Remerciements

Je remercie du fond du cœur toutes les personnes qui ont contribué directement ou indirectement à ce projet.

Je tiens avant tout à remercier **Léopold**, mon cher époux, pour le soutien inestimable que tu m'as apporté tout au long de ces sept dernières années. Tu as été un collègue plus qu'exceptionnel.

Je remercie également mes parents et ma belle-famille pour leur support inconditionnel et leurs précieux encouragements.

Je remercie mon promoteur, **Pr. Raphaël Frédérick**, pour m'avoir accueillie dans son laboratoire au début de mon master et m'avoir fait suffisamment confiance pour que je puisse y réaliser un doctorat. Merci pour l'autonomie scientifique que vous m'avez octroyée. Ces cinq années de thèse ont été un grand enrichissement pour moi tant sur le plan scientifique que personnel.

Je remercie également mon co-promoteur, **Pr. Benoît Van den Eynde**. Merci pour vos lectures attentives et pour m'avoir permis de travailler dans votre laboratoire où j'ai pu étendre mes horizons de chimiste médicinale et rencontrer des scientifiques formidables.

I would like to warmly thank all the jury members of this thesis: Professors **Bernard Gallez**, **Moreno Galleni**, **Johan Wouters**, **Ute Röhrig** and **Wim De Borggraeve**. Thank you for the precious time that you took to read my long manuscript so attentively. Thank you for all your suggestions and the fruitful discussions during this project. They were truly essential for making this work as it is today.

Merci à tous les membres de la **CMFA team**. Merci pour votre amitié et le soutien que nous nous sommes apportés. Merci pour cette ambiance et cet état d'esprit qui ont rendu le travail avec vous si agréable. Je regrette que nous n'ayons pas pu nous voir autant que nous l'aurions souhaité ces deux dernières années.

Merci à toi **Marine**. Tu es rapidement devenue une de mes amies les plus proches. Merci pour les trampolines, les spas, la pole, les road-trips et toutes les autres activités qu'on a pu faire ensemble et qui ont grandement contribué à mon bien-être et donc forcément à ma thèse.

Merci **Julien**. Beaucoup d'années se sont écoulées depuis nos débuts dans la team arginase et je suis contente d'avoir été là tout au long de ton parcours. Le laboratoire n'aurait pas pu se passer de toi. Nos sessions d'analyse objective autour d'un thé vont me manquer.

Merci **Esra** d'avoir toujours été autant disponible et surtout de si bonne humeur. Merci pour ton aide tout au long de ma thèse, que ce soit pour mes manips ou pour m'aider à retrouver les millions de choses que j'ai « perdu ». Les doctorants du labo ont beaucoup de chance de t'avoir !

Romain, je te remercie d'avoir rempli si admirablement ton rôle d'antagoniste, tu as été un némésis comme on en trouve peu. Je pense que nos débats creux et paris divers me manqueront (parfois).

Je remercie également **Karine**, la dernière arrivée. Ce fut à chaque fois un plaisir de discuter avec toi. Bien que tu sois arrivée il y a à peine quelques mois, j'ai l'impression qu'on se connaît depuis bien plus longtemps.

Merci **Maxime** pour toutes nos discussions (très souvent distancielles). Merci pour ce que tu as apporté au laboratoire et félicitations monsieur maître de conf' !

Merci à toi **Quentin**, j'ai adoré t'avoir comme collègue. Nos discussions de bureau sur 1000 sujets différents et les paris prétextes pour faire des restos resteront pour moi de très bons moments de début de thèse.

Merci à la dernière génération de doctorants que, à mon grand regret, ces deux dernières années m'ont un peu moins permis de fréquenter. **Chiara**, on t'a tout de suite adopté quand tu es arrivée comme étudiante et tu as été une collègue adorable pour tout le monde. Merci **Marine #2** pour la relève que tu pris pour faire revivre la « team animation CMFA ». Merci aussi à **Perrine** et **Juhans**, je vous souhaite tout le meilleur pour la suite de vos thèses.

Je tiens aussi à remercier les personnes suivantes qui ont fait partie plus ou moins longtemps de l'équipe du **CMFA** lors des sept dernières années. Merci **Caroline**, **Simon D.**, **Alice**, **Bouazza** et **Séverine**.

Merci également aux nombreuses personnes du **LDRI** que j'ai côtoyé durant ces années et tout particulièrement aux membres de **GNOS**, **BPBL** et **REMA**. Merci tout particulièrement à **Maude** et **Marie-France** pour votre aide précieuse et votre disponibilité.

Merci aux membres du **LICR** et du **De Duve**. Passer vous voir pour discuter, que ce soit de science ou de la vie, ainsi que travailler avec vous a été un réel plaisir.

Je voudrais particulièrement remercier **Vincent** pour les nombreuses discussions, ainsi que les conseils et les remarques pertinentes qui m'ont beaucoup aidé tout au long de cette thèse.

Merci beaucoup à **Bénédicte**. Désolée si j'ai pu parfois apporter un peu trop d'échantillons, mais maintenant promis c'est fini.

Grand merci **Luc** pour ta disponibilité et pour m'avoir appris tout ce que je sais des cellules. Ton aide a été très précieuse.

Merci **Simon K**. Bien que nous ayons partagé la même enzyme, on ne partageait pas vraiment les mêmes connaissances et j'ai apprécié apprendre des choses sur TDO sous un autre angle. Merci pour ta disponibilité et ta curiosité scientifique.

Merci également à **Nicolas** pour votre patience et toute l'aide avant, pendant et après les manips.

Finalement, je voudrais remercier mes chères amies **Angéline**, **Táňa** et **Yasmine**. Merci pour votre soutien, votre présence aux moments importants de ces années de thèse. J'ai eu énormément de chance de vous rencontrer lors de ces études de pharmacie (*100 % worth it!*).

Enfin, je remercie messire **Archibald Kozbault** pour son soutien moral indéfectible et sa présence apaisante à mes côtés, particulièrement lors de la défense privée.

ABBREVIATIONS

3-HAA	3-hydroxyanthranilic acid
3-HK	3-hydroxykynurenine
AHR	Aryl hydrocarbon receptor
AMPA	α-amino-3-hydroxy-5-methyl-4-isoxazolepropionic acid
APC	Antigen-presenting cells
ARG	Arginases
ARG1	Arginase 1
BBB	Blood-brain barrier
BCG	Bacillus Calmette-Guerin
Boc	*Tert*-butyloxycarbonyl
Bregs	Regulatory B cells
CAFs	Cancer-associated fibroblasts
CAR T	Chimeric antigen receptor T cells
CD28	Cluster of differentiation 28
cGAS	Cyclic-GMP-AMP Synthase
CNS	Central nervous system
COX-2	Cyclooxygenase-2
CRS	Cytokine release syndrome
CTL	Cytotoxic T cell
CTLA4	Cytotoxic T-lymphocyte associated protein 4
DAMPs	Damage-associated molecular patterns
DCs	Dendritic cells
DMSO	Dimethylsulfoxide
DMAB	*p*-dimethylaminobenzaldehyde
FACS	Flow cytometry
FOXP3	Forkhead box P3
GCN2	General control non-derepressible 2 nutrient-sensing sensing kinase
GPXs	Glutathione peroxidase
ICIs	Immune checkpoint inhibitors

ICs	immune checkpoints
IDO1	Indoleamine 2,3-dioxygenase 1
IFN	Interferon
IFN-γ	Interferon-γ
IL	Interleukin
IL-2	Interleukin 2
IMAC	Immobilised metal affinity chromatography
iNOS	inducible nitric oxide synthase
IPTG	Isopropyl 1-thio β galacto-pyranoside
IRAEs	Immune-Related Adverse Events
K_d's	Dissociation constants
KMO	Kynurenine monooxygenase
KP	Kynurenine pathway
KYN	L-kynurenine
KYNA	Kynurenic acid
L-Arg	L-Arginine
LE	Ligand efficiency
LICR	Ludwig Institute for Cancer Research
LLE	Lipophilic ligand efficiency
L-Trp	L-tryptophan
MCP1	Monocyte chemoattractant protein 1
MDSC	Myeloid-derived suppressor cells
MHC I	Major histocompatibility complex class I
MIDA	Methyliminodiacetic acid
MST	Microscale thermophoresis
mTOR	Mammalian target of the rapamycin
NAD^+	Nicotinamide adenine dinucleotide
NanoDSF	Nanoscale Differential Scanning Fluorimetry
NEFAs	Non-esterified fatty acids
NFK	N'-formylkynurenine
NF-κB	Nuclear factor-kappa B
NK	Natural killer (cells)
nM	Nanomolar

NMDA	N-methyl-D-aspartate
NO	Nitric oxide
NOE	Nuclear Overhauser effect
NOS	nitrogen reactive species
NSCLC	Non-small cell lung carcinoma
OXPHOS	Oxidative phosphorylation
OL	Organic layer
PAMPs	Pathogen-associated molecular patterns
PD-1	Programmed cell death receptor 1
PD-L1	Programmed cell death ligand 1
PGE2	Prostaglandin E2
PI	Propidium iodide
PIM	4-phenylimidazole
PMB	*p*-methoxybenzyl
PROTACs	Proteolysis-targeting chimaeras
PRRs	Pathogen recognition receptors
QUIN	Quinolinic acid
RLU	Relative luminescence units
ROS	oxygen reactive species
Rp-HPLC	Reversed-phase high-performance liquid chromatography
Sec	Selenocysteine
Sem	Selenomethionine
Sepp1	Selenoprotein P
shIDO1-ST	shRNA plasmid targeting IDO1
SMI	Small-molecule inhibitors
STD	Saturation transfer difference
STING	Stimulator of IFN Genes
TAMs	Tumour-associated macrophages
TCA	Trichloroacetic acid
TCR	T-cell receptor
TDO2	Tryptophan 2,3-dioxygenase 2
TFA	Trifluoroacetic acid

TGF-β	tumour growth factor β
TLRs	Toll-Like Receptors
TME	Tumour microenvironment
Tregs	Regulatory T cells
TRXRs	Thioredoxin reductase

TABLE OF CONTENTS

1. INTRODUCTION

1.1. Actors of the immune system and immune cancer surveillance

Cancer cells can be differentiated from healthy self cells by their biochemical makeup, antigenic structure and biologic behaviour. The myriad of genetic and epigenetic alterations characteristic of all cancers provides a diverse set of antigens that the immune system can use to distinguish tumour cells from their healthy counterparts.[1] The immune system is essential for detecting these differences and initiate a response to prevent further tumour development. This process is referred to as "cancer immune surveillance" and requires both innate and adaptive immunity actors. Both of these immunity actors are not mutually exclusive and closely related.[2]

Innate immunity refers to defence mechanisms that act within hours of an antigen's appearance in the body. They are orchestrated by various types of immune cells from both myeloid and lymphoid lineage. The myeloid lineage include dendritic cells (DCs), monocytes, macrophages, polymorphonuclear and mast cells, while natural killer (NK) cells and γδ T cells are of lymphoid origin (**Figure 1**).[3]

Upon detection of pathogen-associated molecular patterns (PAMPs) and damage-associated molecular patterns (DAMPs), these cells initiate a non-specific immune response leading to downstream inflammatory reactions. This recognition is

orchestrated by various receptor-ligand-like interactions between the target cell and the immune cell. A first response to recognizing PAMPs or DAMPs includes phagocytosis of the foreign body by antigen-presenting cells (APC), namely DCs, macrophages, and polymorphonuclear cells.[3,4] Conversely, NK cells possess potent cytolytic function and proinflammatory cytokine production.[5] In addition to being the first-line defence against pathogens, the innate immune system plays a crucial role in priming the antigen-specific responses of B and T cells that belong to the adaptive immune system (**Figure 1**).

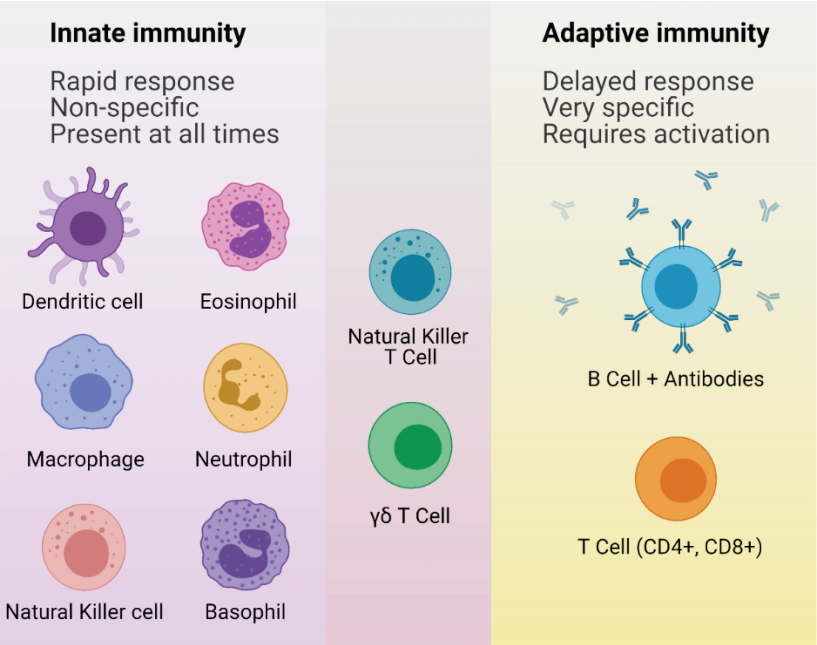

Figure 1. A brief overview of innate and adaptive immunities and their actors. Adapted from Nature Reviews Cancer, 4, 11-22, 2004.[6]

Adaptive immunity corresponds to a specific response tailored for a given antigen. It includes a memory that makes future responses against this specific antigen more efficient. This memory allows the immune system to recognise a previously identified antigen and initiate a more rapid and vigorous immune response upon re-exposure. Once an antigen has been recognised, the adaptive immune system creates an army of immune cells specifically designed to attack it.

The adaptive immune system consists of CD4+ T helper, CD8+ T cytotoxic and B lymphocytes. Once activated, CD8+ T cells play a central role in anti-cancer immunity due to their capacity to kill malignant cells upon recognition of specific antigenic peptides by the T-cell receptor (TCR). CD4+ T cells are involved in regulating anti-tumour immunity by helping the priming of CD8+ T cell response through activation of APC and an increase in antigen presentation by major histocompatibility complex class I (MHC I).[7] Furthermore, through specific and poorly understood molecular mechanisms, CD4+ T cells optimise cytotoxic T cell (CTL) response by downregulating co-inhibitory receptors and increasing migration capacities.[8] On the other hand, a subset of CD4+ T cells with cytotoxic activity (CD4+ CTL) was observed in various immune responses.[9] Another subpopulation of CD4+ T cells, known as regulatory T cells (Tregs), demonstrates potent suppressive abilities and plays a role in maintaining self-tolerance and immune homeostasis by regulating CD8+ T cells and B cells as well as innate immunity cells responses.[10] In cancer, Treg activity was shown to promote tumour progression.[11] For this reason,

targeting intra-tumoural Tregs appears as an attractive strategy to improve anti-tumour immunity. In contrast, an abundance of infiltrating lymphocytes often correlates with a favourable prognosis.[12]

The past decade resulted in extensive research regarding the various implications of T cells in immune-oncology. However, the role of B cells in cancer has only recently started to gain more attention.[13] B cells appear to play both negative and positive roles in cancer progression, depending on the tumour. B cells can inhibit tumour development by producing tumour-reactive antibodies, promoting tumour killing by NK cells, phagocytosis by macrophages, and priming CD4+ and CD8+ T cells.[14] On the other hand, B cells can promote tumour development by producing auto-antibodies and tumour growth factors.[14] Regulatory B cells (Bregs), a subpopulation of B cells, can, directly and indirectly, suppress Th1 and CD8+ cytolytic T cell responses.[13,14]

Of note, NK cells and γδ T cells belong to both innate and adaptive immunity. γδ T cells are a subset of T cells that express a distinct T cell receptor (TCR) composed of one γ-chain and one δ-chain, instead of the α- and β-chains that comprise the TCR on the majority of T cells. Like NK cells, γδ T cells are considered to be a bridge between innate and adaptive immunity.[5] Although NK cells are components of the innate immune system, they show characteristics of the adaptive immune system, such as the expansion of pathogen-specific Treg cells, the generation of long-lasting

"memory" cells able to persist upon cognate antigen encounter, and the possibility to induce an increased secondary recall response.[15]

While the immune system is a powerful tool against cancer, it can also enhance tumour development and progression.[16] Inflammation and angiogenesis mediated by the innate immune system are recognised as enabling characteristics of cancer development.[17] Additionally, the tumour microenvironment (TME) allows the elusion of anti-tumour responses by exploiting multiple suppressive pathways. This ability to avoid the immune response was added as the next generation of hallmarks of cancer.[16] The following section is an overview of these mechanisms.

1.2. Cancer immune escape at a glance

During tumourigenesis, cancer cells adapt to survive in an adverse environment. To that end, tumour cells use multiple mechanisms to drive the immune system to become tolerant towards them. Cancer cells can generate a tolerogenic microenvironment by (**1**) remodelling their metabolism, (**2**) dysregulating T-cell immune checkpoints and antigen presentation, (**3**) releasing immunosuppressive factors and enzymes and (**4**) recruiting immunosuppressive cells (**Figure 2**).

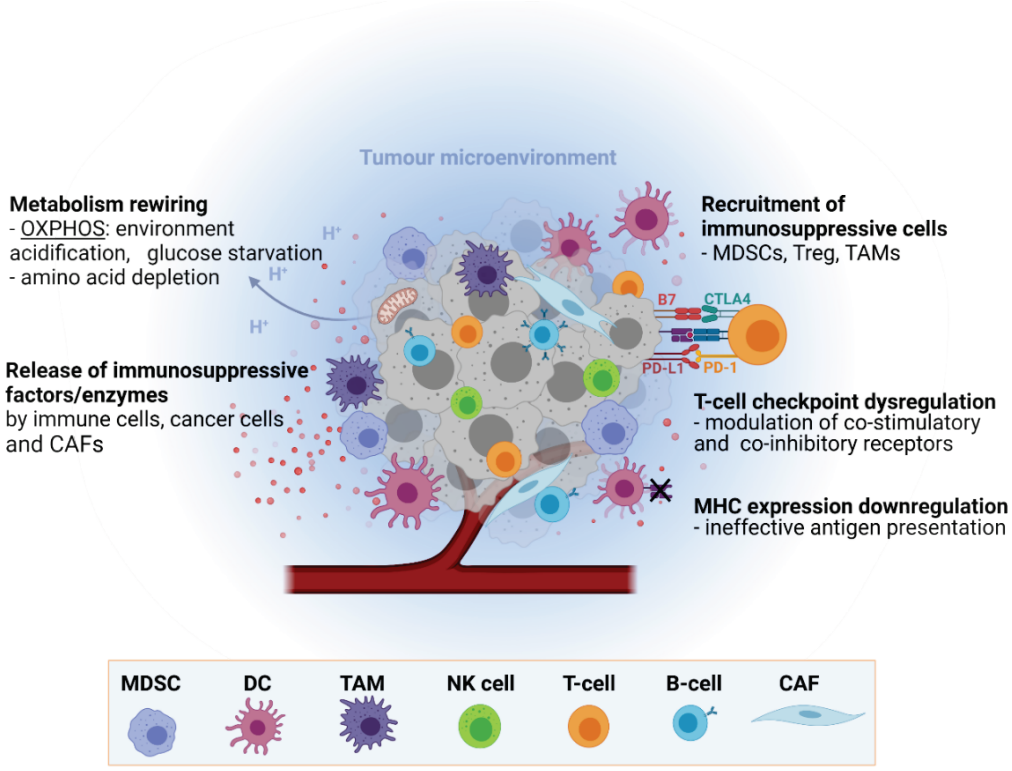

Figure 2. Overview of immunosuppressive strategies taking place in the tumour microenvironment. Created with BioRender.com

1.2.1. Metabolism rewiring

Developing tumours must acquire important amounts of nutrients to ensure growth, survival, proliferation, and long-term maintenance, which leads to a rewiring of their metabolism.[18,19] A widespread adaptation of tumour cells to sustain their anabolic growth is a simultaneous increase of aerobic glycolysis and decrease in oxidative phosphorylation (OXPHOS). This phenomenon is called the Warburg effect. The Warburg effect enables rapid ATP synthesis and provides intermediate biosynthetic materials, both of which are essential for meeting the high proliferative demands of cancer cells.[20] The high demand for glucose in cancer cells creates competition in the tumour microenvironment that harms neighbouring (immune) cells.[19] In addition to this direct starvation, extracellular acidification due to the increased glycolysis confers immune evasion ability to cancer cells by impairing T and NK cells cytotoxicity.[20] Acidosis induced by tumours can also promote macrophage polarisation toward a tumour-associated macrophage phenotype that will sustain tumour growth.[21]

Furthermore, the increase of glycolysis flux produces immunosuppressive metabolites such as lactate, the export of which also leads to a pH decrease.[19] This acidic environment impairs T cell and NK cell cytotoxicity. In turn, lactate production negatively impacts interferon-gamma (IFN-γ) production by tumour-infiltrating T cells and NK activation.[22] Moreover, lactate also enhances the

proportion of myeloid-derived suppressor cells (MDSC),[19] and may also promote macrophage polarization to an M2 phenotype.[23]

Besides glucose, tumour cells require high availability of amino acids as protein building blocks for their proliferation. The metabolic demand for amino acids in the tumour microenvironment is so high that amino acids are the most depleted substances in tumours.[24] Thus, cancer cells increase amino acid metabolism, which starves T cells and blocks the immune response. Competitions for amino acids such as L-Tryptophan or L-Arginine lead to immune suppression through direct starvation of immune cells and activation of specific pathways developed later in sections *1.3.3.* and *1.4.* of the present work.

1.2.2. Recruitment of immunosuppressive cells

Tumours can also decrease their immunogenicity by recruiting and polarizing specific immune suppressive cells such as cancer-associated fibroblasts (CAFs), regulatory T cells (Tregs), myeloid-derived suppressor cells (MDSCs) and tumour-associated macrophages (TAMs).

Cancer-associated fibroblasts (CAFs). CAFs are the most abundant cells in tumour stroma. CAFs correspond to a heterogeneous cell population that arises from progenitor cells from the circulating pool of hematopoietic cells, such as circulating fibrocytes and bone marrow-derived cells.[25] During tumour development, these CAF-progenitors are continuously recruited into cancer tissue. CAFs provide

mechanical support and promote proliferation, survival, angiogenesis, metastasis, immunogenicity, and resistance to therapies.[26] Their immunosuppressive mechanisms include the recruitment of myeloid cells (via monocyte chemoattractant protein 1 (MCP1)) and induction of their pro-tumoural phenotypes.[27,28] A study also reported that a subset of CAFs attracts CD4+CD25+ cells via CXCL12 secretion and promotes differentiation into the tolerogenic forkhead box P3 ($FOXP3^{+}$) Tregs cells.[29] Furthermore, CAFs also hinder anti-tumour immune responses and impede T cells' function in the TME by affecting the antigenic presentation capacity of DCs by secreting interleukin (IL) 6 and tumour growth factor β (TGF-β).[25]

Regulatory T cells (Tregs). Treg cells can arise from the thymus (natural Tregs) or differentiate from naïve T cells under certain cytokine conditions in peripheral tissues (induced Tregs).[30,31] Both families have similar phenotypical features and share the ability to maintain immunological tolerance.[32] Their differentiation and function have been linked with the expression of transcription factor Foxp3, whose function itself is tightly regulated by various post-translational modifications.[33,34] The tumour microenvironment contains a range of factors able to attract Tregs and facilitate their proliferation.[35] Treg suppressive mechanisms include the secretion of soluble immunosuppressive cytokines such as TGF- ß1, expression of the T cell co-inhibitory receptors Cytotoxic T-Lymphocyte Associated Protein 4 (CTLA4) and reduction of T cell-stimulatory capacity of APCs.[36,37]

Myeloid-derived suppressor cells (MDSCs) and tumour-associated macrophages (TAMs). MDSCs and TAMs are heterogeneous populations of suppressive cells from myeloid lineage, elevated in virtually all patients with malignancies.[38] MDSCs are in an immature state and replenished by bone marrow precursors, while TAMs exhibit markers present in mature macrophages.[39] In response to tumour signalling pathways, TAMs can arise following the polarization of tissue-resident macrophages and circulating monocytes or differentiate from MDSCs. These last ones are also able to skew macrophages into an M2-like phenotype, known for supporting angiogenesis and expressing immunosuppressive molecules.[40,41]

In addition to promoting tumour progression through the facilitation of angiogenesis, MDSCs and TAMs regulate both innate and adaptive immunities by impairing NK and T-cell function.[42–44] Both drive the differentiation of T cells towards the Treg phenotype and stimulate their expansion.[45] TAMs and MDSCs also contribute to L-Arg or L-Trp exhaustion by expressing arginases (ARG), inducible nitric oxide synthase (iNOS) or indoleamine 2, 3-dioxygenase (IDO1). MDSCs and TAMs starve T cells and inhibit their responses by downregulation of the CD3ζ chain in the TCR complex.[46,47] TAMs and MDSCs can also promote immune suppression by producing oxygen and nitrogen reactive species (ROS, RNS).[48] These short-lived reactive species hinder the activation of T cells and drive them towards apoptosis.[49]

MDSCs' and TAMs' suppressive nature is also due to their ability to express membrane surface ligands of T cell co-inhibitory receptors CTLA-4, cluster of differentiation 28 (CD28) and programmed cell death receptor 1 (PD-1).[50,51] These receptors are commonly referred to as immune checkpoints (ICs) because of their crucial role in maintaining self-tolerance. However, they are also widely implicated in tumour escape mechanisms, developed in the next section. However, ICs expression is also one of the major immune escape mechanisms, developed in the following section.

1.2.3. Dysregulation of T cell checkpoints

Even when an endogenous immune response is observed against tumour cells, it is not always efficient.[52] Indeed, tumours can induce tolerance among tumour-specific T cells and hijack the immune checkpoint system by expressing ligands that bind to inhibitory receptors on T cells.[52] T cells require two signals to initiate an efficient response.[53] The first signal originates from the interaction between the antigen and the TCR and gives specificity to the immune response. In the case of T cells, the amplitude and quality of the effector response following antigen recognition by the TCR is regulated by ICs' co-stimulatory and co-inhibitory signals.[54] Under normal physiological conditions, immune checkpoints are crucial for maintaining self-tolerance or amplify the immune response following a pathogenic infection.[55,56] Tumours use the expression of these immune checkpoints as a way to escape the immune system.

The most studied ICs are the axis of CTLA-4 and the programmed cell death receptor 1 and its ligand (PD-1/PD-L1) .[57] CTLA-4 and PD-1 signalling both result in negative effects on T-cell activity; however, the responsible signalling mechanisms and the expression patterns between these two immune checkpoints differ.[58]

CTLA-4 is an immunoglobulin-related receptor expressed by both $CD4^+$ and $CD8^+$ T cells. Its endogenic ligands are membrane proteins CD80 and CD86, collectively called B7 molecules and located at the surface of APCs as well as on immune cells of the tumour microenvironment, on stromal cells and tumour cells.[59] The exact mechanism remains unclear, but the CTLA-4 axis is thought to act in the early stages of an immune response, primarily to reduce T-cell responses to self-antigens and prevent autoimmunity.[60] CTLA-4 ligation antagonises early T cell activation by inhibiting interleukin 2 (IL-2) production, cell cycle progression and TCR signalling.[61] CTLA-4 is the counteracting homologue of the co-stimulatory receptor CD28, their co-stimulations act as a thermostat for self-tolerance. The potent regulation of immune response by CTLA-4/B7 signalling was demonstrated by the fact that knockout mice die after 2 – 3 weeks due to fatal lymphocytic infiltration and autoimmune destruction of major organs.[62]

PD-1 receptors have a broader expression and are present on activated T cells, B cells, and myeloid cells.[63,64] Its ligands, PD-L1 and (to a lesser degree) PD-L2, are present on the surface of malignant cells, and immune cells and vascular

endothelial cells in the tumour microenvironment.[65] Their expression is induced as activated T cells express high levels of PD-1. Unlike CTLA-4, which expression is limited to T cells, PD-1 is present on activated T cells, B cells, and myeloid cells.[63,64] While CTLA-4 functions during the priming phase of T-cell activation, PD-1 functions during the effector phase, predominantly within peripheral tissues.[64] Binding between PD-1 and PD-L1 or PD-L2 triggers inhibitory signalling to attenuate immune responses of T cells already engaged in an effector response.[66–68] If a T cell experiences coincident TCR and PD-1 binding, PD-1-generated signals prevent phosphorylation of key TCR signalling intermediates, terminating early TCR signalling and reducing activation of T cells.[69,70] PD-1 expression is a hallmark of "exhausted" T cells that have experienced high levels of stimulation or reduced $CD4^+$ T-cell help.[68] This state of exhaustion, which occurs during chronic infections and cancer, is characterised by T-cell dysfunction, resulting in suboptimal infection tumour control.[58]

Intense efforts were devoted to the development of agonists of co-stimulatory receptors or antagonists of inhibitory signals, both of which result in the amplification of antigen-specific T cell responses. Such an approach represents the majority of the compounds in current clinical testing. The blockade of immune checkpoints seems to unleash the potential of the anti-tumour immune response. *The current state regarding the blockade of ICs is the subject of section 1.3.1.*

1.2.4. Major histocompatibility complex I downregulation

MHC I constitutes a crucial factor in the initiation of an adaptive immune response.[71] Nucleated cells express MHC-I to present peptides from intracellular proteins for recognition by the $CD8^+$ TCR.[72] However, tumours can avoid tumour-associated antigen presentation by downregulating the surface display of these MHC-I, which results in the suppression of CD8+ T cell-mediated immunity.[73,74] Downregulation of MHC-I has been described in 40–90% of human tumours, often correlating with a worse survival prognosis.[73] This downregulation can be reversible or irreversible and is regulated by complex mechanisms.[74,75] Irreversible MHC-I downregulation can arise from chromosomal alterations in the heavy and/or light chain genes.[76,77] In contrast, reversible MHC-I dysregulations can occur due to (post-)transcriptional downregulation of the HLA class I chains or components of the antigen processing machinery.[78,79] Reversible MHC-I downregulations represent a potential target for cancer immunotherapy.[74]

1.2.5. Release of immunosuppressive factors and expression of immunomodulatory enzymes

Tumour or tumour-associated cells exert suppressive effects on the immune system by synthesising many biologically active agents.[80] One of the main immunosuppressive factors is TGF-β, a pleiotropic immunosuppressive cytokine that inhibits T cell activation, proliferation, and differentiation.[81] Tumours cells can also induce proinflammatory cyclo-oxygenase-2 (COX-2) to stimulate prostaglandin

E2 (PGE2) signalling, promoting apoptotic resistance and proliferation, angiogenesis, inflammation, invasion, and metastasis of cancer cells.[82]

Finally, enzymes that catabolise essential or semi-essential amino acids such as iNOS, ARG1, IDO1, TDO2 or IL4I1, are also often used in TME.[83] Their expression leads to nutrient/building block depletion and the generation of suppressive catabolites. The inhibition of these enzymes is exploited as a strategy for cancer treatment.

1.3. Cancer immunotherapy as a treatment strategy

While the idea of harnessing the immune system to treat cancer is an old idea, human trials over the following years were, however, very unsuccessful and led to hypothesis dereliction and dismissal of the entire idea of cancer immunotherapy for decades.

Dr William Coley, considered as the father of immunotherapy, searched for a more effective method than surgery to treat sarcoma. In 1891, Dr Coley began injecting patients' tumours with a mixture of live and inactivated *Streptococcus pyogenes* and *Serratia marcescens* (Coley's toxin). By doing so, he achieved remarkable responses, including durable and complete remissions for patients with various malignancies, including sarcoma, lymphoma, and testicular cancer.[84,85]

Modern immunotherapy emerged again with bacillus Calmette-Guerin (BCG) therapy, an example of a very successful cancer therapy involving activated macrophages in tumour rejection. In 1976, a trial was conducted to examine the use of BCG, the tuberculosis vaccine, to prevent the recurrence of bladder cancer.[86] A solution of attenuated bacilli was injected into the bladder of patients with superficial bladder cancer. Following the course of the treatment, no tumours were found in the treated cases, and biopsies revealed an intense granulomatous reaction, indicating that an immune-inflammatory reaction had occurred.[87]

Today, cancer immunotherapy is a validated approach for treating cancer patients. Several types of immunotherapeutic treatments are available and were successfully applied to patients and significantly prolonged the survival of patients with life-threatening cancers. In 2018, the Nobel prize for physiology or medicine acknowledged the importance of immunotherapy and awarded the discovery of CTLA-4 by James P. Allison and PD-1 / PD-L1 by Tasuku Honjo.[88]

The present section summarises the current strategies used in cancer immunotherapy and some of the potential future approaches (**Figure 3**).

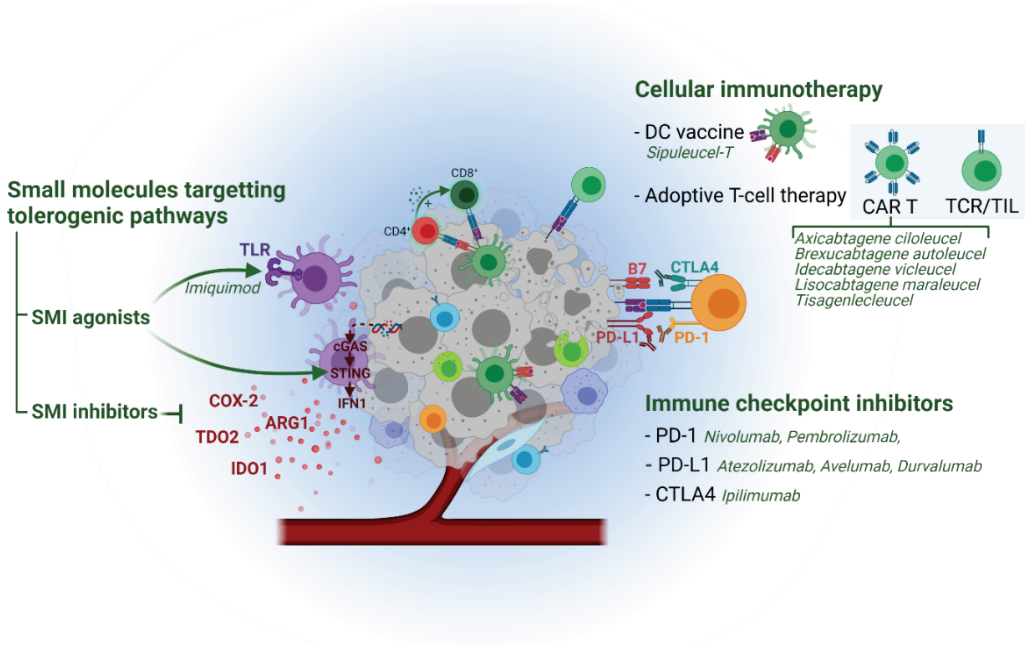

Figure 3. Overview of existing immunotherapeutic approaches in cancer. Created with BioRender.com

1.3.1. Immune checkpoint inhibitors (ICIs)

As stated in the previous chapter, tumours can induce tolerance by expressing ligands that bind to inhibitory receptors on T cells. The blockade of these immune checkpoint inhibitory pathways constitutes a central cancer immunotherapy approach. Nowadays, several FDA-approved drugs target these immune checkpoints and most notably CTLA4 and PD-1.[89] Overall, the use of these drugs led to an increased survival rate compared to chemotherapy alone.

In 2014, humanised and fully human anti-PD-1 monoclonal IgG4 antibodies **pembrolizumab** (**KEYTRUDA®**) and **nivolumab** (**OPDIVO®**) became the first FDA approved PD-1- targeted therapeutics for refractory and unresectable melanoma.[90–93] Since then, their use was extended for more than ten other cancer types, including lung cancer, urothelial cancer, head and neck squamous cell carcinoma, renal cell cancer and Hodgkin's disease.[88,94] In 2021, six different ICIs FDA-approved antibody drugs are targeting the PD-1/PD-L1 axis, one is targeting CTLA4, and a staggering number of ongoing clinical trials involve existing and emerging ICIs.[95]

ICIs targeting the PD-1/PD-L1 axis or CTLA4 are used in monotherapy or combination with other anti-cancer agents (i.e. chemotherapy, radiotherapy or immunomodulatory agents) and create an immunogenic tumour microenvironment with subsequent improvement of patients' survival rate.[88,96,97]

Despite its obvious benefit for cancer treatment, ICIs therapy has two significant hinders. Firstly, while some tumour types have a moderate response rate to ICIs therapy, the response rate for the vast majority of tumours is low (~15% objective response rate across indications), and most tumours exhibit adaptive escape mechanisms.[98,99] Secondly, treatment with ICIs is frequently accompanied by Immune-Related Adverse Events (IRAEs).[100,101] IRAEs may affect any tissue, but most frequently involve the skin (rash, pruritis, bullous, lichenoid, eczema-like and psoriasis-like manifestations), the gut (colitis), lungs (pneumonitis), liver (hepatitis) and endocrine glands (hypophysitis, thyroiditis).[52,100] They are estimated to occur in up to 90% of patients subjected with an anti-CTLA-4 antibody and 70 % of those treated with anti-PD-1 or anti-PD-L1 antibodies.[100] IRAEs are believed to be the off-target effects of the activated immune response due to eliminating immune checkpoints.[52] Treatment of IRAEs is based on corticosteroids and anti-TNF α antibody (**infliximab**) in severe cases.[102] While anti-TNF treatment seems to have an only mild impact on immune activity, corticosteroids present a significant negative impact on anti-tumour immune responses, thus hindering the clinical efficacy of ICIs treatment.[102]

The higher incidence of IRAEs in anti-CTLA4 treated patients could be explained by the lack of specificity in T cell expansion, coupled with the fundamental importance of CTLA4 as an immune checkpoint in the formation of de novo immune response.[103] The more favourable toxicity profile of the PD1- and PD-L1 blocking

agents suggests the benefits of specifically targeting the properties of cancer that inhibit the immune response rather than non-specifically activating the immune system with CTLA4 blockade.

1.3.2. Cellular immunotherapy

Cellular immunotherapies are based on the administration of live autologous or allogeneic cells to patients to take advantage of the anti-tumour capabilities of the immune system. Current cellular immunotherapies belong to two different categories: (**1**) DC-based cancer vaccines (active immunotherapy) and (**2**) Adoptive T-cell therapies (passive immunotherapy). Briefly, the general principle of cellular immunotherapies is the isolation of autologous immune cells (DCs or T cells) by leukapheresis followed by their ex-vivo modification using tumour antigens and their administration back into the patient. Once reinjected, these cells can generate or induce tumour antigen-specific immune responses.[104]

In 2010, **sipuleucel-T** (**PROVENGE®**), a DC-based vaccine, was the first FDA-approved cellular immunotherapy and is used to treat asymptomatic or minimally symptomatic prostate (hormone-refractory) cancer with metastases. It is a generally well-tolerated therapy with minor adverse effects related to the injection site.[105]

Chimeric antigen receptor T cells (CAR T) include **tisagenlecleucel** and **axicabtagen-ciloleucel**, in which T cells are engineered to express an anti-CD19 chimeric antigen

receptor. Both products received their approval in 2017 and are used to treat blood malignancies (diffuse large B-cell lymphoma, lymphoblastic leukaemia, B cell acute lymphoblastic leukaemia, non-Hodgkin's lymphoma, chronic lymphocytic leukaemia).[105] CAR T cell therapy is particularly appropriate in B cell malignancies since the transmembrane glycoprotein CD19 is only expressed on the B cell lineage.[106] CAR T therapy is associated with severe and life-threatening side effects (cytokine release syndrome (CRS)). While CAR T therapy demonstrated durable remission/cure in patients with blood malignancies, its use in solid tumours remains uncertain—one reason being the suppressive nature of the TME.[107] New strategies are currently under investigation, including the combination of CAR T with ICIs.[108]

1.3.3. Opportunities for small molecules in cancer immunotherapy

Current cancer immunotherapy mainly revolves around biologics and is unfortunately successful in only a minor fraction of responsive tumours. Furthermore, multiple immune resistance mechanisms are often involved within a tumour microenvironment, hampering the immune response and leading to the failure of currently available treatments.[109,110]

As previously mentioned, tumours employ a number of enzymatic pathways to suppress anti-tumour immunity. Due to the inability of antibodies to reach intracellular targets, a desirable approach to targeting these escape mechanisms may reside in developing small molecule inhibitors (SMIs). Furthermore, SMIs are

not limited to enzymatic targets and can be applied to other suppressive mechanisms such as membrane receptors. Among these, immune checkpoints and toll-like receptors are amongst the currently explored candidates.

Using SMIs to target tolerogenic pathways is an attractive strategy for cancer immunotherapy. The advantages of SMIs reside in their ability to reach a wide array of intracellular targets, the possibility to fine-tune their ADME properties, as well as their superior cost-effectiveness compared to biologics.[111,112]

Within this context, small molecular scaffolds are a rapidly expanding area of research, as exemplified by the increasing number of patent applications and compounds currently under evaluation at preclinical and clinical stages, both as stand-alone or combination therapies.[111–113] Many compounds targeting various targets and pathways are currently in the pipeline, some of which are exemplified hereafter.

The PD-1/PDL-1 axis. The development of small molecules for the PD-1/PDL-1 axis is a strategy currently explored to palliate the IRAEs and poor tumour penetration of the mAbs (150 kDa).[114] However, the development of small-molecule-based therapeutics is challenging as the interaction between PD-1 and PD-L1 is a protein-protein interaction and thus corresponds to a wide, shallow and hydrophobic surface poorly suitable for chemical compounds.[115,116] Another challenge resides in the fact that conformational changes occur during the interaction.[117] Nonetheless,

there is an increasing number of patent applications and preclinical studies involving small-molecule modulators of the PD-1/PD-L1 pathway. So far, the only compound to have reached clinical evaluation is **CA-170** (Aurigene/Curis, structure not disclosed). **CA-170** shows promising results, especially against non-small cell lung carcinoma (NSCLC) and Hodgkin's lymphoma. **CA-170** is orally bioavailable and displays significantly better biosafety than monoclonal antibodies as no dose-dependent toxicity was observed so far.[118]

Toll-Like Receptors (TLRs). TLRs are transmembrane proteins that belong to the family of pathogen recognition receptors (PRRs) in the innate immune system.[119] TLRs recognise PAMPs and DAMPs and trigger the expression of inflammatory cytokines, chemokines and IFNs.[119,120] Evidence suggests that activation of TLRs may be useful as immunotherapy adjuvants to increase treatment efficacy.[121,122] Presently, the TLR7 agonist **imiquimod** (**Figure 4**) is the only FDA-approved immunotherapy small molecule and is used topically in basal cell carcinoma.[123] However, several clinical trials are ongoing to broaden its applications.

TLRs activation presents several challenges. Firstly, TLRs agonists can induce immune stimulation against normal cells.[124] When they enter the bloodstream, these compounds are likely to systematically produce excess proinflammatory cytokines, resulting in cytokine storms or even tissue damage. For this reason, most of these molecules have been approved for only local or topical treatment.[125]

Secondly, due to the heterogeneity of both TLRs receptors and tumours, inflammation and oncogenesis were observed in some settings.[126] The challenge resides in the difficulty of predicting these specific outcomes.[122]

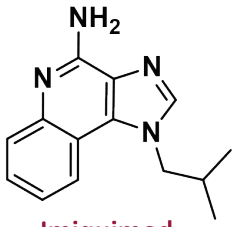

Imiquimod
EC_{50} 2.1 μM

Figure 4. Structure of TLR7 agonist **imiquimod**. EC_{50} value from ref.[127]

Cyclic-GMP-AMP Synthase (cGAS)/Stimulator of IFN Genes (STING) Pathway. The DNA-sensing cGAS–STING pathway is another signalling axis of innate immunity. It comprises the synthase for the second messenger cyclic GMP–AMP (cGAS) and the cyclic GMP–AMP receptor stimulator of interferon genes (STING).[128] cGAS-STING is activated upon the detection of pathogenic DNA and initiates an immune response involving the expression of type I interferon (IFN).[129]

In cancer, malignant transformation usually accompanies cytosolic chromatin fragments and micronuclei, increasing the probability of DNA leakage in a tumour cell or tumour cell-derived DNA uptake by DCs.[130] Disruptions in the cGAS–STING pathway were observed in some tumours as an immune escape mechanism.[131] It is worth mentioning that chemotherapeutic drugs such as **cisplatin** and **etoposide**

may partly attribute their anti-tumour activity by triggering STING-dependent innate immune activity by inducing DNA damage.[132]

The discovery of STING in 2008 resulted in intense efforts to find STING agonists for cancer immunotherapy.[133] So far, several compounds have entered clinical trials.

The synthetic cyclic dinucleotide **ADU-S100** (**Figure 5**) was the first to enter clinical trials in 2017 for the treatment of advanced/metastatic solid tumours or lymphoma.[134,135] Other cyclic (**MK-1454** and **SB11285**) and non-cyclic (**MK-2118**, **GSK3745417**, **TAK-676**, **SNX281**) dinucleotides are currently in clinical development both as single agents and in combination with an ICI. Another clinical trial on advanced lymphoma and solid tumours is also recruiting to evaluate a macrocyclic peptide (**E7766**) as a single agent.[136] Finally, a plethora of STING-targeting compounds with improved structural properties and potency are currently at a preclinical stage.[137]

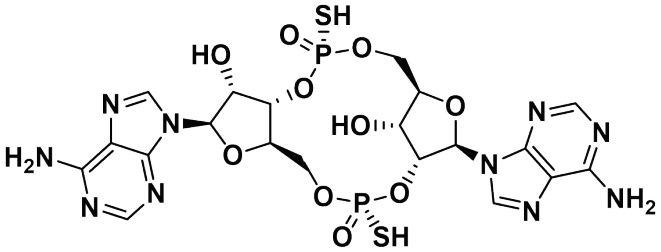

ADU-S100

Figure 5. Structure of cyclic dinucleotide STING agonist **ADU-S100**.

The prostaglandin pathway (COX-2). Cyclooxygenase 2 (COX-2) is an inducible enzyme that catalyses the metabolism of arachidonic acid generates prostanoids, including PGE2, which activates specific prostaglandin receptors (EP1 to EP4) expressed on immune cells.[138] COX-2 is overexpressed in most solid tumours and participates in immune evasion by suppressing adaptive and innate immune responses and creating a tolerant immune environment.[139] COX-2 activity inhibits the maturation of DCs and the activation and proliferation of T and NK cells while enhancing the differentiation of immunosuppressive M2 macrophages and Treg cells.[3] These findings led to the clinical evaluation of **celecoxib** (**Figure 6**), a selective COX-2 inhibitor already used to treat osteoarthritis, rheumatoid arthritis and ankylosing spondylitis in adults.[140] Preclinical results suggest that COX-2 inhibition in patients carrying tumours expressing IDO1 constitutively leads to decreased IDO1 expression, increased T-cell infiltration, and increased responsiveness to anti-PD-1/ Programmed cells Death Ligand-1(PD-L1) therapy.[141,142]

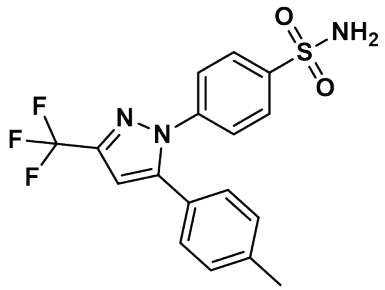

Celecoxib
IC_{50} COX-1 10 µM
COX-2 0.04 µM

Figure 6. Structure of selective COX2 inhibitor **celecoxib**.

L-Arginine (L-Arg) catabolism by Arginase 1 (ARG1) and inducible nitric oxide synthase (iNOS). The overexpression of L-Arg catabolizing enzymes ARG1 and iNOS by TAMs, MDSCs and DCs is another important regulator of innate and adaptive immune responses.[143] The interest in inhibition of key enzymes ARG1 and iNOS as an approach to treat cancer already emerged in early 90s.[144,145]

In T cells, the resulting L-Arg starvation leads to the downregulation of CD3ζ chain expression, which is the principal signal transduction element of the TCR.[146] Furthermore, ARG1 degrades L-Arg to produce L-ornithine, which serves as a precursor for the synthesis of polyamines, L-proline and collagen, promoting tumour cell growth.[143] On the other hand, iNOS hydrolyses L-arginine into nitric oxide (NO) + L-citrulline and can play both pro- and anti-tumourigenic roles, depending on its concentration, the tumour microenvironment and the tumour type.[147,148] In vivo studies demonstrated that expression of iNOS in melanoma and triple-negative breast cancer led to a poor prognosis and that administration of iNOS inhibitors could halt tumour cell proliferation, migration and reduce metastases.[149,150]

The development of ARG1 inhibitors constituted major challenges as all inhibitors heavily rely on the boronic acid function.[151,152] The use of this moiety in drug design is relatively recent as the boron atom was long considered toxic. However, since the approval in 2003 of the protease inhibitor **bortezomib** (**VELCADE®**), interest in

boronic acids has steadily increased, and they are now generally considered safe.[153,154] A boron-containing ARG1 inhibitor **CB-1158** (**INCB001158**) (**Figure 7**) is currently in Phase I and Phase II trials either as a single agent or combined with ICI **pembrolizumab** or chemotherapy for advanced/metastatic solid tumours. So far, data indicates that **CB-1158** is well-tolerated, did not impact the occurrence of IRAES and showed responses both in mono- and in combination therapies.[155,156]

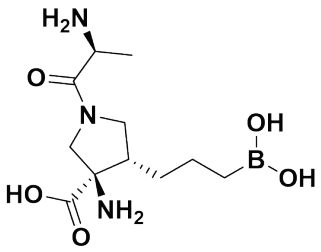

CB-1158 (INCB001158)
IC_{50} ARG1 86 nM

Figure 7. Structure of selective ARG1 inhibitor **CB-1158**/**INCB001158**. Enzymatic IC_{50} is from ref.[157]

Tryptophan metabolism and its targeting in cancer therapy. Tryptophan degradation is considered one of the major immunosuppressive pathways and has been at the centre of intense research for cancer immunotherapy over the past decade. These efforts led to several compounds that reached clinical trials over the past decades.[158] The present work relates the development of compounds targeting L-Tryptophan (L-Trp) metabolism. Therefore, more attention will be drawn to this subject, and the following chapter is dedicated to L-Trp metabolism and its targeting.

1.4. Tryptophan metabolism in cancer immunotherapy and beyond

L-Trp is an essential amino acid and is thus exclusively obtained through dietary intake. Besides its obvious use for protein synthesis (for which its amount is also limiting), L-Trp is the precursor of several critical pathways.

Unlike other amino acids, L-Trp is mainly bound to albumin in the plasma. This bound form accounts for around 90 % of all circulating L-Trp and is not available for blood-brain barrier (BBB) crossing.[159] This equilibrium is regulated by the concentration of non-esterified fatty acids (NEFAs) that displace L-Trp from its binding site.[160] Elevations in NEFAs occur following sympathetic β-adrenoceptor-mediated lipolysis following a sustained physical exercise.[161] This dissociation is an important factor for L-Trp intake into the extracellular fluid of the central nervous system (CNS) through a competitive transport carrier.[162]

Once in the CNS, L-Trp is metabolised into several neuroactive compounds, including serotonin, melatonin and tryptamine.[163] It is estimated that 1% of ingested L-Trp is converted through the serotonin – melatonin pathway.[164,165] This synthesis also occurs in the gastrointestinal tract.[166]

The overwhelming majority of L-Trp (~95 %) is degraded following the kynurenine pathway (KP). This cascade of enzymatic reactions, illustrated in **Figure 8**, is necessary for the de novo synthesis of the crucial energy and redox cofactor,

nicotinamide adenine dinucleotide (NAD^+), in the liver and the kidney.[167] Additionally, the KP also ubiquitously produces a series of immunomodulatory, neuroactive and inflammatory catabolites, called kynurenines.

The KP is best studied in the context of immune regulation. Indeed, the KP is known for contributing to immune privilege both by (**1**) the depletion of L-Trp, resulting in the suppression of effector T-cell response against antigens and (**2**) the accumulation of kynurenine and its metabolites, able to control the inflammation, thus maintaining a tolerogenic environment.[168,169] Physiologically, the KP contributes to protecting immune-privileged sites such as placenta.[170]

The following subchapter is a more in-depth discussion around the KP and its physio-pathological implications.

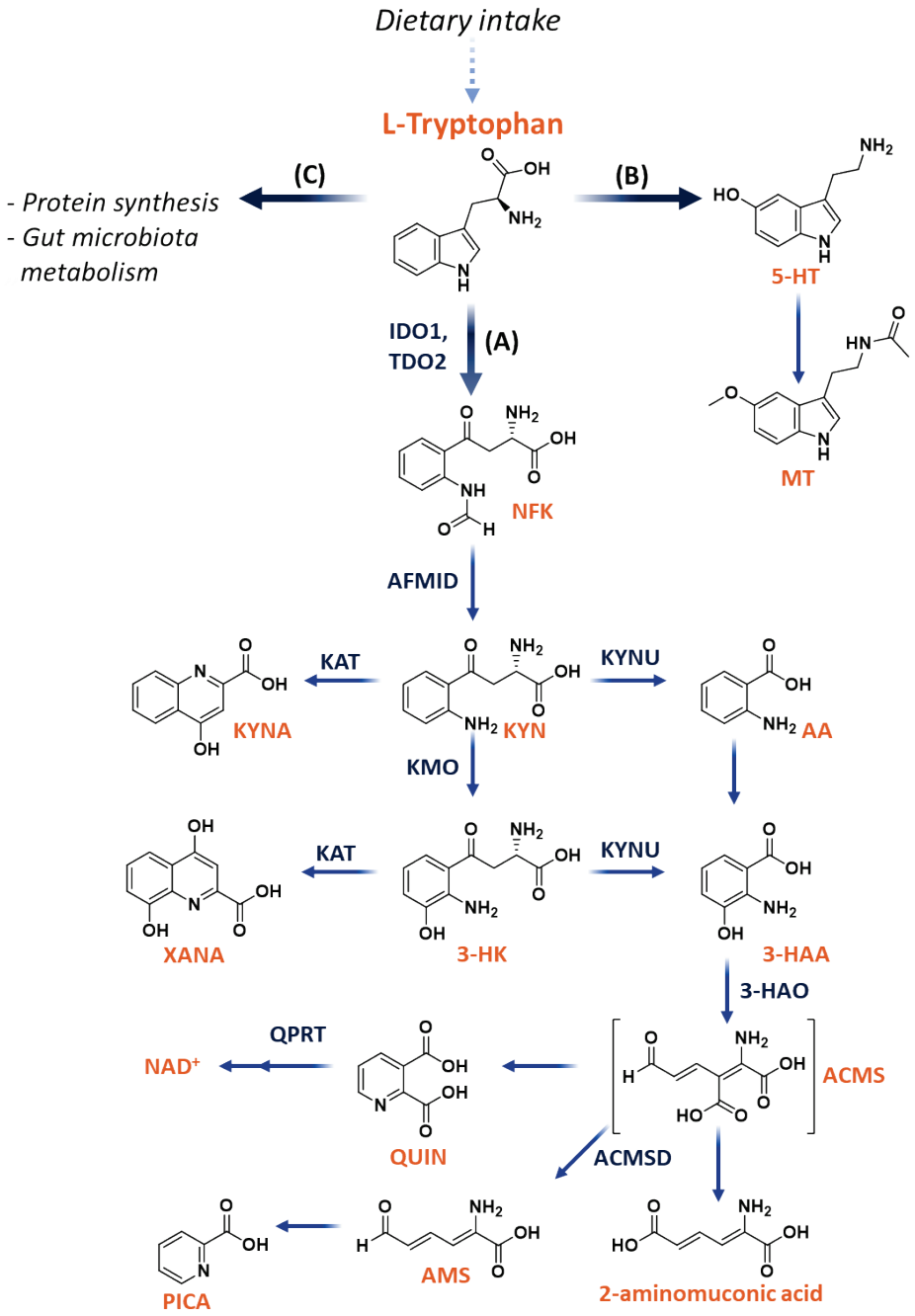

Figure 8. Catabolic fate of L-Trp.

L-Trp can be used in different ways following its ingestion (**A**, **B**, **C**). **(A)** The kynurenine pathway (KP) accounts for the vast majority of L-Trp catabolism. The KP involves numerous enzymatic and non-enzymatic reactions, leading to various compounds that modulate inflammation and immunity and NAD+. **(B)** L-Trp is metabolised to 5-HT, which can be further metabolised to MT. **(C)** In addition to its use for protein synthesis, L-Trp is metabolised by the gut microbiota into several molecules, such as indole derivatives, tryptamine, and skatole. Abbreviations: 3-HAA, 3-hydroxyanthranilic acid; 3-HAO, 3-hydroxyanthranilic acid 3,4-dioxygenase; 3-HK, 3-hydroxykynurenine; 5-HT, serotonin; ACMS, 2-amino-3-carboxymuconic acid-6-semialdehyde; ACMSD, 2-amino-3-carboxymuconate-semialdehyde decarboxylase; AFMID, kynurenine formamidase; IDO1, indoleamine 2,3-dioxygenase; KAT, kynurenine aminotransferase; KMO, kynurenine monooxygenase; KYNA, kynurenic acid; KYNU, kynureninase; KYN, L-kynurenine; MT, melatonin; NAD, nicotinamide adenine dinucleotide; PICA, picolinic acid; QPRT, quinolinate phosphoribosyltransferase; QUIN, quinolinic acid; TDO, tryptophan 2,3-dioxygenase; XANA, xanthurenic acid.

1.5. Kynurenine pathway: Physiological implications and therapeutic relevance

The first and rate-limiting step of the KP is independently catalysed by either indoleamine 2, 3-dioxygenase (IDO1) or tryptophan 2, 3-dioxygenase (TDO2), two cytosolic heme-containing oxidoreductases. IDO1 and TDO2 perform the oxidative cleavage of L-Trp's pyrrole ring, forming N'-formylkynurenine (NFK) (**Figure 8**). The latter is rapidly converted into L-kynurenine (KYN) both by spontaneous and enzymatic hydrolysis. KYN is further degraded into a plethora of metabolites with various biological activities and functions. These metabolites are usually collectively referred to as kynurenines.

Expression of IDO1 and TDO2 is used by more than half of human tumours as an immune escape mechanism.[171] The resulting catabolism of L-Trp promotes an

immunosuppressive environment both through the depletion of the essential amino acid and the accumulation of kynurenine (KYN) metabolites.[170]

Firstly, the decrease in L-Trp levels results in a blockage of CD8+ and CD4+ T-cells, in the G1 cell cycle phase, due to their susceptibility to the amino acid shortage.[172] Secondly, it has been often proposed that the L-Trp decrease led to the activation of the general control non-derepressible 2 (GCN2) "stress", nutrient-sensing kinase. GCN2 activation in response to amino acid starvation induces a signalling pathway involved in the up- and down-regulation of gene expression to maintain cellular homeostasis, further hindering CD8+ T-cell proliferation.[46,173] Although more recent data suggest that, at least in melanoma, GCN2 expression in T cells does not mediate tumour immune escape in response to tryptophan catabolism.[174] Finally, immunosuppression from L-Trp deprivation was also linked to the inhibition of the mammalian target of the rapamycin (mTOR) pathway.[175] Administration of L-Trp mimetic **indoximod** (**Figure 9**) was able to reactivate the function of mTOR and prevent the activation of GCN2 by creating an artificial Trp-sufficiency signal.[176]

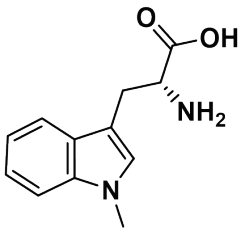

Indoximod

Figure 9. Structure of 1-methyl-D-tryptophan, also known as indoximod.

On the other hand, along with its catabolites, kynurenine (KYN) favours Tregs, MDSCs and TAMs through several mechanisms. One of the currently proposed mechanisms is the interaction between KYN and the ligand-activated transcription factor aryl hydrocarbon receptor (AHR), leading to the polarization of CD4+ T-cells into Tregs.[177–179] By activating AHR, KYN can also upregulate PD-1 expression in $CD8^+$ T cells, further enhancing tumour immune escape.[179,180] Other studies also showed that KYN-AhR activation promotes Tregs expansion by activating the forkhead box p3 (Foxp3) in naïve T-cells, preventing the maturation of Th17 cells.[181,182] Th17 are a subset of CD4+ T helper cells that generally stimulate immune responses by producing activating cytokines.[183] IDO1-induced Tregs appear to play an essential role in the recruitment and activation of suppressive MDSCs.[184] Additionally, TAMs also retain an immunosuppressive pro-tumoural function through the engagement of the AHR pathway in the presence of high IDO1 or TDO2 expression.[180] A recent study also highlighted an AHR-driven upregulation of the ectonucleotidase CD39 (an immune checkpoint mediator) in TAMs, which promoted T cell dysfunction.[185]

Regarding the immunomodulatory activity of other KP metabolites, 3-Hydroxyanthranilic acid (3-HAA) appears to have the highest immunomodulatory capacity on monocytic cells and lymphocytes through different mechanisms.[182] First, 3-HAA impairs NO synthesis in macrophages due to inhibition of nuclear factor-kappa B (NF-κB) and iNOS activity.[186,187] Furthermore, 3-HAA induces apoptosis in effector T cell populations and limits their antigen-dependent and

independent proliferation by reducing the number of T-cells entering the cell cycle.[188] 3-HAA also appears to specifically enhance the differentiation of Tregs.[189] Finally, 3-HAA, but also 3-hydroxykynurenine (3-HK) and quinolinic acid (QUIN), readily oxidise under physiological conditions to form immunomodulatory and neurotoxic peroxide and hydroxyl radicals.[190]

In conclusion, excessive KP activation promotes carcinogenesis and tumour cell growth by reducing T-cell proliferation, suppressing natural killer cells (NK), promoting Treg differentiation, and activating, recruiting, and expanding MDSCs and TAMs.[191,192]

The interest regarding KP inhibition is not limited only to cancer immunotherapy, as its role in psychiatric and neurodegenerative diseases is drawing increasing attention. Dysregulations in the KP were linked to neuropsychiatric disorders such as schizophrenia, depression, amyotrophic lateral sclerosis, and Huntington's, Alzheimer's and Parkinson's diseases.[193–196] Alterations in kynurenic acid (KYNA) and QUIN levels were characterised in several neuropathological states.[196,197] Indeed, KYNA has potent neuroprotective actions. It is an inhibitor of N-methyl-D-aspartate (NMDA), kainate, α-amino-3-hydroxy-5-methyl-4-isoxazolepropionic acid (AMPA), and α7 nicotinic acetylcholine receptors.[198] On the other hand, QUIN is an excitotoxin that selectively activates NMDA receptors and has a role in iron-dependent oxidative effects.[198,199]

KP enzyme kynurenine monooxygenase (KMO) is increasingly pointed as an attractive drug target for previously enumerated neurological diseases as it is located at a key KP branch point. Indeed, KMO inhibition is expected to increase concentrations of the neuroprotective KYNA while reducing QUIN.[200] Neuroprotective effects were observed even following administration of a non-BBB-penetrating inhibitor, which suggests that peripheral administration of KMO inhibitors could change the concentrations of KP metabolites within the central nervous system (CNS).[201,202]

While KMO is an emerging target in neurodegenerative diseases, the targeting of IDO1 and TDO2 to reverse tumour immune resistance remains the principal therapeutic interest of the KP. The subsequent chapters provide more details on these essential enzymes.

1.6. Overview of IDO1 and TDO2 structure and function

The proposed catalytic mechanism of IDO1 and TDO2 is illustrated below (**Figure 10**). In this mechanism, a ternary complex [Fe(II)-O_2-L-Trp] comprised of the ferrous enzyme, L-Trp and O_2, appears to be the starting point of the subsequent chemical steps. The reaction starts with a radical addition of the ferric heme iron-bound superoxide to the C2 of the Trp to generate an "alkylperoxo" intermediate. Then, this intermediate is homolytically cleaved to generate a ferryl and Trp-epoxide intermediate. Afterwards, the ammonium group of the Trp protonates this epoxide ring, which opens up, allowing the addition of the ferryl oxygen to C2 of the Trp to make the final product, NFK. This mechanism is supported by additional computational and experimental studies and is now widely accepted in the field.[203] A Criegee-type rearrangement involving electron transfer from the deprotonated L-Trp to the heme-bound O_2, followed by radical recombination to generate the 3-indolenylperoxy intermediate, has also been proposed by *Leeds et al.*[204] Nevertheless, none of the postulated intermediates, except for the dioxygen-bound intermediate, have been identified experimentally in either IDO1 or TDO2.[205]

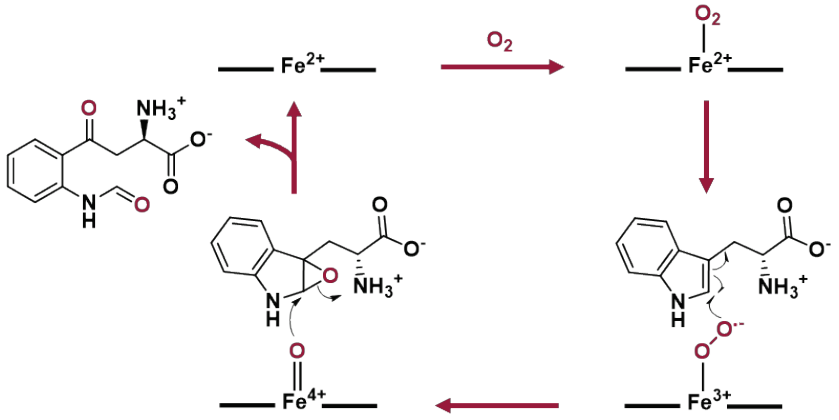

Figure 10. Ferryl-based mechanism of L-Trp dioxygenation reaction catalysed by IDO1 and TDO2. In this mechanism, molecular oxygen binds to the ferrous heme, forming a ferric heme bound to a superoxide. The superoxide radical attacks the C2-C3 double bond of L-Trp to form an alkylperoxo intermediate. Then, the O – O bond is cleaved to afford the epoxide intermediate and the ferryl. Finally, the ferryl attacks this epoxide, resulting in the formation of NFK and reduction of the ferryl back to its ferrous state.[206]

Even though they catalyse the same reaction and share a similar active site structure, IDO1 and TDO2 are two genetically unrelated and fundamentally different enzymes, sharing 10 % sequence identity. [205,207] IDO1 is a monomeric 45 kDa enzyme with a broader substrate specificity than TDO2, catalysing the cleavage of the pyrrole ring of not only L-Trp but also serotonin, melatonin, and other indoleamine derivatives.[208] IDO1 is expressed in various tissues, including lungs, small intestine, placenta and in some specific subsets of antigen-presenting cells.[209,210] Expression of IDO1 is inducible under inflammatory conditions by stimuli such as IFN-γ or following TLRs activation.[211,212] The activity of IDO1 is also regulated directly by substrate inhibition, following the binding of a Trp molecule inside an

inhibitory binding site on the proximal side of the heme.[213] IDO1 is by far the most studied enzyme of the KP due to its validated effects in the context of immune regulation. Already in 1998, *Munn et al.* demonstrated that IDO1 activity in mice placenta was essential to prevent foetus rejection by maternal T cells.[214] However, while the original postulate was that local L-Trp depletion was responsible for the foeto-maternal tolerance, years of research led to the understanding that this immune suppression was due to the production of KYN metabolites.[215–217] In 2003, *Uyttenhove et al.* showed that most human tumours constitutively expressed IDO1 and that the subsequent L-Trp degradation led to tumour immune resistance.[218]

As with IDO1, TDO2 is highly expressed in a range of human cancers. TDO2 is a homotetrameric 190 kDa enzyme that is highly specific for L-Tryptophan, its only substrate.[219] Crystal structures of human TDO2 in a ternary complex with L-Trp and O_2 and in a binary complex with the reaction product NFK were published in 2016 and provided a better understanding of binding modes and catalysis mechanism.[220] TDO2 has different tissue expression and expression patterns from IDO1: it is mainly expressed in the liver, where, among its physiological roles, it controls blood homeostasis of L-Trp. To a lesser extent, TDO2 is also expressed in the brain.[221] Numerous human tumours, including glioblastoma, melanoma and liver, bladder, pancreatic and colon carcinomas, express TDO2 at various levels to exploit the KP as an immune escape mechanism.[171,222] TDO2 inhibitors would be particularly relevant in hepatocarcinoma, 100 % of which express this enzyme.[171,223] Contrary

to IDO1, whose induction is cytokine-dependent, TDO2 expression is regulated hormonally (e.g. glucocorticoids, noradrenaline) at the transcriptional step.[224,225] Activity of TDO2 is regulated by controlling the lifespan of the protein. Indeed, TDO2 possess an Exo binding site for L-Trp, 42 Å away from the active site. L-Trp binding at this exo site does not affect enzyme catalysis but instead protects TDO2 from degradation through the ubiquitin-dependent proteasomal pathway (**Figure 11**).[220]

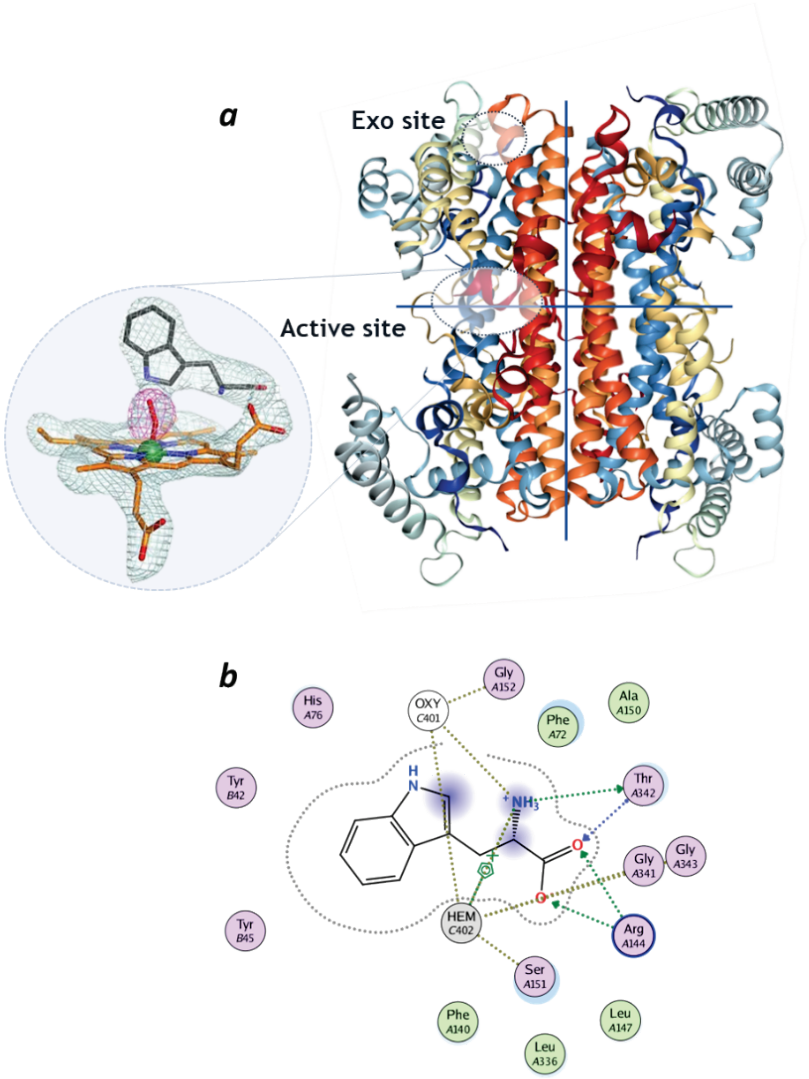

Figure 11. (**a**) Crystallographic structure of *h*TDO2 tetramer (PDB code: 5TIA) with indicated locations of the active site and exo site. The close-up view represents Omit Fo–Fc map (grey) for heme, L-Trp and O_2 (pink) adapted from *Lewis-Ballester et al.*[220] (**b**) Representation of interactions between L-Trp and the active site of hTDO2 (PDB code: 5TIA)

1.7. Targeting of IDO1 and TDO2 in cancer immunotherapy and beyond

1.7.1. Indoleamine 2,3-dioxygenase 1 (IDO1)

Findings regarding IDO1 ability to suppress the immune system were followed by a rapid clinical development of IDO1 inhibitors. After several preclinical studies demonstrated promising efficacy for combinations of IDO1 inhibitors and an anti-PD1 antibody, in which anti-tumour immunity was restored,[226,227] multiple companies rushed to invest in IDO1 inhibitors for application in various cancer types. Thereby, Incyte developed **epacadostat** (**INCB-24360**) from their previously discovered lead compound **5l**.[228,229] Together with Merck, they began testing the **epacadostat/ KEYTRUDA®** (**pembrolizumab**) combination.[230,231] Bristol-Myers Squibb acquired Flexus and began a trial of their own **OPDIVO®** (**nivolumab**) with **linrodostat** (**BMS-986205**).[232] NewLink Genetics' alliance with Genentech led to **navoximod** (developed based on the heme-binder **4-phenylimidazole** (**PIM**), **Figure 12**) and evaluated in combination with **TECENTRIQ®** (**atezolizumab**).[233,234] Finally, Pfizer's partnership with iTEOS led to the study of **PF-06840003** as a single agent therapy (**Figure 12**).[235]

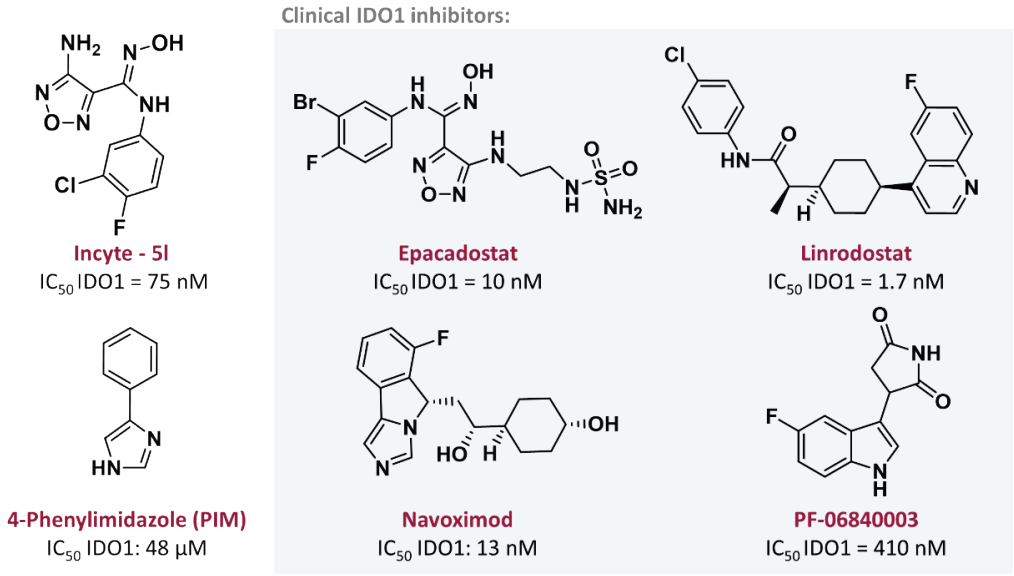

Figure 12. Enzymatic IC_{50}s and structures of IDO1 inhibitors **5I**[228], **PIM**[236] and clinical candidates **epacadostat**[237], **linrodostat**[238], **navoximod**[239] and **PF-06840003**[235].

After encouraging results of a phase I/II (ECHO-202/KEYNOTE-037) trial evaluating the **epacadostat/ KEYTRUDA®** combination on sixty-two patients with advanced solid tumours,[240] a large scale Phase III (ECHO-301/KEYNOTE-252) trial was initiated. This randomised trial included more than seven hundred patients with metastatic melanoma and failed to demonstrate a benefit from **epacadostat** addition.[241] Following these disappointing results, Incyte/Merck decided to put on hold or convert to Phase II their other ongoing Phase III trials. This announcement resulted in a severe drawback for the development of IDO1 inhibitors. Multiple reasons that could explain the negative outcome of the ECHO-301 trial were summarised in several review articles.[242,243] Some of the raised concerns are

mentioned hereafter. Firstly, IDO1 expression in tumours of enrolled patients was not assessed. This expression is adaptive in melanoma and especially important in inflamed tumours. As these tumours are already more responsive to the ICI, the potential benefit of IDO1 inhibition in such tumours would be less noticeable. Secondly, the dosage of **epacadostat** might have been insufficient to achieve complete inhibition of IDO1 activity. Finally, compensatory expression of enzymes such as TDO2 or IDO2 cannot be excluded but was not considered. Finally, anti-PD1 therapy might not have been the best combination choice.

Several clinical trials are still ongoing for most of the previously cited IDO1 inhibitors. Although murine models do not always transpose well in human evaluation, there is still an abundance of preclinical data supporting the interest for IDO1 inhibition and demonstrating the worsened prognosis of IDO1-expressing tumours.[184,218,244,245] For these reasons, IDO1 could remain a relevant target in the future, pending that we achieve the right approach to block it. As of today, **indoximod**, **epacadostat** and **linrodostat** remain under evaluation in several phases I and II studies in various combination therapies for cancer therapy.

Several recent publications use different delivery strategies to target IDO1 in cancer and autoimmune diseases with encouraging results. Treatment with attenuated Salmonella typhimurium delivering an shRNA plasmid targeting IDO1 (shIDO1-ST) markedly delays tumour growth in two immunocompetent colorectal mouse

models, and this appears to be a superior therapeutic strategy compared to **epacadostat** or blocking anti-PD1 antibody therapy in colon cancer.[246] The use of dual IDO1/TDO2 inhibitors might also improve the clinical response.[247] Some publications investigated the use of proteolysis-targeting chimaeras (PROTACs) strategy with **epacadostat**.[248]

Furthermore, the design of IDO1 inhibitors remains an active area of research, and several recent publications gave new insights that may help with the future design of inhibitors. In 2019, using a combination of X-ray co-crystallography, spectroscopic experiments, and in silico approaches, *Röhrig et al.* published a thorough characterisation of IDO1 inhibitors' binding mechanisms.[249] More recently, in 2021, a different crystallographic study performed by *Pham et al.* highlighted the unusual conformational plasticity of IDO1 involved in the substrate-ligand interaction.[203] These understandings may provide us with novel scaffolds able to demonstrate a superiority of action compared to the predecessors and a better modulation of the pathway.[250]

1.7.2. Tryptophan 2,3-dioxygenase (TDO2)

Interest in TDO2 inhibition was initially driven by depression therapy. The first series of selective inhibitors was developed in 1994 by *Salter et al.* (Wellcome Research Laboratories) as combined TDO/serotonin reuptake inhibitors.[251] This series included compound **680C91** (**Figure 13**). The importance of TDO2 activity in

the context of cancer immunotherapy was exposed almost two decades later when *Opitz et al.* showed that TDO2 expression by glial tumours promoted tumour cell survival and invasiveness while suppressing anti-tumour immune responses.[252] *Pilotte et al.* demonstrated in 2012 that around 35 % of human cancer cell lines express TDO2, making it a very attractive target in cancer immunotherapy.[171]

Our previous research eventually led to the identification of **LM10** (**Figure 13**), characterised by a trans-vinyl tetrazole side chain in the 3-position of a 6-fluoroindole scaffold and a low micromolar potency.[253] The administration of **LM10** restored the immune response and promoted tumour rejection in a mouse model. **LM10** was, to our knowledge, the very first soluble and bioavailable TDO2 inhibitor demonstrating preclinical anti-tumour efficacy and thus the proof-of-concept of TDO2 inhibition for anti-cancer immunotherapy.[171] Lately, inhibition of TDO2 was also demonstrated to be beneficial for the efficacy of immune checkpoint inhibitors like anti-PD1 and anti-CTLA4 monoclonal antibodies.[222] Interestingly, the benefit of TDO2 blockade persisted even in the absence of its tumoural expression, probably due to the increased availability of circulating L-Trp levels.[222]

In addition to TDO2 inhibitor research for cancer immunotherapy, TDO2 has attracted some interest due to its involvement in neurodegenerative diseases and is the subject of intensive research. Indeed, inhibition of TDO2 was showed to be

beneficial in several neurodegenerative disease models, such as Alzheimer's and Parkinson's.[254]

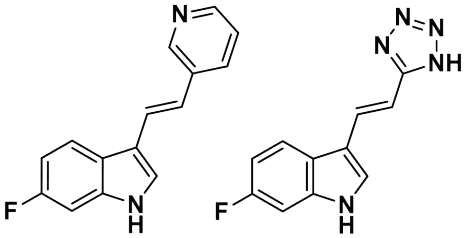

Figure 13. Structures and inhibition constants (Ki) and cellular IC_{50}s (P815B cells) of selective TDO2 inhibitors **680C91** and **LM10**.

Another *in vivo* study was published in 2020 using compound **PF06845102/EOS200809** (**Figure 14**) as a TDO2 selective inhibitor, which was more potent than previously described **680C91** and **LM10**, and more drug-like than the poorly soluble **680C91** that also had an issue regarding CYP inhibition.

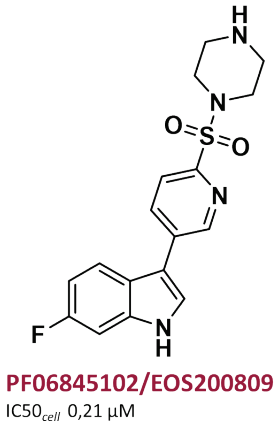

Figure 14. Structure of **PF06845102/EOS200809** and cellular IC_{50} in P815B cells.

Compound **PF06845102/EOS200809** was the first TDO2-selective inhibitor with a described pharmacokinetic/pharmacodynamic profile.[222] This characterisation allowed its preclinical evaluation *in vivo* in mouse tumour models and its potential subsequent clinical development. Using TDO2-expressing tumours cells, *Schramme et al*. demonstrated that TDO2 inhibitors could improve the efficacy of an immune checkpoint inhibitor.[222]

In the last few years, several companies began developing TDO2 inhibitors, and it remains an active area of research. However, no clinical trials are currently ongoing for a selective TDO2 inhibitor.

Existing IDO1 inhibitors disclosed in patent filings have already been summarised in 2013 by *Dolušić et al.* and in 2018 by *Cheong et al.* and *Xi Feng in 2020*,[255–257] however, no such review has been previously done for TDO2. Thus, existing applications of dual IDO1/TDO2 and TDO2-selective inhibitors, categorised by chemical structure, are summarised in this work, as well as relevant inhibitors described in peer-reviewed literature. When available, structure-activity relationships (SARs) are provided; however, it should be noted that many of the presented inhibitors were tested using cell-based assays and that biochemical inhibition data was not always reported. Furthermore, the frequently used Ehrlich assay, in which kynurenine is reacted with *p*-dimethylaminobenzaldehyde (DMAB) to form a Schiff base with an absorption maximum at 480 nm,[258] is known to give

promiscuous results due to potential cross-reactions with other compounds presenting chemical functionalities such as ketones, aldehydes, hydrazines, and indoles [259,260], thus also possibly reacting with other KYN metabolites. For these reasons, SARs are limited or could not be established for certain groups of compounds. Unless stated otherwise, the presented data is in humans.

1.7.3. TDO2 inhibitors: literature and patent activity

1.7.3.1. Phenylimidazoles analogues and other fused-ring derivatives

Several companies have developed IDO1 and TDO2 inhibitors using as a starting point **PIM** (IDO1 IC_{50}(enz): 48 μM) with a binding preference to the enzyme at its inactive ferric state. Following its identification in 1989 by *Sono et al*.,[236] the SARs of various PIM analogues have been extensively studied, leading to the discovery of new analogues selectively targeting IDO1 (**Figure 15**).[261] In 2016, IOmet patented a PIM-inspired series of 4-phenylisoxazol-5-amine and 5-phenylisoxazol-4-amine derivatives (**WO2016026772**, **Table 1**),[262] more selective towards TDO2. The majority of these compounds showed an IC_{50} below 3 μM in TDO2-expressing A172 glioblastoma cell lines. In 2018, *Pei et al.* published a series of aminoisoxazoles compounds as TDO2 inhibitors. [263] Starting from the 4-phenylisoxazol-5-amine (**2i**) scaffold, they investigated the replacement of the phenyl group. Their optimised compounds showed modest TDO2 selectivity over IDO1, ranging from 6- to 14-fold.

In 2012, the first set of tricyclic IDO1 inhibitors, containing the 4-phenylimidazole scaffold (or a derivative) was published by NewLink Genetics (**WO2012142237**).[264] This series included **navoximod** (**NLG919**) (**Figure 15**), a racemic compound licensed to Roche and used in several clinical trials as mentioned previously in this work. In 2014, claims concerning some of the isomeric imidazoindoles of this tricyclic series were expanded to inhibitors of both IDO1 and TDO2. In **WO2014159248**,[265] the most potent compound (**8i**), an imidazoisoindole derivative, had an IC_{50} of <1 μM on both enzymes. The replacement of the hydroxyl group by a ketone group resulted in a slight affinity loss for IDO1 (**9i**, IC_{50}: 1-10 μM) but did not affect TDO2 inhibition. Replacement of the 9*H*-imidazo[1,5-*a*]indole structure with an 8*H*-[1,2,3]triazolo[5,1-*a*]isoindole (**10i**) led to a decrease of potency on both enzymes. In **WO2016165613**,[266] the Hangzhou Innogate Pharma company proceeded to the replacement of the cyclohexane ring by several other aliphatic ring systems such as adamantane, adamantanols (e.g. **11i**: IC_{50} IDO1 < 100 nM, IC_{50} TDO2 < 200 nM), bicyclo[2,2,2]octane as well as N-substituted piperidines (e.g. **12i** IC_{50} IDO1 < 500 nM, IC_{50} TDO2 < 200 nM). Although, no precise enzymatic inhibition data is available in this application, there seems to be no gain in potency compared to **NLG919**, who is reported to have an enzymatic IC_{50} of 13 nM on IDO1 and 140 nM on TDO2.

Table 1. Representative compounds from WO2016026772. IDO1/TDO2 inhibitors based on the 4-phenylisoxazol-5-amine and 5-phenylisoxazol-4-amine scaffold. The compounds' number in the patent is indicated in parenthesis.

N°	Structure	Cellular pIC_{50}		Biochemical pIC_{50}	
		TDO2 (A172)	IDO1 (SKOV3)	TDO2	IDO1
1i *(1)*	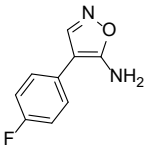	> 5.50	4.50 – 5.49	4.50 – 5.49	4.50 – 5.49
2i *(7)*	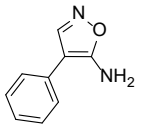	> 5.50	4.50 – 5.49	4.50 – 5.49	4.50 – 5.49
3i *(8)*	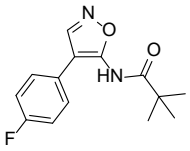	< 4.00	4.50 – 5.49	N.T.	N.T.
4i *(11)*	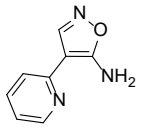	4.50 – 5.49	4.50 – 5.49	N.T.	N.T.
5i *(26)*	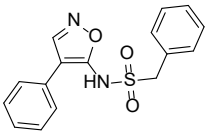	4.00 – 4.49	4.50 – 5.49	N.T.	N.T.
6i *(81)*	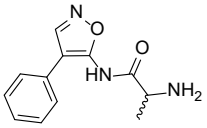	> 5.50	4.50 – 5.49	4.00 – 4.49	< 4.00
7i *(56)*	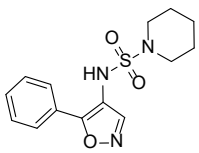	< 4.00	4.50 – 5.49	N.T.	N.T.

N.T. = not tested.

In 2016, Redx Pharma showed in their two applications (**WO2016051181**,[267] **WO2016059412**[268]) that replacing the 1-cyclohexylethan-1-ol moiety by an N-phenylamine or a phenylether (**WO2016051181**) led to enhanced TDO2 selectivity and inhibitory potency, with biochemical IC_{50}s as low as 12 nM (**13i**, **14i**) while keeping IDO1 inhibition in the low micromolar range (**Figure 15**). In **WO2016059412**, with their series of 6,7-heterocyclic fused 5H-pyrrolo[1,2-*c*]imidazole derivatives, Redx also showed that the replacement of the initial imidazo(iso)indole scaffold did not allow any gain in potency for TDO2. Their most potent compound (**15i**) had an IC_{50} of 101 nM for TDO2.

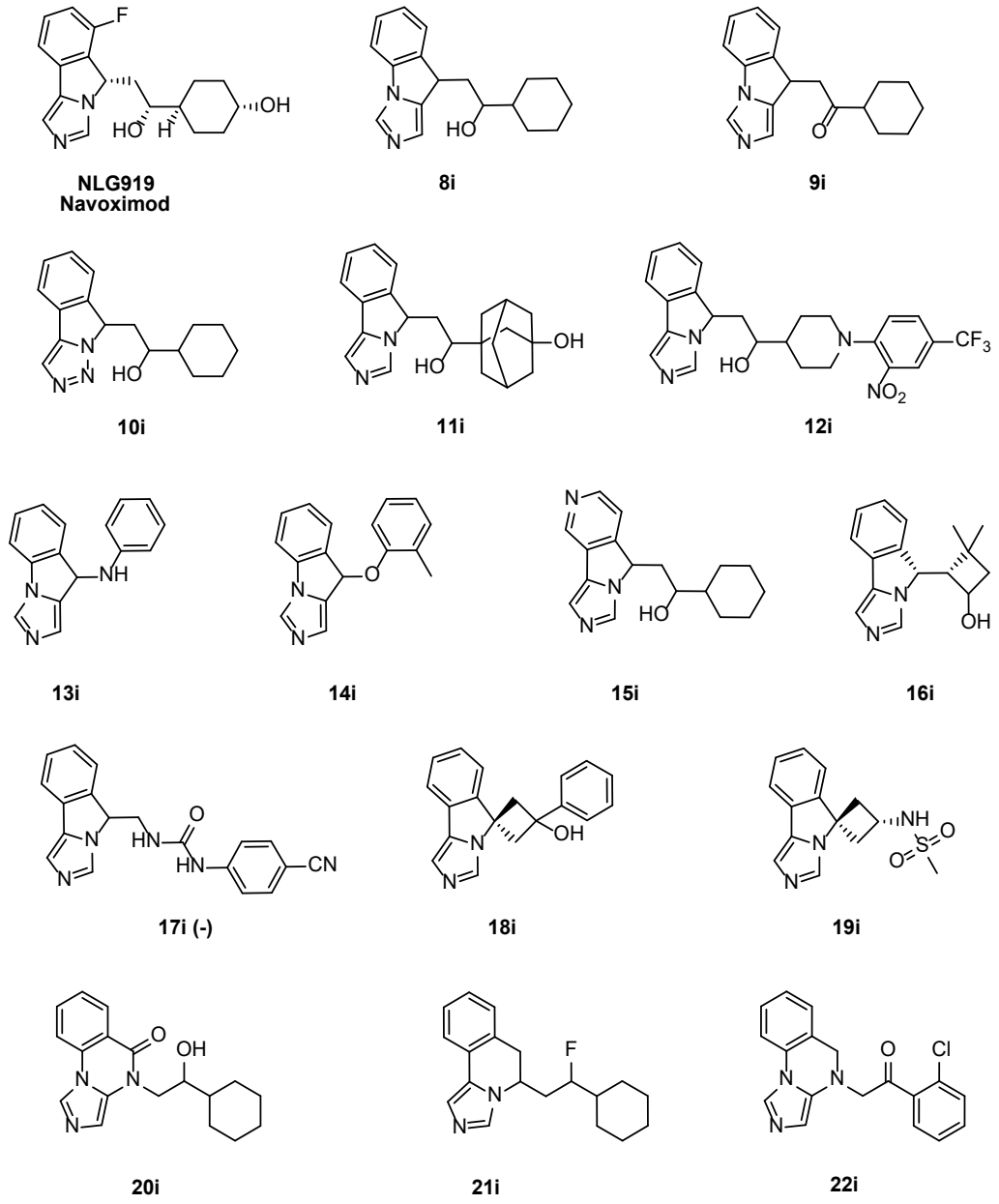

Figure 15. Fused-ring tricyclic derivatives of 4-phenylimidazole. The first series of which was published by NewLink Genetics.

In **WO2017107979**,[269] Genentech showed that integrating the hydroxyl from the initial ethan-1-ol moiety into a 4-, 5-, or 6- membered (hetero)cycle leads to a loss in potency for IDO1 (EC_{50} between 1 and >25 μM), but does not affect the affinity for TDO2, that remains in the low micromolar range. Their cellular EC_{50}s range between 0.016 μM (for compound **16i**) and >25 μM for the least potent compounds.

In **WO2016131381**,[270] Shanghai De Novo Pharmatech reported a series of fused-ring compounds based on the initial imidazoisoindole tricyclic scaffold but introducing a methylurea linker (**Figure 15**). Only one data is available for TDO2 in this application (levogyrous isomer of **17i**, **17i (-)**: IC_{50} < 0.5 μM). As for IDO1, the most potent compounds had an IC_{50} below 0.05 μM (**17i**: IC_{50} < 0.05 μM). Finally, in **WO2018082567**,[271] the Shanghai Institute of organic chemistry showed that a spiro cyclobutane linker (**18i**, **19i**) could result in a dual inhibition with biochemical IC_{50}s below 10 μM for both enzymes.

Both SciFluor Life Sciences Inc. and Emcure Pharmaceuticals Ltd. focused on evaluating the modification of the central ring of the imidazoisoindole. In their application (**US20170121325**)[272], SciFluor reported around 20 compounds with modified ring systems. Compared to the initial tricyclic scaffold, the modified analogues with a six-membered central ring did not show an increase in inhibitory potency (**21i**) (**Figure 15**). In **WO2017149469**,[273] Emcure disclosed a series of dual

IDO1/TDO2 inhibitors in which a cyclisation between the imidazole and the phenyl group was performed through an amide bond (**20i**). As compared to **NLG919**, this resulted in a loss of potency since these compounds were described with IC_{50}s in the low micromolar range (IC_{50} >10 μM). Their most potent TDO2 inhibitor (**22i**) is characterised by an enzymatic IC_{50} below 1 μM.

In 2020, *Parr et al.* (Genentech) optimised the tricyclic imidazoisoindole scaffold via structure-based drug design into TDO2-selective compounds.[274] These rigidified compounds were up to 85 fold more selective towards TDO2 and had cellular EC_{50}(TDO2) below 100 nM (**Figure 16**).

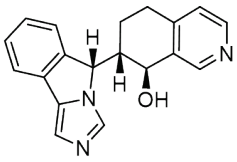

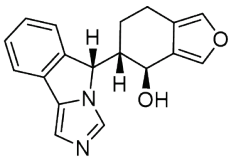

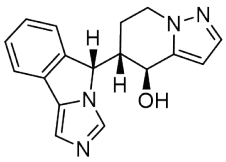

Entry[a]	**20**[a]	**29**[a]	**30**[a]
TDO2 EC_{50} (μM)	0.050	0.054	0.13
IDO1 EC_{50} (μM)	1.4	4.6	4.5

Figure 16. Compounds from *Parr et al.* that were advanced on to mouse in vivo studies.
[a]Entry numbers are from *Parr et al.* publication.[274]

1.7.3.2. Benzofuranes, benzothiophenes and their aza analogues (thieno[2,3-*c*]pyridines, furo[2,3-*c*]pyridines)

In 2014, Curadev Pharma published an application (**WO2014186035**)[275] reporting a series of benzofurans and benzothiophenes derivatives as IDO1 and/or TDO2 inhibitors (**Figure 17**).

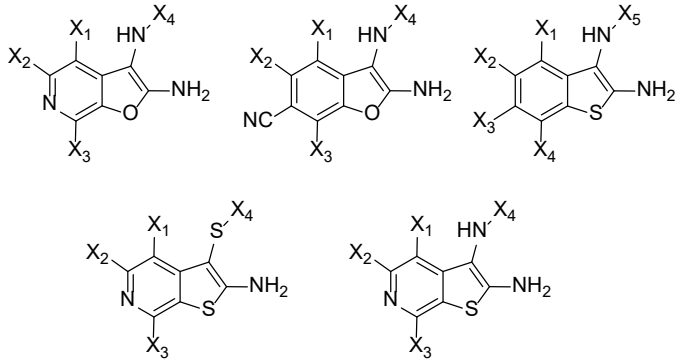

Figure 17. Pharmacophores of heterocyclic IDO1 and TDO2 inhibitors disclosed in WO2014186035 by Curadev Pharma.

All the compounds were tested in a cellular assay with *h*TDO2-transfected CHO-K1 cells. The most potent compounds demonstrated an IC_{50} below 500 nM on TDO2 and under 200 nM on IDO1 (**Table 2**). Compounds bearing an ortho-substituted phenyl ring were usually found to be less active than other analogues. Moreover, when the phenyl was para-substituted with larger groups such as phenyl or morpholine, a decrease in potency was noted.

Table 2. Heterocyclic IDO1/TDO2 inhibitors from WO2014186035. Compounds' number in patent is indicated in parenthesis.

N°	Structure	Cellular IC_{50} (nM)	
		TDO2 (CHO-K1)	IDO1 (HeLa)
23i *(3)*	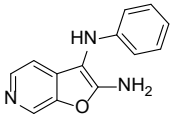	< 500	< 200
24i *(66)*	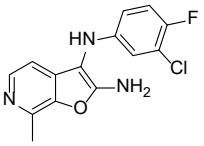	< 500	< 200
25i *(81)*	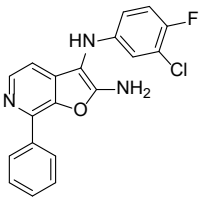	< 500	< 200
26i *(103)*	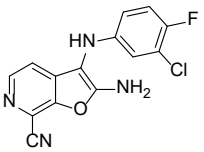	< 500	< 200
27i *(117)*	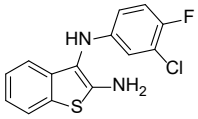	< 500	< 200

1.7.3.3. Indol-3-yl derivatives

Several companies have filed applications on various indol-3-yl-based compounds. This scaffold is present in the first ever-described TDO2 inhibitors, the fluoroindoles **680C91** and **LM10** (and analogues).

iTEOS therapeutics reported several series of compounds based on the indol-3-yl scaffold (**Figure 18**). In 2015, they published the first applications focused on targeting *h*TDO2 selectively.

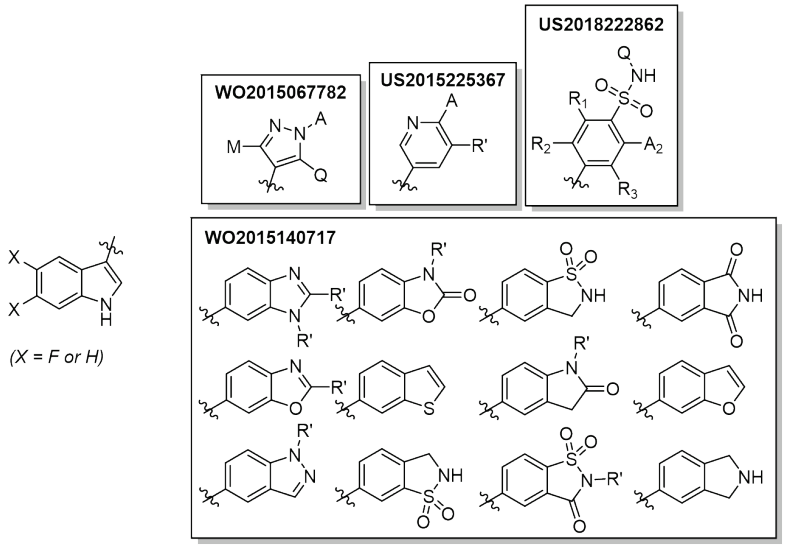

Figure 18. TDO2 inhibitors scaffolds patented by iTEOS in WO2015067782, US2015225367, US2018222862 and WO2015140717.

In **WO2015067782**[276] and **US2015225367**[277], they reported two series, each comprising around 100 compounds based on 4-(indol-3-yl)-pyrazole (**Table 3**) and 3-(indol-3-yl)-pyridine scaffold (**Table 4**). The 4-(indol-3-yl)-pyrazoles (113

compounds) show enzymatic IC_{50}s in the low micromolar range, usually between 1 and 10 μM, while 18 of them are reported as having an IC_{50} below 1 μM. The 3-(indol-3-yl)-pyridines have a similar affinity, with IC_{50}s ranging between 0.29 μM and 39000 μM.

Table 3. Representative compounds from WO2015067782, published by iTEOS. Compounds' number in the patent is indicated in parenthesis.

N°	Structure	IC_{50} (μM)	
		Enzyme	Cell (P815)
28i *(2)*	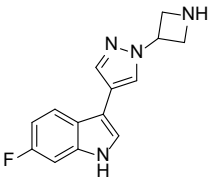	< 1	< 1
29i *(7)*	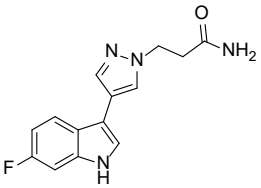	< 1	< 1
30i *(16)*	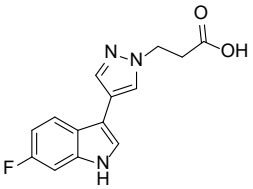	1 – 10	N.T.
31i *(33)*	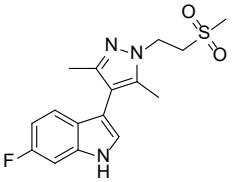	10 – 100	N.T.
32i *(55)*	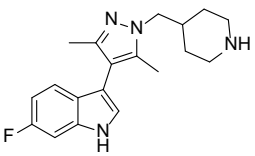	< 1	N.T.

33i *(56)*	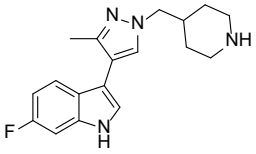	10 – 100	N.T.
34i *(70)*	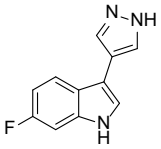	< 1	< 1
35i *(112)*	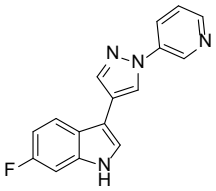	< 1	< 1

N.T. = not tested.

Table 4. Representative compounds from WO2015067782, published by iTEOS. Compounds' number in patent is indicated in parenthesis.

N°	Structure	IC_{50} (nM)	
		Enzyme	Cell (A172)
36i *(1)*	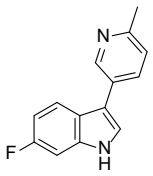	370	180
37i *(4)*	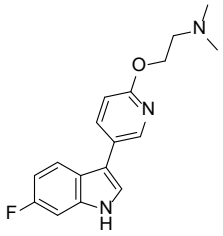	39000	680
38i *(9)*	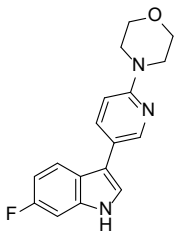	540	210
39i *(14)*	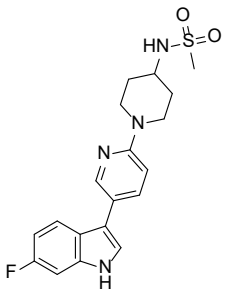	970	610
40i *(27)*	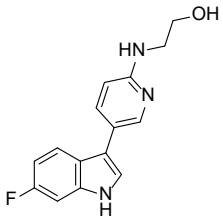	490	190

41i *(49)*	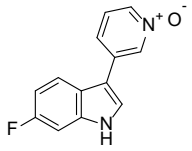	11000	N.T.
42i *(78)*	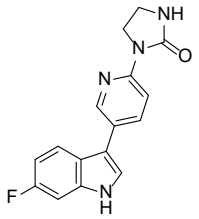	16000	N.T.

N.T. = not tested.

In **WO2015140717**,[278] iTEOS reported another series of 3-indol substituted derivatives containing benzene-fused heterocycles (such as benzimidazoles or benzisoxazoles) as shown in **Table 5**, with enzymatic IC_{50} ranging on average in the low micromolar range as the previous two series of compounds. They later published **US2018222862**,[279] another TDO2 targeted patent, describing a series of 3-indol substituted compounds bearing a phenylsulfonamide moiety, with enzymatic activities (IC_{50}) between 120 nM (**47i**, **48i**) and 4700 nM (**Figure 19**).

Table 5. 3-indole substituted derivatives from WO2015140717 (iTEOS). In the enzymatic assay, compound 25 was the most potent compound of the series. The highest enzymatic IC_{50} was measured for compound 7. Compounds' number in the patent is indicated in parenthesis.

N°	Structure	IC_{50} (nM)		
			Cell	
		Enzyme	P815	A172
43i *(65)*	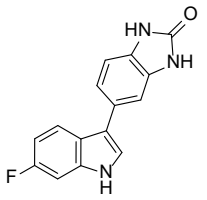	N.T.	109	335
44i *(7)*	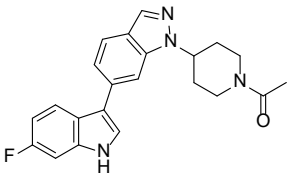	13770	N.T.	N.T.
45i *(10)*	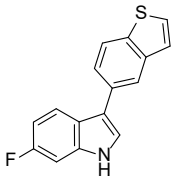	N.T.	N.T.	442
46i *(20)*	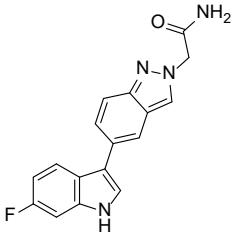	421	N.T.	169

N.T. = not tested.

The Netherlands Translational Research Center published in **WO2018011227,**[280] a series of substituted 3-phenyl-1H-indole derivatives as selective TDO2 inhibitors. The measured IC_{50} values of these compounds were all found to be below 5 μM in the biochemical assay, but most compounds had a measured IC_{50} of < 1 μM (e.g. **52i**, **53i**, and **54i**) (**Figure 19**). In the cellular assay, all the IC_{50} were between 200 nM and 2 μM.

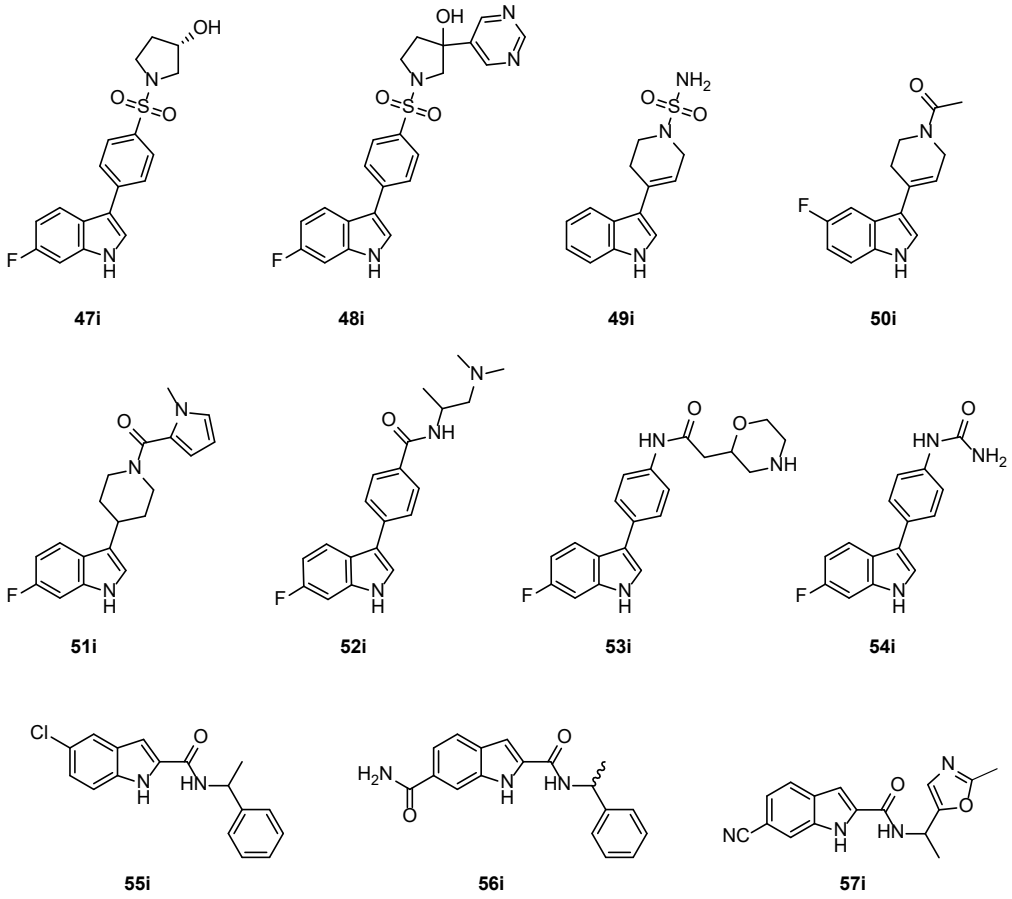

Figure 19. Inhibitors based on an indole-based pharmacophore, representative of publications from iTEOS (US2018222862), IOmet (WO2015082499 and WO2015150097) and the Netherlands Translational Research Center (WO2018011227).

In the same year as the first iTEOS' patents, IOmet published **WO2015082499,**[281] disclosing a series of 4-(indol-3-yl)-3,6-dihydro-2H-pyridines as potential IDO1 and TDO2 inhibitors (**Figure 19**). 319 compounds were exemplified, among these; most of them are inhibitors of TDO2 in the low micromolar range (e.g. **49i**, **50i**) while only

one of them has shown an inhibitory potency below 100 μM on IDO1 in a biochemical assay (**51i**, pIC_{50} IDO1: 4 – 4.99 TDO: <4.00). Using the cell-based assay for detection of kynurenine with Ehrlich's reagent, the best compounds had an IC_{50} below the micromolar for TDO2 (on glioblastoma A172 cells) (e.g. **55i**, **56i** and **57i**) and between 1 and 10 μM for IDO1 (ovarian carcinoma SKOV3 cells). In the same year, they reported in **WO2015150097**[282] a series of 275 indole-2-carboxamides. These compounds were tested using the same cell types and cell-based assay. No biochemical results were reported. These compounds inhibited IDO1 more potently than TDO2 in the cell-based assay. Indeed, 57 % of the reported molecules had a measured pIC_{50} above 5.50 for IDO1, while only 9 (e.g. **55i**, **56i** and **57i**) compounds were reported as having this potency on TDO2.

1.7.3.4. Isoquinoline derivatives

In **WO2016071283,**[283] IOmet/Merck reported 58 compounds with an isoquinoline or tetrahydroisoquinoline as a core structure with inhibitory potency similar to their previous publications. **61i** and **62i** showed a promising dual inhibition in the cellular assay compounds, with IC_{50} of below 3 μM on both enzymes (**Table 6**). Most substitutions are in position 5. Several analogues were synthesised with an 8-substitution, but their inhibitory potency was below their 5-substituted analogues. There is biochemical data for 11 compounds. Among them, compound **6i** had the best results, with < 3 μM IC_{50} on both enzymes; however, it did not perform well in the cellular assay with IC_{50} on TDO2 between 30 and 100 μM.

Table 6. Representative N-(isoquinolin-5-yl)sulfonamides and an N-(tetrahydroisoquinolin-5-yl)sulfonamide (**65i**) published by IOmet Pharma in WO2016071283. Compounds' number in the patent is indicated in parenthesis.

N°	Structure	Cellular pIC_{50}	
		TDO2 (A172)	IDO1 (SKOV3)
60i *(9)*	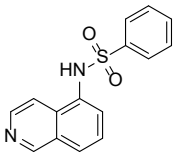	≥ 5.50	4.50 – 5.49
61i *(14)*	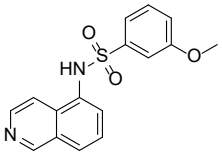	≥ 5.50	4.50 – 5.49
62i *(18)*	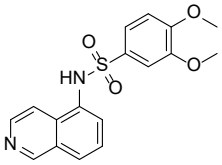	< 4.00	4.00 – 4.49
63i *(19)*	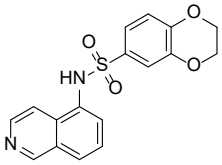	≥ 5.50	≥ 5.50
64i *(20)*	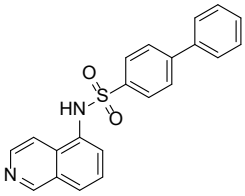	≥ 5.50	≥ 5.50
65i *(50)*	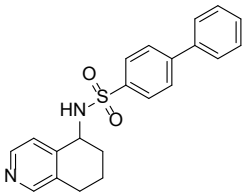	< 4.00	≥ 5.50

1.7.3.5. Imidazopyridines

BeiGene published **US20180072716**[284] in early 2018, reporting 5 or 8-substituted imidazo[1, 5-a]pyridines derivatives as inhibitors of IDO1 and/or TDO2 (**Table 7**). Around 150 compounds are exemplified. The most promising compounds show potency in the low nanomolar range for both enzymes; some of the compounds are more selective towards IDO1. The binding of one of the analogues (**66i**), which is the most promising dual inhibitor of this series with IC_{50} of 9.6 nM on IDO1 and 29 nM on TDO2, was confirmed by co-crystallisation with IDO1. The compound was shown to bind in the active site. The imidazole part interacts with the iron atom of the heme, while the hydroxyl interacts with heme propionate.

Compounds substituted in position 7 of the imidazo[1, 5-a]pyridine seem to have an increased affinity for TDO2 ($Cl > Br > CF_3$), while a substituent bigger than fluorine in position 6, leads to a lower TDO2 affinity. A cyclopentane instead of cyclohexane seems to favour the inhibitory activity on TDO2, while not changing the inhibition of IDO1. As for dual inhibition, compounds having chlorine in position 7 present the best dual profile. The stereochemistry of the chiral centre seems important; S conformation is more potent than R for both enzymes.

Table 7. Imidazopyridines from US20180072716, published by BeiGene. Compounds' number in the patent is indicated in parenthesis.

N°	Structure	Cellular IC_{50} (nM)	
		TDO2	IDO1
66i *(A101a)*	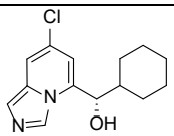	29	9.6
67i *(A101)*	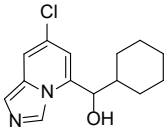	68	29
68i *(A116)*	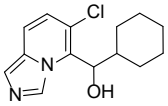	270	7.5
69i *(A118)*	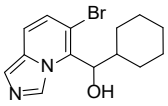	5700	15
70i *(A103)*	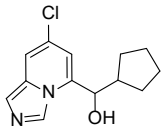	22	22
71i *(A148)*	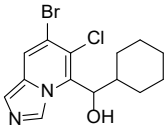	420	39
72i *(A149)*	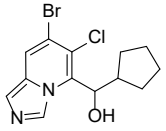	160	35
73i *(A150)*	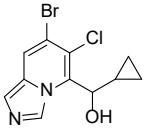	200	130

1.7.3.6. Isoxazolopyridines

In **WO2016024233**[285] and **WO2017034420**[286], Auckland Uniservices Ltd. disclosed around a hundred and twenty compounds with [1,2]-oxazolo[5,4-*b*]pyridine (isoxazolo[5,4-*b*]pyridin-3-amine) as a core scaffold. Their application is focused on IDO1 inhibition, though data regarding TDO2 inhibition is available for five compounds (**Table 8**).

Table 8. Compounds for which data regarding TDO2 inhibition are reported. **74i**, **75i**, **76i**, and **77i** are from WO2016024233, **78i** and **79i** are from WO2017034420. Compounds' number in the patent is indicated in parenthesis.

N°	Structure	Cellular IC_{50} (μM)	
		TDO2	IDO1
74i *(3)*	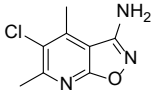	10 – 100	< 1
75i *(11)*	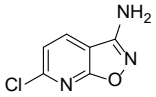	< 1	< 1
76i *(66)*	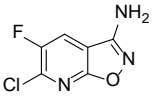	< 1	< 1
77i *(89)*	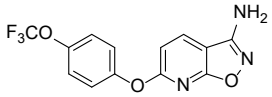	10 – 100	10 – 100
78i *(4)*	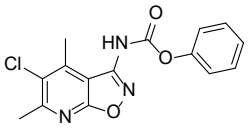	10 – 100	< 1
79i *(15)*	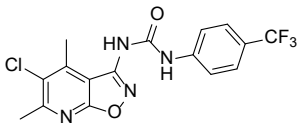	10 – 100	10 – 100

1.7.3.7. Tryptanthrin derivatives

Derivatives of the tryptanthrin alkaloid were initially reported as IDO1 inhibitors in 2013, before being published as dual acting compounds in 2018.[287–290] Starting from the initial scaffold **80i** (**Table 9**), variously substituted analogues were reported (i.e. **81i**, **82i**).[288,289,291] These series demonstrated an uncompetitive or mixed-uncompetitive mode of inhibition, enzymatic IC_{50} below the micromolar. According to the predicted binding modes, the oxygen atom of the five-membered ring coordinates the heme iron, while the rest of the compound interacts with hydrophobic residues of the active site.[288]

Table 9. Representative tryptanthrin and 1-phenyl-1*H*-naphtho[2,3-*d*][1,2,3]triazole-4,9-dione derivatives. IC_{50}(cell) of compounds **80i** and **81i** were evaluated in HEK293 cells.[287,288] IC_{50}(cell) of compound **82i** was evaluated in HeLa cells.[291]

N°	Structure	IC_{50}(enz) (μM)		IC_{50}(cell) (μM)	
		TDO2	IDO1	TDO2	IDO1
80i	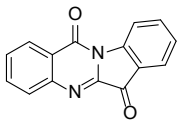	3.94	7.15	0.140	0.054
81i	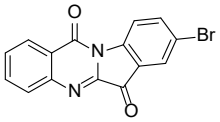	0.937	0.574	0.053	0.054
82i	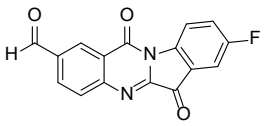	0.06	0.46	N.T.	0.16

1.7.4. Overview regarding TDO2 inhibition

The search for TDO2 inhibitors expanded very quickly in the last few years, after the demonstrations regarding the benefit of TDO2 inhibition to reverse tumoural immune resistance.[171] Additionally, encouraging early clinical outcomes for IDO1 inhibitors further contributed to an eager development of IDO1 and TDO2 inhibitors. In 2014, it led NewLink Genetics to publish the first application focusing on both IDO1 and TDO2 inhibition, in which they expanded their claims regarding their fused tricyclic imidazoisoindoles derivatives to include TDO2 as its other target. Afterwards, new programs were quickly launched by numerous pharmaceutical companies, resulting in the discovery of the following chemical classes of TDO2 inhibitors: I) Phenylimidazole analogues and its fused-ring derivatives II) Benzofuranes, benzothiophenes and their aza analogues (thieno[2,3-*c*]pyridines, furo[2,3-*c*]pyridines) III) Indol-3-yl derivatives IV) Isoquinolines V) Imidazopyridines, VI) Isoxazolopyridines and VII) Tryptanthrin derivatives. Among these categories, the indol-3-yl derivatives were the only ones to exhibit inhibition exclusively on TDO2 and to be patented as selective TDO2 inhibitors. However, despite their selectivity, these molecules were often found to be of lower affinity, with IC_{50}s usually fell in the high-nanomolar/low-micromolar range. Conclusively, existing TDO2 inhibitors remain of limited structural diversity.

The development of potent TDO2 inhibitors may, however, turn out to be challenging. Indeed, the active site of TDO2 in the neighbourhood of the heme

prosthetic group is characterised by its lipophilicity and its relatively small size, which might restraint the chemical diversity of substituents, as shown by *Dolušić et al*.[292]

Finally, the vast majority of TDO2 inhibitors are little documented and concentrated in patents, with often unavailable enzymatic inhibition values and chemical modulations that would allow the obtention of SARs. Though, the design of future potent TDO2 inhibitors would undeniably benefit from such data.

2. OBJECTIVES AND STRATEGY

The main objective of this thesis is the discovery of new TDO2-selective or IDO1/TDO2 dual-acting inhibitory scaffolds.

As previously stated, there are few SARs data studies performed on series of TDO2 inhibitors, resulting in a poor understanding of what affects TDO2 affinity and binding.

As a starting point for the rational part of this work, we used the structures **680C91**, **LM10** and the previously established SARs for 3-(2-(pyridyl)ethenyl)indole scaffold (**Figure 20**).[253] In these previously obtained results, the inhibitory potency could not be much improved to reach a cellular efficacy below the μM threshold. Furthermore, a replacement for the electrophilic vinyl linker could not be found. This moiety is prone to chemical instability (trans-cis isomerization) and could potentially result in side reactions (Michael acceptor) and metabolic liabilities.[253] To summarise, all investigated replacements of indole moiety led to inactive compounds, even when changes were minor (5-azaindole or indazole). Moreover, the nitrogen of the indole group should remain free, and only the substitution in C5 or C6 with small lipophilic substituents such as fluorine led to increased potency. As suggested by molecular docking, the 3-pyridyl group of **680C91** is located in the vicinity of Arg144 guanidinium. Coherently, the replacement of this 3-pyridyl with H-bond acceptors or negatively charged groups provided more soluble compounds

that could be further stabilised in the TDO2 binding cleft through ionic interactions.[253] Replacement of the trans-vinyl linker to longer, shorter, or a more flexible ethyl spacer resulted in inactive or poorly active derivatives. Thus, it appeared that TDO2 was particularly susceptible to minor modifications of the inhibitor. Recent crystallographic studies revealed that the active site of *h*TDO2 was, in fact, more rigid than that of *h*IDO1, which has a broader substrate specificity.[203]

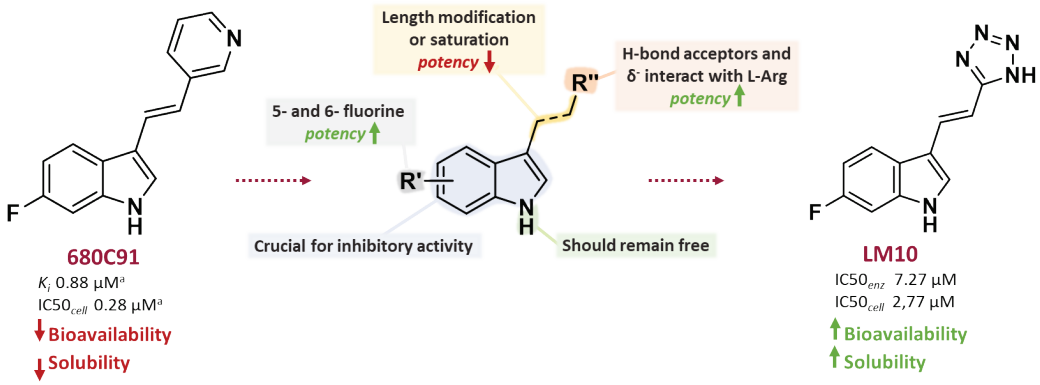

Figure 20. Structure-activity relationship data previously obtained by *Dolušić et al*. starting from **680C91** and leading to the optimised compound **LM10**.

In the present work, to optimise the previous series and further expand SARs data for TDO2 and provide a better molecular framework for TDO2 inhibitors, we designed a fused-cycle scaffold that would theoretically result in compounds with enhanced stability.

We reasoned that the rigidification of the lateral *trans*-vinyl present in the **680C91** and **LM10** scaffolds could improve the TDO2 inhibitory potency by conformational restriction and provide a molecular template devoid of chemical liabilities (**Figure 21**). Moreover, several fused-cycle scaffolds were previously reported in a patent regarding TDO2 inhibitors, suggesting that such rigidification could lead to potent TDO2 inhibitors.[278] This strategy would result in the synthesis of the benzotriazole moiety depicted in **Figure** (**Figure 21.1**). Following this cyclization, our optimization included benzotriazole substitutions with various side chains to probe TDO2 active-site while considering the potency and physicochemical characteristics of the studied compounds. Next, we further modulated the benzotriazole ring by (1) replacement with a triazolo-pyridine scaffold and (2) substitution on the 6-membered ring of the benzotriazole. This work constitutes the **2nd chapter** of this thesis.

Finally, we decided to further study this scaffold by replacing the benzotriazole central nitrogen with elements from the chalcogen periodic table group and

studying their bioisostery regarding target affinity, cellular toxicity and metabolic stability. (**Figure 21.2**). This work constitutes the **3rd chapter** of this thesis.

The evaluation of the potential TDO2 inhibitors required the production of human TDO2 and the setup of an enzymatic assay. These data are described in the first and following chapter.

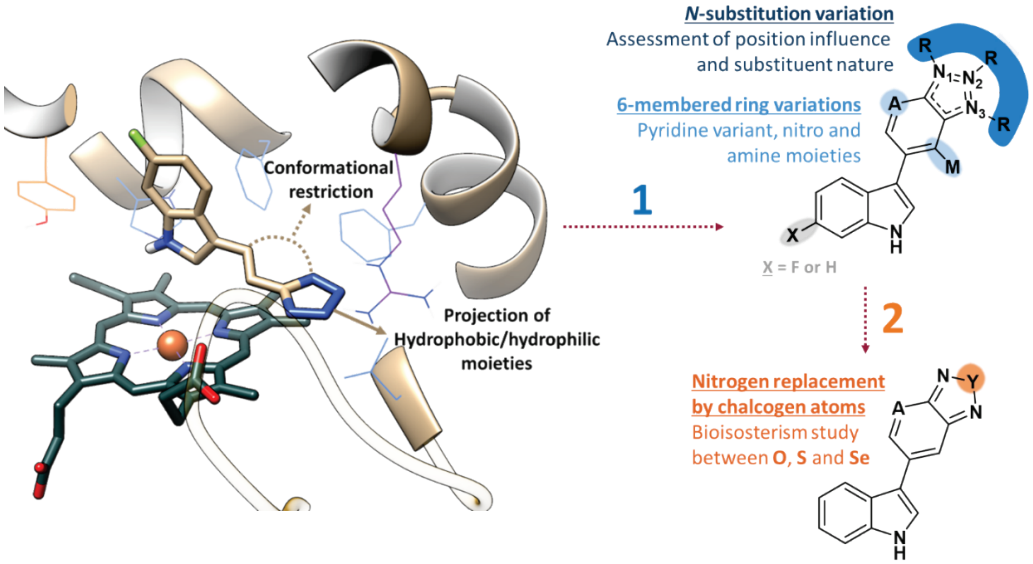

Figure 21. Molecular modelling of **LM10** inside *h*TDO2 active site (PDB code 5TI9) and the two rational design strategies explored during this PhD thesis.

3. CHAPTER 1: ENZYME PRODUCTION, PURIFICATION AND ENZYMATIC ASSAY SETUP

In the early beginning of this project, full-length (His-tag) recombinant *h*TDO2 (*h*TDO2fl) was purified and initially used for evaluation. Unfortunately, several drawbacks prevented its use during the whole duration of the project. Firstly, the purification yield was relatively modest at around 3 mg/litre of culture. Common issues described regarding *h*TDO2fl production include a high tendency to aggregate in free solution and form inclusion bodies when expressed in Escherichia coli.[205] Moreover, purified *h*TDO2fl displayed poor stability after storage due to a loss of activity over freezing. Indeed, thawed aliquots of *h*TDO2fl did not present a thermal unfolding profile in Nanoscale Differential Scanning Fluorimetry (NanoDSF), suggesting that the enzyme was not correctly folded. NanoDSF is a fluorescence-based assay used to characterise protein thermal stability and folding integrity.[293] NanoDSF measures the changes in protein intrinsic fluorescence intensity ratio (350:330 nm) as a function of temperature. The resulting thermogram is a plot of the intrinsic fluorescence intensity ratio or its first derivative as a function of temperature. Ultimately, NanoDSF allows the obtention of the unfolding temperature of the tested protein in given conditions.[293] Finally, full-length *h*TDO2 purity was insufficient for the envisioned biophysical experiments and evaluation (~70%) (**Figure 22a**).

To palliate the issues mentioned above, a truncated version of *h*TDO2 (*h*TDO2tr) was produced and used for all assays and evaluations of the work presented herein. The sequence of *h*TDO2tr corresponds to *h*TDO2fl truncated for residues 1–17 and 389–406. This sequence was first described by *Batabyal and Yeh*[205] and corresponds to a deletion of residues that are not present in bacterial TDOs indicating that they are not critical for the structure and function of *h*TDO2.

A pET-28 vector coding *h*TDO2tr was designed and transferred into the *E. coli* strain BL21 (DE3) (Rosetta). The expression of *h*TDO2tr was induced by isopropyl 1-thio β galacto-pyranoside (IPTG) and cultured with a final hemin concentration of 10 µM to ensure complete heme integration, as previously suggested in the literature.[205] Protein purification carried out using immobilised metal affinity chromatography (IMAC) to yield a highly pure (**Figure 22b**) and enzymatically active *h*TDO2tr, with a high yield of 60 mg per litre of culture. The obtained enzyme was catalytically active, presented a similar Km that the reported Km of the full-length version. Furthermore, it presented a sharp transition in nanoDSF, indicating the high homogeneity of the sample (**Figure 22c**).

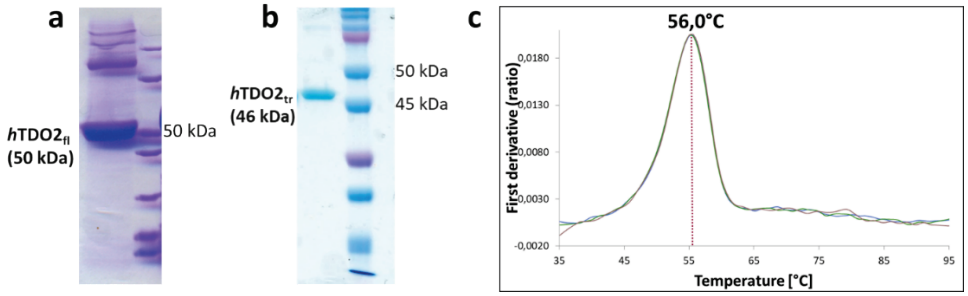

Figure 22. (a) Sodium dodecyl sulfate polyacrylamide gel electrophoresis (SDS-PAGE) of purified hTDO2fl (right) with molecular weight standard (left) (b) SDS-PAGE of purified hTDO2tr (right) with molecular weight standard (left). (c) Nano Differential Scanning Fluorimetry (nanoDSF) showing a melting temperature of 56.0 °C for the produced *h*TDO2tr.

Concerning IDO1, we relied on a batch of enzyme kindly provided by the Ludwig Institute for Cancer Research (LICR).

Regarding the enzymatic evaluation, we optimised and applied the most commonly described assay for IDO1 and TDO2 activity. This assay follows the formation of the enzymatic product NFK after hydrolysis with trichloroacetic acid (TCA) into KYN and reaction with DMAB (**Figure 23**) to provide a Schiff base that we monitor by measuring the absorbance at 490 nm.[259,294]

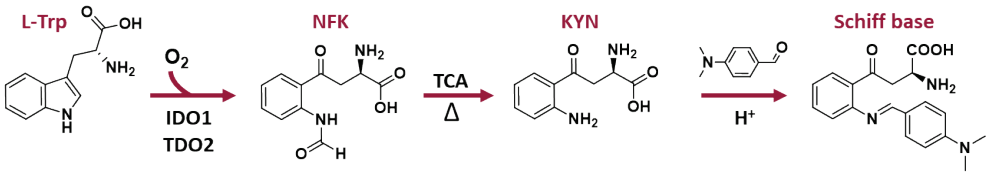

Figure 23. Principle of the enzymatic assay used for compound evaluation.

The recommended concentrations of components were used as a base for the optimization of the incubation medium.[259] The fine-tuning of these conditions included the assessment of sensitivity to the presence of co-solvents that were essential for solubilising lipophilic scaffolds. Initially, we evaluated the effect of dimethylsulfoxide (DMSO). We noted that while *h*IDO1 activity was not influenced by the presence of DMSO up to 5 %, *h*TDO2tr demonstrated a dose-dependent sensitivity (**Figure 24a**). However, in nanoDSF, the addition of DMSO showed a decrease in *h*TDO2tr melting temperature without impacting the overall profile of denaturation (**Figure 24c**). These similar profiles suggested that when needed, the use of DMSO could be considered. Nonetheless, we decided to test other potential co-solvents and showed that the use of ethanol and methanol could be tolerated at 5 % (**Figure 24b**).

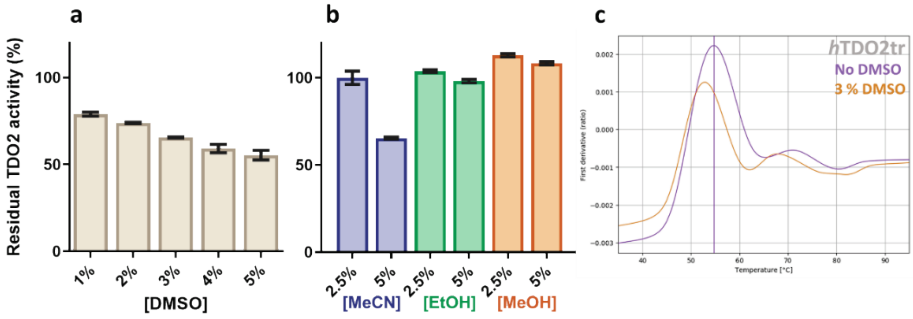

Figure 24. Solvent tolerance for *h*TDO2tr. (**a**) DMSO has a concentration dependent influence on *h*TDO2tr catalytic activity in the spectrophotometric assay. (**b**) Ethanol and methanol did not impact the activity of *h*TDO2tr. Acetonitrile was deleterious at 5%. (**c**) The addition of DMSO has a slight impact on stability in nanoDSF but does not seem to disturb the proper folding.

Next, we set out to measure the Km of the enzymes (**Figure 25**) to identify the optimal L-Trp concentrations for the evaluation of competitive inhibitors. The Km values were close to the ones previously reported in the literature, with ~47 μM for *h*IDO1 and ~105 μM for *h*TDO2tr.

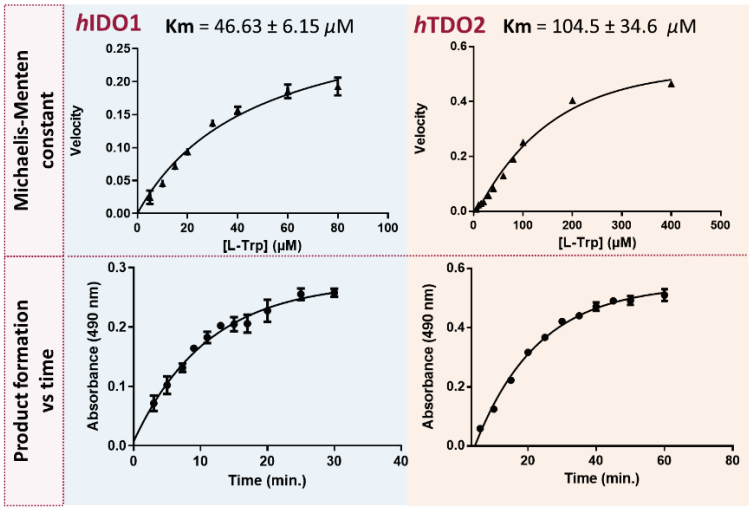

Figure 25. Above: Km determination for *h*IDO1 and *h*TDO2tr. Below: Product formation vs time graphs for *h*IDO1 and *h*TDO2tr.

Finally, we evaluated the optimum time of incubation before quenching the reaction with TCA. To achieve maximal sensitivity, we selected an early time of incubation to allow for a linear relationship between time and product formation. Final conditions are summarised in **Table 10**. These optimised conditions were used to evaluate the compounds described in the following chapters. For more clarity, hTDO2tr is referred to as hTDO2 in the rest of this work.

Table 10. Final conditions of the spectrophotometric assay for *h*IDO1 and *h*TDO2tr.

Variable	*h*IDO1	*h*TDO2
IDO1/TDO2	~30 nM	~80 nM
L-Tryptophan	60 μM	100 μM
Sodium L-ascorbate	20 mM	
Methylene blue	10 μM	
Catalase	~200 nM	
Buffer	KH_2PO_4/K_2HPO_4 100 mM, pH 6.5	
Detergent	Triton X-100 0.01 %	
Duration	8 min.	18 min.

4. CHAPTER 2: RATIONAL DESIGN OF ORIGINAL FUSED-CYCLE SELECTIVE INHIBITORS OF TDO2

This chapter is based on the following manuscript: Kozlova, A.; Thabault, L.; Liberelle, M.; Klaessens, S.; Prévost, J.R.C.; Pilotte, L.; Stroobant, V.; Van den Eynde, B.; Frédérick, R. Rational Design of Original Fused-cycle Selective Inhibitors of Tryptophan 2,3-Dioxygenase, 2021. DOI: 10.1021/acs.jmedchem.1c00323

4.1. Design of TDO2 Inhibitors

To investigate our rigidification hypothesis, we synthesised several fused-cycle analogues of **680C91** and **LM10** (**1 - 6**, **Table 11**). As indicated by our previous results, fluorine substitution in the 6-position of the indole usually leads to a slight increase in TDO2 inhibitory potency.[292] However, we first decided to avoid 6-fluorine derivatives as their synthesis resulted, in our experience, to lower yields compared to their non-fluorinated counterparts. Evaluation of these compounds in enzyme and cell-based assays on IDO1 and TDO2 demonstrated their ability to selectively inhibit TDO2. Interestingly, inhibition data on isolated enzyme assay often lacks for reported TDO2 inhibitors. Indeed, several reported series of TDO2 inhibitors were characterised only by cell-based inhibition assays, limiting the SARs understanding and hence the future development of inhibitors.[274,295] We used the most commonly described assay for IDO1/TDO2 activity which follows the formation of the enzymatic product NFK after hydrolysis with trichloroacetic acid and reaction with DMAB.[259,294] Regarding cell-based evaluation, we used a

previously described assay using *h*TDO2-expressing P815B murine mastocytoma cell line.[171]

Compounds **1** to **6** all exhibited low μM range enzymatic IC_{50}s and mid-nanomolar (nM) to low μM activities in cells. Interestingly, these compounds also presented very low cellular toxicity, as assessed by our MTS assay (**Table 11**).

Table 11. 680C91, **LM10** and their fused-cycle analogues (**1** – **6**) with their inhibition data.

	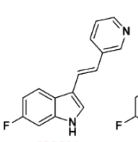 680C91	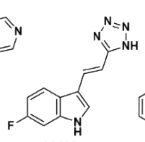 LM10	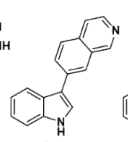 1	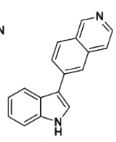 2	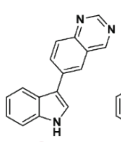 3	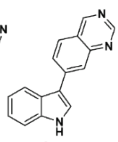 4	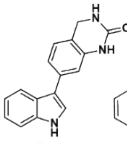 5	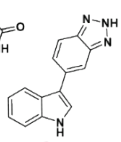 6
*h*TDO2 **IC50**$_{enz}$[a] (μM) **IC50**$_{cell}$[a]	Ki 0.88[d] 0.28[d]	[6.1 – 8.7] [1.74 – 6.62]	[5.6 – 7.1] [0.07 – 0.12]	[4.9 – 6.6] [0.10 – 0.14]	[12.8 – 16.9] [0.27 – 0.40]	[21.2 – 32.6] [0.49 – 0.66]	[12.7 – 22.9] [0.83 – 1.16]	[2.0 – 3.4] [0.70 – 1.02]
*h*IDO1 **IC50**$_{enz}$ **IC50**$_{cell}$	*NI*[e]	*NI*	*NI*	*NI*	*NI*	*NI*	*NI*	*NI*
LD50[b] (μM)	> 80[d]	> 100	> 20	> 30	> 100	> 100	> 30	> 100
cLogD$_{7.4}$[c]	3.34	0.15	3.49	3.49	3.17	3.17	2.60	3.01
LLE	2.72	4.99	1.76	1.75	1.67	1.46	2.18	2.56
LE	0.46	0.41	0.38	0.38	0.35	0.33	0.33	0.42

[a] 95 % confidence intervals. Reported IC_{50} values are calculated from measurements performed in triplicates, in at least two separate experiments. [b] Toxicity was determined using an MTS assay on P815B cell. [c] $LogD_{7.4}$ were calculated using Chemicalize. [d] Previously obtained data from *Pilotte et al.*[171] [e] *NI*: No inhibition.

To rank and compare these initial hits, we normalised their respective affinities using ligand efficiency (LE: $1.4(-\log IC_{50})/(\text{heavy atom count})$) and lipophilic ligand efficiency (LLE: $pIC_{50} - \text{clog}D_{7.4}$) metrics.[296,297] These values allow us to consider both activity and lipophilicity,[2] an equally important attribute in drug design affecting ligand association and ADME properties.[298]

Isoquinoline analogues **1** and **2** were the most active compounds in cells, whereas quinazolines (**3**, **4**) showed a loss in their potency and LE/LLE values. Despite being less potent in cells than **1** and **2**, hit compound **6**, bearing a triazole moiety, had the lowest IC_{50}(enz) on *h*TDO2, and overall more favourable metrics due to its higher hydrophilicity and heteroatoms count. In addition to the absence of cell toxicity even at high concentrations (> 100 μM), incubation of cells with **6** did not affect the cell cycle distribution, which was determined by flow cytometry with propidium iodide DNA staining (PI) (**Figure 26**).

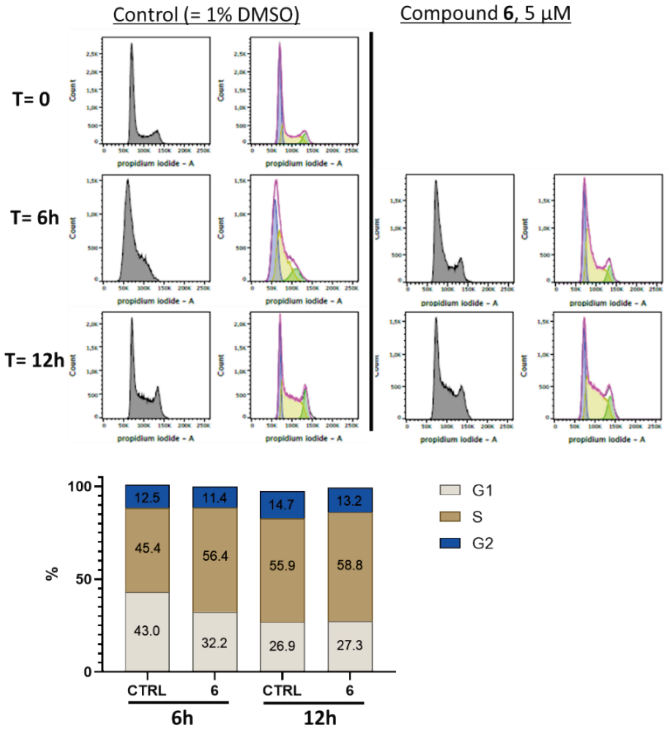

Figure 26. Evaluation of influence of compound 6 (5-(1H-indol-3-yl)-1H-benzo[*d*][1,2,3]triazole) on P815B cell cycle. Cell cycle phase distribution was determined at 6h and 12 h by flow cytometry. The bar diagram represents the distribution of cells in different phases of the cell cycle.

Evaluation of *h*TDO2 inhibition by **6** demonstrated an $IC_{50}(CI_{95\%})$ of 2.7 μM in the enzymatic assay (IC_{50} (enz)) and 0.8 μM in cell-based settings (IC_{50} (cell)), while **LM10** had an IC_{50} (enz) of 7.3 μM and an IC_{50} (cell) of 2.8 μM. Consequently, we decided to use **6** as a starting point for designing variously N-substituted original indole 3-benzotriazoles. However, compound **6** displayed worsened parameters (LLE = 2.56, $cLogD_{7.4}$=3.01) compared to **LM10** (LLE=4.99, $cLogD_{7.4}$=0.15) due to the loss of the tetrazole function, ionised at the physiological pH of 7.4. Thus, our optimization included benzotriazole substitutions of various hydrophobicity ranges to probe TDO2 inhibition while considering their potency and physicochemical characteristics. Then, we further modulated the benzotriazole ring by (i) replacement with a triazolo-pyridine scaffold and (ii) substitution on the 6-membered ring of the benzotriazole (**Figure 27**).

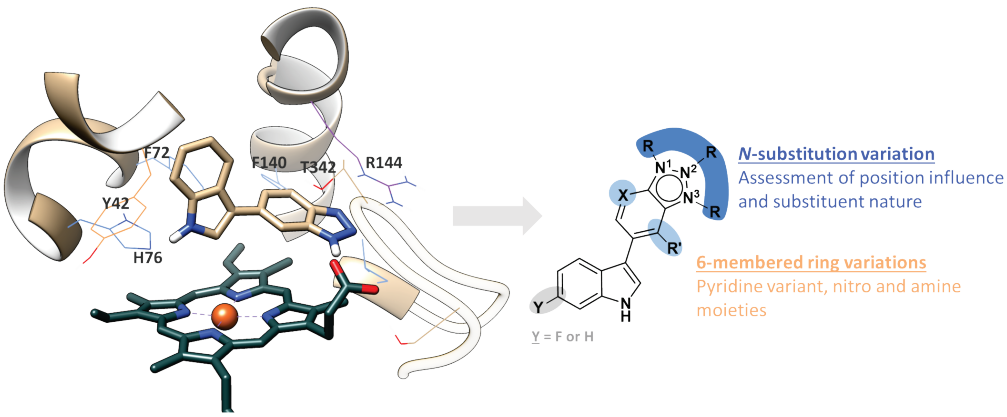

Figure 27. Molecular modelling of **6** inside *h*TDO2 active site (PDB code 5TI9) and envisioned modulations around this scaffold.

4.2. Structure-Activity Relationships of Benzotriazole Analogues

We next synthesised a chemical library of benzotriazole analogues and evaluated the synthesised compounds for their ability to inhibit TDO2 both *in vitro*, using a purified truncated form of TDO2, and *in cellulo* using TDO2-expressing P815B cells.[205] To remain under initial velocity conditions, the assay was optimised so that cells consume less than 25 % of the available L-Trp (**Figure 28**). The same evaluation was performed on IDO1 to assess the selectivity towards TDO2 and demonstrated that none of these compounds could inhibit IDO1 (data not shown).

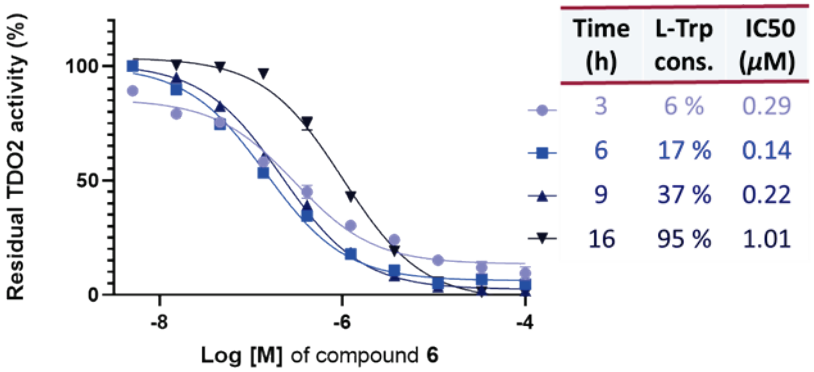

Figure 28. Influence of incubation time and L-Trp consumption of P815B cells on the observed IC_{50} of compound **6**. After 3 hours, the system is too noisy, giving the impression of a lower plateau. Around 6 hours is the optimal incubation time in the initial velocity conditions. After 16 hours, almost all L-Trp was consumed, and the inhibition curve has shifted. Performed in duplicates (n=2).

The active site of TDO2 is highly hydrophobic and relatively small, suggesting that an increase in potency could be achieved by adding lipophilic substituents to the initial scaffold of **6** (IC_{50}(enz): 2.7 μM/ IC_{50}(cell): 0.8 μM). To that end, we examined if the *N*-alkylation of the benzotriazole moiety would result in more potent compounds. Interestingly, The *N*-methyl analogues (**7**, **8**, **9**) displayed a significant gain in IC_{50}(cell) (up to 5-fold for ***7***) compared to their parent compound **6**, while maintaining a similar IC_{50}(enz) (**Table 12**). These results can be explained by the increase in the $LogD_{7.4}$ value resulting from the *N*-methylation. For SARs purposes, we next took an interest in further modifying the *N*-methyl analogues (**7**, **8**, **9**). We thus synthesised and evaluated compounds **10** to **16**, modified on the 6-membered ring of the benzotriazole. Our docking studies suggested that molecules **10**, **11**, **12** could form an H-bond with heme propionate through their aniline. The most potent molecule remained the N_2 analogue **10**. The affinity of these compounds was not significantly different from their precursors, but their lower $cLogD_{7.4}$ value resulted in a better LLE (**Table 12**). Of note, the replacement of the benzotriazole by a 4-*aza*-benzotriazole in compounds **13**, **14** and **15**, did not result in better activities.

Next, we investigated the impact of bulkier *N*-chain substituents in N_1 and N_3 positions of the benzotriazole (compounds **17** to **40**). As the N_2 substitution was poorly available to alkylation, which only occurred through direct methylation of the benzotriazole, we investigated only N_1 and N_3 substitutions. Lipophilic substituents such as trifluoroethyl (**17**, **18**) and ethyl-cyclopropyl (**19**, **20**) yielded

potent compounds, as expected from their higher $cLogD_{7.4}$. We quickly noticed that N_1-substitution was generally more favorable than N_3 for the activity. Interestingly, this trend was not apparent for the smaller methyl group as compounds **7**, **8** and **9** exhibit the same activity. For example, N_1-substitution with a trifluoroethyl (**18**, IC_{50}(enz):1.9 μM/ IC_{50}(cell)$_I$: 0.19 μM) resulted in a 3 to 7-fold increase in activity compared to N_3 substitution of the same moiety (**17**, IC_{50}(enz): 15.0 μM/ IC_{50}(cell): 0.44 μM). However, *N*-substitution by the less lipophilic acetamide moiety (**21**, **22**) resulted in less potent TDO2 inhibitors with similar affinity, although the N_1 substituted compound **22** appeared 2-fold more potent in cells than its isomer. Surprisingly, their hydrolysed counterparts **23** and **24** displayed a loss of activity in both cellular and biochemical assays, suggesting that a low membrane permeability was not the only reason that could account for their poor activity. Compounds **25** and **26**, displaying a 2-(dimethylamino)ethyl moiety, shared a similar potency, perhaps due to the more flexible nature of their *N*-substituent. A further increase of *N*-substituent size with physiologically non-ionised moieties (**27** to **32**) led to a systematic loss of activity and an increasing gap between cellular and enzymatic potencies. Interestingly, the introduction of longer *N*-substituents with H-bond donors such as piperidine (**33**, **34**) and pyrrolidine (**35**, **36**) led to a better activity for N_3-substituted compounds. Of note, these compounds had the best LLE values of all studied compounds due to their predominantly protonated state at physiological pH, resulting in low $cLogD_{7.4}$ values.

We also investigated a substitution of the indole ring H_6 to fluorine, with the synthesis of compounds **8a** and **37a**. As expected from previous results,[292] substitution with fluorine in this position of the indole was beneficial for the activity, and compound **37a** demonstrated a 5-fold increase in activity in both cellular and enzymatic assays (IC_{50}(enz): 5.2 μM/ IC_{50}(cell): 0.23 μM) compared to **37** (IC_{50}(enz): 24.9 μM/ IC_{50}(cell): 0.74 μM). The same gain in activity occurred for **8a** in cells (IC_{50}(enz): 1.1 μM , IC_{50}(cell): 0.02 μM) compared to **8**.

Table 12. Inhibitory affinities (IC_{50}) of compounds against *h*TDO2 in the spectrophotometric assay and P815B cells.

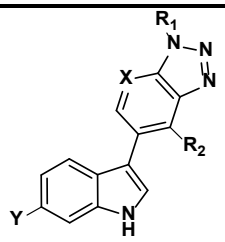

N_1

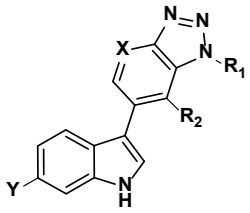

N_3

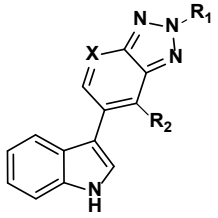

N_2

N°	N_x	Y	X	R_2	R_1	IC_{50}[a] (μM) Enz.	IC_{50}[a] (μM) Cell	Log$D_{7.4}$[b]	LLE	LE
7	N_2					4.0	0.17	3.23	2.17	0.39
8	N_3					3.87	0.22	3.17	2.24	0.39
9	N_1					6.02	0.38	3.17	2.05	0.38
10	N_2			NH_2		3.85	0.42	2.34	3.07	0.37
11	N_3			NH_2		5.01	0.98	2.34	2.96	0.36
12	N_1			NH_2		3.93	0.97	2.34	3.07	0.37
13	N_2		*N*			13.06	0.48	2.73	2.15	0.33
14	N_3		*N*			7.83	0.40	2.71	2.40	0.35
15	N_1		*N*			9.08	0.71	2.66	2.38	0.35
16	N_1			NO_2		1.32[c]	0.54	2.52	3.36	0.37
8a	N_3	*F*				1.1	0.02	3.31	2.65	0.41
17	N_3				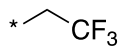	15.0	0.44	4.13	0.69	0.29
18	N_1					1.9	0.19		1.59	0.34
19	N_3				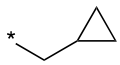	13.5	0.98	3.95	0.92	0.30
20	N_1					3.9	0.10		1.46	0.34
21	N_3				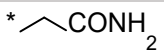	39.7	1.62	1.84	2.56	0.28
22	N_1					36.1	0.68		2.60	0.28
23	N_3				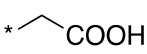	173.8	NI[d]	- 1.00	4.76	0.22
24	N_1					104.5	NI		4.98	0.25
25	N_3				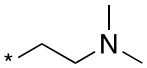	36.9	1.93	1.70	2.73	0.26
26	N_1					24.6	1.64		2.91	0.27
27	N_3				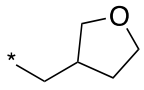	44.1	1.86	3.19	1.16	0.25
28	N_1					21.9	0.41		1.44	0.26
29	N_3				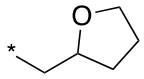	36.9	2.53	3.59	0.81	0.25
30	N_1					21.1	0.50		1.08	0.27
31	N_3				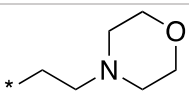	118.6	3.73	2.84	1.20	0.21
32	N_1					52.6	1.60		1.46	0.23

33	N_3		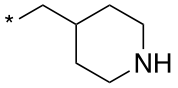	17.73	0.93	0.50	4.25	0.26
34	N_1			25.51	1.15		4.09	0.25
35	N_3		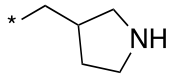	26.10	0.62	- 0.28	4.86	0.27
36	N_1			45.65	1.78		4.62	0.26
37	N_3		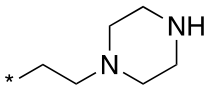	24.9	0.74	0.96	3.64	0.24
38	N_1			45.0	1.43		3.39	0.23
37a	N_3	*F*		5.2	0.23	0.97	4.32	0.28
39	N_3		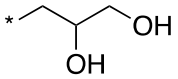	17.0	0.75	1.85	2.64	0.27
40	N_1			25.2	2.27		2.35	0.25

[a] Reported IC_{50} values are calculated from measurements performed in triplicates, in at least two separate experiments. 95 % confidence intervals of the values can be found in the Supporting Information. [b] $LogD_{7.4}$ were calculated using Chemicalize. [c] Residual activity of ~ 30 %. [d]NI: no inhibition. Unless indicated otherwise, Y and R_2 = H, X = CH.

4.3. STD-NMR Study of Interaction Between the Active Site and the Inhibitor

To better understand the observed SARs and notably how the nature and positioning of the lateral *N*-substituent influenced the binding of the inhibitor inside the active pocket, we performed epitope mappings on several couples of regioisomers using saturation transfer difference NMR (STD-NMR). In STD-NMR, selective saturation of *h*TDO2 in solution is transferred to the bound ligand through intermolecular NOEs between protons of the inhibitor and the active site's residues. Consequently, the ligand's protons interacting more closely display intense STD signals, while a decrease in STD intensity correlates with lower interaction.[299] Due to solubility issues, we focused our investigation on compounds bearing solubilising moieties to attain a high compound concentration (up to 200 μM) in an aqueous buffer, suitable for the present evaluation. We mapped the epitopes of regioisomers **25 - 26**, **35 - 36** and **31 - 32** (**Figure 29**). Epitope mapping of all six compounds suggested that N_3-substitutions led to an improper position of the indole ring compared to N_1-substitutions (data regarding compounds **25 - 26** and **35 - 36** can be found in supporting information, **Figure S1**). Indeed, as pictured in **Figure 29**, epitope mapping on the different compounds showed that the indole ring displays the highest saturation transfer for protons H_5, H_6 and H_7 (around 100%). Concurrently, co-crystallographic structures of *h*TDO2 with L-Trp show that this part of the indole tightly interacts with a cluster of several hydrophobic

residues involving L120, F5, Y24, Y27 and L28.[220] In the case of L-Trp, the indole H_2 position is located very close to the heme.[220]

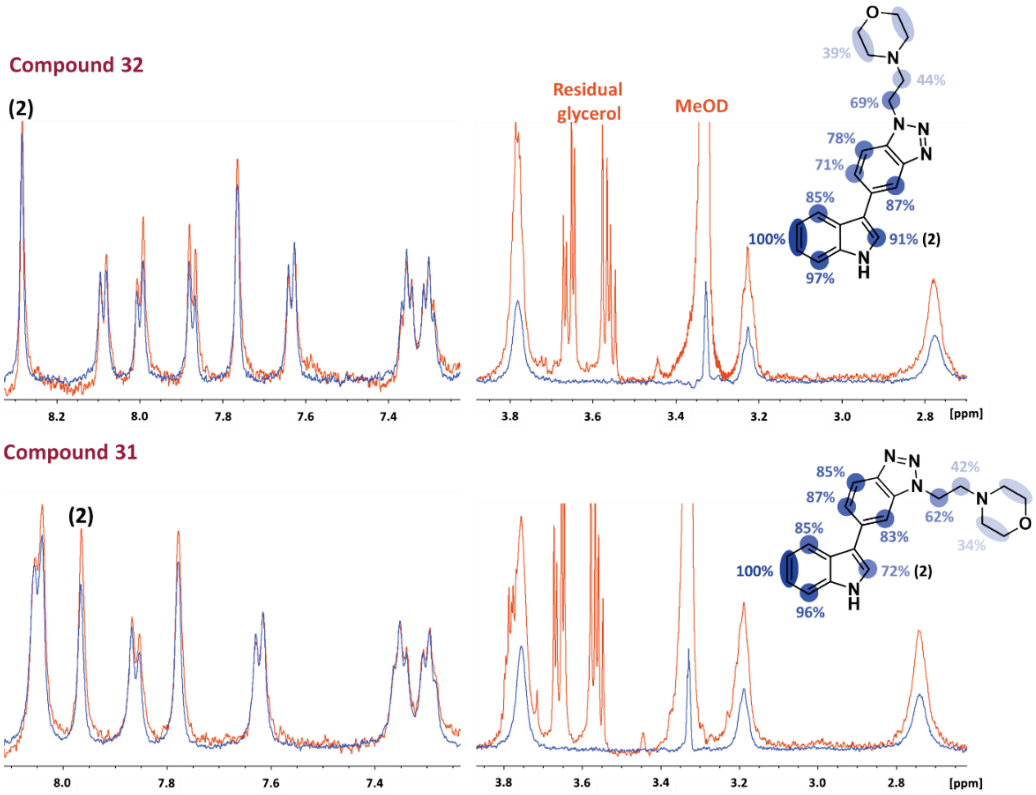

Figure 29. Epitope mapping for regioisomers **32** (IC_{50} 52.6 μM (enz), 1.6 μM (cell) and **31** (IC_{50} 118.6 μM (enz), 3.7 μM (cell). One-dimensional NMR ^{1}H proton spectra (blue) overlaid with STD spectra (orange). Corresponding compounds are represented above each set of spectra. Blue circles represent the protons at the designated position(s), with percentages represent STD intensity of the respective proton(s). Two of the ethylene protons could not be seen as their shift coincide with the water signal.

Similarly, **26**, **36** and **32** all exhibited a saturation transfer of around 90 % for H_2. However, we observed that the less active N_3 substituted analogues **25**, **35** and **31**, systematically displayed a 20 to 30 % decrease in saturation transfer for H_2

compared to their regioisomers substituted in N_1. Overall, these results suggest a shift in the position of the indole core for N_3 substituted compounds, resulting in the misplacement of H_2. This apparent shift of the indole position could partially explain the difference in activity between N_1 and N_3 substituted compounds.

Interestingly, the sidechain of the different isomers always showed a similar and low saturation transfer compared to the aromatic protons. Therefore, the nature of the sidechains does not appear to be useful for the interaction with *h*TDO2, which opens the door to further modulation to fine-tune this family of inhibitor physicochemical properties.

4.4. Molecular docking of benzotriazole analogues

Our molecular docking studies suggested two main hindrances for the accommodation of different ligands in the active site of *h*TDO2. The first identified hinder was Arg144, as a shift in its sidechain was required for the binding of the inhibitors. Displacement of this sidechain increased with the size of the *N*-substituent and was more important for N_3 regioisomers. We noticed that wider Arg144 shifts correlated with lower enzymatic activity. The second hinder was the flexible 338 – 346 loop, suggesting that an induced-fit type binding was perhaps needed for larger compounds. It was previously described that disordering of this loop allows NFK to diffuse out and enables de binding of a new L-Trp molecule.[220]

Its mobility was particularly noticeable when *h*TDO2 was co-crystallised with an NLG919-type analogue, widely opening the active site.[274]

Regioisomers displayed a similar binding pose, as shown in **Figure 30** for analogues **17** (IC_{50}(enz): 15.0 μM/ IC_{50}(cell): 0.44 μM) and **18** (IC_{50}(enz): 1.9 μM, IC_{50}(cell): 0.19 μM) with a particularly noticeable affinity difference. However, docking of N_1-substituted compounds resulted in a more favourable geometry for the indole core placement. Indeed, N_3-substituted compounds display a shift of the indole core from the position naturally adopted by the indole of L-Trp, with a shift of C2, disturbing the interaction with the aromatic hotspots. Regarding compounds bearing a longer sidechain with an H-bond donor (compounds **33** to **40**), our docking results suggested a possible interaction with the propionate of the heme or with an H-acceptor sidechain (such as Ser345) from the mobile loop. This interaction could potentially explain the slightly better activity observed for N_3 analogues.

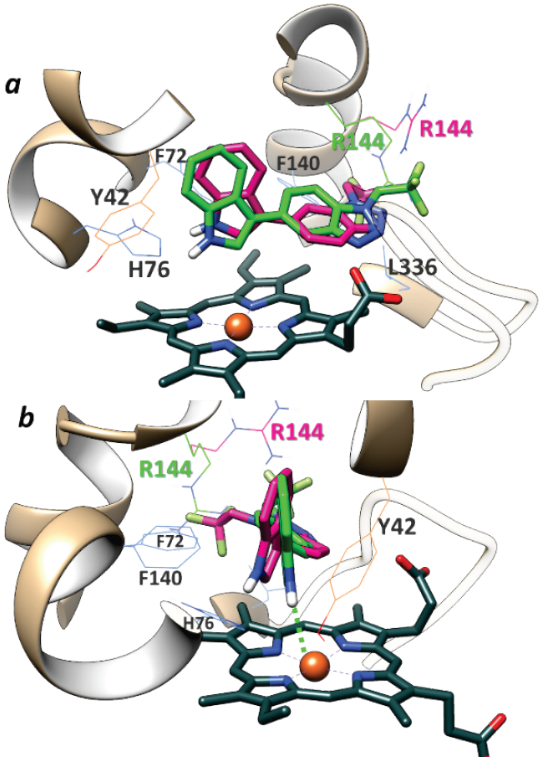

Figure 30. Molecular modelling of regioisomers **17** (pink) and **18** (green), bearing a trifluoroethyl from the front (***a***) and the side (***b***) (PDB code: 5TI9).[220]

4.5. Phase I metabolic stability and electrophilic reactivity

The potential reactivity of **LM10** as Michael acceptor was assessed with a thiol-trapping assay using cysteamine as S-nucleophile and compared to that of the unsubstituted benzotriazole **6**.[300–302] Following incubation with cysteamine, the ^{1}H NMR spectrum of **LM10** quickly changed to reveal the apparition of several new aromatic signals. In contrast, the compound **6** spectrum stayed the same (**Figure 31**). Accordingly, LC/MS analysis of **LM10** ($[M + H]^{+}$= 230.1) confirmed the

appearance of a secondary product ($[M + H]^+$= 305.1) upon cysteamine addition while **6** was not impacted.

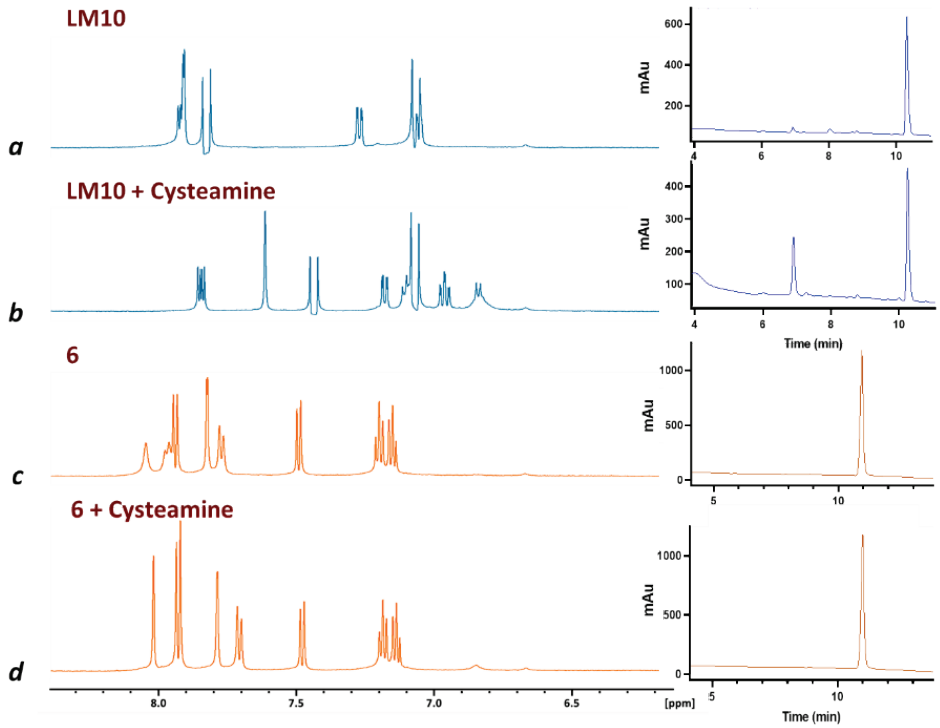

Figure 31. Aromatic regions of ^{1}H NMR in DMSO-*d6* spectra of 1 mM of **LM10** (***a***) and **6** (***c***) before and after (***b, d***) addition of 10 equivalents of cysteamine. Spectra were recorded 30 minutes after the addition of cysteamine. Spectrum ***b*** (**LM10** + cysteamine) shows several new aromatic signals, while proton integrations of compound **6** remain unchanged but displayed a slight shift in the presence of cysteamine.

Then, we evaluated the microsomal half-life of **LM10** and several representative benzotriazoles (**Table 13**). The recovery percentage of **LM10** after 24 hours remained close to the initial concentration. Regarding the present series, we noticed that the nature of the *N*-substituent was determinant for the recovery rate of the compounds. The presence of fluorine on the indole did not impact the microsomal stability in compounds **8a** and **37a** compared to their non-fluorinated analogues. Furthermore, in isomers **37** and **38**, the localization of the *N*-substituent did not impact the microsomal stability.

Table 13. Microsomal stabilities (half-lives) of representative compounds

N°	N_x	R_1	**Microsomal half-life**(min.)
LM10	/	/	> 1440
6	/	H	62
8	N_3		24
8a	N_3		22
18	N_1	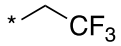	45
26	N_1	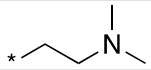	43
35	N_3	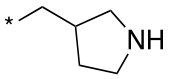	> 1440
37	N_3	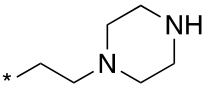	> 1440
37a	N_3		> 1440
38	N_1		> 1440

The stability values were obtained in duplicates in two separate experiments. Graphs of stability curves can be found in supporting information **(Figure S2).**

Overall, these data demonstrate that the structural rigidification results in a scaffold that does not exhibit Michael acceptor behaviour. Nonetheless, the microsomal stability studies contrast our initial idea that this template rigidification would necessarily lead to more metabolically stable compounds. Indeed, the present series display considerable heterogeneity in metabolic stability, which appears heavily dependant on the nature of the *N*-substituent.

4.6. Chemistry of the fused-cycle analogues

The target compounds were synthesised by Suzuki-Miyaura cross-coupling between halogenated benzotriazole analogues and the appropriate indole boronic ester. Compounds **1 – 5** were obtained following reaction between brominated isoquinolines, quinazolines and **42**. The synthesis of **680C91**-type analogues was performed using the same strategy, starting from **3** in the cross-coupling reactions (**Scheme 1**). Several routes were attempted to synthesise compound **6**, bearing an unsubstituted benzotriazole, leading to the synthetic pathway depicted in **Scheme 2**. We used *p*-methoxybenzyl (PMB) as a protecting group for 5-Bromo-benzotriazole, which led to the formation of two regioisomers. Then, we performed the cross-coupling using the MIDA boronate **43** following a procedure adapted from *D.M. Knapp et al*.[303] The MIDA boronate allows a continuous release of the boronic acid over several hours. This unique capacity enabled us to obtain the cross-coupled product with an almost quantitative yield. The cross-coupled intermediate was first

deprotected from its phenylsulfonyl (SO_2Ph) using KOH, after what the PMB was removed in pure trifluoroacetic acid (TFA) at reflux temperature for 16 hours to afford **6**. We noted that no degradation of the scaffold occurred despite the harsh basic and acidic conditions of both deprotection.

Two different routes, depicted in **Scheme 3** and **Scheme 4** were used to synthesise *N*-substituted benzotriazoles, either by direct alkylation of commercially available 5-halo-benzotriazole (**Scheme 3**) or by nucleophilic aromatic substitution starting from bromofluoronitrobenzene derivatives (**Scheme 4**), followed by reduction of the aromatic nitro group and treatment of the resulting compounds by sodium nitrite in acetic acid to get the final alkylated benzotriazoles (**7b – 23b**, **18d – 41d**). To assess the substitution influence on the 6-membered ring, we took advantage of a highly electron-rich position between the halogen and the carbon between the two cycles to perform nitration using KNO_3 in H_2SO_4. A reduction using $Fe_{(s)}/NH_4Cl$ was then performed to reduce the aromatic nitro group (**Scheme 5**).

The halogenated benzotriazoles (**7b – 23b**, **18d – 41d**) were reacted with indole derivatives bearing a pinacol or MIDA boronate in the 3-position and a phenylsulfonyl (SO_2Ph) or a *tert*-butyloxycarbonyl (Boc) as a protecting group to afford the cross-coupled intermediates (**Scheme 6**). Finally, the target compounds **7 - 41** were eventually obtained after appropriate deprotection.

Scheme 1. General synthetic procedure for compounds 1 - 5.[a]

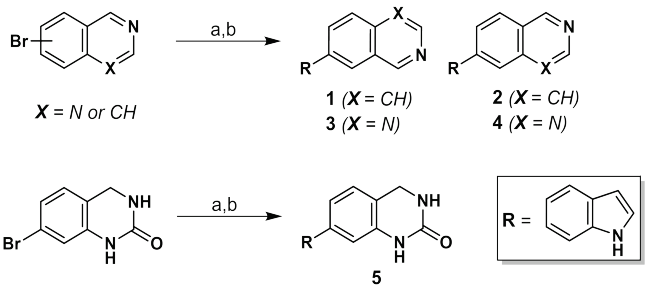

[a] Reagents and conditions: (a) **3** (1-(phenylsulfonyl)-3-(4,4,5,5-tetramethyl-1,3,2-dioxaborolan-2-yl)-1H-indole **42** (1.2 eq), 5 mol % $Pd(dppf)Cl_2$, 10 mol % SPhos, K_3PO_4 (2.0 eq), Dioxane/H_2O (5:1), 60°C, 3-6h, Under N_2. (b) KOH 2.5M in MeOH/H_2O (1:1), reflux 30 min. – 48h.

Scheme 2. Synthesis of compound 5-(1H-indol-3-yl)-1H-benzotriazole (6).[a]

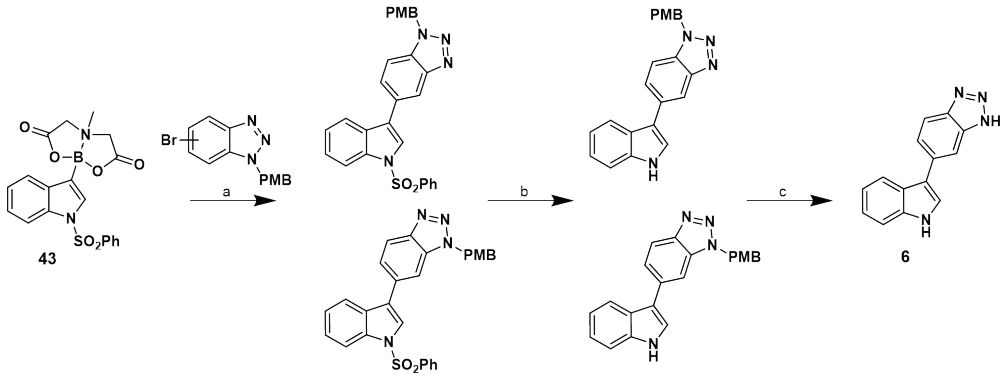

[a] Reagents and conditions: (a) 5 mol % $Pd(dppf)Cl_2$, 10 mol % SPhos, K_3PO_4 (2.0 eq), Dioxane/H_2O (5:1), 60°C, 6h, Under N_2. (b) KOH 2.5M in H_2O/MeOH (1:1), reflux, 1h. (c) 100 % TFA, reflux, 16h. Overall yield: 24 %

Scheme 3. Synthetic Routes for the *N*-substituted 5- and 6-halobenzotriazoles.[a]

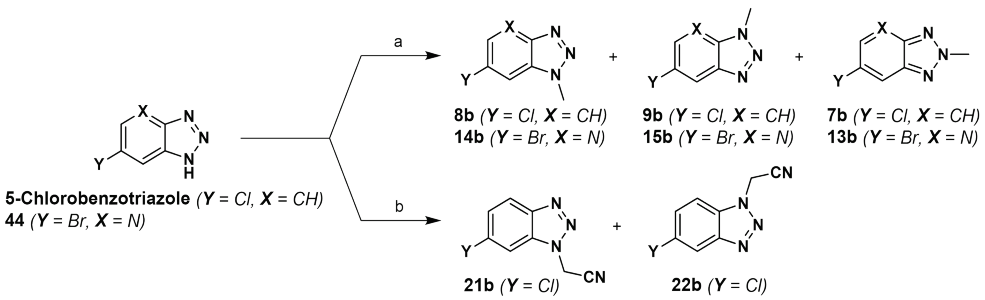

[a] Reagents and conditions: (a) Me_2SO_4 (1.6 eq), $NaOH_{aq}$ 2M, r.t., 1h30 (b) $ClCH_2CN$ (1.5 eq), Et_3N, DMF, reflux, 16h.

Scheme 4. Synthetic Route for N-substituted 5-bromobenzotriazoles and 6-bromobenzotriazoles.[a]

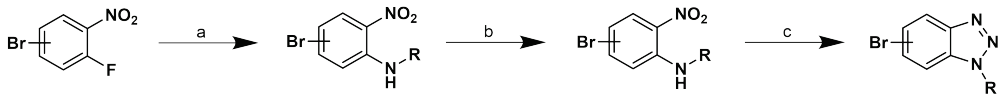

R:	6-Br	5-Br	6-Br	5-Br	6-Br	5-Br
2,2,2,-trifluoroethyl	**17b**	**18b**	**17c**	**18c**	**17d**	**18d**
cyclopropylmethyl	**19b**	**20b**	**19c**	**20c**	**19d**	**20d**
2-(dimethylamino)ethyl	**25b**	**26b**	**25c**	**26c**	**25d**	**26d**
(tetrahydrofuran-2-yl)methyl	**27b**	**28b**	**27c**	**28c**	**27d**	**28d**
(tetrahydrofuran-3-yl)methyl	**29b**	**30b**	**29c**	**30c**	**29d**	**30d**
2-morpholinoethyl	**31b**	**32b**	**31c**	**32c**	**31d**	**32d**
tert-butyl 4-ethylpiperidine-1-carboxylate	**33b**	**34b**	**33c**	**34c**	**33d**	**34d**
tert-butyl 3-ethylpyrrolidine-1-carboxylate	**35b**	**36b**	**35c**	**36c**	**35d**	**36d**
tert-butyl 4-ethylpiperazine-1-carboxylate	**37b**	**38b**	**37c**	**38c**	**37d**	**38d**
butane-1,2-diol	**39b**	**40b**	**39c**	**40c**	**39d**	**40d**

[a] Reagents and conditions: (a) primary amine derivative, Et_3N (1.3 eq), EtOH or THF, r.t. or reflux, 30 min. – overnight; (b) $Fe_{(s)}$ (10 eq), $EtOH/H_2O$ (4:1), reflux, 30 min. – overnight; (c) $NaNO_2$ (2.5 eq), glacial acetic acid, sonication, r.t., 1h.

Scheme 5. Synthetic Route for nitration and reduction to anilines of chloro-methyl-benzotriazoles.[a]

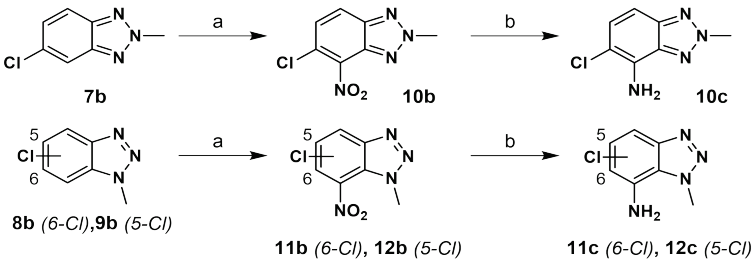

[a] Reagents and conditions: (a) KNO_3 (3.0 eq) in H_2SO_4, 50°C, 1h30 (b) $Fe_{(s)}$ (10.0 eq), EtOH/H_2O (4:1), reflux, 30 min.

Scheme 6. General synthetic procedure for cross-coupling and deprotection of 6-(1H-indol-3-yl)-benzotriazole derivatives.[a]

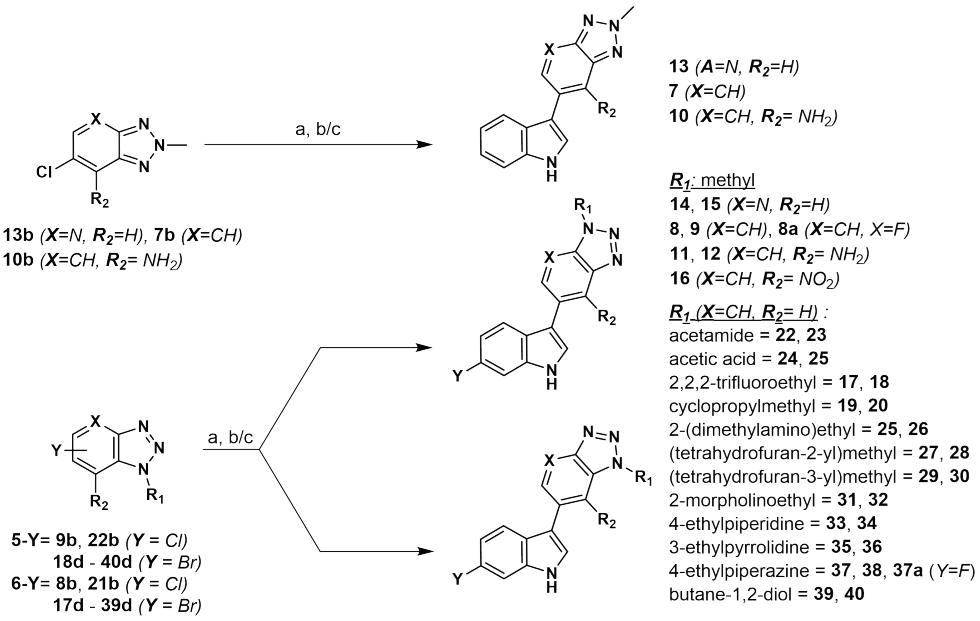

[a] Reagents and conditions: (a) Boronic ester derivative (**41**, **42** or **43)** (1.2 – 1.5 eq.), 5 mol % Pd(dppf)Cl_2, 10 mol % SPhos, K_3PO_4 (2.0 eq), Dioxane/H_2O (5:1), 60°C, 3-6h, Under N_2. (b) HCl 4.0 M in MeOH/H_2O (1:1), reflux, 30 min. – 5h for Boc deprotection, (c) KOH 2.5M in in MeOH/H_2O (1:1) or 1 M TBAF in THF, reflux 30 min. – 48h. for SO_2Ph deprotection.

4.7. Intermediate conclusion

In this work, we designed a series of original TDO2 inhibitors, devoid of the potentially problematic vinyl linker of the reference compound **LM10**. We evaluated these compounds through a SAR study completed by STD epitope mapping and stability evaluation. These compounds present a wide range of lipophilicity and various chemical characteristics, showing the possibility of fine-tuning these inhibitors' molecular and pharmacokinetic characteristics for potential ADME purposes. Compared to existing potent TDO2 inhibitors (**Figure 32a**), the present series shows similar or slightly better (**8a**) cellular affinities up to the nanomolar range (**Figure 32b**). Previously, we reported that the enzyme seemed to be susceptible to small modifications of the inhibitor. However, we bring nuance to that affirmation, as TDO2 appears to allow bulkier substitutions for this series of compounds.

Interestingly, this series of compounds showed a systematically better activity on cells than on isolated enzyme. Such difference was previously observed for other indole-based patented TDO2 inhibitors.[277,278] Moreover, other previous works preferred focusing on cellular activities and did not include enzymatic inhibition values (i.e., preclinical compound **PF06845102/EOS200809**, evaluated here in the biochemical assay, **Figure 32a**).[222,274,295] Different parameters could account for this discrepancy. Firstly, the enzymatic assay that uses ascorbate, methylene blue, and

catalase to maintain a reduced state could mimic poorly the physiological protein environment.[304] Furthermore, some inhibitors could also bind to the apo form of the protein, inhibiting its activity in a way the enzymatic assay would not detect.

Finally, the isoquinolines and quinazolines derivatives reported in this work (**1** – **5**) also constitute attractive, and highly functionalisable scaffolds for the future development of TDO2 inhibitors.

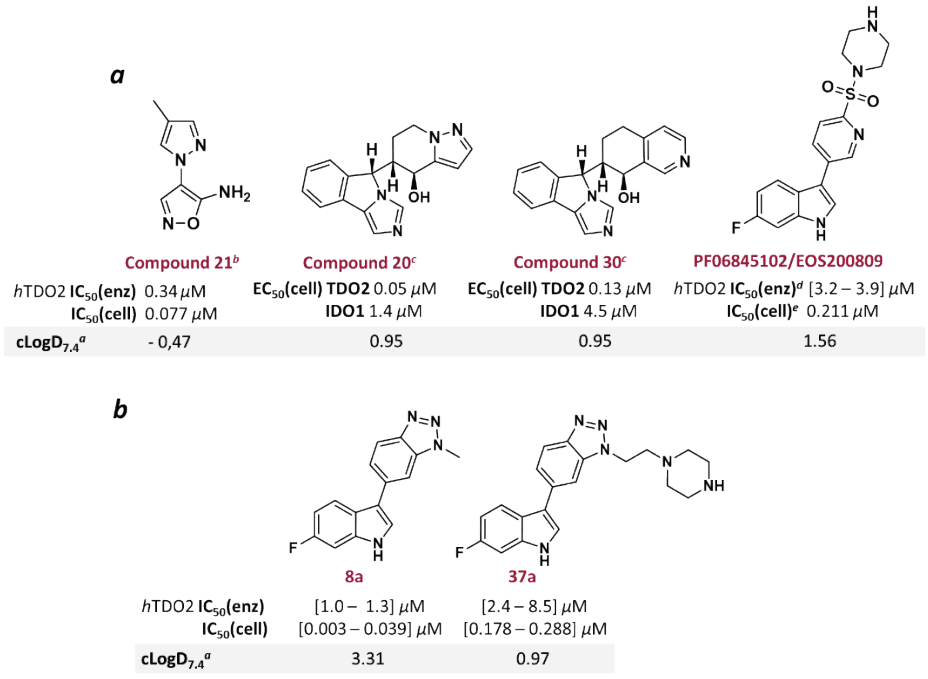

Figure 32. Examples of potent TDO2 inhibitors (**a**) and representative examples of the series developed in the present work (**8a** and **37a**). [a]$LogD_{7.4}$ were calculated using Chemicalize.[b] Compound **21** and its inhibition values are from *Pei et al.* 2018.[263] [c]Compounds **20**, **30** and their inhibition values are from *Parr et al.*[274] [d]Cellular potency of **PF06845102/EOS200809** is from *Schramme et al.* 2020.[222] [e]The biochemical IC_{50} was measured in the present work.

5. CHAPTER 3: CHALCOGEN BIOISOSTERIC REPLACEMENT IN A SERIES OF HETEROCYCLIC INHIBITORS OF TDO2

This chapter is based on the following manuscript: Kozlova, A.; Thabault, L.; Dauguet N; Liberelle, M.; Pilotte, L.; Stroobant, V.; Van den Eynde, B.; Frédérick, R. Investigation of chalcogen bioisosteric replacement in a series of heterocyclic inhibitors of Tryptophan 2,3-Dioxygenase, 2021.

In this subset of the project, we present and a small series of compounds closely related to the benzotriazole series, for which we evaluate the impact of oxygen, Sulphur, selenium bioisosteric replacement.

5.1. Bioisostery in medicinal chemistry

Isosteric replacement is a commonly used strategy in rational drug design. This strategy assumes that functional groups with similar physicochemical properties can be interchanged to modulate efficacy, ADME/Tox, and off-target profiles.[305] Atoms from the chalcogen family, oxygen (O), sulfur (S) and selenium (Se), are a perfect example of this isosteric strategy. While O/S replacements are common in medicinal chemistry, integrating Se into drug-like structures only recently began to gain popularity and thus represents an underexplored research area.[306] The chalcogens share similar physicochemical properties and identical functional group types but present some notable differences. Indeed, the gradual increase in the atom size, particularly evident between O and S, results in lower electronegativity (respectively 3.44 and 2.58) and greater polarizability (**Figure 33**).[307] In turn, these

parameters lead to higher reactivity due to weaker bonding.[308] Moreover, the higher electronegativity of O allows it to be a great hydrogen bond acceptor. However, although they were long overlooked as hydrogen-bond acceptors, S and Se can also participate in hydrogen bonding interactions.[309,310] Finally, S and Se also have a more extensive range of oxidation states than O, allowing them to participate in various redox reactions.[311]

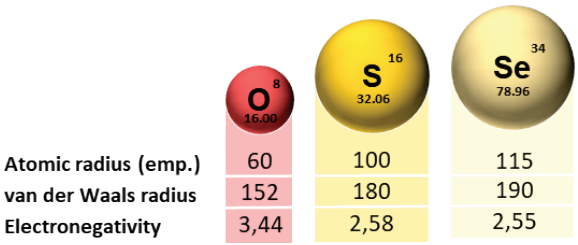

Figure 33. Comparison of oxygen, sulfur and selenium atoms. Radii are expressed in picometers. Atomic radii values are empirical.[307,312]

Se is a toxic yet essential trace element crucial for the regulation of cellular antioxidant systems.[313] It naturally occurs in the form of selenomethionine (Sem) or selenocysteine (Sec). The latter is present in the active sites of selenoproteins such as glutathione peroxidase (GPXs), thioredoxin reductase (TRXRs) and selenoprotein P (Sepp1).[314] Selenoproteins rely on dietary Se intake and a common set of cofactors for their synthesis.[315] Se deficiency is associated with numerous diseases and conditions, including neuromuscular and cardiovascular disorders, inflammation, neurodegeneration, endocrine disorders and higher cancer

incidence and mortality rates.[315] It is thus not surprising that even despite the underwhelming outcomes of the Selenium and Vitamin E Cancer Prevention Trial (SELECT) a few years ago, many efforts aimed at designing and developing pharmaceutical agents that are Se-based or that target specific aspects of Se metabolism.[316,317] Today Se continues to draw interest in medicinal chemistry.[318]

The clinical drug **ebselen** (2-phenyl-1,2-benzoselenazol-3-one, **Figure 34**), evaluated for different applications and diseases, is the most famous example of a Se-containing compound administered to humans. **ebselen** catalyses the reduction of hydroperoxides (ROS) in a glutathione-dependent manner and can act as lithium mimetic.[319–321] While there were initial concerns regarding toxicity due to selenium liberation from **ebselen**, it appears that there is no extrusion of the element from the heterocycle.[322] Multiple human clinical trials are currently ongoing, including one against SARS-CoV-2, as **ebselen** inhibits its main protease.[323,324] An **ebselen** analogue, **ethaselen**, an inhibitor of the mammalian thioredoxin reductase (TrxR), is currently evaluated in non-small cell lung carcinoma.[325] These examples demonstrated that a Se-containing drug is a realistic prospect, at least when the Se atom is in a cyclic moiety.

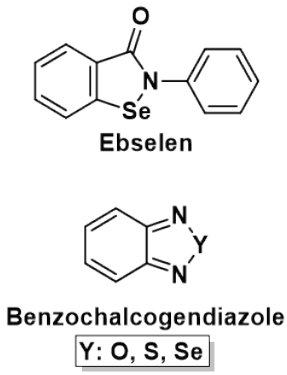

Figure 34. Structures of the clinical drug **ebselen** and the bicyclic benzochalcogendiazole scaffold exploited in this work.

A few examples of bioisosteric replacement in the chalcogen series exist in the literature. In 2011, Achilleon Pharmaceuticals replaced the thiophene group with selenophene in their type IIA Bacterial Topoisomerase inhibitors. The resulting compounds had similar on-target activity, a lower hERG channel inhibition and significant cytotoxicity or microsomal stability issues.[326] Other examples of chalcogen substitutions in non-cyclic moieties also led to non-toxic compounds.[327,328]

To our knowledge, there is no example of benzoxazole, benzothiadiazole and benzoselenodiazole replacement. The benzochalcogendiazole is a bicyclic scaffold consisting of an unsaturated 6-membered ring fused to a five-membered ring of two nitrogen atoms in positions 1, 3 and one chalcogen atom in between (**Figure 34**). It is a drug-like scaffold, present for instance, in the α2 adrenoceptor agonist

drug **tizanidine** (**SIRDALUD**®) and reported in the literature for various biological activities such as antiproliferative and apoptogenic effects on tumour cells.[329,330] Moreover, 5-Bromobenzo[*c*][1,2,5]selenadiazole and Benzo[*c*][1,2,5]selenadiazole did not exhibit any cytotoxicity on various cancer cell lines, suggesting that this moiety might not present any intrinsic liabilities.[331] Finally, other Se-containing derivatives displayed free radical-scavenging activity.[332]

In the present work, we set out to study the equivalence of benzochalcogendiazole replacement in a small series of novel TDO2 inhibitors. These compounds were designed to optimise our benzotriazole-based TDO2 inhibitors, discussed in the second chapter of this work.[333] In the present study, we replaced the benzotriazole with benzochalcogendiazole moieties (**Figure 35**).

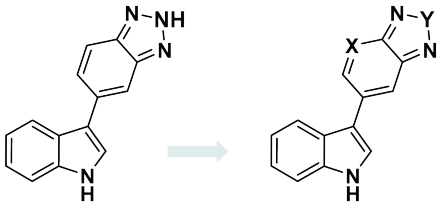

N°	X	Y
45	CH	O
46	CH	S
46*p*	N	S
47	CH	Se
47*p*	N	Se

Figure 35. On the left, [a] Compound **6** from *chapter 2*.[333] On the right, analogues synthesised and evaluated as TDO2 inhibitors displayed in the present work.

Firstly, we hypothesised that 5-(1H-indol-3-yl)benzo[*c*][1,2,5]oxadiazole (**45**) could be accommodated in the enzymatic cavity by potentially forming a hydrogen bond with Arg144 (**Figure 36**). Based on positive results with **45**, we next decided to study

the impact of O isosteric replacement by S (**46**, **46*p***) or Se (**47**, **47*p***) on inhibitory potency and selectivity against IDO1, lipophilicity, microsomal stability and cellular toxicity.

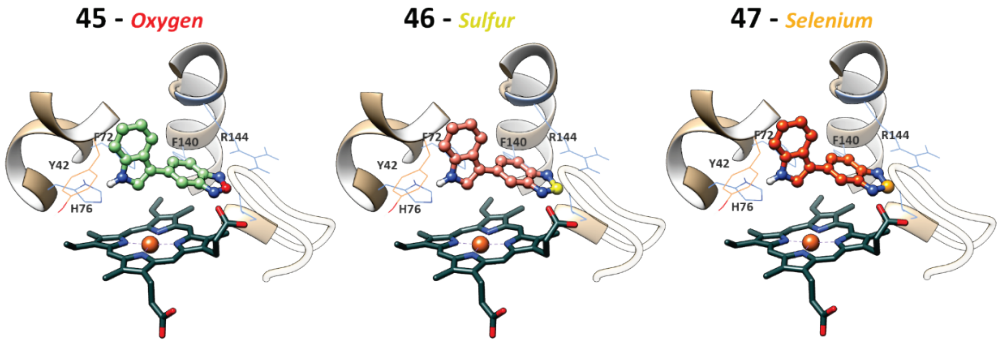

Figure 36. Molecular modelling of **45** (green-oxygen), **46** (pink-sulfur), **47** (red-selenium) inside TDO2 pocket (PDB structure: 5TI9) shows the same pose for the three isomers. The chalcogen atoms are represented to scale.

5.2. Synthesis of benzochalcogendiazoles

Like the compounds from the previous chapter, all final compounds were synthesised by a Suzuki-Miyaura type cross-coupling between an aryl bromide and the appropriate boronic ester. Firstly, the thiadiazole derivatives **48** and **49** (**Scheme 7**, **a**) and selenadiazoles **50** and **51** (**Scheme 7**, **b**) were prepared starting from the commercially available 4-Bromo-1,2-diaminobenzene and 5-bromopyridine-2,3-diamine. 5-bromobenzoxadiazole was purchased from a commercial source. The obtained aryl bromides were then used to perform the synthesis of cross-coupled products.

Scheme 7. Synthesis of 5-bromobenzochalcogendiazoles (48 – 51) [a]

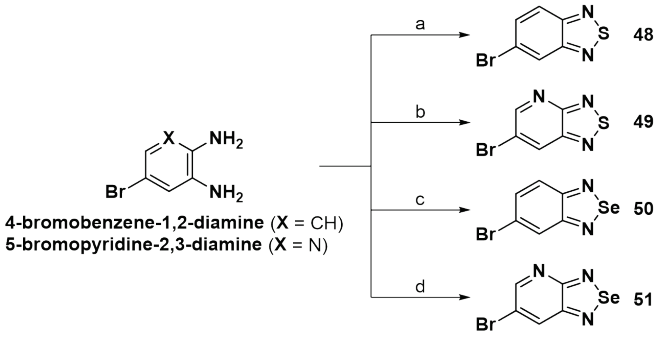

[a]Reagents and conditions: (a) $SOCl_2$, H_2SO_4, atm, 2 h, reflux. Yield: 80 % ; (b) $SOCl_2$, toluene/DMF, atm, overnight, reflux. Yield: 77 %; (c) SeO_2, EtOH, atm, 10 min reflux. Yield: quantitative ; (d) SeO_2, 5 min, Yield: quantitative.

Surprisingly, we could not apply the same synthetic route to obtain all final molecules, as we found significant differences in the reactivity during either the cross-coupling reaction or the final deprotection of the indole nitrogen. Indole boronates are known for being intrinsically unstable due to fast protodeboronation.[303,334] Therefore, we used two different boronic esters in the present work. In accordance with our previous experience of coupling reactions with indoles, we started all synthetic attempts with 1-(phenylsulfonyl)indole-3-boronic acid pinacol ester (**42**). This boronic ester is air-stable, inexpensive, easily accessible synthetically and, usually allows better yields in our optimised conditions than the indole protected with a Boc group.

Starting from **42** and bromobenzoxadiazole, we obtained (5-(1-(phenylsulfonyl)-1H-indol-3-yl)benzoxadiazole) following the optimised procedure with an 80 %

yield (**Scheme 8**). Finally, deprotection in strong basic conditions using potassium hydroxide afforded final compound **45** with an overall yield of 80 %.

Scheme 8. Synthesis of 5-(1H-indol-3-yl)benzoxadiazole (45) [a]

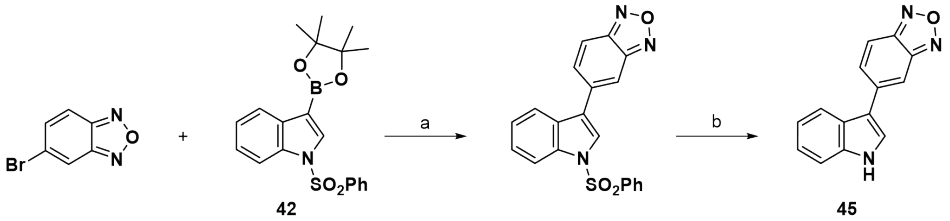

[a] Reagents and conditions: (a) **42** (1.2 – 1.5 eq.), 5 mol % $Pd(dppf)Cl_2$, 10 mol % SPhos, K_3PO_4 (2.0 eq), Dioxane/H_2O (5:1), 60°C, 3h, Under N_2; (b) KOH 2.5M in in MeOH/H_2O (1:1), reflux, 1h. Yield over 2 steps: 80 %.

We next applied the same procedure to the synthesis of aryl-thiadiazole compounds **46** and **46*p***. However, we noticed that while the cross-coupled product was formed, it readily degraded during SO_2Ph deprotection in strong basic conditions. We also evaluated milder conditions that all resulted in the same degradation (e.g. 1M TBAF in THF). Thus, we decided to modify the boronate derivative in a way that would require acidic deprotection conditions. We chose Boc as the new protecting group and simultaneously tried two different routes (**Scheme 9**), both of which were successful.

Scheme 9. Synthesis of 5-(1H-indol-3-yl)benzothiadiazole (46) and 6-(1H-indol-3-yl)-[1,2,5]thiadiazolo[3,4-b]pyridine (46*p*). [a]

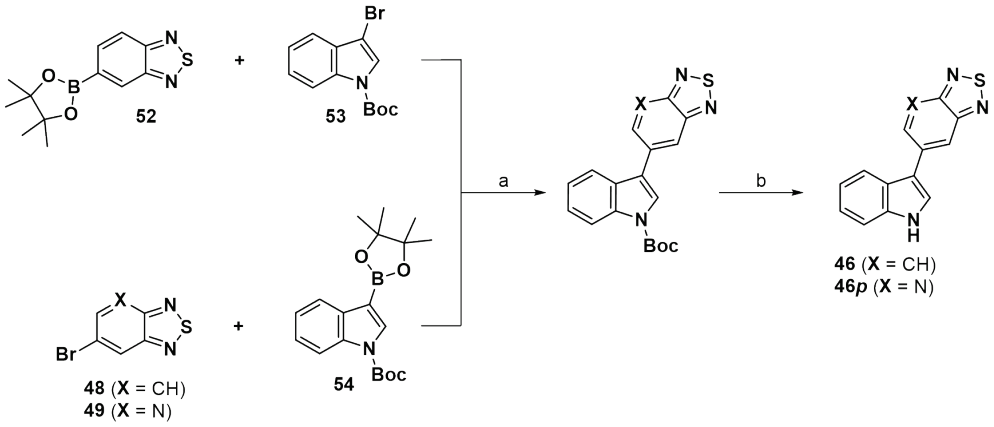

[a]Reagents and conditions: (a) Boronic ester (**52**/**54**) (1.2 – 1.5 eq.), 5 mol % $Pd(dppf)Cl_2$, 10 mol % SPhos, K_3PO_4 (2.0 eq), Dioxane/H_2O (5:1), 60°C, 3h, Under N_2; (b) HCl 4.0 M in MeOH/H_2O (1:1), reflux, 2h. Yield over 2 steps: 76 % for **46**, 42 % for **46*p***.

Finally, we applied the synthetic pathway of compound **45** to synthesise the selenium analogues **47** and **47*p***. However, we did not detect the formation of a cross-coupling product under these conditions. Thus, we decided to modify the nature of the boronic ester and selected the MIDA ester boronate. Compared to other esters, MIDA boronates can slowly release the boronic acid, thus resolving the potential loss of yield due to protodeboronation.[303] There are no available data regarding the reactivity of aryl benzoselenadiazoles derivatives in Suzuki-Miyaura couplings. Using the MIDA boronate **43**, we obtained the cross-coupled compounds **47** and **47*p*** with a high yield of 90 % of the pure compound after flash chromatography. We performed the deprotection in strong basic conditions and

obtained the deprotected final compound in quantitative yield for **47** and around 40 % for **47*p*** due to loss during purification (**Scheme 10**).

Scheme 10. Synthesis of 5-(1H-indol-3-yl)benzoselenadiazole (47) and 6-(1H-indol-3-yl)-[1,2,5]selenadiazolo[3,4-b]pyridine (47*p*)

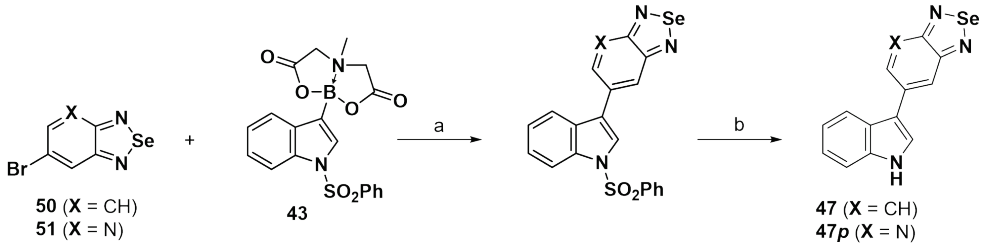

[a]Reagents and conditions: Boronic ester **43** (1.2 eq), 5 mol % $Pd(dppf)Cl_2$, 10 mol % SPhos, K_3PO_4 (2.0 eq), Dioxane/H_2O (5:1), 60°C, 3h, Under N_2; (b) KOH 2.5 M in MeOH/H_2O (1:1), reflux, 1h. Yield over 2 steps: 79 % for **47**, 34 % for **47*p***.

5.3. Evaluation of Tryptophan 2, 3-dioxygenase inhibition, lipophilicity parameters and microsomal stability

Next, we evaluated the synthesised isosteric inhibitors **45**, **46** and **47** and the two aza-analogues **46*p*** and **47*p*** in enzymatic and cellular assays for their ability to inhibit TDO2. The selectivity of these compounds towards TDO2 was also evaluated by performing the same assays against IDO1, which presents a similar active site.[203] Overall, cellular and enzymatic IC_{50} indicated similar activities against TDO2, demonstrating that affinity loss did not occur following the chalcogen replacement (IC_{50} curves are depicted in **Figure 37**, CI95% IC_{50} values in **Table 14**).

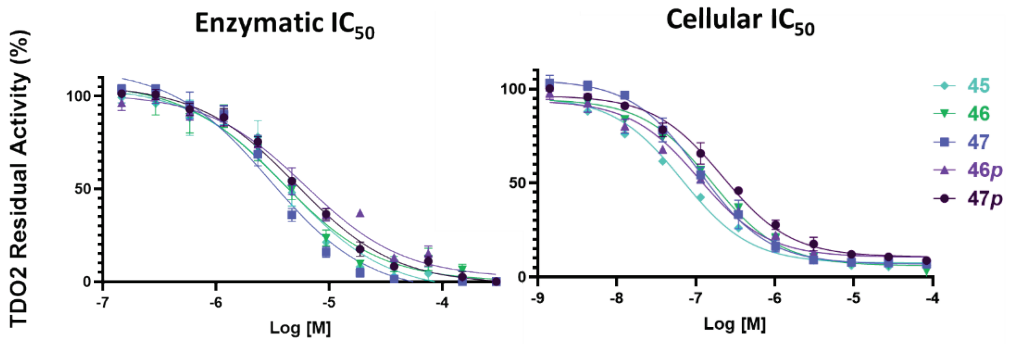

Figure 37. IC_{50} curves of inhibitors on TDO2. Data was obtained in quadruplicates in at least two separate experiments and analysed with GraphPad Prism 8.

S to Se replacement even allowed a slight affinity gain even though the lipophilicity decreased between **46** and **47**. Interestingly, none of the compounds could inhibit IDO1 (**Table 14**), suggesting that the observed inhibition of TDO2 did not stem from a non-specific effect, such as oxidation of the heme prosthetic group or by unspecific binding. Of note, the latter mechanism was reported for **ebselen**, which inhibits IDO1 by binding to several cysteine residues with an apparent inhibition constant of 94 +/- 17 nM .[259,335]

Table 14. Enzymatic and cellular inhibition values on TDO2 and experimentally determined Log K_w (methanol/water), calculated LogP and microsomal stability half-lives.

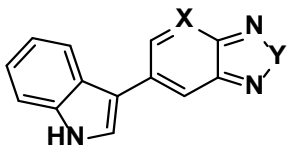

N°	X	Y	TDO2 IC_{50}[a] (μM) Enz.	TDO2 IC_{50}[a] (μM) Cell.	IDO1 IC_{50}[a] (μM) Enz. / Cell.	Log K_w[b]	*c*LogP[c]	Microsomal stability half-life (min.)
45	CH	O	[3.4 – 5.6]	[0.051 – 0.088]	> 100	4.1	3.41 (3.07)	[24.6 – 28.1]
46	CH	S	[3.0 – 4.9]	[0.129 – 0.199]	> 100	4.1	3.64 (3.86)	[35.6 – 50.1]
46p	N	S	[4.7 – 8.0]	[0.082 – 0.147]	> 100	3.6	2.83 (2.97)	[22.0 – 45.0]
47	CH	Se	[2.5 – 3.7]	[0.094 – 0.133]	> 100	3.6	3.10 (3.67)	[70.2 – 100.8]
47p	N	Se	[4.5 – 5.9]	[0.171 – 0.271]	> 100	3.2	2.36 (2.83)	[28.3 – 47.6]

[a] Reported 95 % confidence intervals IC_{50} values are calculated from measurements in triplicate. [b] Log K_w traces and stability curves can be found in supporting information (**Figure S2** and **S3**).[c] *c*LogP were calculated using ACD/Percepta 14.1.0 and Chemicalize (values reported in parenthesis).[336,337] [d] Reported 95 % confidence intervals for microsomal half-life were obtained in duplicates in two separate experiments. The error between two independent determinations is < 0,05 Log K*w* unit.

We next evaluated the impact of chalcogen substitution on lipophilicity. Very few lipophilicity-related experimental data are available for Se species, leading to potentially unreliable software predicted data. Such data are of great importance for the future discovery of novel drug-like Se compounds in medicinal chemistry. In a recent paper, the replacement of an OCF_3 moiety by SCF_3 or $SeCF_3$ resulted in a 0.5 logP-units increase in lipophilicity.[327] In another example of rhodamine derivatives, integration of Se lead to more hydrophilic compounds.[338] Thus, chalcogen replacement could prove helpful to modulate physicochemical properties and hence ADME parameters but still need further exemplification.[327]

To evaluate the impact of chalcogen replacement on lipophilicity, we performed an experimental determination of Log K_w and compared them to calculated LogP values using the Chemicalize software (ChemAxon). Determining the Log K_w index using reversed-phase high-performance liquid chromatography (RP-HPLC) is a rapid and convenient method to estimate a molecule's lipophilicity. Log K_w is performed by measuring a compound's retention time in multiple methanol/water mobiles phases (isocratic elution) on a C18 silanised silica gel column. The obtained retention values form a linear regression curve of which Log K_w is the intercept. Log K_w values usually have a very good correlation with the LogP value.[339–341]

We expected **45** to be the least hydrophobic compound due to its usually better capacity for hydrogen bonding. However, compounds **45** and **46** presented approximately the same Log K_w value of 4.1 (**Table 14**). Surprisingly, Se compounds resulted in a drop of around 0.5 LogK_w-units of lipophilicity in both **47** (Log K_w= 3.6) and **47*p*** (Log K_w= 3.2) compared to their S analogues **46** (Log K_w= 4.1) and **46*p*** (Log K_w= 3.6). This confirms that chalcogen replacement is a valid strategy to modulate the compound's lipophilicity but suggests that an increase in chalcogen size does not systematically lead to an increase in lipophilicity.

Interestingly, we found that the chalcogen atom replacement also had a significant impact on the microsomal stability (**Table 14**). Indeed, Se compound **47** was the most stable, with a half-life between 70.2 and 100.8 minutes, while the least stable

was O compound **45**. Pyridine analogues **46*p*** and **47*p*** showed a decrease of half-life compared to their parent compounds.

5.4. Cellular Toxicity Evaluation

Next, we evaluated the cellular toxicity of the synthesised analogues on three different TDO2 expressing cell lines using an MTS assay. We used P815B murine mastocytoma cell line, A172 human glioblastoma cell line and human embryonic kidney 293 cells, HEK293 (**Table 15**). The assay was performed after 6h of exposition to assess whether compound exposure caused acute cell death. Furthermore, 6h is also the duration of an IC50 cellular assay on P815B cells. Additionally, we also performed the assay after 24h of exposition.

Compounds **45**, **46** and **47** all demonstrated similar toxicity patterns in the MTS assay. However, in few conditions (P815B (24h) and HEK293), compound **47** displayed slightly more toxicity than the other two chalcogen derivatives. On the other hand, compounds **46*p*** and **47*p*** displayed almost no toxicity and were only toxic on P815B cells after 24h treatment at high concentrations (above 30 μM, more than 150-fold $IC50_{cell}$ value). Interestingly, the presence of Se in **47*p*** did not influence the toxicity pattern. Following these results, we decided to use P815B cells to evaluate whether cells died from apoptosis or necrosis and if the Se-containing compounds were responsible for ROS elevation.

Table 15. Toxicity of P815, A172 and HEK293 cell lines.

	LD50 (μM)[a]					
	P815B		**A172**		**HEK293**	
	6h	*24h*	*6h*	*24h*	*6h*	*24h*
45	[10 – 30]	[10 – 30]	[30 – 80]	[30 – 80]	> 80	> 80
46	[30 – 80]	[10 – 30]	[30 – 80]	[30 – 80]	> 80	> 80
46*p*	> 80	[30 – 80]	> 80	> 80	> 80	> 80
47	[30 – 80]	[3 – 10]	[30 – 80]	[30 – 80]	[30 – 80]	[10 – 30]
47*p*	> 80	[30 – 80]	> 80	> 80	> 80	> 80

[a]Values obtained using the MTS assay, performed in triplicates. The curves can be found in supporting information (**Figure S4**).

Following 24h of treatment with 1 and 10 μM of inhibitors (as well as 5 μM for **47**), we next analysed the cell death using Annexin V-FITC and propidium iodide (PI) staining followed with bi-parametric analysis by flow cytometry (FACS). As shown in **Figure 38a**, treatment with **47** at 10 μM caused an increase of cells undergoing a late apoptotic/necrotic cell death (Annexin V+/PI+, **Figure 38b**), while the other analogues did not increase cellular death at 1 μM and 10 μM (**Figure 38a**).

The same experiment was performed using shorter treatment times to assess whether we could see an early apoptosis population. We did not observe any elevation of cell death after 3 hours of treatment with 10 μM of compound **47**. However, after 6 hours, 30.4 % of cells were dead, with 27.6 % in the double-positive square, suggesting a necrosis-type cell death (**Figure S5**).

To investigate the underlying mechanism of this observed toxicity, we evaluated the impact of a 24h treatment of 5 μM of **47** on cell cycle distribution of P815B cells using PI DNA staining. The FACS analysis revealed that incubation of cells with **47** did not result in an arrest of the cell cycle in G1 or G2 phases, thus further indicating a necrosis-type cell death (**Figure 38c**).

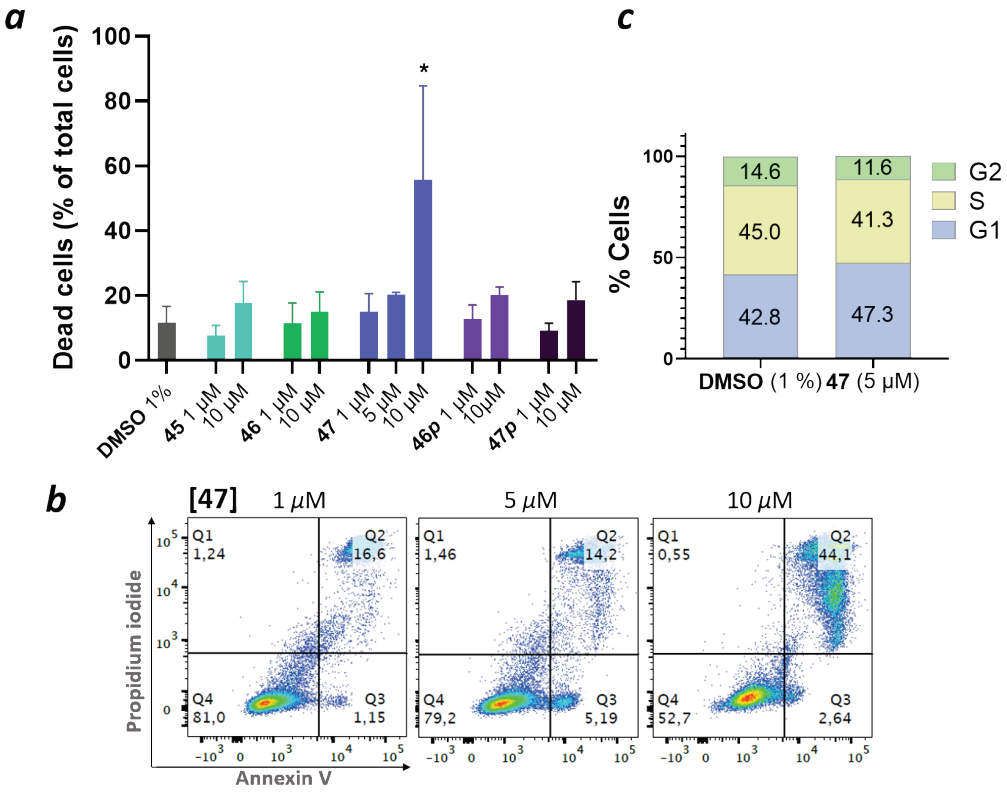

Figure 38. P815B cells were cultured with 1 to 10 μM of test compounds for 24h. Cells were double-stained with Annexin V-FITC/PI and analysed by flow cytometry. The percentages correspond to Annexin V and/or PI-positive cells (**a**). (**b**) Cell death induction by compound **47** in an Annexin V-FITC/PI assay (analysed by flow cytometry) on P815B cells after 24h of treatment. (**c**) Bar diagram of cell distribution in different phases (G2, S, G1) of the cell cycle after 24h of treatment. At 5 μM, **47** had very little influence on cell viability and cell cycle. *P<0.05 in regard to the negative control.

As Se compounds are known for their redox capacities, we decided to investigate whether the observed toxicity of **47** could be attributed to oxidative stress. Therefore, we performed an H_2O_2 production assay in a cellular environment to evaluate whether the present scaffold could generate ROS (**Figure 39**). We measured a slight elevation of H_2O_2 levels at high concentrations of both **47** and the non-toxic analogue **47*p***. Overall, these results suggest that, while compound **47** shows cellular toxicity at high concentration, this toxicity does not appear to be due to a non-specific redox effect of the Se as (i) the pyridine analogue (**47*p***) does not exhibit any similar toxicity and (ii) the toxicity does not seem to arise from ROS generation.

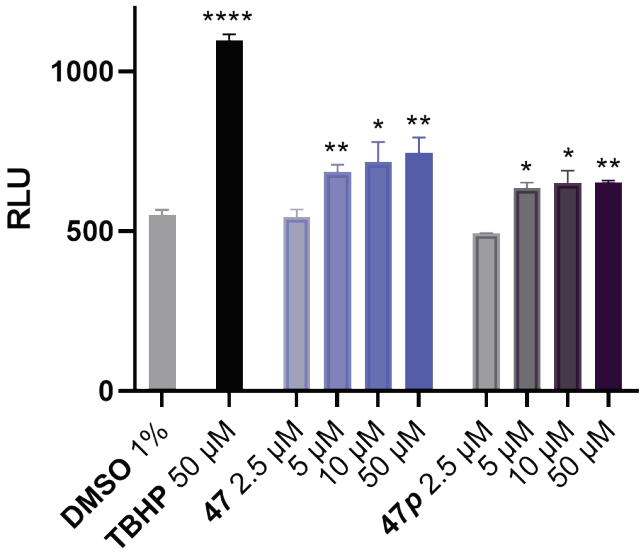

Figure 39. Production of ROS following treatment with Se compounds **47** and **47*p*** using the bioluminescent ROS-Glo™ H_2O_2 assay (Promega, USA). Data is shown in relative luminescence units (RLU). The assay was performed in triplicates in two separate experiments. tert-butylhydroperoxide (TBHP) was used as positive control. ****P<0.0001, **P<0.005, *P<0.05 in regard to the negative control.

5.5. Intermediate conclusion

In the work herein, we designed, synthesised and compared isosteric replacement of O, S and Se aryl-chalcogendiazoles on TDO2 inhibitors. We showed that chalcogen replacement did not significantly impact TDO2 affinity and that introducing a Se did not lead to unspecific inhibition of IDO1, an enzyme with a similar active site. Interestingly, Se substitution influenced the compound's lipophilicity and microsomal stability. In the present case, the two Se compounds were the least lipophilic and presented the most stable. Se compound **47** displayed more cellular toxicity than its O and S isosteres in all three evaluated cell lines. However, the observed toxicity occurred at a concentration close to 100 times above the IC_{50} value. Furthermore, this toxicity did not appear to be Se-related, as the second Se compound **47*p***, bearing a [1,2,5]selenadiazolo[3,4-*b*]pyridine instead of a benzo[*c*][1,2,5]selenadiazole, displayed the lowest toxicity in our experimental settings. Both Se compounds could only induce ROS at high concentrations, contrary to the common preconception regarding Se-containing molecules. These data suggest that liabilities observed at higher concentrations of **47** may not be solely attributed to the presence of Se or that Se-related toxicity is heavily dependent on the scaffold. The introduction of Se in drug-like structures should thus be worthy of consideration in medicinal chemistry designs, and new data of Se containing scaffolds are crucial for future lipophilicity and ADME/Tox predictions. Regarding the chemistry, it would give more insights into their synthetic

accessibility and reactivity. As of today, an increasing amount of publications seems to suggest that Se might someday be a part of the chemical drug space.

6. CONCLUSIONS AND PERSPECTIVES

6.1. General conclusion

Immunotherapy is now a well-accepted paradigm in cancer therapy but currently relies mainly on biologics. While very effective in some situations, these compounds exhibit several drawbacks, such as low cost-effectiveness, IRAEs issues and an inability to reach intracellular targets. Small molecules that selectively target cancer determinants could address these shortcomings. SMIs of immunosuppressive pathways have been the subject of intense research for the past decade. Among the explored immunosuppressive pathways, the KP and, more precisely, IDO1 probably attracted the most attention due to its immense involvement in establishing immune privilege.[218,342] However, the first clinical studies are dating back to the last decade. Early (pre)clinical data propelled the development of IDO1 inhibitors into a short-lived, fast-moving wave of excitement that ended quite abruptly around 2018 following the disappointing outcomes of the ECHO-301/KN-252 (**Epacadostat**/ **Pembrolizumab**) trial.[240] While cancer research needs to move at a fast pace, it should also follow sufficient rationale in the design of clinical trials. There is sufficient preclinical evidence suggesting that targeting L-Trp metabolism could benefit cancer treatment and multiple tracks left to explore regarding IDO1/TDO2 inhibition.[243]

In the present work, we presented the design, synthesis and pharmacological evaluation of a series of heterocyclic fused-cycle of TDO2 inhibitors.

Firstly, rigidified analogues of reference inhibitors **LM10** and **680C91** were synthesised and evaluated. The obtained compounds resulted in increased potency and higher hydrophobicity, especially when comparing **LM10** ($cLogD_{7.4}$ 0.15) and the benzotriazole compound **6** ($cLogD_{7.4}$ 3.01). Next, we functionalised the benzotriazole moiety in different positions on the nitrogen and the six membered-ring. The compounds were obtained following Suzuki-Miyaura type cross-couplings between the halogenated heterocycles and the indole bearing an appropriate boronic ester derivative. The resulting series of compounds presented a wide range of hydrophobicity and chemical functions. Pharmacological evaluation of this series demonstrated cellular activities ranging from low micromolar to the nanomolar range, which provided insights regarding their binding inside the TDO2 active site. For instance, we observed that the position of the N-sidechain impacted the inhibitor's activity. Generally, N_1-substituted compounds were more active. However, sidechains with H-bond donors presented a better activity when they were N_3-substituted. In both cases, STD-NMR suggested a more favourable placement of the indole moiety with N_1-substituted compounds. While the *N*-substituent did not appear to be useful for the interaction with *h*TDO2, its nature was determinant for microsomal stability. These results suggest that multiple other

modulations could be envisioned to fine-tune physicochemical and ADME properties of this series.

In the second part of this work, we substituted the benzotriazole moiety with benzoxazoles, benzothiadiazole, and benzoselenodiazole to investigate the potential of these scaffold for bioisosteric replacement. To our knowledge, although several chalcogen bioisosteric studies were published in the past few years due to a regain of interest for the inclusion of atypical elements in the chemical drug space, no studies provided a direct comparison of these moieties. We individually adapted the synthetic procedures to obtain these scaffolds, which demonstrated some differences in their respective reactivities. These compounds acted in the high nanomolar range in cells. While chalcogen replacement did not significatively impact the potency, it allowed to modulate the compounds' lipophilicity and microsomal stability. Se compound **47** had the longest microsomal half-life and was less hydrophobic than compounds **45** (O) and **46** (S). In the MTS cellular assay on three different cell lines, all the isosteres displayed toxicity far above their IC_{50} range. While Se compound **47** exhibited the highest toxicity, the other Se compound **47*p*** did not display the same toxicity pattern. When we evaluated cells treated with **47** in an Annexin V/PI assay, it appeared that cell death was occurring most probably by necrosis. Naturally, we suspected ROS production to be responsible for this toxicity. However, **47** was not a potent ROS inducer in our settings. These data suggest and reinforce other related studies that propose

that Se is worthy of consideration in medicinal chemistry and contribute to an unexplored research area regarding the integration of Se in drug-like structures.

Overall, this work extended the existing data and knowledge available regarding TDO2 inhibition and provided new perspectives for the therapeutic targeting of this enzyme. The following chapter encompasses some of the prospects that the present work unravelled.

6.2. Perspectives

6.2.1. Extension of the (iso)quinoline/(iso)quinazoline (680C91 analogues) series

Although the present work could not further develop the (iso)quinoline and quinazoline analogues series, these moieties offer many possibilities for functionalization and are very drug-like. Indeed, both of these heterocyclic scaffolds are considered to be “privileged scaffolds” in medicinal chemistry.[343,344] Meaning that they often appear in bioactive substances with widely distinctive therapeutic uses.[345,346] Privileged scaffolds were successfully used as the core structures for synthesis and optimal starting points for the library design of ligands with an affinity to certain molecular targets.[346] Consequently, synthetic pathways are particularly well established and allow an accessible functionalisation.[343] Thus, giving the opportunity to generate a new series of original compounds with potentially other insights regarding binding to TDO2 and PK/PD parameters. In our

case, apart from various N-alkylations, interesting functionalization would include the addition of hydrogen bond donors and acceptors, as well as halogenations.

6.2.2. Repurposing of the benzotriazole series – Design of bifunctional molecules

An interesting feature of the benzotriazole series resides in the high degree of substitution in N_1 and N_3 that can be accommodated by TDO2. Indeed, the N-sidechains do not appear to play a role in binding, as demonstrated by the SARs and supported by the STD-NMR and molecular modelling experiments. These N_1 and N_3 substitutions would be located outside the pocket and thus solvent-exposed. Therefore, such substitution could be used to graft a functional moiety to a linker and hence produce bifunctional compounds.

PROteolysis-TArgeting Chimeras (PROTACs) are an example of bifunctional molecules that could constitute an interesting way of repurposing the benzotriazole series. This strategy is continuously gaining attention both from academia and industry as a new way to inhibit challenging targets.[347,348] PROTACs are bifunctional hybrid molecules, in which a small molecule binder of a target protein is chemically linked to an E3 ubiquitin ligase-recruiting moiety.[349] By bridging a protein of interest to the E3 ubiquitin ligase, PROTACs engage the ubiquitin-proteasome system to degrade the protein of interest.[350] Because PROTACs function by degrading their target protein instead of inhibiting it, different kinds of resistance, such as target overexpression, could be conquered using this strategy.[348] Furthermore, compared

with the parent small-molecule that can only inhibit protein activity, PROTACs exhibit both enhanced potency and specificity.[351] Following promising efficacy data, the development of PROTACs is rapidly increasing, and the first clinical candidate (ARV-110) is currently recruiting for Phase 1/Phase 2 first-in-human PROTAC trial for the treatment of metastatic prostate cancer.[352]

Regarding this work, an E3 ligase warhead could be attached through N_1 or N_3 substitution to the benzotriazole TDO2 inhibitors synthesised during this project. Synthesizing such compounds could allow us to explore the PROTAC strategy for TDO2 (**Figure 40**). The use of PROTACs on TDO2 could increase serum L-Trp concentrations more drastically than an SMI and thus lead to a better anti-tumour immune response. Especially in combination with an ICI.[222]

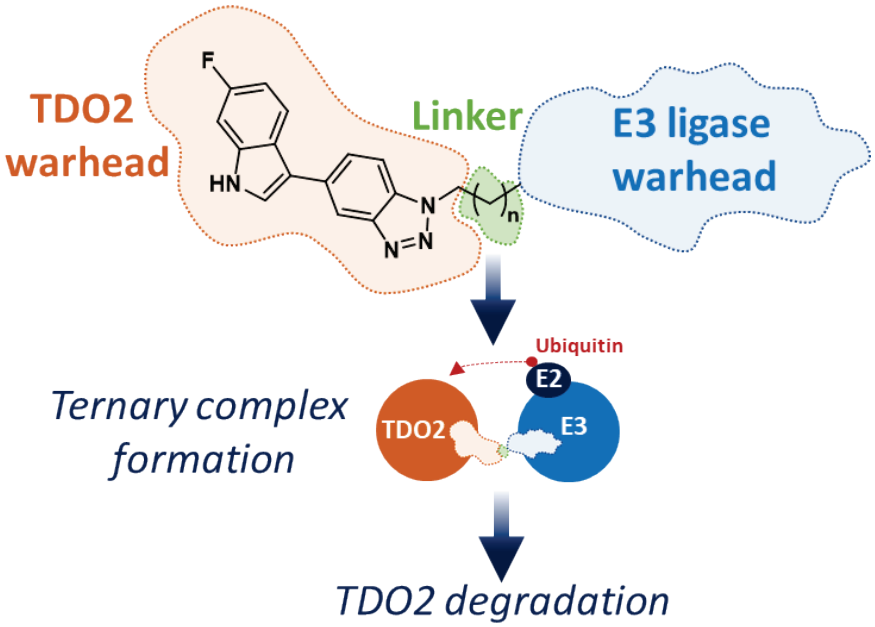

Figure 40. Application of the PROTAC strategy to the benzotriazole inhibitors series.

6.2.3. Biophysical assay development: application of microscale thermophoresis (MST)

The *in vitro* evaluation of the compounds presented in this work relied on their ability to inhibit TDO2 catalytic activity in our biochemical assay. However, this bioassay does not reflect physiological conditions as it imposes a non-physiological redox cycling to TDO2 using L-ascorbate, methylene blue and catalase. This system appears flawed as TDO2 seems to quickly lose its catalytic activity in this buffer, despite no modifications of its nanoDSF pattern. This could suggest that TDO2 does not efficiently regenerate its ferrous form after its catalytic cycle. Besides, TDO2 activity appears to be highly sensitive to the amount of co-solvent we put in solution, which might further hinder the reliability of the enzymatic assays. Moreover, catalytic activity is only a proxy of a compound potency, and many parameters unrelated to a compound affinity can affect protein activity in an *in vitro* assay. In this context, it would be interesting to study the binding of the benzotriazole series to TDO2 to obtain dissociation constants (K_ds) instead of IC_{50}s.

Microscale thermophoresis (MST) is a biophysical technique that relies on the change of the thermophoretic mobility of a fluorescently labelled protein upon binding of a ligand.[353] MST experiments were already performed on IDO1 and provided insights into the binding properties of inhibitors to the ferric form of IDO1,

offering novel clues for future development of more efficient IDO1 inhibitors.[354] We attempted to develop an MST biophysical assay on TDO2 to evaluate the K_d of the different inhibitors. While we obtained convincing results regarding the interaction of TDO2 and L-Trp (**Figure 41a**), we did not achieve to obtain a consistent K_d of the different inhibitors due to a poor signal-to-noise ratio (S/N). Further evaluation revealed that this poor S/N could result from TDO2 inhomogeneity in the biophysical assay. Indeed, mass photometry experiments (**Figure 41b**), as well as analysis of the protein Soret band (**Figure 41c**), revealed that TDO2 behaved as a mixture of tetramer and dimer in solution, partly due to incomplete heme integration. In future steps, homogenization of recombinant TDO2 could prove to be a key parameter in developing biophysical assays towards a better understanding of TDO2 inhibitors.

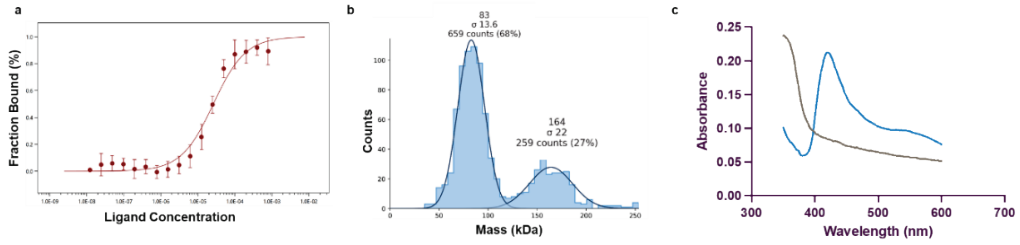

Figure 41. TDO2 inhomogeneity in solution hampers the development of biophysical assays. a) Evaluation of the K_d for L-Trp using MST at a 10 s "on time" (K_d = 23μM +/- 5 μM). b) Mass photometry of TDO2 in solution without heme, with the calculated molecular weights of the complex in solution and their relative intensity indicated above the peaks (theoretical molecular weight of the monomer is 46 kDa). c) Absorbance of TDO2 with (blue) or without (grey) the addition of heme.

7. Experimental section

7.1. Molecular docking

Molecular docking jobs were performed with AutodockVina 1.1.2,[355] using the disclosed tryptophan 2,3-dioxygenase structure (PDB ID: 5TI9) with the orthosteric binding site occupied by natural ligand tryptophan, heme and dioxygen. This structure was chosen as it displayed the full 338-346 loop that is part of this binding site. Hydrogens and charges were added, then L-Trp and dioxygen were removed, centring the searching box 15 Å around this region. During the process, sidechain flexibility was allowed for several residues of the binding site and later only for the Arg144 that appeared critical for accommodating compounds bearing bigger N-substituents. Binding poses were analysed for their binding mode and assessed in comparison with crystallised analogue and with L-Trp.

7.2. Protein Expression and Purification

The sequence of the truncated form of *h*TDO2 in which 1–17 and 389–406 fragments were deleted (**His6Thrb-TDO2tr)**, [205] described by Batabyal and Yeh, was inserted in a pET-28 plasmid, ordered from Genecust. The recombinant plasmid was transferred into the *E. coli* strain BL21 (DE3) (Rosetta). The transformant was selected from a single colony on an LB kanamycin agar plate and was used to

inoculate an LB medium (50 μg/mL kanamycin and 34 μg/mL chloramphenicol) and were cultured at 37 °C until an optical density of 0.6 was reached. The expression of *h*TDO2 was induced by isopropyl 1-thio β galacto-pyranoside (IPTG), with a final concentration of 1 mM. An aliquot of hemin in NaOH 0.5M, with a final concentration of 8–10 µM, was added to the culture. The culture was grown at 20 °C for 20 h. Cells were harvested by centrifugation at 5000 rpm, 4 °C for 25 min. Cell pellets were resuspended in a lysis buffer (Tris-HCl 50 mM, pH 8.5, $MgCl_2$ 10 mM, NaCl 300 mM, imidazole 5 mM, and glycerol 10%) supplemented with protease inhibitors (Roche) and then disrupted by sonication, followed by centrifugation at 4 °C, 10 000 rpm for 30 min. The supernatant was collected, and 1 μL/mL of supernatant of β-mercaptoethanol was added before loading onto 1 mL of His-trap FF-crude columns (GE Healthcare) according to the manufacturer's instructions. Protein concentrations were measured using the Bradford method with the Biorad protein assay kit, and sample homogeneity was assessed using sulfate−polyacrylamide gel electrophoresis (SDS−PAGE) with Coomassie brilliant blue as a staining agent. Purified TDO2tr was then dialysed overnight in a pH 7.6 buffer containing 50mM sodium phosphate, 100mM NaCl, 20% glycerol and 10mM L-Trp.

7.3. Nano differential scanning fluorimetry (NanoDSF)

NanoDSF experiments were performed on a Tycho NT.6 device (NanoTemper Technologies). According to the standard manufacturer's procedures, samples were poured into capillaries and heated up to 95 °C in 3 min while following fluorescence emission at 330 and 350 nm. Melting temperatures were extracted from the derivative of the 350/330 nm fluorescence ratios upon increasing temperature.

7.4. Nuclear Magnetic Resonance STD experiments

All experiments were performed at 277K on a Bruker Ascend Avance III 600 MHz system equipped with a broadband cryoprobe (Bruker). For 1D Saturation transfer difference (STD) studies, samples were prepared at 200 μM in PBS with 5% deuterated methanol. The concentration of *h*TDO2$_{tr}$ was 15 µM. Ligand binding was detected using an STD stddiffesgp.3 sequence with a 2s saturation time. Water signal suppression was achieved using an excitation-sculpting scheme, and a 50 ms spinlock was used to suppress protein background signals. For each experiment, 2048 scans were collected for on- and off-resonance experiments (respectively at 0 and 40 ppm) to achieve a sufficient signal to noise ratio for the epitope mapping.

7.5. Enzymatic Assay

All the graphs were obtained with GraphPadPrism 8 software (San Diego, CA). The UV spectra were recorded at room temperature on a Spectramax® M2E spectrophotometer (Molecular Devices, LLC, Sunnyvale, CA) in 96-well flat-bottom plates. The assay was initiated by adding 15 μL of buffer containing approximately 80 nM of *h*TDO2$_{tr}$ (no L-Trp, no DMSO) to 85 μL of buffer (with L-Trp and the tested inhibitor concentration in DMSO). After 15 minutes, 20 μL 30 % m/v of trichloroacetic acid (TCA) in water were added and the plates were heated at 65°C for 15 minutes. Then, 100 μL of a 2% m/v DMAB solution in pure acetic acid was added to each well. After 10 minutes, absorbance reading was performed at 490 nM.

For testing against IDO1, 30 nM of purified *h*IDO1 were used, and the incubation time was shortened to 8 minutes before quenching with TCA to remain under initial velocity conditions.

7.6. Cellular Assays

Cells were cultured in Gibco Iscove's Modified Eagle Medium (DMEM) supplemented with 10 % of fetal bovine serum (FBS), GlutaMAX™ (Thermo Fisher Scientific) and PenStrep (Gibco) at 37°C and 5 % CO_2.

7.6.1. Measurement of IC_{50} values

The assay was performed in 96-well flat-bottom plates seeded with 1×10^5 cells (P815B-hTDO2, clone 19) in a final volume of 200 μL of Iscove's modified Dulbecco medium (80 mmol/L Trp) supplemented with 2% FCS in the presence of the TDO2 inhibitor at different concentrations (1–25,000 nM) for 7 hours when substrate consumption was below 25 %. Cells were centrifuged 10 min at 300 RCF, after what 60 μL of supernatant were collected and mixed with 60 μL of 12% (wt/vol) trichloroacetic acid. After centrifugation at 4°C, 23000 RCF, 70 μL of supernatant was diluted with 70 μL of HPLC grade H_2O. The resulting solution was used to quantify L-Trp and L-Kyn concentrations by ultra-performance liquid chromatography (UPLC) based on the retention time and the UV absorption.

The same protocol was applied for *h*IDO1 counter-screening (P815B-*h*IDO1), but the plates were seeded with 2×10^5 cells and incubated for 24h to achieve a similar L-Trp consumption.

7.6.2. MTS-PMS toxicity assay

The effect of the compounds on cancer cell viability was determined by the MTS assay uptake method. Briefly, after incubation for the appropriate amount of time (6 and 24h), 21 μL (20 μL of PMS and 1 μL of MTS) were added to well containing the cells in 200 μL in DMEM containing 5% of FBS and different concentrations of test compounds in triplicates (HEK293 cells were seeded at 30.000 cells/well, A172

at 20.000 cells/well and P815B at 50.000 cells/well). Then, the cells were incubated until complete development of the colouration (usually around 2 to 4 hours) at 37 °C, absorbance at 490 nm was measured. Graphpad Prism software was used to calculate the residual viability of cells.

7.6.3. Cell cycle assay

Prior to the assay, the cells were deprived of serum for the duration of 1 cell cycle. The cells, cultivated in a 10 % FBS, GlutaMax (1X) + PenStrep (1X) IMDM medium were centrifuged and then re-suspended in 0% FCS + PenStrep (1X) IMDM medium. Following serum starvation, cells were harvested, centrifuged for 5 min. at 300 RCF and resuspended in 10 % FBS, GlutaMax (1X) + PenStrep (1X) IMDM medium (300 000 cells/mL). The cells were plated in 6-well flat-bottom plates (5 mL/well), and 50 μL of DMSO (with or without test compound) were added. After the appropriate incubation time, $5x10^5$ cells were harvested from each well, transferred into 15 mL tubes, centrifuged at 300 RCF for 5 min., washed with PBS and centrifuged again. The pellet was resuspended with 200 μL PBS and fixated by gradually adding 800 μL of cold (-20°C) 70% EtOH absolute while vortexing at the lowest speed. The samples were either stored at -20°C awaiting FACS analysis. Fixed cells were washed with 1× PBS and suspended in 200 μL PI staining solution (40 μg of DNase-free RNase A and 14 μg of PI in PBS). After staining for 15 min in the dark at r.t., the cells were analysed by a BD FACSVerse (BD Biosciences) for total DNA content.

7.6.4. Annexin V/PI assay

In a 12-well flat-bottom plate, cells were cultured in IMDM 5% FBS medium with 1 % DMSO (with or without test compound) for the desired time: $4x10^5$ in 2.5 mL. Following incubation, $1x10^6$ cells were washed 2X with annexin binding buffer (BD Biosciences Pharmingen), then resuspended in annexin binding buffer (final concentration of $1x10^6$ cells/mL). 100 μL of the cell suspension was transferred into a 1.5 mL tube, and 5 μL of FITC Annexin V (Biolegend) and 10 μL of PI solution (Sigma) were added. The resulting mix was gently vortexed and incubated in the dark at room temperature. 400 μL were added to each tube, and analysis by FACS was performed.

7.6.5. ROS-Glo™ assay

The detection of ROS was performed according to the manufacturer protocol of ROS-Glo™ bioluminescent assay (Promega). Briefly, the assay was performed in a white opaque 96-well flat-bottom plate, in which cells were suspended in IMDM and desired compound (final DMSO concentration 1%) in a total volume of 80 μL. Then, 20 μL of H_2O_2 substrate were added. After incubation for the desired time (at 37°C, 5% $CO)_2$, 100 μL of ROS-Glo detection solution was added in each well. The final mix was incubated for 20 minutes at r.t. before recording the relative luminescence units.

7.7. Microsomal stability assay

Liver microsomes (20 mg protein/ml), NADPH regenerating system solutions A & B and 10 mM stock compound solution (100% DMSO) are prepared. The reaction mixture finally contains 713 µL purified water, 200 µL 0.5 M potassium phosphate pH 7.4, 50 µL NADPH regenerating system solution A (BD Biosciences Cat. No. 451220), 10 µL NADPH regenerating system solution B (BD Biosciences Cat. No. 451200) and 2 µL of the compound stock solution (10 µM final concentration). A control experiment was realised for each compound by substituting NADPH regenerating solutions A and B for 60 μl of purified water. The reaction mixture is warmed to 37°C for 5 minutes in a water bath, and the reaction is initiated by the addition of 25 µL of liver microsomes (0.5 mg protein/ml final concentration). At different time points (0 min –60 min –180 min – 360 min – 24h), 100 µL is withdrawn and added to 400 µL cold acetonitrile on ice. Then the mixtures are centrifuged at 13 000 rpm for 5 min at 4°C. Finally, 450μl of the supernatant is recovered, evaporated using a speedvac and evaluated by UPLC. 7-Ethoxycoumarine was used as a positive control.

7.8. Chemistry

7.8.1. Chemicals and Reagents

All chemical reagents and solvents were used as obtained from various commercial sources (Merck/Sigma, Fluorochem, TCI, VWR) and were all used without further purification. Unless stated otherwise, reactions were performed under atmospheric pressure. Thin-layer chromatography (TLC) was performed using silica gel 60 F254 plates, with observation under UV at 254 and 366 nm Camag Lamp. For purification, flash-column chromatography on silica gel was performed. Compounds were characterised using ^{1}H and ^{13}C NMR, recorded on a 400 MHz Bruker Ultrashield Advance II spectrometer, and their spectra were analysed using the TopSpin 3.1. software. NMR analysis was performed in either $CDCl_3$, DMSO-*d6* or MeOD, all purchased from Eurisotop. Chemical shifts are in parts per million (ppm), coupling constants (J) are in hertz (Hz). Standard abbreviations indicating multiplicity were used as follows: s = singlet, d = doublet, t = triplet, dd = double doublet, q = quartet, qn= quintet, m = multiplet, br = broad. Melting ranges were determined using an electrothermal IA9000 apparatus are reported uncorrected. LC-MS analysis were performed on an Agilent 6200 series TOF mass spectrometer equipped with ESI and APCI as ionization sources and TOF (Time of Flight) detector, coupled with an Agilent 1200 series LC system with a flux of 0.25 mL/min. A C18 “brand” column was used. Water (A) and CH_3CN (B) were used as eluents. Both were prepared to contain a final concentration of 0.1 % of trifluoroacetic acid (TFA).

The wavelength for UV detection was 210, 230 and 254 nm. HPLC purities of final compounds that underwent biological assessment were ≥ 95%. High-resolution mass spectra were carried out on a Thermofisher Scientific LTQ-Orbitrap XL hybrid mass spectrometer (Thermo Fisher Scientific, Bremen, Germany).

7.8.2. Chemical synthesis

Content:

1. Synthesis of boronic esters

1.1. *tert-butyl 6-fluoro-3-(4,4,5,5-tetramethyl-1,3,2-dioxaborolan-2-yl)-1H-indole-1-carboxylate* (**41**)

- *tert-butyl 6-fluoro-1H-indole-1-carboxylate* (**41a**)

To a 0.4 M solution of 6-fluoro-1H-indole (4g, 29.62mmol, 1equi) in DCM at r.t. were added di-tert-butyl dicarbonate (8.4 g, 38.5 mmol, 1.3 equi), Et_3N (0.60 mg, 5.92 mmol, 0.2 equi) and 4-dimethylpyrridine (0.72g, 5.92mmol, 0.2 equi). The solution was stirred under atm. P for 3h, then washed with H_2O and Brine, dried with $MgSO_4$ and concentrated *in-vacuo*. The product **41a** was obtained as a orange/brown oil and was used without further purification. Quantitative yield. ^{1}H NMR (400MHz, $CDCl_3$): δ 1.70 (9H, s), 6.55 (1H, d, J=3,35Hz), 7.00 (1H, td, J=8.92Hz, J=2.37Hz), 7.49 (1H, dd, J=8.98Hz, J=5.45Hz), 7.59 (1H, d, J=3.12Hz), 7.90 (1H, d, J=8.50Hz). ^{13}C NMR (100 MHz,$CDCl_3$): δ 28.16 ; 84.09 ; 102.55 (d, J=28.18 Hz) ; 107.02 ; 110.91 (d, J=24,49 Hz) ; 121.46 (d, J=10.04 Hz) ; 126.19 ; 126.77 ; 135.35 (d, J=12.83 Hz) ; 149.54 ; 160.85 (d, J=238.88 Hz).

- *tert-butyl 3-bromo-6-fluoro-1H-indole-1-carboxylate* (**41b**)

To a 0.1 M solution of **41a** (6,97g, 29,62mmol, 1eq) in DCM was added N-bromosuccinimide (NBS) (6.85g, 38.50 mmol, 1.1 equi). The solution was stirred at atm. P. under reflux for 6h. 0.1 equi of NBS were added after 2h, 4h, and 5h (If added all at once, the reaction led to the formation of an undesired dibrominated compound). The reaction mixture was subsequently washed with H_2O, 1M NaOH and Brine, dried with $MgSO_4$ and concentrated in-vacuo. The obtained residue was crystallised in EtOH. Pink crystals. Yield: 80 %. ^{1}H NMR (400MHz, $CDCl_3$): δ 1.69 (9H, s), 7.08 (1H, td, J=8.81Hz, J=1.9Hz), 7.47 (1H, dd, J=8.56Hz, J=5.3Hz), 7.63 (1H, s), 7.91 (1H, s). ^{13}C NMR (100 MHz,$CDCl_3$): δ 28.11 ; 84.77 ; 97.59 ; 102.84 (d, J=29.07 Hz) ; 111.69 (d, J=24.70 Hz) ; 120.43 (d, J=10.03 Hz) ; 125.04 ; 125.74 ; 134.72 (d, J=11.67 Hz) ; 148.63 ; 161.57 (d, J=241.79 Hz).

- *tert-butyl 6-fluoro-3-(4,4,5,5-tetramethyl-1,3,2-dioxaborolan-2-yl)-1H-indole-1-carboxylate* (**41**)

In a flame-dried RB flask under N_2, tert-butyl 3-bromo-6-fluoro-1H-indole-1-carboxylate (**41b**) (6 g, 19,09 mmol, 1eq) was dissolved in dry THF (70 mL). The solution was stirred at -78°C several minutes before dropwise addition of n-BuLi (27,5mL of a 2.5M solution in hexanes, 68,75mmol, 3,6eq). After 30 min., a solution of bispinacolatodiboron (9,7g, 38,19mmol, 2eq) in 24mL of dry THF was added to the reaction mixture. After 3h, the reaction was quenched with saturated NH_4Cl_{aq}.The mixture was extracted 3x with EtOAc. The combined OL was washed with H2O and Brine, dried with Na_2SO_4 and concentrated in-vacuo. The residue was

purified by flash chromatography in Cyclohexane/EtOAc (9 :1). Optionally, when purity was insufficient, a crystallisation in MeOH was performed. White powder. Yield : 43 %. ^{1}H NMR (400MHz, $CDCl_3$): δ 1.39 (12H, s), 1.67 (9H, s), 7.03 (1H, td, J=9.00Hz, J=2.30Hz), 7.89 - 7.92 (2H, m), 7.99 (1H, s). ^{13}C NMR (100 MHz,$CDCl_3$): δ 24.90 ; 28.16 ; 83.47 ; 84.29 ; 102.26 (d, J=28.59Hz) ; 111.08 (d, J=23.83Hz) ; 123.23 (d, J=9.81Hz) ; 129.62 ; 135.53 (d, J=3.19 Hz); 136.26 (d, J=12.79Hz) ; 149.17 ; 160.85 (d, J=239.66Hz).

1.2. *1-(phenylsulfonyl)-3-(4,4,5,5-tetramethyl-1,3,2-dioxaborolan-2-yl)-1H-indole* (**42**).

- *3-bromo-1H-indole* (**42a**)

Indole (10 g, 85.36 mmol) was dissolved in 100 mL of pyridine. After what, pyridinium tribromide (1.25 eq, 34 g) in 100 mL pyridine was added dropwise using a dropping funnel and the reaction was left to stir for 1 hour. Next, ice water was added and the reaction mixture was extracted with Et_2O (3x). The OL was washed with 6N HCl and saturated $NaHCO_3$, dried with $MgSO_4$, filtered and concentrated *in vacuo* to afford 12.7 grams of (**42a**) as a beige powder, which was used as such in the next step. Yield= 76 %. ^{1}H-NMR (400 MHz, $CDCl_3$): δ 14.27 (bs, 1H), 9.03 (d, J= 5.34 Hz, 2H), 8.56 (t, J= 7.82 Hz, 1H), 8.10 (t, J= 6.94 Hz, 2H). EI-MS (m/z): 337 $[M]^+$

- *3-bromo-1-(phenylsulfonyl)-1H-indole* (**42b**)

A 2-necked round bottom (RB) flask was charged with 3-bromo-1H-indole (12.5 g, 63.77 mmol) and TBAHS (3.25 g, 9.56 mmol) in 300 mL toluene at 0°C. Next 300 mL of a 50 % aqueous NaOH solution and benzenesulfonyl chloride (16.9 g, 12.3 mL, 95.66 mmol) were added dropwise. The reaction mixture was left to stir at rt overnight. After TLC showed full conversion, the OL layer was separated, acidified with 1N HCl, neutralised with $NaHCO_3$, washed with brine, dried with Na_2SO_4 and concentrated in vacuo to be used as such. **42b** was obtained as a beige powder in quantitative yield. The compound is poorly stable, it was stored at -20°C in the dark and used <24h after synthesis. ^{1}H-NMR (400 MHz, $CDCl_3$): δ 7.35 (1H, t, J=7.45 Hz), 7.41 (1H, t, J=7.32 Hz), 7.48 (2H, t, J=7.77 Hz), 7.53 (1H, d, J=7.82 Hz), 7.58 (1H, t, J=7.46 Hz), 7.66 (1H, s), 7.92 (2H, d, J=7.61 Hz), 8.03 (1H, d, J=8.29 Hz). ^{13}C NMR (100 MHz, $CDCl_3$): δ 136.52; 134.91; 133.55; 130.02; 129.07; 126.82; 126.15; 125.63; 124.47; 119.77; 113.45; 98.92. EI-MS (m/z): 337 $[M]^+$

- *1-(phenylsulfonyl)-3-(4,4,5,5-tetramethyl-1,3,2-dioxaborolan-2-yl)-1H-indole* (**42**)

A RB flask was charged with 3-bromo-1-(phenylsulfonyl)-1H-indole (**42b**) (10 g, 29.76 mmol), bis(pinacolato)diboron (10.2 g, 40.18 mmol) and KOAc (8.8 g, 89.3 mmol) in 100 mL DMF. The reaction mixture was degassed for 20 min, after which

$Pd(dppf)Cl_2$ (659 mg, 3 mol%) was added. The reaction was stirred at 80°C overnight. After TLC showed full conversion, EtOAc was added and the mixture was filtered over a pad of celite. The OL was evaporated in vacuo. The crude product was purified using flash chromatography (hexane/EtOAc: 4/1) to obtain 7.7 g of the desired product (67 %). ^{1}H-NMR (400 MHz, $CDCl_3$): δ 1.26 (12H, s), 7.30 (2H, t, J=7.38 Hz), 7.36 (1H, d, J=7.96 Hz), 7.42 (3H, t, J=7.85 Hz), 7.46 – 7.54 (3H, m, J=7.27 Hz), 7.63 (1H, s), 7.88 (2H, d, J=7.73 Hz), 8.00 (1H, d, J=8.31 Hz). ^{13}C-NMR (100 MHz, $CDCl_3$): δ 25.04; 83.52; 99.84; 113.56; 120.11; 124.01; 124.72; 125.88; 126.85; 129.44; 134.18; 137.74.EI-MS (m/z): 383 $[M]^+$

1.3. *Synthesis of 1-(phenylsulfonyl)-3-indolylboronic acid MIDA ester (4-methyl-8-(1-(phenylsulfonyl)-1H-indol-3-yl)dihydro-4l4,8l4-[1,3,2]oxazaborolo[2,3-b][1,3,2]oxazaborole-2,6(3H,5H)-dione)* (**43**)

The synthesis was adapted from *J. Am. Chem. Soc.* 2009, 131, 20, 6961–6963. To a round-bottom flask equipped with a stir bar was added 1-(phenylsulfonyl)-3-indoleboronic acid (1 equi, 1 g, 3.32 mmol, purchased from Fluorochem), N-methyliminodiacetic acid (1.5 equi, 0.732 g, 4.96 mmol), toluene (21 mL) and DMSO (11 mL). The flask was fitted with a Dean-Stark trap and the Dean-Stark trap was fitted with a reflux condenser vented to ambient atmosphere. The stirred mixture was heated to reflux for 1h30, after what the reaction was complete. Toluene was evaporated *in vacuo*. The product was precipitated with cyclohexane and filtered over a glass filter funnel. The final compound was obtained as a white powder with 85 % yield. ^{1}H NMR (400MHz, $CDCl_3$): δ 2.56 (3H, s), 4.19 (2H, d, J=17.21 Hz), 4.39 (2H, d, J=17.25 Hz), 7.22 – 7.29 (1H, d, J=26.01 Hz), 7.32 (1H, t, J=7.62 Hz), 7.52 – 7.63 (3H, m), 7.69 (1H, t, J=7.30 Hz), 7.74 (1H, s), 7.90 (1H, d, J=8.16 Hz), 8.03 (2H, d, J=7.80 Hz). ^{13}C NMR (100MHz, $CDCl_3$): δ 47.76; 62.29; 113.51; 122.77; 123.94; 124.81; 127.27; 130.26; 132.54; 133.83; 135.10; 135.63; 137.40.

1.4. *Synthesis of 5-(4,4,5,5-tetramethyl-1,3,2-dioxaborolan-2-yl)benzo[c][1,2,5]thiadiazole* (**52**)

A flame dried two-necked RB flask under N_2 atmosphere was charged with 5-bromobenzo[*c*][1,2,5]thiadiazole (**48**) (2 g, 9.3 mmol, 1 eq.), Bis(pinacolato)diboron (4.7 g, 18.6 mmol, 2eq.) and potassium acetate (3 g, 30 mmol, 3 eq.). Then, 60 mL of dry DMF were added. After 5 minutes, $Pd(dppf)Cl_2$ (5 mol %, 340 mg) was added and the reaction was left under agitation overnight, at 80°C. The conversion was total. The reaction mixture was filtered on a celite pad and the filtrate was extracted with ethyl acetate and water. The OL was concentrated and the residue was purified by flash chromatography in a cyclohexane/ethyl acetate gradient. Yield: 68 %. ^{1}H RMN (400MHz, DMSO) : δ 1.35 (12H, s), 7.86 (1H, d, J=8.80 Hz), 8.08

(1H, d, J=8.80 Hz), 8.34 (1H, s). ^{13}C RMN (100 MHz, DMSO): δ 25.14; 84.87; 121.39; 128.95; 133.84; 154.39; 155.95.

2. Synthesis of N-substituted benzotriazoles

2.1. *Bromo-1-(4-methoxybenzyl)-1H-benzo[d][1,2,3]triazole*

- *6-bromo-1H-benzo[d][1,2,3]triazole*

4-bromobenzene-1,2-diamine (1 g, 5.35 mmol) was dissolved in 10 mL of glacial acetic acid, to this solution were added 2.5 equivalents of $NaNO_2$ (0.92 g, 13.35 mmol) and the resulting mixture was sonicated for 20 minutes. The reaction mixture is poured onto H_2O and the off-white precipitate was filtered and washed with H_2O until neutrality. Yield: 86 %. ^{1}H NMR (400MHz, $CDCl_3$): δ 7.57 (1H, dd, J=1.29, 8.76 Hz), 7.91 (1H, d, J=8.75 Hz), 8.21 (1H, s).

- *6-bromo-1-(4-methoxybenzyl)-1H-benzo[d][1,2,3]triazole + 5-bromo-1-(4-methoxybenzyl)-1H-benzo[d][1,2,3]triazole (***6b***)*

6-bromo-1H-benzo[d][1,2,3]triazole (396mg ,2 mmol), was dissolved in 20 mL DMF. To this solution were added 4-methoxybenzyl chloride (0.6 mL, 2.2 equi), TBAB (130 mg, 0.2 equi) and NaH 60% (168 mg, 2.1 equi). Agitated overnight at atm. P. and r.t. After completion, saturated NH_4Cl_{aq} was added and the mixture was extracted with EtOAc. The combined OL was washed with $CuSO_{4(aq)}$ and Brine, dried with Na_2SO_4 and concentrated *in vacuo*. The residue was purified by flash chromatography (Cyclohexane/EtOAc 4:1). The product is obtained as a mix of two regioisomers that co-elute. ^{1}H NMR (400MHz, $CDCl_3$): δ 3.79 (6H, d, J=3.90 Hz), 5.75 (4H, d, J=11.92 Hz), 6.87 (4H, dd, J=6.44, 8.41 Hz), 7.20 – 7.26 (m), 7.44 (1H, dd, J=1.45, 8.80 Hz), 7.47 (1H, dd, J=1.51, 8.78 Hz), 7.54 (1H, s), 7.92 (1H, d, J=8.78 Hz), 8.21 (1H, d, J=0.86 Hz).

2.2. *Synthesis of N-methylated 6-chloro-1H-benzo[d][1,2,3]triazoles (***7b**, **8b**, **9b***)*

The procedure previously described by *Carta et al.* in *Heterocycles, 65(10), 2471-2481; 2005*

The commercially available 5-Chlorobenzotriazole (CAS = 94-97-3, 10 mmol) was dissolved in 25 mL of $NaOH_{aq}$ 2M. 1.6 equi. of Me_2SO_4 (16 mmol) were added. The reaction mixture was agitated at room temperature for 1h30. The product gradually appeared in the form of an off-white precipitate and contained 3 N-methylated regioisomers. A flash chromatography was performed using cyclohexane/EtOAc (4:1) as eluent. The structures were confirmed using diffraction X-Ray crystallography. Compounds eluted in the following order:

- *5-chloro-2-methyl-2H-benzo[d][1,2,3]triazole* (**7b**)

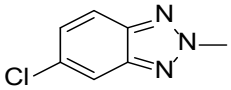

^{1}H-NMR (400 MHz, $CDCl_3$): δ 4.50 (3H, s), 7.33 (1H, dd, J=1.73, 9.03 Hz), 7.78 (1H, d, J=9.04 Hz), 7.84 (1H, d, J=1.11 Hz). ^{13}C-NMR (100 MHz, $CDCl_3$): δ 43.37 ; 116.96 ; 119.06 ; 127.82 ; 132.13; 143.01; 144.87. White powder. Yield = 23 %. Melting point = 57°C

- *6-chloro-1-methyl-1H-benzo[d][1,2,3]triazole* (**8b**)

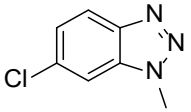

^{1}H-NMR (400 MHz, $CDCl_3$) δ 4.28 (3H, s), 7.33 (1H, dd, J=1.58, 8.83 Hz), 7.53 (1H, d, J=0.99 Hz), 7.97 (1H, d, J=8.83 Hz). ^{13}C-NMR (100 MHz, $CDCl_3$) δ 34,36 ; 112,20 ; 121,14 ; 121,65 ; 127,61 ; 134,51 ; 144,78. White powder. Yield = 31 %. Melting point = 120°C

- *5-chloro-1-methyl-1H-benzo[d][1,2,3]triazole* (**9b**)

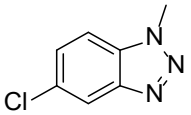

^{1}H-NMR (400 MHz, $CDCl_3$): δ 4.30 (3H, s), 7.46 (2H, d, J=1.18 Hz), 8.01 – 8.05 (1H, m). ^{13}C-NMR (100 MHz, $CDCl_3$): δ 34.49; 110.14; 119.31; 128.32; 129.84; 132.18 ; 146.53. White powder.Yield = 27 %. Melting point = 85°C

2.3. *2-(5-chloro-1H-benzo[d][1,2,3]triazol-1-yl)acetonitrile & 2-(6-chloro-1H-benzo[d][1,2,3]triazol-1-yl)acetonitrile* (**21b**, **22b**)

The commercially available 5-Chlorobenzotriazole (CAS = 94-97-3, 20 mmol) was dissolved in anhydrous DMF (30 mL). Triethylamine (22.86 mmol, 3.81 mL) and chloroacetonitrile (31.26 mmol, 2mL) were added and the reaction was refluxed overnight (16h). The solution was basified to remove unreacted 5-Chlorobenzotriazole and the desired product was extracted using EtOAc. A column was performed using a gradient of Cyclohexane/EtOAc (1:0 ➔ 3:1) as both products have very similar *R*f values. The compounds eluted in the following order: **21b** then **22b**. However, a significant number of fractions contained both products. Each product was crystallised in the same conditions: Cyclohexane was added to the obtained powder and heated until boiling. EtOAc was gradually added until complete dissolution.

While conversion was total, reported yields are low due to purification process. Structures were confirmed with NOESY-NMR and X-ray diffraction crystallography.

- *2-(6-chloro-1H-benzo[d][1,2,3]triazol-1-yl)acetonitrile* (**21b**)

Crystals were obtained as white long needles. Yield= 15 %. ^{1}H-NMR (400 MHz, $CDCl_3$) δ 8.06 (d, J= 8.84 Hz, 1H), 7.70 (d, J= 0.83 Hz, 1H), 7.45 (dd, J= 8.84, 3.44 Hz, 1H), 5.59 (s, 2H). ^{13}C-NMR (100 MHz, $CDCl_3$) δ 35.77; 108.69; 112.07; 121.69; 126.36; 132.85; 135.71; 144.84.

- *2-(5-chloro-1H-benzo[d][1,2,3]triazol-1-yl)acetonitrile* (**22b**)

Crystals were obtained as white flakes. Yield= 10 %. ^{1}H-NMR (400 MHz, DMSO) δ 8.31 (d, J= 0.82 Hz, 1H), 8.04 (d, J= 8.85 Hz, 1H), 7.74 (dd, J= 8.82, 3.43 Hz, 1H), 6.20 (s, 2H). ^{13}C-NMR (100 MHz, DMSO) *δ 36.42; 112.59; 115.37; 119.37; 129.49; 129.88; 131.89; 146.22.*

2.4. Substituted benzotriazoles synthesised from 4-bromo-1-fluoro-2-nitrobenzene or 4-bromo-2-fluoro-1-nitrobenzene

General procedure: The N-substituted benzotriazoles (**18d–40d**) were synthesised using the following three-step general procedure. (**Step 1**) To a 0.5 M solution of 4-bromo-1-fluoro-2-nitrobenzene or 4-bromo-2-fluoro-1-nitrobenzene (1 equiv) in ethanol was added the primary amine (1.5 equiv) and triethylamine (2 equiv). The resulting mixture was stirred under reflux until complete conversion (30 min to 16 h), before being evaporated in vacuo. The residue was extracted using EtOAc and water, and the organic layer was dried with Na_2SO_4 and concentrated to afford the desired compound, used in the next step without further purification (unless stated otherwise). (**Step 2**) The nitro group of N-substituted 4-bromo-2-nitroaniline or 5-bromo-2-nitroaniline (1 equiv) obtained in step A was reduced into an amine using iron powder (10 equiv) in a mixture of $NH_4Cl_{sat.}$/EtOH (1:4) stirred under reflux for 30 min to 16 h. Upon complete conversion, the reaction mixture was filtrated over a celite pad, washed with EtOAc. After extraction, the organic layer was dried over Na_2SO_4 and concentrated in vacuo. Unless stated otherwise, the obtained residue was used for step C without further purification. (**Step 3**) The cyclization of mono-N-substituted 4-bromobenzene-1, 2-diamine or 5-bromobenzene-1, 2-diamine was performed using $NaNO_2$ in acetic acid using a sonication bath for 30 min to 1 h. The reaction mixture was then poured onto ice water and extracted with EtOAc. The combined organic layers were washed with saturated Na_2CO_3 solution and brine, dried with Na_2SO_4, and concentrated *in vacuo*. The N-substituted benzotriazole was

purified using flash chromatography on silica gel with an EtOAc/cyclohexane gradient.

2.4.1. N-substituted benzotriazoles obtained starting from 4-Bromo-1-fluoro-2-nitrobenzene [CAS 364-73-8]:

- *5-bromo-1-(2,2,2-trifluoroethyl)-1H-benzo[d][1,2,3]triazole (***18d***)*

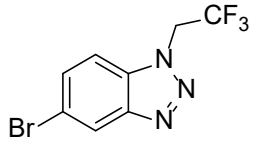

- *4-bromo-2-nitro-N-(2,2,2-trifluoroethyl)aniline (***18b***)*: 4-Bromo-1-fluoro-2-nitrobenzene (500 mg, 2.27 mmol) and trifluoroethanolamine.HCl were dissolved in anhydrous THF (4mL) and DIEA (1.16 mL, 6.82 mmol) under N_2. The resulting mixture was refluxed for 16h. After cooling to room temperature, the solvent was removed *in-vacuo*. Then, the residue was resuspended in 10 mL water and extracted 3 times with EtOAc. The OL was dried with Na_2SO_4 and evaporated to yield 620 mg (2.07 mmol) of a bright yellow powder containing **19b**. Yield = 91 % Used without further purification in the next step. ^{1}H-NMR (400 MHz, $CDCl_3$): δ 3.98 (2H, qn, J=8.12 Hz), 6.88 (1H, d, J=9.12 Hz), 7.59 (1H, dd, J=2.09, 9.11 Hz), 8.21 (1H, dd, J=2.35, 6.51 Hz), 8.36 (1H, d, J=2.23 Hz).

- *4-bromo-N^1-(2,2,2-trifluoroethyl)benzene-1,2-diamine (***18c***)*. Obtained following the general reduction procedure. After evaporation, the crude extract was immediately engaged in the next step.

- *5-bromo-1-(2,2,2-trifluoroethyl)-1H-benzo[d][1,2,3]triazole (***18d***)* was obtained using the general procedure. Flash chromatography purification: Cyclohexane/EtOAc (9:1). Beige powder. Yield over two steps: 60 %. 5.27 – 5.15 (m, 2H), 7.56 (d, J= 8.72 Hz, 1H), 7.78 (s, 1H), 7.99 (d, J= 8.76 Hz, 1H). ^{13}C-NMR (100 MHz, $CDCl_3$) δ 49.23 & 49.60 (-**C**F_3); 110.40; 117.96; 123.13; 132.12; 132.24; 147.26. Yield: 56 %.

- *5-bromo-1-(cyclopropylmethyl)-1H-benzo[d][1,2,3]triazole (***20d***)*

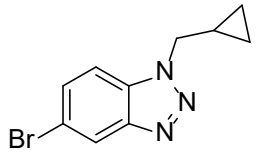

- *4-bromo-N-(cyclopropylmethyl)-2-nitroaniline (***20b***)* was synthesised according to the general procedure using *cyclopropylmethanamine*. Quantitative yield.

Obtained as a bright orange oil. ^{1}H-NMR (400 MHz, $CDCl_3$): δ 0.35 – 0.30 (m, 2H), 0.69 – 0.63 (m, 2H), 1.21 – 1.14 (m, 1H), 3.14 (dd, J= 6.37, 5.41 Hz), 6.73 (d, J= 9.16 Hz, 1H), 7.48 (d, J= 9.16 Hz, 1H), 8.11 (bs, 1H), 8.32 (s, 1H). ^{13}C-NMR (100 MHz, $CDCl_3$): 48.18; 106.24; 115.60; 128.94; 138.90.

- *4-bromo-N1-(cyclopropylmethyl)benzene-1,2-diamine (***20c***).* Obtained by reducing **20b** using the general procedure, reaction time= 1h. The crude extract was immediately used in the following step.

- *5-bromo-1-(cyclopropylmethyl)-1H-benzo[d][1,2,3]triazole (***20d***)* was obtained by using the general cyclisation procedure. Reaction time= 30 min. The compound was purified using flash chromatography (cyclohexane/EtOAc 3:1) and obtained as a dark red oil that solidified overnight. Yield over two steps = 62 %. ^{1}H-NMR (400 MHz, $CDCl_3$): δ 8.23 (s, 1H), 7.59 (dd, J= 8.75, 1.13 Hz, 1H), 7.47 (d, J= 8.76 Hz, 1H), 4.51 (d, J= 7.11 Hz, 2H), 1.42 – 1.35 (m, 1H), 0.70 – 0.66 (m, 2H), 0.52 – 0.47 (m, 2H). ^{13}C-NMR (100 MHz, $CDCl_3$): δ 3.83; 10.27; 48.18; 106.24; 115.60; 128.94; 138.90.

- *2-(5-bromo-1H-benzo[d][1,2,3]triazol-1-yl)-N,N-dimethylethan-1-amine (**26d**)*

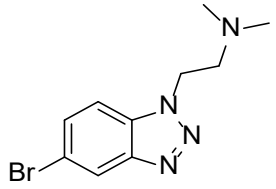

*N^1-(4-bromo-2-nitrophenyl)-N^2,N^2-dimethylethane-1,2-diamine (***26b***)* was synthesised according to the general procedure using *N^1,N^1-dimethylethane-1,2-diamine*. Yield: 84%. Orange powder. ^{1}H NMR (400MHz, $CDCl_3$): δ 2.30 (6H, s), 2.63 (2H, t, J=6.18 Hz), 3.32 (2H, dd, J=5.92, 11.05 Hz), 6.74 (1H, d, J=9.16 Hz), 7.48 (1H, dd, J=2.09, 9.13 Hz), 8.28 – 8.38 (2H, m). ^{13}C NMR (100MHz, $CDCl_3$): δ 40.77; 45.26; 57.20; 106.08; 115.71; 128.92; 132.21; 138.80; 144.27.

*4-bromo-N1-(2-(dimethylamino)ethyl)benzene-1,2-diamine (***26c***)* Obtained by reducing **26b** using the general procedure. The crude extract was immediately used in the following step.

*2-(5-bromo-1H-benzo[d][1,2,3]triazol-1-yl)-N,N-dimethylethan-1-amine (***26d***).* Flash chromatography (cyclohexane/EtOAc 3:1 ➔ 0:1). Yield over two steps: 65 %. Dark brown powder. ^{1}H NMR (400MHz, $CDCl_3$): δ 2.30 (6H, s), 2.88 (2H, t, J=6.65 Hz), 4.71 (2H, t, J=6.65 Hz), 7.47 (1H, d, J=8.75 Hz), 7.57 (1H, dd, J=1.22, 8.76 Hz),

8.20 (1H, s). ^{13}C NMR (100MHz, $CDCl_3$): δ 45.56; 46.84; 58.41; 110.92; 117.11; 122.56; 130.64; 132.25; 147.09.

- *5-bromo-1-((tetrahydrofuran-3-yl)methyl)-1H-benzo[d][1,2,3]triazole (**28**)*

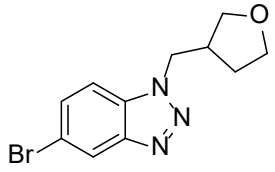

*4-bromo-2-nitro-N-((tetrahydrofuran-3-yl)methyl)aniline (**28b**).* Synthesised according to the general procedure using *(tetrahydrofuran-3-yl)methanamine.* Compound was obtained in quantitative yield as an orange powder. ^{1}H-NMR (400 MHz, $CDCl_3$): δ 1.65 – 1.81 (1H, m), 2.14 – 2.25 (1H, m), 2.61 – 2.73 (1H, m), 3.22 – 3.36 (2H, m, J=4.31 Hz), 3.67 (1H, dd, J=4.83, 8.89 Hz), 3.80 (1H, dd, J=7.90, 15.69 Hz), 3.90 (1H, dd, J=6.94, 8.77 Hz), 3.94 – 4.02 (1H, m), 6.78 (1H, dd, J=1.64, 9.08 Hz), 7.02 (1H, d, J=1.48 Hz), 8.04 (1H, d, J=9.08 Hz), 8.08 – 8.19 (1H, m). ^{13}C-NMR (100 MHz, $CDCl_3$): δ 26.91; 30.07; 38.47; 46.27; 67.72; 71.27; 116.31; 118.98; 128.21; 131.01; 131.83; 145.69.

*4-bromo-N^1-((tetrahydrofuran-3-yl)methyl)benzene-1,2-diamine (**28c**).* Obtained following the general reduction procedure. After evaporation, the crude extract was immediately engaged in the next step.

*5-bromo-1-((tetrahydrofuran-3-yl)methyl)-1H-benzo[d][1,2,3]triazole (**28d**).* Obtained following the general cyclisation procedure. The obtained compound was purified using flash chromatography (cyclohexane/EtOAc, 4:3). Dark brown oil. Overall yield = 54 %. ^{1}H-NMR (400 MHz, $CDCl_3$): δ 1.71 – 1.82 (1H, m), 2.03 – 2.14 (1H, m), 2.96 – 3.08 (1H, m), 3.68 (1H, dd, J=4.69, 9.10 Hz), 3.76 – 3.85 (2H, m), 4.57 (2H, d, J=7.74 Hz), 7.49 (1H, dd, J=1.35, 8.80 Hz), 7.74 (1H, d, J=0.66 Hz), 7.95 (1H, d, J=8.80 Hz).

- *5-bromo-1-((tetrahydrofuran-2-yl)methyl)-1H-benzo[d][1,2,3]triazole (**30d**)*

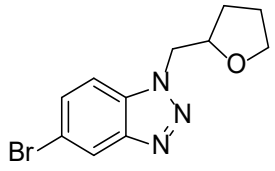

- *4-bromo-2-nitro-N-((tetrahydrofuran-2-yl)methyl)aniline (**30b**)* Synthesised according to the general procedure using *2-(aminomethyl)tetrahydrofuran*. The reaction mixture was agitated for 1h at room temperature. After cooling to 0°C, the

precipitate was filtered and washed with cold EtOH. The product was obtained as a bright orange powder with an 82 % yield. ^{1}H-NMR (400 MHz, $CDCl_3$): δ 1.65 - 1.79 (m, 1H), 1.93-2.01 (m, 2H), 2.05-2.13 (m, 1H), 3.29 - 3.36 (m, 1H), 3.42 - 3.46 (m, 1H), 3.79 - 3.86 (m, 1H), 3.91 - 3.99 (m, 1H), 4.15 - 4.22 (m, 1H), 6.81 (d, J= 9.17 Hz, 1H), 7.48 (d , J= 9.12Hz, 1H), 8.23 (bs, 1H), 8.31 (s, 1H). ^{13}C-NMR (100 MHz, $CDCl_3$) δ 25.86; 29.15; 30.95; 47.07; 68.57; 106.44; 115.71; 128.93; 132.40; 138.84; 144.56.

- *4-bromo-N-((tetrahydrofuran-2-yl)methyl)benzene-1,2-diamine (***30c***).* Obtained following the general reduction procedure. After evaporation, the crude extract was immediately engaged in the next step.

- *5-bromo-1-((tetrahydrofuran-2-yl)methyl)-1H-benzo[d][1,2,3]triazole (***30d***).* Obtained following the general cyclisation procedure. The obtained compound was purified using flash chromatography (cyclohexane/EtOAc, 4:3). Dark red oil. Overall yield 37 %. ^{1}H-NMR (400 MHz, $CDCl_3$): δ 1.56 - 1.64 (m, 1H), 1.68 - 1.76 (m, 1H), 1.79 - 1.89 (m, 1H), 2.03 - 2.12 (m, 1H), 3.64 - 3.73 (m, 2H), 4.35 - 4.41 (m, 1H), 4.68 (dd, J= 14.49, 5.39 Hz, 1H), 4.80 (dd, J=14.49Hz, 3.48 Hz, 2H), 7.54 – 7.63 (m, 2H), 8.19 (s, 1H). ^{13}C-NMR (100 MHz, $CDCl_3$): δ 25.67; 28.54; 52.47; 68.53; 112.17; 117.17; 122.23; 130.71; 132.83; 147.10.

- *4-(2-(5-bromo-1H-benzo[d][1,2,3]triazol-1-yl)ethyl)morpholine (***32d***)*

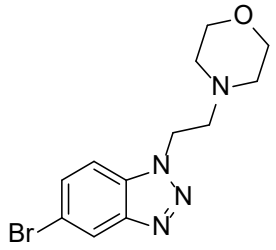

- *4-bromo-N-(2-morpholinoethyl)-2-nitroaniline (***32b***).* Synthesised according to the general procedure using 4-(2-aminoethyl)morpholine. The precipitate was filtered and washed with cold EtOH. The product was obtained as a bright orange powder. Yield = 90 %. ^{1}H-NMR (400 MHz, $CDCl_3$): δ 2.52 (4H, m), 2.72 (2H, t, J=6.06 Hz), 3.34 (2H, dd, J=10.83, 5.63 Hz), 3.76 (4H, t, J=4.39 Hz), 6.73 (2H, d, J=9.13 Hz), 7.49 (2H, dd, J=1.70, 9.08 Hz), 8.32 (2H, d, J=1.94 Hz), 8.53 (1H, s). ^{13}C-NMR (100 MHz, $CDCl_3$) δ 39.40; 53.14; 55.87; 67.00; 106.20; 115.75; 128.99; 132.30; 138.85; 144.17.

- *4-bromo-N-(2-morpholinoethyl)benzene-1,2-diamine (***32c***).* Obtained following the general reduction procedure. Brown oil. Yield: 89 %. ^{1}H-NMR (400 MHz, $CDCl_3$): δ 2.43 – 2.53 (4H, m), 2.67 (2H, t, J=5.76 Hz), 3.13 (2H, t, J=5.77 Hz), 3.47 (2H, s),

3.72 (4H, t, J=4.33 Hz), 6.49 (1H, d, J=8.35 Hz), 6.82 (1H, d, J=1.59 Hz), 6.89 (1H, q, J=3.32 Hz).

- *4-(2-(5-bromo-1H-benzo[d][1,2,3]triazol-1-yl)ethyl)morpholine (***32d***).* Obtained following the general cyclisation procedure. The crude was purified using flash chromatography cyclohexane/EtOAc (1:1 ➔ 2:1). The compound was obtained as a brown powder. Yield = 43 %. ^{1}H-NMR (400 MHz, $CDCl_3$) δ 2.46 - 2.55 (4H, m). 2.93 (2H, t, J= 6.43 Hz), 3.59 - 3.67 (4H, m), 4.74 (2H, t, J= 6.43 Hz), 7.47 (1H, d, J= 8.68 Hz), 7.58 (1H, d, J= 8.53 Hz), 8.22 (1H, s). ^{13}C-NMR (100 MHz, $CDCl_3$) δ 46.13; 53.64; 57.63; 66.84; 110.89; 117.14; 122.65; 130.62; 132.29; 147.11.

- *tert-butyl 4-((5-bromo-1H-benzo[d][1,2,3]triazol-1-yl)methyl)piperidine-1-carboxylate (***34d***)*

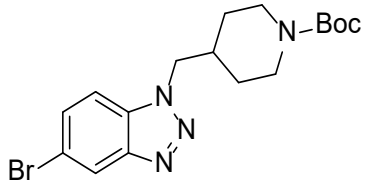

*tert-butyl 4-(((4-bromo-2-nitrophenyl)amino)methyl)piperidine-1-carboxylate (***34b***).* Synthesised according to the general procedure using *tert-butyl 4-(aminomethyl)piperidine-1-carboxylate*. An orange oil was obtained following evaporation under reduced pressure. Yield: 86 %. ^{1}H-NMR (400 MHz, $CDCl_3$): δ 1.36 – 1.49 (11H, m), 1.59 – 1.71 (1H, m), 1.78 (2H, d, J=10.40 Hz), 2.83 (2H, t, J=11.76 Hz), 3.08 (2H, t, J=5.82 Hz), 3.28 (2H, d, J=11.92 Hz), 4.66 – 4.76 (1H, m), 7.07 (1H, d, J=8.48 Hz), 7.22 (1H, s), 7.66 (1H, d, J=8.64 Hz).

*tert-butyl 4-(((2-amino-4-bromophenyl)amino)methyl)piperidine-1-carboxylate (***34c***).* Obtained following the general reduction procedure. Yield: 73 %. ^{1}H-NMR (400 MHz, $CDCl_3$): δ 1.32 – 1.42 (2H, m), 1.46 (9H, d, J=4.06 Hz), 1.52 – 1.66 (1H, m), 1.80 (2H, d, J=12.27 Hz), 2.55 (2H, t, J=11.39 Hz), 3.04 – 3.18 (4H, m), 3.92 (3H, s), 4.64 (1H, s), 6.59 (3H, t, J=6.60 Hz), 7.00 (2H, dd, J=1.80, 8.37 Hz), 7.04 (2H, s).

*tert-butyl 4-((5-bromo-1H-benzo[d][1,2,3]triazol-1-yl)methyl)piperidine-1-carboxylate (***34d***).* Obtained following the general cyclisation procedure. The crude was purified using flash chromatography cyclohexane/EtOAc (1:1 ➔ 0:1). The compound was obtained as a brown powder. Overall yield = 55 %. ^{1}H-NMR (400 MHz, $CDCl_3$): δ 1.21 – 1.35 (2H, m), 1.44 (9H, s), 1.52 – 1.63 (2H, m), 2.15 – 2.27 (1H, m), 2.65 (2H, t, J=11.90 Hz), 4.01 – 4.23 (2H, m), 4.50 (2H, d, J=7.18 Hz), 7.40 (1H, d, J=8.75 Hz), 7.60 (1H, q, J=3.37 Hz), 8.23 (1H, d, J=0.73 Hz). ^{13}C-NMR (100 MHz,

$CDCl_3$) δ 28.42; 29.78; 37.22; 53.53; 79.72; 110.51; 117.24; 122.75; 130.88; 132.36; 146.98; 154.65.

- *tert-butyl 3-((5-bromo-1H-benzo[d][1,2,3]triazol-1-yl)methyl)pyrrolidine-1-carboxylate (***36d***)*

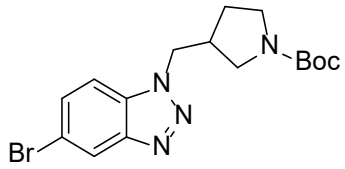

*tert-butyl 3-(((4-bromo-2-nitrophenyl)amino)methyl)pyrrolidine-1-carboxylate (***36b***).* Synthesised according to the general procedure using *tert-butyl 3-(aminomethyl)pyrrolidine-1-carboxylate*. Agitated at reflux temperature for 2h30. The reaction media was extracted with EtOAc. After evaporation the product was obtained as an orange oil that was used without further purification in the next step. Quantitative yield. ^{1}H-NMR (400 MHz, $CDCl_3$): δ 1.46 (9H,s), 1.67 – 1.80 (1H, m), 2.08 – 2.19 (1H, m), 2.52 – 2.65 (1H, m), 3.07 – 3.20 (1H, m), 3.21 – 3.70 (5H, m), 6.76 (1H, d, J=9.16 Hz), 7.51 (1H, dd, J=1.59, 9.08 Hz), 8.03 – 8.15 (1H, m), 8.33 (1H, d, J=1.61 Hz). ^{13}C-NMR (100 MHz, $CDCl_3$): δ 28.42; 39.59; 55.39; 58.46; 79.73; 116.74; 118.52; 128.19; 131.01; 131.56; 145.57; 154.75.

*tert-butyl 3-(((2-amino-4-bromophenyl)amino)methyl)pyrrolidine-1-carboxylate (***36c***).* Obtained following the general reduction procedure as an orange oil. Quantitative yield. ^{1}H-NMR (400 MHz, $CDCl_3$): δ 1.47 (9H, s), 1.64 – 1.77 (1H, m), 2.04 – 2.13 (1H, m), 2.43 – 2.56 (1H, m), 3.04 – 3.20 (3H, m), 3.21 – 3.66 (6H, m), 6.49 (2H, d, J=8.39 Hz), 6.84 (1H, s), 6.90 (2H, d, J=8.14 Hz).

*tert-butyl 3-((5-bromo-1H-benzo[d][1,2,3]triazol-1-yl)methyl)pyrrolidine-1-carboxylate (***36d***).* Obtained following the general cyclisation procedure. Flash chromatography: Cyclohexane/EtOAc: 1:0 ➔ 1:4. Yield: 70 %. ^{1}H-NMR (400 MHz, $CDCl_3$): δ 1.45 (9H, s), 1.68 – 1.78 (1H, m), 1.91 – 2.03 (1H, m), 2.85 – 2.99 (1H, m), 3.11 – 3.62 (5H, m), 4.61 (3H, s), 7.41 (3H, d, J=8.72 Hz), 7.60 (3H, d, J=8.48 Hz), 8.24 (2H, s). ^{13}C-NMR (100 MHz, $CDCl_3$): δ 28.48; 39.35; 44.62; 49.25; 50.26; 79.68; 110.27; 117.36; 122.85; 131.03; 147.06; 154.44.

- *tert-butyl 4-((5-bromo-1H-benzo[d][1,2,3]triazol-1-yl)methyl)piperazine-1-carboxylate (***38d***)*

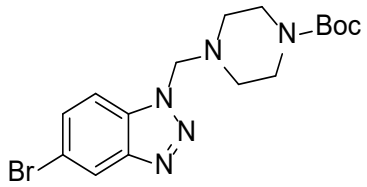

*tert-butyl 4-(((4-bromo-2-nitrophenyl)amino)methyl)piperazine-1-carboxylate (***38b***).* Synthesised according to the general procedure using *tert-butyl 4-(aminomethyl)piperazine-1-carboxylate*. Agitated at reflux temperature for 2h30. Yellow powder. Quantitative yield. ^{1}H-NMR (400 MHz, $CDCl_3$): δ 1.46 (9H, s), 2.47 (4H, s), 2.73 (2H, t, J=5.90 Hz), 3.34 (2H, dd, J=5.29, 10.25 Hz), 3.48 (4H, s), 6.76 (1H, d, J=9.04 Hz), 7.00 (1H, s), 8.03 (1H, d, J=9.04 Hz), 8.54 (1H, s). ^{13}C-NMR (100 MHz, $CDCl_3$) δ 28.51; 37.52; 38.42; 45.18; 45.73; 49.62; 60.42; 79.54; 106.80; 115.33; 129.06; 132.36; 139.05; 144.18; 154.49.

*tert-butyl 4-(((2-amino-4-bromophenyl)amino)methyl)piperazine-1-carboxylate (***38c***).* Obtained following the general reduction procedure as a clear oil. Quantitative yield. ^{1}H-NMR (400 MHz, $CDCl_3$): δ 1.46 (9H, s), 2.42 (4H, s), 2.68 (2H, t, J=5.79 Hz), 3.13 (2H, t, J=5.64 Hz), 3.34 (2H, bs), 3.38 – 3.49 (5H, m), 6.56 (2H, d, J=8.09 Hz), 6.72 (2H, d, J=1.85 Hz), 6.76 (2H, dd, J=2.02, 8.09 Hz).

*tert-butyl 4-((5-bromo-1H-benzo[d][1,2,3]triazol-1-yl)methyl)piperazine-1-carboxylate (***38d***).* Obtained following the general cyclisation procedure. Flash chromatography: Cyclohexane/EtOAc 1:0 ➔ 1:2. Yield: 80 %. Brown powder. ^{1}H-NMR (400 MHz, $CDCl_3$): δ 1.45 (9H, s), 2.46 (4H, s), 2.93 (2H, t, J=6.38 Hz), 3.37 (4H, s), 4.72 (2H, t, J=6.38 Hz), 7.46 (1H, dd, J=8.80, 1.37 Hz), 7.79 (1H, d, J=0.68 Hz), 7.92 (1H, d, J=8.80 Hz). ^{13}C-NMR (100 MHz, $CDCl_3$): δ 28.40; 46.28; 53.06; 57.28; 79.80; 112.78; 121.18; 121.52; 127.57; 134.38; 144.80; 154.62.

- *3-(5-bromo-1H-benzo[d][1,2,3]triazol-1-yl)propane-1,2-diol (***40d***).*

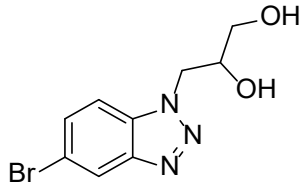

*3-((4-bromo-2-nitrophenyl)amino)propane-1,2-diol (***40b***).* Synthesised according to the general procedure using *3-aminopropane-1,2-diol*. Orange powder. Quantitative yield. ^{1}H NMR (400MHz, DMSO): δ 3.22 – 3.31 (1H, m), 3.36 – 3.41 (1H, m), 3.42 – 3.52 (2H, m), 3.69 – 3.77 (1H, m), 4.81 (1H, t, J=5.57 Hz), 5.18 (1H, d, J=4.98 Hz), 7.08 (1H, d, J=9.31 Hz), 7.67 (1H, dd, J=2.14, 9.24 Hz), 8.18 (1H, d, J=2.30

Hz), 8.35 (1H, t, J=4.97 Hz). ^{13}C NMR (100MHz, DMSO): δ 46.16; 64.07; 69.77; 105.52; 117.72; 128.24; 131.79; 139.31; 145.11.

*3-((2-amino-4-bromophenyl)amino)propane-1,2-diol (***40c***).* Obtained following the general reduction procedure. After evaporation, the crude extract was immediately engaged in the next step.

*3-(5-bromo-1H-benzo[d][1,2,3]triazol-1-yl)propane-1,2-diol (***40d***).* Obtained following the general cyclisation procedure. Flash chromatography: EtOAc (100 %). Yield: 80 %. Brown powder. ^{1}H NMR (400MHz, MeOD): δ 3.33 (1H, s), 3.62 (2H, d, J=5.49 Hz), 4.07 – 4.19 (1H, m), 4.63 – 4.74 (1H, m), 4.86 (1H, d, J=3.52 Hz), 7.55 (1H, q, J=3.28 Hz), 7.91 (1H, d, J=8.82 Hz), 8.13 (1H, s).^{13}C NMR (100MHz, MeOD): δ 51.06; 63.24; 70.94; 113.99; 119.79; 121.07; 127.61; 135.16; 144.10.

2.4.2. N-substituted benzotriazoles obtained starting from 4-Bromo-2-fluoro-1-nitrobenzene [CAS 364-73-8]:

- *6-bromo-1-(2,2,2-trifluoroethyl)-1H-benzo[d][1,2,3]triazole (***17d***).*

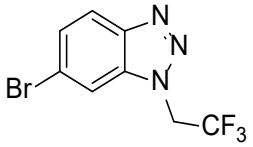

- *5-bromo-2-nitro-N-(2,2,2-trifluoroethyl)aniline (***17b***).* 4-Bromo-2-fluoro-1-nitrobenzene (500 mg, 2.27 mmol) and trifluoroethanolamine.HCl were dissolved in anhydrous THF (4mL) and DIEA (1.16 mL, 6.82 mmol) under N_2. The resulting mixture was refluxed for 16h. After cooling to room temperature, the solvent was removed *in-vacuo*. Then, the residue was resuspended in 10 mL water and extracted 3 times with EtOAc. The OL was dried with Na_2SO_4 and evaporated to yield 620 mg (2.07 mmol) of a bright yellow powder containing **17b**. Quantitative yield. Used without further purification in the next step. ^{1}H NMR (400MHz, $CDCl_3$): δ 3.97 (2H, qn, J=8.08 Hz), 6.94 (1H, dd, J=1.43, 9.04 Hz), 7.11 (1H, s), 7.47 (1H, d, J=8.95 Hz), 7.51 (1H, d, J=10.16 Hz), 7.98 (1H, t, J=8.29 Hz), 8.08 (2H, d, J=9.05 Hz), 8.28 (1H, s). ^{13}C NMR (100MHz, $CDCl_3$): δ 44.67 (CF_3, q, J=34.76 Hz), 116.29; 120.91; 122.09 (d, J=23.60 Hz); 125.53; 127.17 (d, J=2.33 Hz); 128.21 (d, J=13.52 Hz); 131.89; 144.42.

- *5-bromo-N1-(2,2,2-trifluoroethyl)benzene-1,2-diamine (***17c***).* Obtained following the general reduction procedure. After evaporation, the crude extract was immediately engaged in the next step.

- *6-bromo-1-(2,2,2-trifluoroethyl)-1H-benzo[d][1,2,3]triazole (***17d***)* was obtained using the cyclisation general procedure. Flash chromatography purification: Cyclohexane/EtOAc (9:1). Beige powder. Yield over two steps: 68 %. ^{1}H NMR (400MHz, $CDCl_3$): δ 5.21 (2H, q, J=8.02 Hz), 7.56 (1H, d, J=8.67 Hz), 7.78 (1H, s), 7.99 (1H, d, J=8.68 Hz). ^{13}C NMR (100MHz, $CDCl_3$): δ 49.29 (m, CF_3); 112.17; 121.28; 121.60; 123.25; 124.06; 128.50; 134.28; 144.91.

- *6-bromo-1-(cyclopropylmethyl)-1H-benzo[d][1,2,3]triazole (***19d***)*

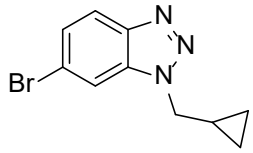

- *5-bromo-N-(cyclopropylmethyl)-2-nitroaniline (***19b***).* Synthesised according to the general procedure using *cyclopropylmethanamine*. Quantitative yield. The product precipitated as yellow crystals that were filtrated. Then, *5-bromo-N1-(cyclopropylmethyl)benzene-1,2-diamine (***19c***)* was obtained following the general reduction procedure. After evaporation, the crude extract was immediately engaged in the next step.

- *6-bromo-1-(cyclopropylmethyl)-1H-benzo[d][1,2,3]triazole (***19d***).* was obtained by using the general cyclisation procedure. Reaction time= 30 min. The compound was purified using flash chromatography (cyclohexane/EtOAc 3:1) and obtained as a dark red oil that solidified overnight. Overall yield = 51 %. ^{1}H NMR (400MHz, $CDCl_3$): δ 0.50 (2H, q, J=5.21 Hz), 0.68 (2H, q, J=6.31 Hz), 1.36 – 1.45 (1H, m), 4.48 (2H, d, J=7.13 Hz), 7.47 (1H, dd, J=1.07, 8.80 Hz), 7.77 (1H, s), 7.93 (1H, d, J=8.80 Hz). ^{13}C NMR (100MHz, $CDCl_3$): δ 4.51; 11.04; 53.16; 112.54; 121.20; 121.52; 127.51; 133.94; 144.92.

- *2-(6-bromo-1H-benzo[d][1,2,3]triazol-1-yl)-N,N-dimethylethan-1-amine (***25d***)*

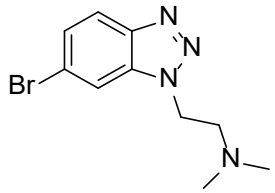

*N^1-(5-bromo-2-nitrophenyl)-N^2,N^2-dimethylethane-1,2-diamine (***25b***)* was synthesised according to the general procedure using *N^1,N^1-dimethylethane-1,2-diamine*. Quantitative yield. Orange powder.^{1}H NMR (400MHz, $CDCl_3$): δ 2.30 (6H, s), 2.63 (2H, t, J=6.08 Hz), 3.31 (2H, dd, J=5.74, 10.80 Hz), 6.73 (1H, q, J=3.53 Hz),

6.99 (1H, d, J=1.14 Hz), 8.02 (1H, d, J=9.07 Hz), 8.36 (1H, s). ^{13}C NMR (100MHz, $CDCl_3$): δ 40.74; 45.22; 57.11; 116.60; 118.38; 128.16; 130.94; 131.51; 145.67.

*5-bromo-N1-(2-(dimethylamino)ethyl)benzene-1,2-diamine (***25c***)* was obtained following the general reduction procedure. After evaporation, the crude extract was immediately engaged in the next step.

*2-(6-bromo-1H-benzo[d][1,2,3]triazol-1-yl)-N,N-dimethylethan-1-amine (***25d***)* was obtained by using the general cyclisation procedure. Flash chromatography (cyclohexane/EtOAc 3:1 ➔ 0:1). Yield over two steps: 55 %. Dark brown oil. ^{1}H NMR (400MHz, $CDCl_3$): δ 2.53 (6H, s), 3.25 (2H, t, J=7.15 Hz), 4.90 (2H, t, J=7.15 Hz), 7.48 (1H, dd, J=1.20, 8.79 Hz), 7.89 (1H, s). ^{13}C NMR (100MHz, $CDCl_3$): δ 44.14; 56.49; 112.64; 121.06; 122.13; 128.02; 134.10; 144.62; 176.16.

- *6-bromo-1-((tetrahydrofuran-3-yl)methyl)-1H-benzo[d][1,2,3]triazole (***27d***)*

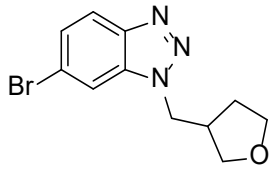

*5-bromo-2-nitro-N-((tetrahydrofuran-3-yl)methyl)aniline (***27b***).* was synthesised according to the general procedure using *(tetrahydrofuran-3-yl)methanamine*. Quantitative yield. ^{1}H-NMR (400 MHz, $CDCl_3$) δ 1.68 – 1.81 (2H, m), 2.14 – 2.25 (2H, m), 2.62 – 2.72 (2H, m), 3.26 – 3.36 (4H, m), 3.63 – 3.69 (2H, m), 3.79 (2H, q, J=7.86 Hz), 3.89 (2H, q, J=5.23 Hz), 3.93 – 4.01 (2H, m), 6.78 (2H, d, J=9.19 Hz), 7.49 (2H, dd, J=2.05, 9.15 Hz), 8.10 (1H, s), 8.26 (2H, d, J=2.19 Hz). ^{13}C-NMR (100 MHz, $CDCl_3$) δ 30.02; 38.52; 46.21; 67.69; 71.22; 106.56; 115.46; 128.80; 132.13; 138.94; 144.29.

*5-bromo-N1-((tetrahydrofuran-3-yl)methyl)benzene-1,2-diamine (***27c***).* was obtained following the general reduction procedure. After evaporation, the crude extract was immediately engaged in the next step.

*6-bromo-1-((tetrahydrofuran-3-yl)methyl)-1H-benzo[d][1,2,3]triazole (***27d***)* was obtained by using the general cyclisation procedure. Purified using flash chromatography (cyclohexane/EtOAc, 4:1). Light brown powder. ^{1}H-NMR (400 MHz, $CDCl_3$): δ 1.71 – 1.81 (2H, m), 2.02 – 2.17 (2H, m), 2.96 – 3.06 (1H, m), 3.63 – 3.72 (1H, m), 3.75 – 3.83 (2H, q, J=7.46 Hz), 3.96 – 4.03 (1H, m), 4.59 (2H, d, J=7.70 Hz), 7.44 (1H, d, J=8.75 Hz), 7.60 (1H, t, J=4.37 Hz), 8.23 (1H, s). ^{13}C-NMR (100 MHz, $CDCl_3$) δ 24.86; 29.74; 39.63; 50.63; 67.52; 70.80; 75.02; 110.36; 117.32; 122.77; 130.96; 132.11; 147.00.

- *6-bromo-1-((tetrahydrofuran-2-yl)methyl)-1H-benzo[d][1,2,3]triazole (***29d***)*

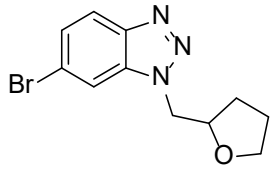

- *5-bromo-2-nitro-N-((tetrahydrofuran-2-yl)methyl)aniline (***29b***).* Synthesised according to the general procedure using *2-(Aminomethyl)tetrahydrofuran*. After cooling the reaction mixture to 0°C, the precipitate was filtered and washed with cold EtOH. The compound was obtained as a yellow powder. Yield: 50 %. ^{1}H-NMR (400 MHz, $CDCl_3$): δ 1.66 - 1.74 (m, 1H), 1.94 - 2.01 (m, 1H), 2.06-2.14 (m, 1H), 3.27 - 3.34 (m, 1H), 3.41 - 3.46 (m, 1H), 3.79 - 3.87 (m, 1H), 3.93 - 4.00 (m, 1H), 4.17 - 4.23 (m, 1H), 6.76 (d, J= 9.08Hz, 1H), 7.05 (s, 1H), 8.03 (d, J =8.69 Hz, 1H), 8.25 (bs, 1H). ^{13}C-NMR (100 MHz, $CDCl_3$): δ 25.87; 29.17; 47.08; 68.57; 116.57; 118.75; 128.18; 131.11; 131.61; 145.92.

- *5-bromo-N-((tetrahydrofuran-2-yl)methyl)benzene-1,2-diamine (***29c***).* Obtained following the general reduction procedure. The compound was immediately engaged in the next step.

- *6-bromo-1-((tetrahydrofuran-2-yl)methyl)-1H-benzotriazole (***29d***).* Obtained following the general cyclisation procedure. Purified using flash chromatography (cyclohexane/EtOAc, 4:1). Light brown powder. Yield = 53 %. ^{1}H-NMR (400 MHz, $CDCl_3$) δ 1.54 – 1.64 (m, 1H), 1.78 – 1.88 (m, 1H), 2.03 – 2.11 (1H, m), 3.67 – 3.70 (m, 2H), 4.35 – 4.40 (m, 1H), 4.68 (dd, J=14.49Hz, J=5.04Hz, 1H), 4.80 (dd, J=14.69 Hz, J=4.01Hz 1H), 7.54 – 7.62 (m, 2H), 8.19 (s, 1H). ^{13}C-NMR (100 MHz, $CDCl_3$) δ 25.67; 28.64; 30.97; 52.43; 68.58; 113.70; 120.86; 121.69; 127.62; 134.85; 144.81.

- *4-(2-(6-bromo-1H-benzo[d][1,2,3]triazol-1-yl)ethyl)morpholine (***31d***)*

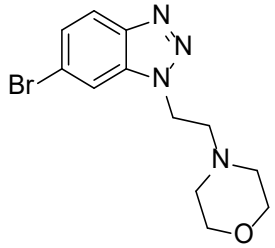

- *5-bromo-N-(2-morpholinoethyl)-2-nitroaniline (***31b***).* Synthesised according to the general procedure using *4-(2-aminoethyl)morpholine*. After cooling the reaction mixture to 0°C, the precipitate was filtered and washed with cold EtOH. Yellow powder. Yield: 78 %. ^{1}H-NMR (400 MHz, $CDCl_3$) δ 2.49 – 2.56 (m, 4H), 2.73 (t, J=

17.93 Hz, 2H), 3.30 – 3.37 (m, 2H), 3.75 (t, J= 4.48 Hz, 4H), 6.75 (d, J= 9,08Hz, 1H), 7.00 (s, 1H), 8.03 (d, J= 9.08 Hz, 1H), 8.55 (s, 1H). ^{13}C-NMR (100 MHz, $CDCl_3$) δ 39.41; 53.13; 55.83; 67.00; 116.72; 118.50; 128.19; 131.02; 131.55; 145.59.

- *5-bromo-N-(2-morpholinoethyl)benzene-1,2-diamine (***31c***).* Obtained following the general reduction procedure. The compound was immediately engaged in the next step.

- *4-(2-(6-bromo-1H-benzo[d][1,2,3]triazol-1-yl)ethyl)morpholine (***31d***).* Obtained following the general cyclisation procedure. The obtained compound was purified using flash chromatography (cyclohexane/EtOAc, 1:1). Light brown powder. Yield = 53 %. ^{1}H-NMR (400 MHz, $CDCl_3$) δ 7.92 (d, J= 8.80 Hz, 1H), 7.80 (s, 1H), 7.48 (d, J= 8.79 Hz, 1H), 4.72 (t, J= 6.38 Hz, 2H), 3.63 - 3.69 (m, 4H), 2.92 (t, J= 6.39 Hz, 2H), 2.50 - 2.55 (m, 4H). ^{13}C-NMR (100 MHz, $CDCl_3$) δ 46.07; 53.62; 60.42; 66.82; 112.85; 121.18; 121.52; 127.59; 134.37; 144.82.

- *tert-butyl 4-((6-bromo-1H-benzo[d][1,2,3]triazol-1-yl)methyl)piperidine-1-carboxylate (***33d***)*

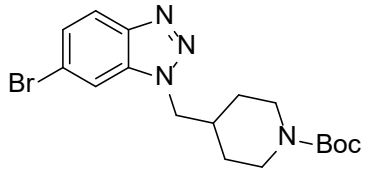

- *tert-butyl 4-(((5-bromo-2-nitrophenyl)amino)methyl)piperidine-1-carboxylate (***33b***).* Synthesised according to the general procedure using *tert-butyl 4-(aminomethyl)piperidine-1-carboxylate*. Agitated overnight at room temperature. An orange oil was obtained following evaporation under reduced pressure. ^{1}H-NMR (400 MHz, $CDCl_3$)*: δ* 1.19 – 1.32 (2H, m), 1.47 (9H, s), 1.77 – 1.92 (3H, m), 2.63 – 2.83 (2H, m), 3.19 (2H, t, J=5.67 Hz), 4.00 – 4.30 (2H, m), 6.76 (1H, d, J=9.09 Hz), 7.00 (1H, s), 8.03 (1H, d, J=9.10 Hz), 8.11 – 8.19 (1H, m).

- *tert-butyl 4-(((2-amino-5-bromophenyl)amino)methyl)piperidine-1-carboxylate (***33c***).* Obtained following the general reduction procedure as a black oil with a yield of 82 %, which was used in the next step without further purification. ^{1}H-NMR (400 MHz, $CDCl_3$)*: δ* 1.05 – 1.21 (3H, m), 1.38 (9H, s), 1.60 – 1.75 (3H, m), 2.56 – 2.70 (2H, m), 2.87 (2H, d, J=5.90 Hz), 3.20 (2H, bs), 3.44 (1H, bs), 3.98 – 4.12 (2H, m), 6.48 (2H, d, J=8.08 Hz), 6.61 (2H, s), 6.65 (2H, d, J=8.07 Hz).

- *tert-butyl 4-((6-bromo-1H-benzo[d][1,2,3]triazol-1-yl)methyl)piperidine-1-carboxylate (***33d***).* Obtained following the general cyclisation procedure. The obtained compound was purified using flash chromatography (cyclohexane/EtOAc,

2:1 ➔ 1:1). Brown powder. Yield = 84 %. ^{1}H-NMR (400 MHz, $CDCl_3$) δ 1.23 – 1.36 (2H, m), 1.45 (9H, s), 1.54 – 1.63 (2H, m), 2.16 – 2.29 (1H, m), 2.61 – 2.73 (2H, m), 4.06 – 4.25 (2H, m), 4.47 (2H, d, J=7.00 Hz), 7.48 (1H, d, J=7.99 Hz), 7.69 (1H, s), 7.94 (1H, d, J=8.75 Hz). ^{13}C-NMR (100 MHz, $CDCl_3$) δ 28.42; 29.77; 37.12; 53.44; 79.71; 112.19; 121.33; 121.86; 127.71; 134.41; 144.68; 154.66.

- *tert-butyl 3-((6-bromo-1H-benzo[d][1,2,3]triazol-1-yl)methyl)pyrrolidine-1-carboxylate (***35d***)*

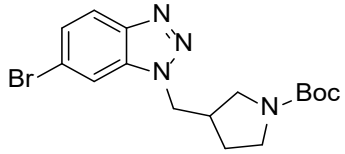

*tert-butyl 3-(((5-bromo-2-nitrophenyl)amino)methyl)pyrrolidine-1-carboxylate (***35b***).* Synthesised according to the general procedure using *tert-butyl 3-(aminomethyl)pyrrolidine-1-carboxylate*. Brown oil. Quantitative yield. ^{1}H-NMR (400 MHz, $CDCl_3$): δ 1.47 (9H, s), 1.68 – 1.82 (1H, m), 2.09 – 2.20 (1H, m), 2.55 – 2.68 (1H, m), 3.09 – 3.20 (1H, m), 3.23 – 3.69 (5H, m), 6.78 (1H, d, J=9.03 Hz), 7.01 (1H, s), 8.02 (1H, d, J=9.07 Hz), 8.08 – 8.12 (1H, m).

tert-butyl 3-(((2-amino-5-bromophenyl)amino)methyl)pyrrolidine-1-carboxylate (**35c**). Obtained following the general reduction procedure. Quantitative yield. ^{1}H-NMR (400 MHz, $CDCl_3$): δ 1.47 (1H, s), 1.64 – 1.76 (1H, m), 2.02 – 2.12 (1H, m), 2.42 – 2.57 (1H, m), 3.00 – 3.20 (3H, m), 3.24 – 3.66 (5H, m), 6.58 (1H, d, J=7.24 Hz), 6.71 (1H, s), 6.77 (1H, d, J=7.88 Hz).

tert-butyl 3-((6-bromo-1H-benzo[d][1,2,3]triazol-1-yl)methyl)pyrrolidine-1-carboxylate (**35d**). Obtained following the general cyclisation procedure. Purified using flash chromatography (cyclohexane/EtOAc, 1:0 ➔ 1:4). Brown powder. Yield = 70 %. ^{1}H-NMR (400 MHz, $CDCl_3$): δ 1.46 (9H, s), 1.69 – 1.79 (1H, m), 1.92 – 2.05 (1H, m), 2.87 – 2.98 (1H, m), 3.17 – 3.26 (1H, d, J=4.44 Hz), 3.28 – 3.62 (3H, m, J=10.21 Hz), 4.60 (2H, d, J=6.79 Hz), 7.48 (1H, d, J=8.62 Hz), 7.72 (1H, s), 7.94 (1H, d, J=8.57 Hz).

- *tert-butyl 4-((6-bromo-1H-benzo[d][1,2,3]triazol-1-yl)methyl)piperazine-1-carboxylate (***37d***)*

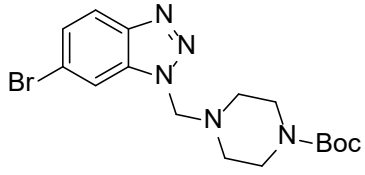

*tert-butyl 4-(((5-bromo-2-nitrophenyl)amino)methyl)piperazine-1-carboxylate (***37b***).* Synthesised according to the general procedure using *tert-butyl 4-(aminomethyl)piperazine-1-carboxylate*. Agitated at reflux temperature for 2h30. Yellow powder. Quantitative yield. ^{1}H-NMR (400 MHz, $CDCl_3$): δ 1.47 (9H, s), 1.52 – 1.65 (1H, m), 1.67 – 1.80 (1H, m), 2.08 – 2.19 (1H, m), 2.59 (1H, d, J=6.84 Hz), 3.07 – 3.20 (1H, m), 3.21 – 3.69 (5H, m), 6.76 (1H, d, J=9.16 Hz), 7.51 (1H, d, J=7.80 Hz), 8.08 (1H, s), 8.33 (1H, s). ^{13}C-NMR (100 MHz, $CDCl_3$): δ 14.21; 21.09; 28.51; 37.52; 38.42; 45.18; 45.73; 49.62; 60.42; 79.54; 106.80; 115.33; 129.06; 132.36; 139.05; 144.18; 154.49.

*tert-butyl 4-(((2-amino-5-bromophenyl)amino)methyl)piperazine-1-carboxylate (***37c***).* Obtained following the general reduction procedure. Quantitative yield. ^{1}H-NMR (400 MHz, $CDCl_3$) δ 1.46 (9H, s), 2.37 – 2.45 (4H, s), 2.65 (2H, t, J=5.80 Hz), 3.11 (2H, t, J=5.78 Hz), 3.38 – 3.47 (4H, m), 3.55 (2H, br s), 6.46 (1H, d, J=8.36 Hz), 6.80 (1H, d, J=2.08 Hz), 6.85 (1H, dd, J=2.05, 8.34 Hz)

*tert-butyl 4-((6-bromo-1H-benzo[d][1,2,3]triazol-1-yl)methyl)piperazine-1-carboxylate (***37d***).* Obtained following the general cyclisation procedure. Purified using flash chromatography (cyclohexane/EtOAc, 2:1 ➔ 1:1). Brown powder. Yield = 80 %. ^{1}H-NMR (400 MHz, $CDCl_3$) δ 1.45 (9H, s), 2.36 – 2.52 (4H, m), 2.94 (2H, t, J=6.40 Hz), 3.25 – 3.47 (4H, s), 4.74 (2H, t, J=6.39 Hz), 7.46 (1H, d, J=8.75 Hz), 7.58 (1H, dd, J=1.48, 8.76 Hz), 8.21 (1H, d, J=0.84 Hz). ^{13}C-NMR (100 MHz, $CDCl_3$) δ 28.39; 46.33; 53.01; 57.27; 79.81; 110.91; 117.13; 122.61; 130.62; 132.31; 147.06; 154.64.

- *3-(6-bromo-1H-benzo[d][1,2,3]triazol-1-yl)propane-1,2-diol (***39d***)*

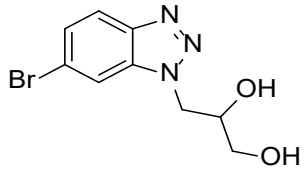

*3-((5-bromo-2-nitrophenyl)amino)propane-1,2-diol (***39b***).* Synthesised according to the general procedure using *3-aminopropane-1,2-diol*. Quantitative yield. ^{1}H NMR (400MHz, DMSO): δ 3.22 – 3.52 (4H, m), 3.73 (1H, s), 4.82 (1H, s), 5.20 (1H, s), 6.84 (1H, dd, J= 1.57, 9.10 Hz), 7.29 (1H, s), 8.00 (1H, d, J=9.10 Hz), 8.35 (1H, t, J=4.86 Hz). ^{13}C NMR (100MHz, DMSO): δ 46.13; 64.04; 69.82; 117.40; 118.53; 128.53; 130.67; 131.47; 146.43.

*3-((2-amino-5-bromophenyl)amino)propane-1,2-diol (***39c***).* Obtained following the general reduction procedure. After evaporation, the crude extract was immediately engaged in the next step.

*3-(6-bromo-1H-benzo[d][1,2,3]triazol-1-yl)propane-1,2-diol (***39d***).* Obtained following the general cyclisation procedure. Flash chromatography: EtOAc (100 %). Yield: 75 %. Brown powder. ^{1}H NMR (400MHz, MeOD): δ 3.33 (1H, s), 3.62 (1H, d, J=5.47 Hz), 4.11 – 4.19 (1H, m), 4.68 – 4.76 (1H, m), 4.86 – 4.89 (1H, m), 7.67 (1H, d, J=8.80 Hz), 7.81 (1H, d, J=8.82 Hz), 8.18 (1H, s). ^{13}C NMR (100MHz, MeOD): δ 51.15; 63.25; 70.92; 112.56; 117.12; 120.92; 130.32; 133.15; 146.34.

3. Synthesis and methylation of 5-Bromotriazolopyridine

- *5-Bromotriazolopyridine (***44***)*

was obtained from the commercially available 5-bromopyridine-2,3-diamine (1504 mg, 8 mmol) using $NaNO_2$ (1104 mg, 16 mmol) in acetic acid (16 mL) using a sonication bath for 1h. ^{1}H-NMR (400 MHz, DMSO) δ 8.82 (1H, d, J=7.83 Hz). ^{13}C-NMR (100 MHz, DMSO) δ 116.93; 127.29; 150.46. Light brown powder. Yield: 83 %.

5-Bromotriazolopyridine (1194 mg, 6 mmol) was dissolved in 15 mL of $NaOH_{aq}$ 2N and 1.6 eq. of Me_2SO_4 (9.6 mmol) were added. The reaction mixture was agitated at room temperature for 1h30, until disappearance of starting material on TLC. The product gradually appeared in the form of an off-white precipitate and contained 3 N-methylated regioisomers. Crude yield: 96 %. The regioisomers were purified by flash chromatography in a gradient of cyclohexane/EtOAc (4:1 ➔ 2:3).

- *6-bromo-1-methyl-1H-[1,2,3]triazolo[4,5-b]pyridine (***14b***)*

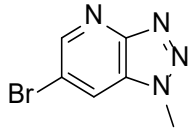

^{1}H-NMR (400 MHz, DMSO): δ 4.33 (3H, s), 8.79 (1H, d, J=1.95 Hz), 8.85 (1H, d, J=1.98 Hz).^{13}C-NMR (100 MHz, DMSO) δ 35.57 ; 118.51 ; 123.40 ; 127.39 ; 149.30 ; 155.67. Beige powder. Purified yield : 13 %

- *6-bromo-3-methyl-3H-[1,2,3]triazolo[4,5-b]pyridine (***15b***)*

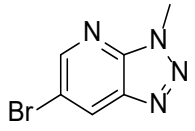

^{1}H-NMR (400 MHz, DMSO): δ 4.31 (3H, s), 8.88 (1H, d, J=1.89 Hz), 8.96 (1H, d, J=1.88 Hz). ^{13}C-NMR (100 MHz, DMSO): δ 33.58; 115.54; 131.06; 137.82; 144.81 ; 151.66. White crystalline powder. Purified yield : 20.5 %

- *6-bromo-2-methyl-2H-[1,2,3]triazolo[4,5-b]pyridine (***13b***)*

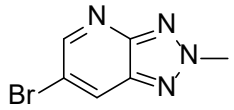

^{1}H-NMR (400 MHz, $CDCl_3$): δ 4.56 (3H, s), 8.39 (1H, d, J=2.06 Hz), 8.80 (1H, d, J=1.96 Hz). ^{1}H-NMR (400 MHz, DMSO): 4.55 (3H, s), 8.84 – 8.87 (2H, m). ^{13}C-NMR (100 MHz, DMSO): δ 44.70 ; 117.64 ; 129.47 ; 137.34 ; 152.92; 154.16. White crystalline powder. Purified yield: 11 %

A loss in purified yield is due to the lack of resolution of the glass column purification.

4. Nitration (A) and reduction (B) of methylated 5-chlorobenzotriazoles

General procedure: 2 mmol of the appropriate chloro-methylbenzotriazole (**7b–9b**) was dissolved in 3.5 mL of concentrated H_2SO_4. To this solution, 6.5 mmol KNO_3 in concentrated H_2SO_4 was added dropwise. The resulting mixture was agitated for 1h30 min at 50 °C. After cooling down to room temperature, the reaction mixture was poured on ice, resulting in precipitate formation (**10b–12b**). The obtained powder was washed with water until neutrality. In accordance with the literature, nitration of 5-chloro-2-methyl-2H-benzo[*d*][1,2,3]-triazole (**7b**) led to the formation of a second dinitrated product, 5-chloro-2-methyl-4,6-dinitro-2H-benzo[*d*][1,2,3]triazole, in addition to the mononitrated 5-chloro-2-methyl-4-nitro-2H-benzo[*d*][1,2,3]-triazole (**10b**).[356] The product of nitration (2mmol) was reduced using 10 equiv. of iron powder ($Fe_{(s)}$) in a mixture of 3 mL of saturated NH_4Cl and 11 mL EtOH under reflux for 30 min. to 16h. Upon completion, the reaction medium is filtrated over a celite pad, washed with EtOAc. After extraction, the OL is dried with Na_2SO_4 and concentrated *in-vacuo* to afford N-methylbenzotriazol-4-amines (**10c–12c**).

4.1. *Nitrated N-methylbenzotriazoles*

- *5-chloro-2-methyl-4-nitro-2H-benzo[d][1,2,3]triazole (***10b***)*

Obtained following the general procedure A using **7b**, 77% yield, white powder. ^{1}H-NMR (400 MHz, $CDCl_3$) δ 8.01 (d, J= 9.03 Hz, 1H), 7.49 (d, J= 9.03 Hz, 1H), 4.58 (s, 3H). ^{13}C-NMR (100 MHz, $CDCl_3$) δ 44.09; 118.83; 122.80; 125.95; 128.53; 138.26; 144.28.

- *5-chloro-2-methyl-4,6-dinitro-2H-benzo[d][1,2,3]triazole*

Obtained as a side product following the general procedure A using **7b**, 23 % yield, white powder. ^{1}H-NMR (400 MHz, $CDCl_3$) δ 8.59 (s, 1H), 4.66 (s, 3H).

- *6-chloro-1-methyl-4-nitro-1H-benzo[d][1,2,3]triazole (***11b***)*

Obtained following the general procedure A using **8b**, quantitative yield, white powder. ^{1}H-NMR (400 MHz, $CDCl_3$) δ 4.26 (3H, s), 7.50 (1H, d, J=8.83 Hz), 8.17 (1H, d, J=8.83 Hz). ^{13}C-NMR (100 MHz, $CDCl_3$) *δ 36.20; 123.73; 125.84; 126.01; 126.55; 146.94.*

- *5-chloro-1-methyl-4 nitro-1H-benzo[d][1,2,3]triazole (***12b***)*

Obtained following the general procedure A using **9b**, quantitative yield, white powder. ^{1}H-NMR (400 MHz, $CDCl_3$) δ 4.39 (3H, s), 7.61 (1H, d, J=8.84 Hz), 7.69 (1H, d, J=8.84 Hz). ^{13}C-NMR (100 MHz, $CDCl_3$) δ 35.02; 113.19; 122.49; 129.53; 133.82; 139.03.

4.2. *N-methylbenzotriazol-4-amines*

- *5-chloro-2-methyl-2H-benzo[d][1,2,3]triazol-4-amine (***10c***)*

Obtained in quantitative yield, starting from **10b**, as a powder. ^{1}H-NMR (400 MHz, DMSO): δ 4.45 (s, 3H), 6.01 (bs, 1H), 7.02 (d, J= 8.92 Hz, 1H), 7.20 (d, J= 8.93 Hz, 1H). ^{13}C-NMR (100 MHz, DMSO) δ 43.54; 104.77; 107.79; 128.91; 135.31; 136.91; 144.02.

- *6-chloro-1-methyl-1H-benzo[d][1,2,3]triazol-4-amine (***11c***)*

Obtained in quantitative yield, starting from **11b**, as a yellow powder. ^{1}H-NMR (400 MHz, $CDCl_3$) δ 4.45 (bs, 2H), 4.52 (s, 3H) 7.20 (d, J= 8.60 Hz, 1H), 7.34 (d, J= 8.60 Hz, 1H). ^{13}C-NMR (100 MHz, $CDCl_3$) δ 36.74; 110.22; 116.31; 125.48; 126.08; 128.38; 146.49.

- *5-chloro-1-methyl-1H-benzo[d][1,2,3]triazol-4-amine (***12c***)*

Obtained starting from **12b**. Purified using a DCM + 1% MeOH flash column. Yield= 73 %. ^{1}H-NMR (400 MHz, $CDCl_3$) δ 7.31 (d, J= 8.68 Hz, 1H), 6.72 (d, J= 8.64 Hz, 1H), 5.08 (bs, 1H), 4.22 (s, 1H). ^{13}C-NMR (100 MHz, $CDCl_3$) δ 34.35; 97.47; 109.71; 129.19; 133.51; 135.25; 136.99.

5. Synthesis of cross-coupled benzotriazole compounds

Prior to the coupling procedures, the solvent 1,4-Dioxane and K_3PO_4 solution in water were degassed by atmosphere exchange with nitrogen in a sonication bath for 45 minutes. The cross-coupling procedure was adapted from *DM Knapp et al.*[303] We found that the use of Pd(dppf)Cl_2 as catalyst significantly increased the yield as compared to Pd(OAc)$_2$.

(A) Coupling procedure adapted for the use of a pinacol boronic ester (41, 42).

Aryl-halide (1mmol, 1 eq) and the boronic ester (1.6 eq), $Pd(dppf)Cl_2$ (5 mol %) and SPhos (10 mol %) were introduced into a 25 ml 2-neck round-bottom flask under inert atmosphere. Then, 10 mL of degassed dioxane were added and the reaction was left under agitation at r.t. for 10 minutes until dissolution of reactants. Finally, 2 mL of degassed distilled water containing K_3PO_4 (3.5 mmol) were added to the media and the reaction was stirred for 3 to 16h at 70°C. When the conversion was complete, the mixture was cooled to room temperature, diluted with 1N NaOH (10 mL) and extracted twice with 10 mL EtOAc. The combined organic fractions were dried over Na_2SO_4 and concentrated in vacuo. The obtained residue was purified by flash chromatography on silica gel with the appropriate gradient of EtOAc in cyclohexane to afford the cross-coupled protected intermediate.

(B) Coupling procedure adapted for the use of a MIDA boronate (43).

The coupling procedure above was slightly adapted when couplings were performed using MIDA boronate **43**. In this modified procedure 1.2 eq of boronate and 7 eq of K_3PO_4 were used.

5.1. General deprotection procedures.

Two different deprotection protocols were used for removing N-phenylsulfonyl present on the indole of cross-coupled compounds depending on the stability of moieties present on the molecule.

(A) Strong deprotection conditions for SO_2Ph

0.5 mmol of starting compound were dissolved in 4 mL of a 1:1 solution of $MeOH/H_2O$ containing 2.5 M of KOH. The resulting mixture was refluxed until completion of the reaction (30 min. – 48h.).

(B) Mild deprotection conditions for SO_2Ph

0.5 mmol of starting compound were dissolved in 4 mL of a 1M solution of TBAF in THF. The resulting mixture was refluxed until completion of the reaction (2h. – 48h.).

(C) Tert-butyloxycarbonyl (*Boc*) deprotection

0.5 mmol of starting compound were dissolved in 4 mL of a 1:1 solution of MeOH/H2O containing 4 M of KOH. The resulting mixture was refluxed until completion of the reaction (30 min. – 48h.).

5.2. Products of cross-coupling and deprotection.

5.2.1. Compounds obtained following cross-coupling procedure B (using 43)

The following compounds were synthesised according to the general coupling procedure and then deprotected using the appropriate deprotection procedure.

- *6-(1H-indol-3-yl)-1H-benzo[d][1,2,3]triazole (***6***)*

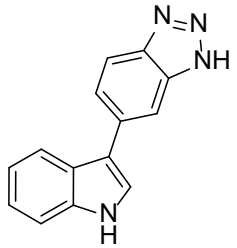

1-(4-methoxybenzyl)-6-(1-(phenylsulfonyl)-1H-indol-3-yl)-1H-benzo[d][1,2,3]triazole was obtained after coupling between compounds **43** and the mixture of 6-bromo-1-(4-methoxybenzyl)-1*H*-benzo[*d*][1,2,3]triazole + 5-bromo-1-(4-methoxybenzyl)-1*H*-benzo[*d*][1,2,3]triazole (**6b**). Purified using flash chromatography (Cyclohexane/ EtOAc 3:1). The obtained white powder underwent general SO_2Ph deprotection procedure A. to afford *6-(1H-indol-3-yl)-1-(4-methoxybenzyl)-1H-benzo[d][1,2,3]triazole*, which was deprotected in pure TFA at reflux temperature. The reaction was left for 16h, after which only around 20 % of the reactant were deprotected a flash chromatography, the rest was starting material. Purification by flash chromatography (cyclohexane/EtOAc) was performed. *6-(1H-indol-3-yl)-1-(4-methoxybenzyl)-1H-benzo[d][1,2,3]triazole* was deprotected again under the same conditions. This procedure was repeated 2 more times. Overall yield: 24 % ^{1}H NMR (600MHz, DMSO): δ 7.14 (1H, t, J=7.05 Hz), 7.19 (1H, t, J=7.10 Hz), 7.48 (1H, d, J=8.02 Hz), 7.76 (1H, dd, J=1.34, 8.59 Hz), 7.82 (1H, d, J=2.53 Hz), 7.94 (1H, d, J=7.90 Hz), 7.97 (1H, d, J=8.58 Hz), 8.04 (1H, s), 11.45 (1H, s). ^{13}C NMR (150MHz, DMSO): δ 110.29; 112.56; 115.88; 116.63; 119.35; 120.30; 122.06; 124.70; 125.48; 134.01; 137.43. HRMS: m/z (EI+), calculated for: $C_{14}H_{10}N_4$ 235.0939 $[M]^+$, found: 235.0639 $[M]^+$. Melting temp. range: 120 – 124 °C.

- *5-(1H-indol-3-yl)-2-methyl-2H-benzo[d][1,2,3]triazole (**7**)*

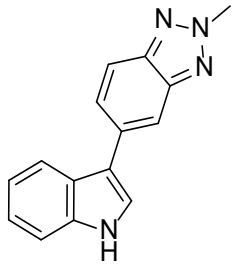

2-methyl-5-(1-(phenylsulfonyl)-1H-indol-3-yl)-2H-benzo[d][1,2,3]triazole was obtained after coupling **43** with **7b**. Purified by flash chromatography (Cyclohexane/EtOAc: 3:1 ➔ 2:1). Off white powder. Yield: 76%. ^{1}H NMR (400MHz, $CDCl_3$): *δ* 4.54 (3H, s), 7.32 (1H, t, J=7.51 Hz), 7.40 (1H, t, J=7.51 Hz), 7.46 (2H, t, J=7.69 Hz), 7.56 (1H, t, J=7.41 Hz), 7.62 (1H, dd, J=8.82, 1.09 Hz), 7.79 (1H, s), 7.83 (1H, d, J=7.86 Hz), 7.94 (3H, t, J=8.33 Hz), 8.09 (2H, t, J=6.11 Hz). ^{13}C NMR (100MHz, $CDCl_3$): *δ* 43.32; 113.91; 116.16; 118.44; 120.42; 123.38; 123.85; 125.21; 126.89; 127.43; 129.21; 129.41; 131.24; 134.01; 135.54; 138.12; 144.06; 145.03.

2-methyl-5-(1-(phenylsulfonyl)-1H-indol-3-yl)-2H-benzo[d][1,2,3]triazole was deprotected following general procedure A to afford **7**. Purified by flash chromatography (DCM/MeOH: 1:0 ➔ 9:1). Off white powder. Yield: 56 %. ^{1}H NMR (600MHz, $CDCl_3$): *δ* 4.54 (3H, s), 7.22 – 7.25 (1H, m), 7.27 – 7.30 (1H, m), 7.47 (1H, dd, J=2.77, 5.30 Hz), 7.73 (1H, dd, J=1.47, 8.82 Hz), 7.91 (1H, d, J=8.81 Hz), 8.01 (1H, d, J=7.93 Hz), 8.11 (1H, s), 8.34 (1H, s). ^{13}C NMR (150MHz, $CDCl_3$): *δ* 43.16; 111.53; 114.50; 117.93; 118.15; 119.77; 120.64; 122.31; 122.70; 125.72; 127.92; 133.90; 136.73; 143.56; 145.45. HRMS: m/z (EI+), calculated for: $C_{15}H_{12}N_4$ 249.1096 $[M]^+$, found: 249.1132 $[M]^+$. Melting temp. range: 157 – 160 °C.

- *5-(1H-indol-3-yl)-2-methyl-2H-benzo[d][1,2,3]triazol-4-amine (**10**)*

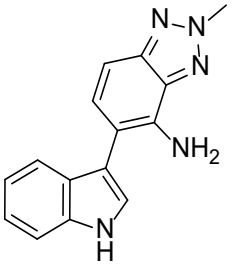

2-methyl-5-(1-(phenylsulfonyl)-1H-indol-3-yl)-2H-benzo[d][1,2,3]triazol-4-amine was obtained after coupling **43** with **10c**. Purified by flash chromatography (Cyclohexane/EtOAc: 3:1 ➔ 1:1). Yield: 64 %. ^{1}H NMR (400MHz, $CDCl_3$): *δ* 4.46 (2H,

s) 4.51 (3H, s), 7.23 – 7.30 (4H, m), 7.39 (1H, t, J=7.62 Hz), 7.50 (3H, q, J=8.21 Hz), 7.58 (1H, t, J=7.41 Hz), 7.72 (1H, s), 7.97 (2H, d, J=7.53 Hz), 8.10 (1H, d, J=8.33 Hz). ^{13}C NMR (100MHz, $CDCl_3$): *δ* 43.16; 106.24; 108.69; 113.87; 120.74; 121.11; 123.58; 124.26; 125.22; 126.90; 129.42; 129.92; 130.29; 134.01; 134.83; 135.24.

2-methyl-5-(1-(phenylsulfonyl)-1H-indol-3-yl)-2H-benzo[d][1,2,3]triazol-4-amine was deprotected following general procedure A to afford **10**.Purified by flash chromatography (Cyclohexane/EtOAc: 2:1 ➔ 0:1). Yield: 50%. ^{1}H NMR (600MHz, DMSO): *δ* 4.52 (3H, s), 5.26 (2H, s), 7.09 (1H, t, J=7.15 Hz), 7.17 (1H, d, J=8.59 Hz), 7.21 (1H, t, J=7.50 Hz), 7.36 (1H, d, J=8.59 Hz), 7.52 (2H, dd, J=3.12, 8.06 Hz), 7.56 (1H, d, J=2.43 Hz), 11.38 (1H, s). ^{13}C NMR (150MHz, DMSO): *δ 43.39; 104.40; 111.10; 112.30; 112.91; 119.48; 119.72; 121.80; 124.54; 126.57; 131.32; 135.09; 136.80; 137.64; 144.43.*

. HRMS: m/z (EI+), calculated for: $C_{15}H_{13}N_5$ 264.1205 $[M]^+$, found: 264.1242 $[M]^+$. Melting temp. range: 135 – 139 °C.

- *6-(1H-indol-3-yl)-1-methyl-1H-benzo[d][1,2,3]triazole (**8**)*

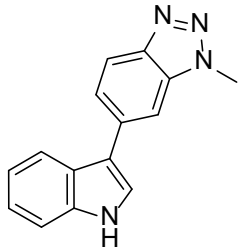

1-methyl-6-(1-(phenylsulfonyl)-1H-indol-3-yl)-1H-benzo[d][1,2,3]triazole was obtained after coupling **43** with **8b**. Purified by flash chromatography (Cyclohexane/EtOAc: 2:1 ➔ 1:1). Off white powder. Yield: 87 %.^{1}H NMR (400MHz, DMSO): *δ* 4.35 (3H, s, 7.34 (1H, t, J=7.20 Hz), 7.42 (1H, t, J=7.38 Hz), 7.48 (2H, t, J=7.69 Hz), 7.58 (1H, t, J=7.45 Hz), 7.62 (1H, dd, J=1.24, 8.62 Hz), 7.71 (1H, s), 7.78 – 7.83 (2H, m), 7.96 (2H, d, J=7.44 Hz), 8.08 – 8.15 (2H, m). ^{13}C NMR (100MHz, DMSO): *δ* 34.35; 107.78; 113.97; 120.21; 120.45; 123.45; 123.68; 123.95; 124.72; 125.38; 126.92; 129.04; 129.47; 132.62; 134.09; 134.12; 135.48; 138.02; 145.44.

1-methyl-6-(1-(phenylsulfonyl)-1H-indol-3-yl)-1H-benzo[d][1,2,3]triazole was deprotected following general procedure A to afford **8**. Purified by flash chromatography (DCM/MeOH: 1:0 ➔ 9:1). Off white powder. Yield: 79 %. ^{1}H NMR (400MHz, DMSO): *δ* 4.36 (3H, s), 7.13 – 7.24 (2H, m), 7.50 (1H, d, J=7.83 Hz), 7.78 (2H, d, J=8.88 Hz), 7.88 (1H, d, J=2.24 Hz), 8.01 – 8.10 (3H, m), 11.54 (1H, s). ^{13}C NMR (100MHz, DMSO): *δ* 34.53; 106.63; 112.56; 115.63; 119.56; 119.73; 120.42;

122.20; 124.57; 125.21; 125.34; 134.73; 135.65; 137.47; 144.00. HRMS: m/z (EI+), calculated for: $C_{15}H_{12}N_4$ 249.1096 $[M]^+$, found: 249.1135 $[M]^+$. Melting temp. range: 230 – 234 °C.

- *6-(1H-indol-3-yl)-1-methyl-1H-benzo[d][1,2,3]triazol-7-amine (**11**)*

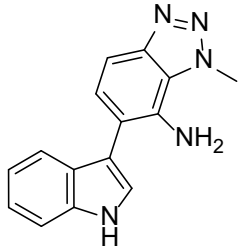

1-methyl-6-(1-(phenylsulfonyl)-1H-indol-3-yl)-1H-benzo[d][1,2,3]triazol-7-amine was obtained after coupling **43** with **11c**. Purified by flash chromatography (Cyclohexane/EtOAc 1:0 ➔ 1:2). Yield: 39%. ^{1}H NMR (400MHz, DMSO): δ 4.08 (2H, s), 4.59 (3H, s), 7.18 (1H, d, J=8.52 Hz), 7.29 (1H, d, J=7.41 Hz), 7.40 (1H, d, J=8.04 Hz), 7.44 (1H, d, J=7.88 Hz), 7.47 – 7.55 (3H, m), 7.60 (1H, t, J=7.42 Hz), 7.70 (1H, s), 7.97 (2H, d, J=7.52 Hz), 8.10 (1H, d, J=8.33 Hz). ^{13}C NMR (100MHz, DMSO): δ 36.96; 110.23; 113.89; 114.63; 119.82; 120.86; 123.77; 124.70; 125.48; 126.92; 127.94; 129.50; 129.75; 129.81; 134.15; 135.18; 138.03.

1-methyl-6-(1-(phenylsulfonyl)-1H-indol-3-yl)-1H-benzo[d][1,2,3]triazol-7-amine was deprotected following general procedure A to afford **11**. Purified by flash chromatography (Cyclohexane/EtOAc 2:1 ➔ 0:1). ^{1}H NMR (400MHz, DMSO): δ 4.55 (3H, s), 4.99 (2H, s), 7.06 (1H, t, J=7.44 Hz), 7.18 (1H, t, J=7.52 Hz), 7.23 (1H, d, J=8.47 Hz), 7.33 (1H, d, J=8.46 Hz), 7.44 (1H, d, J=7.90 Hz), 7.47 – 7.57 (2H, m). ^{13}C NMR (100MHz, DMSO): δ 37.25; 107.93; 112.29; 112.41; 117.09; 119.70; 121.99; 125.06; 126.27; 126.51; 128.81; 131.19; 136.82; 146.79. HRMS: m/z (EI+), calculated for: $C_{15}H_{13}N_5$ 264.1205 $[M]^+$, found: 264.1242 $[M]^+$. Melting temp. range: 299 – 304 °C.

- *5-(1H-indol-3-yl)-1-methyl-1H-benzo[d][1,2,3]triazole (**9**)*

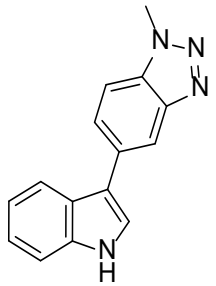

1-methyl-5-(1-(phenylsulfonyl)-1H-indol-3-yl)-1H-benzo[d][1,2,3]triazole was obtained after coupling **43** with **9b**. Purified by flash chromatography (Cyclohexane/EtOAc 3:1 ➔ 0: 1). Yield: 67 %. ^{1}H NMR (400MHz, $CDCl_3$): δ 4.34 (3H, s), 7.32 (1H, t, J=7.53 Hz), 7.40 (1H, t, J=7.64 Hz), 7.46 (2H, t, J=7.69 Hz), 7.55 (1H, t, J=7.43 Hz), 7.60 (1H, d, J=8.55 Hz), 7.72 (1H, dd, J=1.12, 8.55 Hz), 7.76 (1H, s), 7.80 (1H, d, J=7.87 Hz), 7.95 (2H, d, J=7.63 Hz), 8.09 (1H, d, J=8.30 Hz), 8.26 (1H, s). ^{13}C NMR (100MHz, $CDCl_3$): δ 34.42; 109.78; 113.90; 118.56 ; 120.24 ; 123.24 ; 123.46 ; 123.90 ; 125.26 ; 126.88 ; 128.13 ; 129.07 ; 129.21 ; 129.43 ; 133.03 ; 134.06 ; 135.48 ; 138.05 ; 146.56.

1-methyl-5-(1-(phenylsulfonyl)-1H-indol-3-yl)-1H-benzo[d][1,2,3]triazole was deprotected following general procedure A to afford *5-(1H-indol-3-yl)-1-methyl-1H-benzo[d][1,2,3]triazole* (**9**). Purified by flash chromatography (DCM/MeOH 1:0 ➔ 9: 1). ^{1}H NMR (400MHz, $CDCl_3$): δ 4.34 (3H, s), 7.24 (1H, t, J=7.07 Hz), 7.29 (1H, t, J=7.09 Hz), 7.45 (1H, d, J=2.49 Hz), 7.48 (1H, d, J=8.10 Hz), 7.58 (1H, d, J=8.57 Hz), 7.85 (1H, dd, J=1.38, 8.53 Hz), 7.98 (1H, d, J=7.94 Hz), 8.31 (1H, s), 8.37 (1H, s). ^{13}C NMR (100MHz, $CDCl_3$): δ 34.31; 109.26; 111.54; 117.38; 117.73; 119.50; 120.63; 122.12; 122.69; 125.75; 128.33; 131.84; 132.36; 136.67; 146.91. HRMS: m/z (EI+), calculated for : $C_{15}H_{12}N_4$ 249.1096 $[M]^+$, found: 249.1131 $[M]^+$. Melting temp. range: 193 – 195 °C.

- *5-(1H-indol-3-yl)-1-methyl-4-nitro-1H-benzo[d][1,2,3]triazole (***16***)*

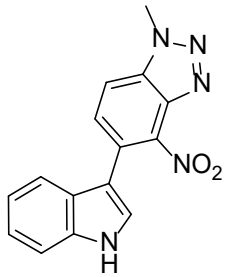

1-methyl-4-nitro-5-(1-(phenylsulfonyl)-1H-indol-3-yl)-1H-benzo[d][1,2,3]triazole was obtained after coupling **43** with **12b**. Purified by flash chromatography (DCM/MeOH 1:0 ➔ 9: 1). Yield: 68 %. ^{1}H NMR (400MHz, $CDCl_3$): δ 4.45 (3H, s), 7.28 (1H, t, J=7.53 Hz), 7.35 – 7.41 (2H, m), 7.42 (1H, s), 7.53 (2H, t, J=7.58 Hz), 7.62 (1H, t, J=7.35 Hz), 7.72 (1H, d, J=8.57 Hz), 7.80 (1H, s), 7.87 – 7.96 (3H, m), 8.03 (1H, d, J=8.30 Hz). ^{13}C NMR (100MHz, $CDCl_3$): δ 34.93; 113.10; 113.75; 117.13; 119.41; 121.93; 124.08; 125.26; 125.57; 126.72; 129.28; 129.48; 130.31; 134.26; 134.65; 137.42; 154.82.

1-methyl-4-nitro-5-(1-(phenylsulfonyl)-1H-indol-3-yl)-1H-benzo[d][1,2,3]triazole was deprotected following general procedure A to afford *5-(1H-indol-3-yl)-1-methyl-4-nitro-1H-benzo[d][1,2,3]triazole (**16**).* Purified by flash chromatography (DCM/MeOH 1:0 ➔ 9: 1). Red powder. Yield: 46 %. ^{1}H NMR (600MHz, DMSO): δ 4.44 (3H, s), 7.10 (1H, t, J=7.48 Hz), 7.21 (1H, t, J=7.55 Hz), 7.45 (1H, d, J=7.98 Hz), 7.51 (1H, d, J=8.15 Hz), 7.61 (1H, d, J=2.50 Hz), 7.89 (1H, d, J=8.63 Hz), 8.23 (1H, d, J=8.62 Hz), 11.66 (1H, s). ^{13}C NMR (150MHz, DMSO): δ 35.40; 109.75; 112.76; 115.22; 118.40; 120.61; 122.58; 124.89; 125.81; 126.03; 131.18; 134.12; 136.80; 137.58; 138.46. HRMS: m/z (EI+), calculated for: $C_{15}H_{13}N_5$ 294.0946 $[M]^+$, found: 294.0987 $[M]^+$. Melting temp. range: 269 – 277 °C.

- *5-(1H-indol-3-yl)-1-methyl-1H-benzo[d][1,2,3]triazol-4-amine (**12**)*

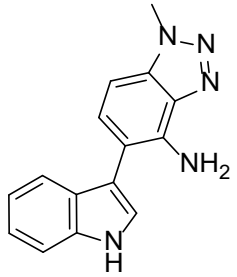

1-methyl-5-(1-(phenylsulfonyl)-1H-indol-3-yl)-1H-benzo[d][1,2,3]triazol-4-amine was obtained after coupling **43** with **12c**. Purified by flash chromatography (Cyclohexane/EtOAc 3:1 ➔ 2:1). Yield: 65 %. ^{1}H NMR (400MHz, $CDCl_3$): δ 4.27 (1H, s), 4.78 (1H, s), 6.85 (1H, d, J=8.32 Hz), 7.24 – 7.30 (1H, m), 7.33 (1H, d, J=8.32 Hz), 7.39 (1H, t, J=7.56 Hz), 7.49 (1H, t, J=7.50 Hz), 7.55 – 7.61 (1H, m), 7.71 (1H, s), 7.97 (1H, d, J=7.56 Hz), 8.10 (1H, d, J=8.24 Hz).

1-methyl-5-(1-(phenylsulfonyl)-1H-indol-3-yl)-1H-benzo[d][1,2,3]triazol-4-amine was deprotected following general procedure A to afford **12**. Purified by flash chromatography (Cyclohexane/EtOAc 4:1 ➔ 1:1). Yield: 74 %. ^{1}H NMR (400MHz, $CDCl_3$): δ 4.27 (3H, s), 4.85 (2H, s), 6.86 (1H, d, J=8.30 Hz), 7.16 – 7.19 (1H, m), 7.27 – 7.30 (1H, m), 7.37 (2H, d, J=2.41 Hz), 7.45 (1H, s), 7.46 (1H, s), 7.49 (2H, d, J=8.19 Hz), 7.60 (2H, d, J=7.57 Hz), 8.36 (1H, br s). ^{13}C NMR (100MHz, $CDCl_3$): δ 34.24; 96.85; 111.10; 111.44; 113.92; 120.11; 120.20; 122.65; 123.03; 126.58; 131.79; 134.10; 136.26; 136.61; 137.47. HRMS: m/z (EI+), calculated for : $C_{15}H_{13}N_5$ 264.1205 $[M]^+$, found: 264.1244 $[M]^+$. Melting temp. range: 177 – 181 °C.

- *2-(6-(1H-indol-3-yl)-1H-benzo[d][1,2,3]triazol-1-yl)acetamide (**21**)*

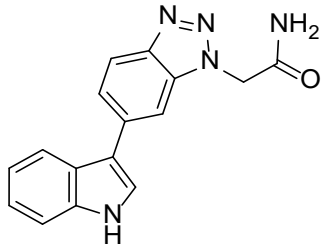

2-(6-(1-(phenylsulfonyl)-1H-indol-3-yl)-1H-benzo[d][1,2,3]triazol-1-yl)acetamide was obtained after coupling **43** with **22b**. The coupling product was obtained bearing an acetamide instead of the initial acetonitrile. Purified by flash chromatography (cyclohexane/EtOAc 3:1). Yield: 80 %. ^{1}H NMR (400MHz, $CDCl_3$): δ 5.50 (2H, s), 7.39 (1H, t, J=7.42 Hz), 7.44 – 7.50 (2H, m), 7.62 (2H, t, J=7.56 Hz), 7.71 (1H, t, J=7.28 Hz), 7.80 (1H, d, J=8.76 Hz), 7.88 (1H, s), 7.96 (1H, d, J=7.92 Hz), 8.06 (1H, d, J=8.24 Hz), 8.09 – 8.17 (4H, m), 8.26 (1H, s).

2-(6-(1-(phenylsulfonyl)-1H-indol-3-yl)-1H-benzo[d][1,2,3]triazol-1-yl)acetamide was deprotected following general procedure **B** to afford **22***.* Purified by flash chromatography (cyclohexane/EtOAc). Yield: 48 %. ^{1}H NMR (600MHz, MeOD): δ 5.53 (2H, s), 7.17 (1H, t, J=7.40 Hz), 7.21 (1H, t, J=7.39 Hz), 7.48 (1H, d, J=8.02 Hz), 7.66 (1H, s), 7.83 (1H, d, J=8.64 Hz), 7.94 (1H, s), 7.99 (1H, d, J=7.88 Hz), 8.03 (1H, d, J=8.66 Hz) Amide protons (N**H$_2$**) and indole N**H** not visible in MeOD. ^{13}C NMR (150 MHz, MeOD): δ 49.43; 106.30; 111.46; 115.90; 118.50; 118.73; 119.76; 121.67; 123.56; 125.02; 125.30; 134.72; 136.85; 137.43; 143.70; 169.28. HRMS: m/z (EI+), calculated for: $C_{16}H_{14}N_5O$ 292.1193 $[M]^+$, found: 292.1197 $[M]^+$. Melting temp. range: 210 – 214 °C.

- *2-(6-(1H-indol-3-yl)-1H-benzo[d][1,2,3]triazol-1-yl)acetic acid (**23**)*

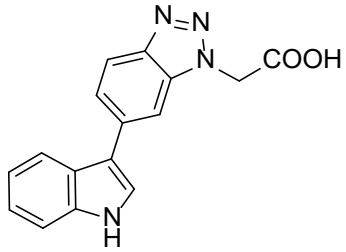

2-(6-(1-(phenylsulfonyl)-1H-indol-3-yl)-1H-benzo[d][1,2,3]triazol-1-yl)acetonitrile was deprotected following general procedure A. After completion, the reaction media was extracted with EtOAc and the OL was discarded. Then, the aqueous layer was acidified to pH 2 and extracted again with EtOAc. The OL containing **24** was dried with Na_2SO_4 and evaporated. White powder. Yield: 72 %. ^{1}H NMR (400MHz,

$CDCl_3$): δ 5.74 (2H, s), 7.13 – 7.25 (2H, m), 7.50 (1H, d, J=7.87 Hz), 7.80 (1H, d, J=8.73 Hz), 7.88 (1H, d, J=1.54 Hz), 8.04 – 8.13 (3H, m), 11.56 (1H, s). ^{13}C NMR (100MHz, $CDCl_3$): δ 49.10; 106.87; 112.56; 115.53; 119.65; 119.77; 120.39; 122.22; 124.60; 125.27; 125.30; 134.95; 135.96; 137.49; 143.92; 169.43. MS: m/z (EI+), calculated for $C_{16}H_{13}N_4O_2^+$: $[M]^+$ 293.1, found: 293.1 $[M]^+$. Melting temp. range: 248 – 255 °C.

- *2-(5-(1H-indol-3-yl)-1H-benzo[d][1,2,3]triazol-1-yl)acetamide (**22**)*

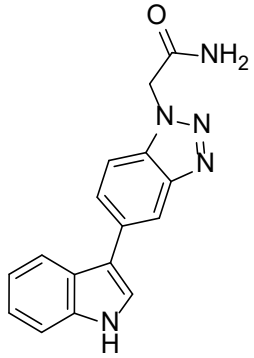

2-(5-(1-(phenylsulfonyl)-1H-indol-3-yl)-1H-benzo[d][1,2,3]triazol-1-yl)acetamide was obtained after coupling **43** with **22b**. The coupling product was obtained bearing an acetamide instead of the initial acetonitrile. Purified by flash chromatography (cyclohexane/EtOAc 3:1). Yield: 83 %. ^{1}H NMR (400MHz, $CDCl_3$): δ 5.48 (2H, s), 7.38 (1H, t, J=7.47 Hz), 7.46 (2H, t, J=7.79 Hz), 7.50 (1H, s), 7.63 (2H, t, J=7.55 Hz), 7.72 (1H, t, J=7.24 Hz), 7.92 (4H, d, J=7.19 Hz), 8.07 (1H, d, J=8.16 Hz), 8.13 (3H, d, J=7.68 Hz), 8.25 (1H, s), 8.37 (1H, s).

2-(5-(1-(phenylsulfonyl)-1H-indol-3-yl)-1H-benzo[d][1,2,3]triazol-1-yl)acetamide was deprotected following general procedure B to afford **23**. Purified by flash chromatography (cyclohexane/EtOAc). Yield: 49 %. ^{1}H NMR (400MHz, DMSO): δ 5.44 (2H, s), 7.14 (1H, t, J=7.32 Hz), 7.19 (1H, t, J=7.33 Hz), 7.44 – 7.54 (2H, m), 7.78 – 7.85 (2H, m), 7.85 – 7.99 (3H, m), 8.23 (1H, s), 11.45 (1H, s). ^{13}C NMR (100MHz, DMSO): δ 50.22; 111.67; 112.51; 115.31; 115.70; 119.31; 120.27; 122.04; 124.47; 125.47; 128.02; 137.38; 146.69; 168.02. HRMS: m/z (EI+), calculated for: $C_{16}H_{14}N_5O$ 292.1193 $[M]^+$, found: 292.1195 $[M]^+$. Melting temp. range: 252 – 254 °C.

- *2-(5-(1H-indol-3-yl)-1H-benzo[d][1,2,3]triazol-1-yl)acetic acid (**24**)*

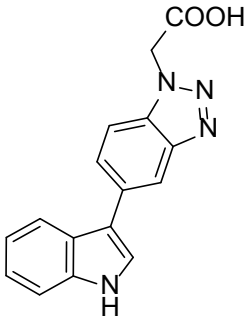

2-(5-(1-(phenylsulfonyl)-1H-indol-3-yl)-1H-benzo[d][1,2,3]triazol-1-yl)acetonitrile was deprotected following general procedure A. After completion, the reaction media was extracted with EtOAc and the OL was discarded. Then, the aqueous layer was acidified to pH 2 and extracted again with EtOAc. The OL containing **25** was dried with Na_2SO_4 and evaporated. White powder. Yield: 63 %. ^{1}H NMR (400MHz, $CDCl_3$): δ 5.69 (2H, s), 7.12 – 7.22 (2H, m), 7.49 (1H, d, J=7.86 Hz), 7.83 (1H, d, J=2.31 Hz), 7.89 – 7.98 (3H, m), 8.25 (1H, s), 11.47 (1H, s), 13.46 (1H, br s). ^{13}C NMR (100MHz, $CDCl_3$): δ 49.22; 111.54; 112.51; 115.36; 115.62; 119.32; 120.29; 122.05; 124.54; 125.45; 128.22; 132.51; 132.59; 137.38; 146.55; 169.27. MS: m/z (EI+), calculated for $C_{16}H_{13}N_4O_2^+$: 293.1 $[M]^+$, found: 293.1 $[M]^+$. Melting temp. range: 250 – 252 °C.

5.2.2. Compounds obtained following cross-coupling general procedure A (pinacol boronic esters)

5.2.2.1. Using 1-(phenylsulfonyl)-3-(4,4,5,5-tetramethyl-1,3,2-dioxaborolan-2-yl)-1H-indole (42)

- *6-(1H-indol-3-yl)-2-methyl-2H-[1,2,3]triazolo[4,5-b]pyridine (**13**)*

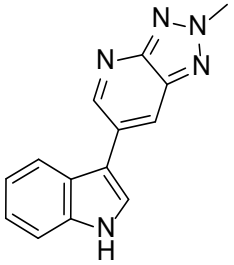

2-methyl-6-(1-(phenylsulfonyl)-1H-indol-3-yl)-2H-[1,2,3]triazolo[4,5-b]pyridine was obtained after coupling **42** with **13**. Purified by flash chromatography (Cyclohexane/EtOAc 4:1 ➔ 1:1). Yield: 77 %. ^{1}H NMR (400MHz, $CDCl_3$): δ 4.40 (3H, s), 7.37 (1H, t, J=7.57 Hz), 7.46 (1H, t, J=8.05 Hz), 7.51 (2H, t, J=7.70 Hz), 7.60 (1H, t,

J=7.47 Hz), 7.76 (1H, d, J=7.93 Hz), 7.87 (1H, s), 7.98 (2H, d, J=7.51 Hz), 8.07 (1H, d, J=1.78 Hz), 8.12 (1H, d, J=8.32 Hz), 9.01 (1H, d, J=1.80 Hz).

2-methyl-6-(1-(phenylsulfonyl)-1H-indol-3-yl)-2H-[1,2,3]triazolo[4,5-b]pyridine was deprotected following general procedure A to afford **13**. Purified by flash chromatography (Cyclohexane/EtOAc 3:1 ➔ 1:1). Yield: 68 % ^{1}H NMR (400MHz, DMSO): δ 4.40 (3H, s), 7.19 (1H, t, J=6.98 Hz), 7.23 (1H, t, J=7.02 Hz), 7.52 (1H, d, J=7.76 Hz), 8.05 (1H, s), 8.11 (1H, d, J=7.75 Hz), 8.33 (1H, s), 8.54 (1H, d, J=1.88 Hz), 9.11 (1H, d, J=1.90 Hz), 11.75 (1H, s). ^{13}C NMR (100MHz, DMSO): δ 35.28; 112.30; 112.70; 114.82; 119.62; 120.69; 122.49; 125.23; 125.91; 126.86; 131.05; 137.45; 148.39; 155.53. HRMS: m/z (EI+), calculated for: $C_{14}H_{11}N_5$ 250.1048 $[M]^+$, found: 250.1086 $[M]^+$. Melting temp. range: 257 – 260 °C.

- *6-(1H-indol-3-yl)-1-methyl-1H-[1,2,3]triazolo[4,5-b]pyridine (**14**)*

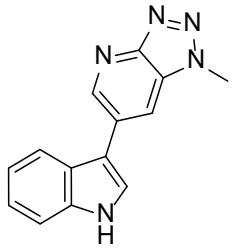

1-methyl-6-(1-(phenylsulfonyl)-1H-indol-3-yl)-1H-[1,2,3]triazolo[4,5-b]pyridine was obtained after coupling **42** with **14**. Purified by flash chromatography (Cyclohexane/EtOAc 4:1 ➔ 1:1). Yield: 49 %. ^{1}H NMR (400MHz, $CDCl_3$): δ 4.60 (3H, s), 7.36 (1H, t, J=7.63 Hz), 7.44 (2H, t, J=7.71 Hz), 7.50 (3H, t, J=7.71 Hz), 7.59 (1H, t, J=7.48 Hz), 7.78 (1H, d, J=7.82 Hz), 7.85 (1H, s), 7.98 (2H, d, J=7.54 Hz), 8.11 (1H, d, J=8.30 Hz), 8.39 (1H, d, J=1.97 Hz), 9.04 (1H, d, J=1.93 Hz).

1-methyl-6-(1-(phenylsulfonyl)-1H-indol-3-yl)-1H-[1,2,3]triazolo[4,5-b]pyridine was deprotected following general procedure A to afford **14**. Purified by flash chromatography (Cyclohexane/EtOAc 3:1 ➔ 1:1). ^{1}H NMR (400MHz, DMSO): δ 4.55 (3H, s), 7.17 (1H, t, J=7.34 Hz), 7.22 (1H, t, J=7.13 Hz), 7.51 (1H, d, J=7.96 Hz), 7.98 (1H, d, J=7.81 Hz), 8.02 (1H, d, J=2.52 Hz), 8.54 (1H, d, J=1.99 Hz), 9.19 (1H, d, J=1.91 Hz), 11.64 (1H, s). ^{13}C NMR (150MHz, DMSO): δ 44.26; 112.63; 112.66; 119.36; 120.72; 120.86; 122.44; 125.31; 125.56; 130.83; 137.07; 137.41; 152.56; 154.31. HRMS: m/z (EI+), calculated for: $C_{14}H_{11}N_5$ 250.1048 $[M]^+$, found: 250.1086 $[M]^+$. Melting temp. range: 206 – 211 °C.

- *6-(1H-indol-3-yl)-3-methyl-3H-[1,2,3]triazolo[4,5-b]pyridine (**15**)*

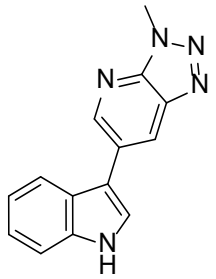

3-methyl-6-(1-(phenylsulfonyl)-1H-indol-3-yl)-3H-[1,2,3]triazolo[4,5-b]pyridine pyridine was obtained after coupling **42** with **14**. Purified by flash chromatography (Cyclohexane/EtOAc 4:1 ➔ 1:1). Yield: 72 %. ^{1}H NMR (400MHz, $CDCl_3$): δ 4.42 (3H, s), 7.36 (1H, t, J=7.32 Hz), 7.44 (1H, t, J=7.72 Hz), 7.50 (2H, t, J=7.69 Hz), 7.59 (1H, t, J=7.46 Hz), 7.74 (1H, d, J=7.87 Hz), 7.83 (1H, s), 7.98 (2H, d, J=7.45 Hz), 8.12 (1H, d, J=8.35 Hz), 8.55 (1H, d, J=1.77 Hz), 8.92 (1H, d, J=1.75 Hz).

3-methyl-6-(1-(phenylsulfonyl)-1H-indol-3-yl)-3H-[1,2,3]triazolo[4,5-b]pyridine was deprotected following general procedure A to afford **15**. Purified by flash chromatography (Cyclohexane/EtOAc 3:1 ➔ 1:1). Yield: 75 %. ^{1}H NMR (400MHz, DMSO): δ 4.33 (3H, s), 7.16 (1H, t, J=7.39 Hz), 7.22 (1H, t, J=7.45 Hz), 7.51 (1H, d, J=7.88 Hz), 7.94 (1H, t, J=3.19 Hz), 8.68 (1H, d, J=1.03 Hz), 9.13 (1H, d, J=1.02 Hz), 11.59 (1H, s). ^{13}C NMR (100MHz, DMSO): δ 33.35 ; 112.30 ; 112.62 ; 119.10 ; 120.67; 122.39; 123.88; 125.21; 125.30; 129.12; 137.25; 137.31; 144.49; 150.71. HRMS: m/z (EI+), calculated for: $C_{14}H_{11}N_5$ 250.1048 $[M]^+$, found: 250.1089 $[M]^+$. Melting temp. range: 207 – 209 °C.

- *6-(1H-indol-3-yl)isoquinoline (**2**)*

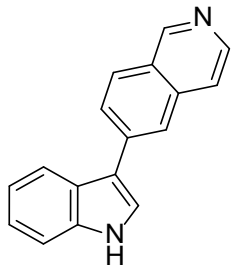

6-(1-(phenylsulfonyl)-1H-indol-3-yl)isoquinoline was obtained after coupling **42** with 6-bromoisoquinoline. Purified by flash chromatography (Cyclohexane/EtOAc 3:1 ➔ 0: 1). Yield: 84 %. ^{1}H NMR (400MHz, $CDCl_3$): δ 7.36 (1H, t, J=7.48 Hz), 7.43 (1H, t, J=7.64 Hz), 7.48 (2H, t, J=7.72 Hz), 7.57 (1H, t, J=7.40 Hz), 7.70 (1H, d, J=5.72 Hz), 7.84 – 7.90 (3H, m), 7.97 (2H, d, J=7.60 Hz), 8.04 – 8.14 (3H, m), 8.56 (1H, d, J=5.72 Hz), 9.28 (1H, s). ^{13}C NMR (100MHz, $CDCl_3$): δ 113.98; 120.36; 120.52; 123.16;

124.00; 124.04; 124.75; 125.40; 126.93; 127.60; 127.79; 128.42; 128.87; 129.47; 134.13; 135.29; 135.57; 136.20; 138.03; 143.50; 152.24.

6-(1-(phenylsulfonyl)-1H-indol-3-yl)isoquinoline was deprotected following general procedure A to afford **2**. Quantitative yield. ^{1}H NMR (400MHz, DMSO): δ 7.18 – 7.27 (2H, d, J=35.64 Hz), 7.53 (1H, d, J=7.49 Hz), 7.90 (1H, d, J=5.40 Hz), 8.03 (1H, s), 8.08 – 8.17 (3H, m), 8.29 (1H, s), 8.48 (1H, d, J=5.55 Hz), 9.26 (1H, s), 11.66 (1H, s). ^{13}C NMR (100MHz, DMSO): δ 112.69; 115.20; 119.88; 120.66; 120.71; 121.66; 122.34; 125.27; 126.01; 126.91; 127.62; 128.36; 136.63; 137.66 ; 138.54 ; 143.60 ; 152.20. HRMS: m/z (EI+), calculated for : $C_{17}H_{11}N_2$ 245.1034 $[M]^+$, found: 245.1073 $[M]^+$. Melting temp. range: 219 – 223 °C.

- *7-(1H-indol-3-yl)isoquinoline (**1**)*

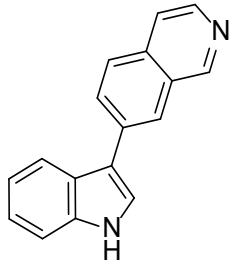

7-(1-(phenylsulfonyl)-1H-indol-3-yl)isoquinoline was obtained after coupling **42** with 5-bromoisoquinoline. Purified by flash chromatography (Cyclohexane/EtOAc 4:1 ➔ 1:4). Yield: 86 %. ^{1}H NMR (400MHz, $CDCl_3$): δ 7.36 (1H, t, J=7.50 Hz), 7.43 (1H, t, J=7.58 Hz), 7.48 (2H, t, J=7.72 Hz), 7.57 (1H, t, J=7.42 Hz), 7.70 (1H, d, J=5.72 Hz), 7.84 – 7.89 (2H, m), 7.92 – 8.00 (4H, m), 8.11 (1H, d, J=8.24 Hz), 8.20 (1H, s), 8.55 (1H, d, J=5.72 Hz), 9.31 (1H, s). ^{13}C NMR (100MHz, $CDCl_3$): δ 113.98; 120.29; 120.40; 123.18; 123.63; 123.97; 125.36; 125.93; 126.91; 127.30; 128.96; 128.99; 129.45; 130.69; 132.18; 134.09; 135.05; 135.55; 138.05; 143.10; 152.48.

7-(1-(phenylsulfonyl)-1H-indol-3-yl)isoquinoline was deprotected following general procedure A to afford **1**. *Quantitative* yield. ^{1}H NMR (400MHz, DMSO): δ 7.22 (2H, m), 7.52 (1H, d, J=7.44 Hz), 7.82 (1H, d, J=5.13 Hz), 7.97 – 8.05 (2H, t, J=9.61 Hz), 8.14 (1H, d, J=7.30 Hz), 8.20 (1H, d, J=8.23 Hz), 8.46 (2H, d, J=8.28 Hz), 9.41 (1H, s). ^{13}C NMR (100MHz, DMSO): δ 112.62; 115.29; 119.80; 120.48; 120.56; 122.24; 122.97; 125.27; 125.30 ; 127.29 ; 129.59 ; 130.78 ; 133.75 ; 135.53 ; 137.58 ; 142.47 ; 152.65. HRMS: m/z (EI+), calculated for: $C_{17}H_{11}N_2$ 245.1034 $[M]^+$, found: 245.1073 $[M]^+$. Melting temp. range: 208 – 214 °C.

- *7-(1H-indol-3-yl)quinazoline (**4**)*

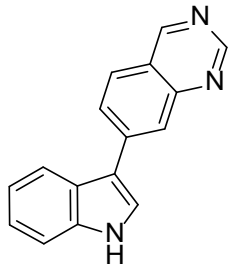

7-(1-(phenylsulfonyl)-1H-indol-3-yl)quinazoline was obtained after coupling **42** with 7-bromoquinazoline. Purified by flash chromatography (Cyclohexane/EtOAc 4:1 ➔ 1:4). Yellow powder. Yield: 56 %. ^{1}H NMR (400MHz, $CDCl_3$): δ 7.37 (1H, t, J=7.48 Hz), 7.44 (1H, t, J=7.66 Hz), 7.49 (2H, t, J=7.72 Hz), 7.59 (1H, t, J=7.40 Hz), 7.94 – 7.99 (5H, m), 8.04 (1H, d, J=8.40 Hz), 8.11 (1H, d, J=8.28 Hz), 8.32 (1H, s), 9.36 (1H, s), 9.43 (1H, s).

7-(1-(phenylsulfonyl)-1H-indol-3-yl)quinazoline was deprotected following general procedure A to afford **4**. Quantitative yield. ^{1}H NMR (400MHz, DMSO): δ 7.18 – 7.27 (2H, m), 7.53 (1H, d, J=7.07 Hz), 8.08 (1H, d, J=7.76 Hz), 8.12 – 8.24 (3H, q, J=9.53 Hz), 8.26 (1H, s), 9.25 (1H, s), 9.51 (1H, s), 11.79 (1H, bs). ^{13}C NMR (100MHz, DMSO): δ 112.88 ; 114.69 ; 119.61 ; 121.06; 122.17; 122.53; 123.20; 125.16; 127.05; 128.05; 128.47; 137.77; 142.80; 150.80; 155.93; 160.04. HRMS: m/z (EI+), calculated for: $C_{16}H_{11}N_3$ 246.0987 $[M]^+$, found: 246.1102 $[M]^+$. Melting temp. range: 221 – 226 °C.

- *6-(1H-indol-3-yl)quinazoline (**3**)*

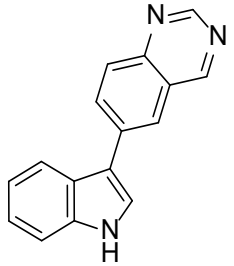

6-(1-(phenylsulfonyl)-1H-indol-3-yl)quinazoline was obtained after coupling **42** with 6-bromoquinazoline. Purified by flash chromatography (Cyclohexane/EtOAc 4:1 ➔ 1:4). Yield: 68 %. ^{1}H NMR (400MHz, $CDCl_3$): δ 7.37 (1H, t, J=7.34 Hz), 7.44 (1H, t, J=7.50 Hz), 7.49 (2H, t, J=7.72 Hz), 7.59 (1H, t, J=7.43 Hz), 7.85 (1H, d, J= 7.95 Hz), 7.88 (1H, s), 7.98 (1H, d, J=7.50 Hz), 8.12 (1H, d, J=8.27 Hz), 8.14 – 8.22 (4H, m), 9.36 (1H, s), 9.47 (1H, s).

6-(1-(phenylsulfonyl)-1H-indol-3-yl)quinazoline was deprotected following general procedure A to afford **3**. Quantitative yield. ^{1}H NMR (400MHz, DMSO): δ 7.16 – 7.26 (2H, m), 7.53 (1H, d, J=7.56 Hz), 7.99 – 8.07 (2H, d, J=8.00 Hz), 8.15 (1H, d, J=7.52 Hz), 8.41 – 8.50 (2H, m), 9.22 (1H, s), 9.68 (2H, s), 11.84 (1H, s). ^{13}C NMR (100MHz, DMSO): δ 112.76; 114.54; 119.75; 120.61; 122.33; 122.42; 125.16; 125.85; 126.05; 128.41; 134.66; 136.18; 137.66; 148.19; 154.54; 160.67. HRMS: m/z (EI+), calculated for : $C_{16}H_{11}N_3$ 246.0987 $[M]^+$, found: 246.1102 $[M]^+$. Melting temp. range: 271 – 275 °C.

- *6-(1H-indol-3-yl)-3,4-dihydroquinazolin-2(1H)-one (**5**)*

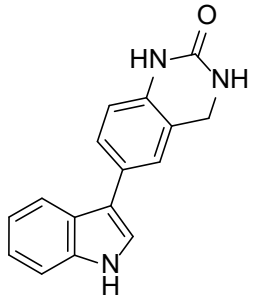

6-(1-(phenylsulfonyl)-1H-indol-3-yl)-3,4-dihydroquinazolin-2(1H)-one was obtained after coupling **42** with 6-bromo-3,4-dihydroquinazolin-2(1H)-one. Purified by flash chromatography (Cyclohexane/EtOAc 4:1 ➔ 1:4). Yield: 72 %. ^{1}H NMR (400MHz, $CDCl_3$): δ 4.61 (2H, s), 5.48 (1H, s), 6.82 (1H, d, J=8.14 Hz), 7.32 (1H, s), 7.24 – 7.32 (2H, m), 7.35 – 7.49 (4H, m), 7.52 – 7.58 (1H, m), 7.64 (1H, s), 7.71 (1H, d, J=7.80 Hz), 7.83 (1H, s), 7.92 (2H, d, J=7.53 Hz), 8.06 (1H, d, J=8.28 Hz).

6-(1-(phenylsulfonyl)-1H-indol-3-yl)-3,4-dihydroquinazolin-2(1H)-one was deprotected following general procedure A to afford **5**. Quantitative yield. ^{1}H NMR (400MHz, DMSO): δ 4.39 (2H, s), 6.84 (1H, d, J=7.96 Hz), 7.10 (1H, td, J=7.19, 27.43 Hz), 7.38 – 7.46 (3H, m), 7.56 (1H, s), 7.84 (1H, d, J=7.69 Hz), 9.02 (1H, br s), 11.25 (1H, br s). ^{13}C NMR (150MHz, DMSO): δ 43.17; 112.30; 114.43; 116.04; 119.02; 119.57; 119.79; 121.74; 122.97; 124.28; 125.45; 126.32; 129.28; 136.23; 137.24; 155.09. HRMS: m/z (EI+), calculated for : 286.0912 $[M+Na]^+$, found: 286.1060 $[M+Na]^+$. Melting temp. range: 256 – 265 °C.

- *1-(cyclopropylmethyl)-6-(1H-indol-3-yl)-1H-benzo[d][1,2,3]triazole (**19**)*

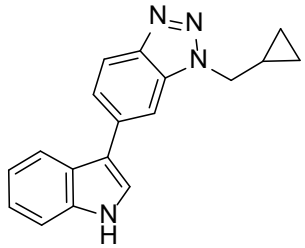

1-(cyclopropylmethyl)-6-(1-(phenylsulfonyl)-1H-indol-3-yl)-1H-benzo[d][1,2,3]triazole was obtained after coupling **42** with **19d**. Purified by flash chromatography (Cyclohexane/EtOAc 4:1). Then, *1-(cyclopropylmethyl)-6-(1-(phenylsulfonyl)-1H-indol-3-yl)-1H-benzo[d][1,2,3]triazole* was deprotected following general procedure A to afford **19***.* Yield over two steps: 69 %. ^{1}H NMR (400MHz, DMSO): δ 0.44 – 0.67 (4H, m), 1.34 – 1.52 (1H, m), 4.67 (2H, d, J=4.76 Hz), 7.10 – 7.28 (2H, s), 7.50 (1H, d, J=5.72 Hz), 7.77 (1H, d, J=7.40 Hz), 7.88 (1H, s), 7.97 – 8.21 (3H, m), 11.54 (1H, s). ^{13}C NMR (100MHz, DMSO): δ 4.43; 11.80; 52.12; 106.89; 112.56; 115.67; 119.65; 120.42; 122.18; 124.58; 125.26; 125.35; 134.15; 135.67; 137.47; 144.12. HRMS: m/z (EI+), calculated for: $C_{18}H_{16}N_4$ 289.1409 $[M]^+$, found: 289.1449 $[M]^+$. Melting temp. range: 129 – 134 °C.

- *1-(cyclopropylmethyl)-5-(1H-indol-3-yl)-1H-benzo[d][1,2,3]triazole (**20**)*

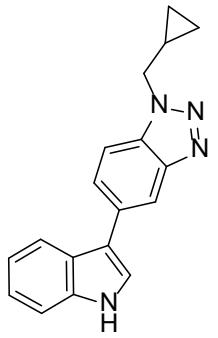

1-(cyclopropylmethyl)-5-(1-(phenylsulfonyl)-1H-indol-3-yl)-1H-benzo[d][1,2,3]triazole was obtained after coupling **42** with **20d**. Purified by flash chromatography (Cyclohexane/EtOAc 4:1). Then, *1-(cyclopropylmethyl)-5-(1-(phenylsulfonyl)-1H-indol-3-yl)-1H-benzo[d][1,2,3]triazole* was deprotected following general procedure A to afford **20**. Yield over two steps: 60 %.^{1}H NMR (400MHz, DMSO): δ 0.47 – 0.54 (2H, m), 0.54 – 0.63 (2H, m), 1.36 – 1.46 (1H, m), 4.63 (2H, d, J=7.17 Hz), 7.14 (1H, t, J=7.36 Hz), 7.19 (1H, t, J=7.44 Hz), 7.49 (1H, d, J=7.83 Hz), 7.83 (1H, d, J=2.36 Hz), 7.89 – 8.03 (3H, m), 8.23 (1H, s), 11.46 (1H, s). ^{13}C NMR (100MHz, DMSO): δ 4.41; 11.81; 52.38; 111.52; 112.51; 115.35; 115.66; 119.32; 120.28; 122.04; 124.51; 125.46; 127.92; 131.75; 132.47; 137.38; 146.69.

HRMS: m/z (EI+), calculated for: $C_{18}H_{16}N_4$ 289.1409 $[M]^+$, found: 289.1447 $[M]^+$. Melting temp. range: 206 – 213 °C.

- *2-(6-(1H-indol-3-yl)-1H-benzo[d][1,2,3]triazol-1-yl)-N,N-dimethylethan-1-amine (**25**)*

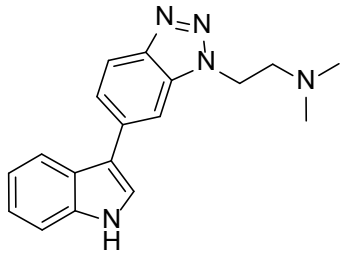

2-(6-((1-(phenylsulfonyl)-1H-indol-3-yl)-1H-benzo[d][1,2,3]triazol-1-yl)-N,N-dimethylethan-1-amine was obtained after coupling **42** with **25d**. Purified by flash chromatography (DCM/$MeOH_{0 \rightarrow 5\ \%}$). Then *N,N-dimethyl-2-(6-(1-(phenylsulfonyl)-1H-indol-3-yl)-1H-benzo[d][1,2,3]triazol-1-yl)ethan-1-amine* was deprotected following general procedure A to afford **25**. Yield over two steps: 50 %. ^{1}H NMR (600MHz, DMSO): δ 2.22 (6H, s), 2.84 (2H, s), 4.86 (2H, s), 7.10 – 7.25 (2H, m), 7.43 – 7.55 (1H, m), 7.71 – 7.80 (1H, m), 7.87 (1H, s), 7.98 – 8.06 (2H, m), 8.09 (1H, s), 11.55 (1H, s). ^{13}C NMR (150 MHz, DMSO): δ 45.62; 46.04; 58.74; 107.06; 112.58; 115.71; 119.59; 120.39; 122.17; 124.52; 125.19; 125.40; 134.52; 135.53; 137.48; 144.03. HRMS: *m/z* (EI+), calculated for: $C_{18}H_{19}N_5$ 306.1674 $[M]^+$, found: 306.1716 $[M]^+$. Melting temp. range: 148 – 149 °C.

- *2-(5-(1H-indol-3-yl)-1H-benzo[d][1,2,3]triazol-1-yl)-N,N-dimethylethan-1-amine (**26**)*

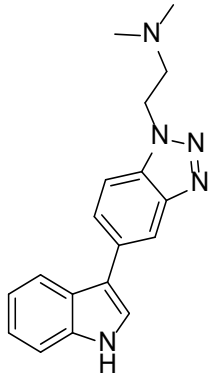

N,N-dimethyl-2-(5-(1-(phenylsulfonyl)-1H-indol-3-yl)-1H-benzo[d][1,2,3]triazol-1-yl)ethan-1-amine was obtained after coupling **42** with **26d**. Purified by flash chromatography (DCM/$MeOH_{0 \rightarrow 5\ \%}$). Then, *N,N-dimethyl-2-(5-(1-(phenylsulfonyl)-*

1H-indol-3-yl)-1H-benzo[d][1,2,3]triazol-1-yl)ethan-1-amine was deprotected following general procedure A to afford **26**. Yield over two steps: 43 %. ^{1}H NMR (400MHz, $CDCl_3$): δ 2.35 (6H, s), 2.95 (2H, t, J=6.90 Hz), 4.77 (2H, t, J=6.90 Hz), 7.23 (1H, t, J=7.36 Hz), 7.29 (1H, d, J=7.12 Hz), 7.42 (1H, s), 7.47 (1H, d, J=7.96 Hz), 7.61 (1H, d, J=8.56 Hz), 7.82 (1H, d, J=7.84 Hz), 7.97 (1H, d, J=7.84 Hz), 8.30 (1H, s), 8.50 (1H, bs). ^{13}C NMR (100MHz, $CDCl_3$): δ 45.64; 46.63; 58.46; 109.59; 111.57; 117.39; 117.68; 119.52; 120.58; 122.18; 122.64; 125.75; 128.29; 131.86; 132.03; 136.69; 146.92. HRMS: *m/z* (EI+), calculated for: $C_{18}H_{19}N_5$ 306.1674 $[M]^+$, found: 306.1716 $[M]^+$. Melting temp. range: 168 – 171 °C.

- *6-(1H-indol-3-yl)-1-((tetrahydrofuran-3-yl)methyl)-1H-benzo[d][1,2,3]triazole (***27***)*

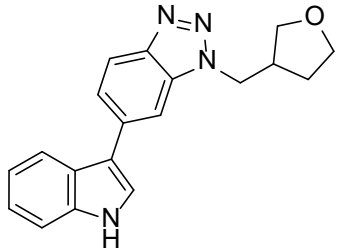

6-(1-(phenylsulfonyl)-1H-indol-3-yl)-1-((tetrahydrofuran-3-yl)methyl)-1H-benzo[d][1,2,3]triazole was obtained after coupling **42** with **27d**. Purified by flash chromatography (Cyclohexane/EtOAc 2:1). Then,*6-(1-(phenylsulfonyl)-1H-indol-3-yl)-1-((tetrahydrofuran-3-yl)methyl)-1H-benzo[d][1,2,3]triazole* was deprotected following general procedure A to afford **27**. Yield over two steps: 40 %.NMR (400MHz, $CDCl_3$): δ 1.77 – 1.84 (1H, m), 2.06 – 2.13 (1H, m), 3.04 – 3.11 (1H, m), 3.71 – 3.75 (1H, m), 3.79 – 3.85 (2H, m), 3.99 – 4.04 (2H, m), 4.64 (4H, d, J=7.00 Hz), 7.24 (1H, t, J=7.47 Hz), 7.29 (1H, t, J=7.45 Hz), 7.45 (1H, d, J=1.95 Hz), 7.48 (1H, d, J=8.07 Hz), 7.59 (1H, d, J=8.52 Hz), 7.84 (1H, d, J=8.46 Hz), 7.98 (1H, d, J=7.92 Hz), 8.32 (1H, s), 8.40 (1H, s). ^{13}C NMR (100MHz, $CDCl_3$): δ 29.86; 39.76; 50.51; 67.61; 70.97; 109.21; 111.58; 117.53; 117.64; 119.50; 120.66; 122.18; 122.73; 125.73; 128.52; 131.98; 132.03; 136.69; 146.87. HRMS: *m/z* (EI+), calculated for : $C_{19}H_{18}N_4O$ 319.1514 $[M]^+$, found: 319.1551 $[M]^+$. Melting temp. range: 216 – 218 °C.

- *5-(1H-indol-3-yl)-1-((tetrahydrofuran-3-yl)methyl)-1H-benzo[d][1,2,3]triazole (***28***)*

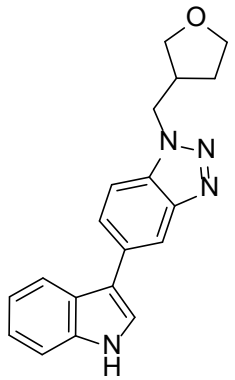

5-(1H-indol-3-yl)-1-((tetrahydrofuran-3-yl)methyl)-1H-benzo[d][1,2,3]triazole was obtained after coupling **42** with **28d**. Purified by flash chromatography (Cyclohexane/EtOAc ➔ 2:1). Yield: 82 %. ^{1}H NMR (400MHz, $CDCl_3$): δ 1.78 – 1.85 (1H, m), 2.06 – 2.13 (1H, m), 3.05 – 3.12 (1H, m), 3.73 – 3.77 (1H, m), 3.78 – 3.86 (2H, m), 4.01 (1H, m, J=5.51 Hz), 4.65 (2H, d, J=7.68 Hz), 7.24 – 7.28 (1H, m), 7.31 (1H, t, J=7.44 Hz), 7.47 – 7.51 (2H, m), 7.71 (1H, d, J=8.58 Hz), 7.75 (1H, s), 7.95 (1H, d, J=7.92 Hz), 8.11 (1H, d, J=8.58 Hz), 8.48 (1H, s). ^{13}C NMR (100MHz, $CDCl_3$): δ 29.88; 39.72; 50.35; 67.62; 70.99; 106.32; 111.74; 117.67; 119.39; 120.23; 120.85; 122.75; 122.91; 125.08; 125.58; 134.01; 135.60; 136.77; 144.71.

5-(1H-indol-3-yl)-1-((tetrahydrofuran-3-yl)methyl)-1H-benzo[d][1,2,3]triazole was deprotected following general procedure **B** to afford **28**. Yield: 55 %. ^{1}H NMR (400MHz, DMSO): δ 1.67 – 1.79 (1H, m), 1.92 – 2.02 (1H, m), 2.90 – 3.01 (1H, m), 3.55 – 3.62 (1H, m), 3.64 – 3.77 (2H, m), 3.81 – 3.89 (1H, m), 4.78 (2H, d, J=7.41 Hz), 7.14 – 7.24 (2H, m), 7.50 (1H, d, J=7.71 Hz), 7.79 (1H, d, J=8.50 Hz), 7.88 (1H, s), 8.05 (1H, t, J=9.23 Hz), 8.12 (1H, s), 11.54 (1H, s). ^{13}C NMR (100MHz, DMSO): δ 29.91; 49.94; 67.29; 70.61; 106.65; 112.55; 115.66; 119.71; 120.44; 122.19; 124.72; 125.34; 134.39; 135.91; 137.48; 143.98. HRMS: *m/z* (EI+), calculated for: $C_{19}H_{18}N_4O$ 319.1514 $[M]^+$, found: 319.1551 $[M]^+$. Melting temp. range: 158 – 162 °C.

- *6-(1H-indol-3-yl)-1-((tetrahydrofuran-2-yl)methyl)-1H-benzotriazole (***29***)*

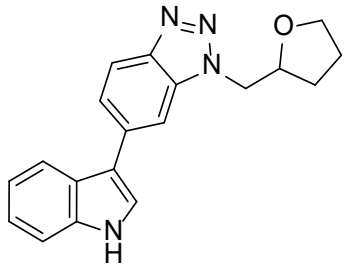

6-(1-(phenylsulfonyl)-1H-indol-3-yl)-1-((tetrahydrofuran-2-yl)methyl)-1H-benzo[d][1,2,3]triazole was obtained after coupling **42** with **29d**. Purified by flash chromatography (Cyclohexane/EtOAc 2:1). Then, *6-(1-(phenylsulfonyl)-1H-indol-3-yl)-1-((tetrahydrofuran-2-yl)methyl)-1H-benzo[d][1,2,3]triazole* was deprotected following general procedure **B** to afford **29**. Yield over two steps: 35 %. ^{1}H NMR (400MHz, $CDCl_3$): δ 1.65 – 1.90 (3H, m), 2.04 – 2.13 (1H, m), 3.72 – 3.84 (2H, m), 4.43 – 4.50 (1H, m), 4.72 (1H, dd, J=14.46, 5.51 Hz), 4.84 (1H, dd, J = 14.46 Hz, 4.08 Hz), 7,23 – 7.31 (2H, m), 7.48 – 7.51 (2H, m), 7.67 (1H,d, J = 4.71 Hz), 7.94 (1H, s), 8.01 (1H ,d J = 7.72 Hz), 8.06 (1H, d, J=8.62Hz), 8.65 (1H, br s). ^{13}C NMR (100MHz, $CDCl_3$): δ 25.69; 28.80; 52.21; 68.60; 77.92; 107.85; 111.73; 117.69; 119.56; 119.72; 120.70; 122.72; 122.77; 124.86; 125.64; 134.60; 135.27; 136.80; 144.72. HRMS: m/z calculated for $C_{19}H_{18}N_4O$ 319.1514 $[M]^+$, found: 319.1550 $[M]^+$. Melting temp. range: 173 – 178 °C.

- *5-(1H-indol-3-yl)-1-((tetrahydrofuran-2-yl)methyl)-1H-benzotriazole (***30***)*

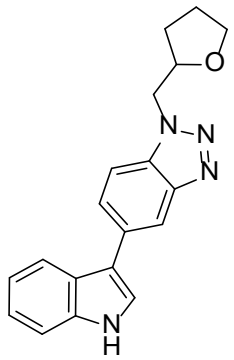

5-(1-(phenylsulfonyl)-1H-indol-3-yl)-1-((tetrahydrofuran-2-yl)methyl)-1H-benzo[d][1,2,3]triazole was obtained after coupling **42** with **30d**. Purified by flash chromatography (Cyclohexane/EtOAc 2:1). Yield: 85 %. ^{1}H NMR (400MHz, $CDCl_3$): δ 1.65 – 1.93 (3H, m), 2.05 -2.17 (1H, m), 3.70 – 3.82 (2H, m), 4.43 (1H, m, J=4.61 Hz), 4.71 (1H, dd, J=5.76, 14.49 Hz), 4.85 (1H, dd, J=3.74, 14.49 Hz), 7.34 (1H, t, J=7.53 Hz), 7.41 (1H, t, J=7.71 Hz), 7.48 (1H, t, J=7.66 Hz), 7.54 – 7.63 (1H, m), 7.80 (1H, s), 7.84 (1H, d, J=7.89 Hz), 7.92 (1H, s), 7.96 (1H, d, J=7.42 Hz), 8.07 – 8.14 (2H, m).

5-(1-(phenylsulfonyl)-1H-indol-3-yl)-1-((tetrahydrofuran-2-yl)methyl)-1H-benzo[d][1,2,3]triazole was deprotected following general procedure **B** to afford **30**. Yield: 39 %. ^{1}H NMR (400MHz, $CDCl_3$): δ 1.69 – 1.81 (3H, m), 1.99 – 2.08 (1H, m), 3.59 – 3.75 (2H, m), 4.30 – 4.40 (1H, m), 4.76 (1H ,dd J = 14.43, 6.82 Hz), 4.84 (1H, dd, J=14.43, 3.75 Hz), 7.11 – 7.23 (2H, m), 7.48 (1H, d, J = 7.88 Hz), 7.81 (1H, s), 7.90 – 7.98 (3H, m), 8.21 (1H, s), 11.45 (1H, s). ^{13}C NMR (100MHz, $CDCl_3$): δ 25.52; 28.81; 51.95; 67.92; 77.67; 112.01; 112.51; 115.16; 115.66; 119.33; 120.28; 122.05;

124.49; 125.45; 127.89; 132.43; 132.49; 137.37; 146.53. HRMS: *m/z* (EI+), calculated for: $C_{19}H_{18}N_4O$ 319,15142 $[M]^+$, found: 319,1550 $[M]^+$. Melting temp. range: 205 – 216 °C.

- *4-(2-(6-(1H-indol-3-yl)-1H-benzotriazol-1-yl)ethyl)morpholine (***31***)*

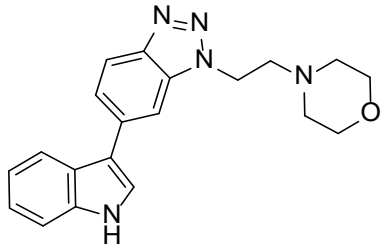

4-(2-(6-(1-(phenylsulfonyl)-1H-indol-3-yl)-1H-benzo[d][1,2,3]triazol-1-yl)ethyl)morpholine was obtained after coupling **42** with **31d**. Purified by flash chromatography (Cyclohexane/EtOAc ➔ 2:1). Yield: 80 %. ^{1}H NMR (400MHz, $CDCl_3$): *δ* 2.55 – 2.45 (4H, m), 2.93 (2H, dt, J = 13.2, 6.7 Hz), 3.61 (2H, d, J = 4.0 Hz), 4.81 – 4.70 (4H, m), 7.30 (2H, t, J = 7.4 Hz), 7.39 (1H, t, J = 7.5 Hz), 7.45 (2H, t, J = 7.7 Hz), 7.62 – 7.51 (2H, m), 7.78 – 7.72 (2H, m), 7.93 (2H, d, J = 7.5 Hz), 8.16 – 7.97 (2H, m).

4-(2-(6-(1-(phenylsulfonyl)-1H-indol-3-yl)-1H-benzo[d][1,2,3]triazol-1-yl)ethyl)morpholine was deprotected following general procedure **A** to afford **31**. Yield: 42 %.^{1}H NMR (400MHz, $CDCl_3$): *δ* 2.48 -2.58 (4H, m), 2.98 (2H, t, J=6.53Hz), 3.63-3.70 (4H, m), 4.78 (2H, t, J=6.64Hz), 7.23-7.30 (2H, m), 7.46-7.51 (2H, m), 7.66 (1H, d, J=8.50Hz), 7.78 (1H, s), 7.95 (1H, d, J=7.75Hz), 8.07 (1H, d, J=8.60Hz), 8.92 (1H, br s). ^{13}C NMR (100MHz, $CDCl_3$): *δ* 45.76 ; 53.71 ; 57.60 ; 66.86 ; 106.62 ; 111.89 ; 117.45 ; 119.33 ; 120.04 ; 120.70 ; 122.77 ; 122.92 ; 125.00 ; 125.55 ; 134.05 ; 135.48; 136.85; 144.69. HRMS: *m/z* (EI+), calculated for $C_{20}H_{21}N_5O$: 348,17797 $[M]^+$, found: 348,1815 $[M]^+$. Melting temp. range: 136 – 140 °C.

- *4-(2-(5-(1H-indol-3-yl)-1H-benzotriazol-1-yl)ethyl)morpholine (***32***)*

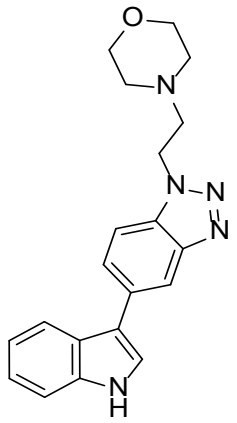

4-(2-(5-(1-(phenylsulfonyl)-1H-indol-3-yl)-1H-benzo[d][1,2,3]triazol-1-yl)ethyl)morpholine was obtained after coupling **42** with **32d**. Purified by flash chromatography (Cyclohexane/EtOAc ➔ 2:1). Quantitative yield. ^{1}H NMR (400MHz, $CDCl_3$): δ 2.55 – 2.45 (4H, m), 2.93 (2H, dt, *J* = 13.2, 6.7 Hz), 3.61 (2H, d, *J* = 4.0 Hz), 4.81 – 4.70 (4H, m), 7.30 (2H, t, *J* = 7.4 Hz), 7.39 (1H, t, *J* = 7.5 Hz), 7.45 (2H, t, *J* = 7.7 Hz), 7.62 – 7.51 (2H, m), 7.78 – 7.72 (2H, m), 7.93 (2H, d, *J* = 7.5 Hz), 8.16 – 7.97 (2H, m).

4-(2-(5-(1-(phenylsulfonyl)-1H-indol-3-yl)-1H-benzo[d][1,2,3]triazol-1-yl)ethyl)morpholine was deprotected following general procedure **A** to afford **32**. Yield: 60 %. ^{1}H NMR (400MHz, $CDCl_3$): δ 2.51 – 2.60 (4H, m), 2.99 (2H, t, J=6.29Hz), 3.64 - 3.72 (4H, m), 4.78 (2H, t, J=6.34Hz), 7.19-7.32 (2H, m), 7.43-7.50 (2H, m) ,7.61 (1H, d, J=8.43H), 7.83 (1H, d, J=8.36Hz), 7.97 (1H, d, J=7.61Hz), 8.30 (1H, s), 8.51 (1H, br s). ^{13}C NMR (100MHz, $CDCl_3$): δ 45.95 ; 53.69 ; 57.68 ; 66.90 ; 109.67 ; 111.62 ; 117.34 ; 117.59 ; 119.49 ; 120.61 ; 122.23 ; 122.68 ; 125.71 ; 128.27 ; 131.93 ; 132.05 ; 136.70 ; 146.91. HRMS: *m/z* calculated for $C_{20}H_{21}N_5O$: 348,17797 $[M]^+$, found: 348,1815 $[M]^+$. Melting temp. range: 155 – 159 °C.

- *3-(6-(1H-indol-3-yl)-1H-benzo[d][1,2,3]triazol-1-yl)propane-1,2-diol (***39***)*

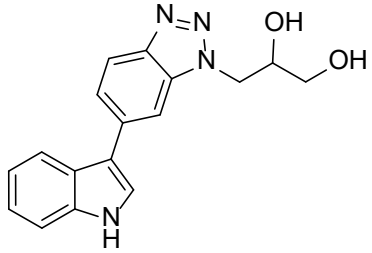

3-(6-((1-(phenylsulfonyl)-1H-indol-3-yl)-1H-benzo[d][1,2,3]triazol-1-yl)propane-1,2-diol was obtained after coupling **42** with **39d**. Purified by flash chromatography ($DCM/MeOH_{0\rightarrow5\%}$).Then, *3-(6-((1-(phenylsulfonyl)-1H-indol-3-yl)-1H-benzo[d][1,2,3]triazol-1-yl)propane-1,2-diol* was deprotected following general procedure A to afford **39**. Yield over two steps: 31 %. ^{1}H NMR (400MHz, MeOD): *δ* 3.65 (2H, d, J=5.05 Hz), 4.21 (1H, bs), 4.67 – 4.81 (2H, m), 7.07 – 7.31 (2H, m), 7.47 (1H, d, J=7.77 Hz), 7.58 (1H, s), 7.84 – 7.97 (3H, m), 8.19 (1H, s). Labile protons not visible. ^{13}C NMR (100MHz, MeOD): *δ* 50.95; 63.35; 70.97; 110.79; 111.42; 114.58; 115.91; 118.51; 119.56; 121.55; 122.82; 125.40; 128.03; 132.52; 133.33; 137.33; 146.06. HRMS: *m/z* (EI+), calculated for : $C_{17}H_{16}N_4O_2$ 309.1307 $[M]^+$, found: 309.1346 $[M]^+$. Melting temp. range: 65 – 73 °C.

- *3-(5-(1H-indol-3-yl)-1H-benzo[d][1,2,3]triazol-1-yl)propane-1,2-diol (***40***)*

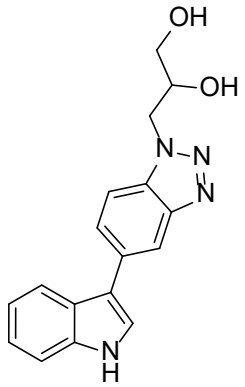

3-(5-((1-(phenylsulfonyl)-1H-indol-3-yl)-1H-benzo[d][1,2,3]triazol-1-yl)propane-1,2-diol was obtained after coupling **42** with **40d**. Purified by flash chromatography ($DCM/MeOH_{0\rightarrow5\%}$). Then, *3-(5-((1-(phenylsulfonyl)-1H-indol-3-yl)-1H-benzo[d][1,2,3]triazol-1-yl)propane-1,2-diol* was deprotected following general procedure A to afford **40**. Yield over two steps: 28 %. ^{1}H NMR (600MHz, DMSO): *δ* 3.40 – 3.52 (2H, m), 3.91 – 4.06 (1H, m), 4.62 – 4.72 (1H, m), 4.82 – 4.97 (2H, m), 5.20 (1H, br s), 7.12 – 7.24 (2H, m), 7.49 (1H, d, J=7.19 Hz), 7.74 (1H, d, J=7.80 Hz), 7.85 (1H, s), 8.03 (2H, d, J=7.44 Hz), 8.09 (1H, s), 11.51 (1H, s). ^{13}C NMR (150 MHz, DMSO): *δ* 51.56; 63.84; 71.58; 107.71; 111.81; 112.56; 115.79; 119.43; 119.64; 120.40; 122.18; 124.46; 125.06; 125.40; 135.20; 135.33; 137.49; 144.05. HRMS: *m/z* (EI+), calculated for : $C_{17}H_{16}N_4O_2$ 309.1307 $[M]^+$, found: 309.1346 $[M]^+$. Melting temp. range: 59 – 65 °C.

5.2.2.2. using tert-butyl 6-fluoro-3-(4,4,5,5-tetramethyl-1,3,2-dioxaborolan-2-yl)-1H-indole-1-carboxylate (41).

- *6-(6-fluoro-1H-indol-3-yl)-1-methyl-1H-benzotriazole (***8a***)*

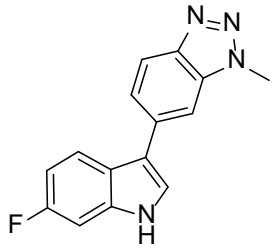

tert-butyl 6-fluoro-3-(1-methyl-1H-benzo[d][1,2,3]triazol-6-yl)-1H-indole-1-carboxylate was obtained after coupling **41** with **8b**. Purified by flash chromatography (AcOEt/Cyclohexane 1:1). Yield: 65 %. ^{1}H NMR (400MHz, CDCl3): δ 1.71 (9H, s), 4.36 (3H, s), 7.09 (1H, t, J=8.77 Hz), 7.64 (1H, d, J=8.55 Hz), 7.69 – 7.82 (3H, m, J=5.58 Hz), 7.98 (1H, d, J=7.89 Hz), 8.14 (1H, d, J=8.57 Hz).

tert-butyl 6-fluoro-3-(1-methyl-1H-benzo[d][1,2,3]triazol-6-yl)-1H-indole-1-carboxylate was deprotected following general procedure **C** to afford **8a**. Yield: Quantitative. ^{1}H NMR (400MHz, DMSO): δ 4.36 (3H, s), 7.02 (1H, ddd, J= 9.23, J=9.21, J= 2.12, J=2.28 Hz), 7.27 (1H, dd, J=7.89, 1.98 Hz), 7.75 (1H, d, J = 8.92 Hz), 7.87 (1H, d, J=2,27 Hz), 8.03 – 8.07 (3H, m), 11.60 (1H, s). ^{13}C NMR (100MHz, DMSO): δ 34,57; 98.46; 106.85; 108.78; 115.86; 119.64; 120.95; 122.24; 124.54; 125.78; 134.70; 135.12; 137.41; 144.10; 161.66. HRMS: *m/z* (EI+), calculated for: $C_{15}H_{10}FN_4Na^+$ 2671041 [M+Na] 288.0782, found: 288.0894 [M+Na] Melting temp. range: 236 – 240 °C.

- *6-(6-fluoro-1H-indol-3-yl)-1-(piperazin-1-ylmethyl)-1H-benzo[d][1,2,3]triazole (***37a***)*

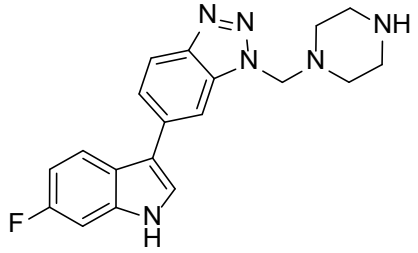

tert-butyl 3-(1-((4-(tert-butoxycarbonyl)piperazin-1-yl)methyl)-1H-benzo[d][1,2,3]triazol-6-yl)-6-fluoro-1H-indole-1-carboxylate was obtained after coupling **41** with **37d**. Purified by flash chromatography (Cyclohexane/EtOAc 1:1). Then, it was deprotected using deprotection procedure **C** to afford *6-(6-fluoro-1H-indol-3-yl)-1-(piperazin-1-ylmethyl)-1H-benzo[d][1,2,3]triazole.* Purified by flash chromatography (Cyclohexane/EtOAc 1:1 ➔ 0:1). Yield over two steps: 18 %.^{1}H

NMR (600 MHz, $CDCl_3$): *δ* 2.36 – 2.43 (3H, m), 2.61 (3H, t, J=4.59 Hz), 2.83 (2H, t, J=6.39 Hz), 4.84 (2H, t, J=6.39 Hz), 6.99 (1H, dt, J=4.14 Hz), 7.26 (1H, dd, J=2.10, 9.84 Hz), 7.81 (1H, s), 7.88 (1H, dd, J=1.35, 8.61 Hz), 7.90 – 7.96 (2H, m), 8.20 (1H, s), 11.58 (1H, s). ^{13}C NMR (150 MHz, $CDCl_3$): *δ* 45.68; 46.03; 54.62; 58.23; 98.40 (1C, d, J=25.36 Hz), 108.64 (1C, d, J=24.25 Hz), 111.74; 115.44; 115.90; 120.51 (1C, d, J=10.13 Hz), 122.40; 125.06; 127.68; 131.91; 132.29; 137.34 (1C, d, J=12.43 Hz); 146.52; 158.58; 160.14. HRMS: *m/z* (EI+), calculated for: 351.1689 $[M]^+$, found: 351.1340 $[M]^+$. Melting temp. range: 195 – 199 °C.

5.2.2.3. Using tert-butyl 3-(4,4,5,5-tetramethyl-1,3,2-dioxaborolan-2-yl)-1H-indole-1-carboxylate (purchased from Fluorochem)

- *6-(1H-indol-3-yl)-1-(2,2,2-trifluoroethyl)-1H-benzo[d][1,2,3]triazole (***17***)*

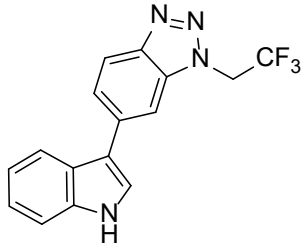

tert-butyl 3-(1-(2,2,2-trifluoroethyl)-1H-benzo[d][1,2,3]triazol-6-yl)-1H-indole-1-carboxylate was obtained after coupling with **17d**. Purified by flash chromatography (Cyclohexane/EtOAc 4:1 ➔ 1:2). Yield: 78 %. ^{1}H NMR (400MHz, $CDCl_3$): *δ* 1.72 (9H, s), 5.29 (2H, q, J=8.24 Hz), 7.35 (1H, t, J=7.40 Hz), 7.42 (1H, t, J=7.68 Hz), 7.73 (1H, d, J=8.60 Hz), 7.77 – 7.86 (3H, m), 8.19 (1H, d, J=8.60 Hz), 8.26 (1H, d, J=7.76 Hz).

tert-butyl 3-(1-(2,2,2-trifluoroethyl)-1H-benzo[d][1,2,3]triazol-6-yl)-1H-indole-1-carboxylate was deprotected using deprotection procedure **C** to afford **17**. Purified by flash chromatography (Cyclohexane/EtOAc 4:1 ➔ 1:2). Yield: 75 %. ^{1}H NMR (400MHz, DMSO): *δ* 5.98 (2H, q, J=9.12 Hz), 7.20 (2H, quint, J=7.28 Hz), 7.51 (1H, d, J=7.47 Hz), 7.85 (1H, d, J=8.73 Hz), 7.91 (1H, d, J=2.15 Hz), 8.08 (1H, d, J=7.62 Hz), 8.12 (1H, d, J=8.71 Hz), 8.22 (1H, s), 11.60 (1H, s). ^{13}C NMR (100MHz, DMSO): *δ* 47.90; 48.24; 106.38; 112.63; 115.27; 119.70; 120.00; 120.56; 122.33; 125.19; 125.61; 134.93; 136.91; 137.52; 143.74. HRMS: *m/z* (EI+), calculated for: $C_{16}H_{11}F_3N_4$ 317.0969 $[M]^+$, found: 317.1006 $[M]^+$. Melting temp. range: 171 – 172 °C.

- *6-(1H-indol-3-yl)-1-(2,2,2-trifluoroethyl)-1H-benzo[d][1,2,3]triazole (***18***)*

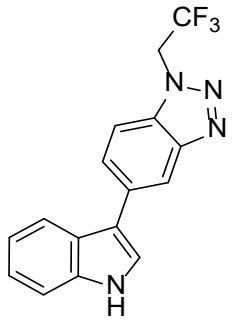

tert-butyl 3-(1-(2,2,2-trifluoroethyl)-1H-benzo[d][1,2,3]triazol-5-yl)-1H-indole-1-carboxylate was obtained after coupling with **18d**. Purified by flash chromatography (Cyclohexane/EtOAc 4:1 ➔ 1:2). Then, the coupling product was deprotected using deprotection procedure **C** to afford **18**. Purified by flash chromatography (Cyclohexane/EtOAc 4:1 ➔ 1:2). Yield: 50 %. ^{1}H NMR (400MHz, DMSO): δ 5.94 (2H, q, J=9.08 Hz), 7.17 (2H, td, J=7.34, 20.39 Hz), 7.49 (1H, d, J=7.85 Hz), 7.86 (1H, d, J=1.90 Hz), 7.98 (2H, t, J=10.34 Hz), 8.03 (2H, s), 8.31 (1H, s), 11.50 (1H, s). ^{13}C NMR (100MHz, DMSO): δ 48.10 ; 48.44; 111.29; 112.54; 115.31; 115.54; 119.32; 120.37; 122.11; 124.78; 125.38; 129.07; 132.37; 133.28; 137.38; 146.49. HRMS: *m/z* (EI+), calculated for: $C_{16}H_{11}F_3N_4$ 317.0969 $[M]^+$, found: 317.1006 $[M]^+$. Melting temp. range: 213 – 214 °C.

- *6-(1H-indol-3-yl)-1-(piperidin-4-ylmethyl)-1H-benzo[d][1,2,3]triazole (**34**)*

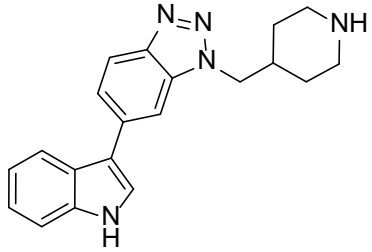

tert-butyl 3-(1-((1-(tert-butoxycarbonyl)piperidin-4-yl)methyl)-1H-benzo[d][1,2,3]triazol-6-yl)-1H-indole-1-carboxylate was obtained after coupling with **33d**. Purified by flash chromatography (Cyclohexane/EtOAc 4:1 ➔ 1:2). Quantitative yield. ^{1}H NMR (400MHz, $CDCl_3$): δ 1.36 – 1.27 (2H, m), 1.43 (9H, s), 1.67 (2H, s), 1.72 (9H, s), 2.34 – 2.20 (1H, m), 2.66 (2H, t, *J* = 12.3 Hz), 4.14 (2H, s), 4.55 (2H, d, *J* = 7.0 Hz), 7.34 (1H, t, *J* = 7.2 Hz), 7.42 (1H, t, *J* = 7.4 Hz), 7.73 – 7.62 (2H, m), 7.81 (2H, d, *J* = 7.4 Hz), 8.14 (1H, d, *J* = 8.5 Hz), 8.25 (1H, d, *J* = 7.8 Hz).

tert-butyl 3-(1-((1-(tert-butoxycarbonyl)piperidin-4-yl)methyl)-1H-benzo[d][1,2,3]triazol-6-yl)-1H-indole-1-carboxylate was deprotected following

procedure **C** to afford **33**. Purified by washing with diethylether. Quantitative yield. ^{1}H NMR (400MHz, DMSO): *δ* 1.02 – 1.12 (1H, m), 1.45 – 1.58 (2H, m), 1.72 (2H, d, J=12.31 Hz), 2.25 – 2.39 (2H, m), 3.22 (1H, d, J=10.72 Hz), 4.75 (2H, d, J=4.50 Hz), 7.13 – 7.24 (2H, m), 7.50 (1H, d, J=6.69 Hz), 7.78 (1H, d, J=8.02 Hz), 7.88 (1H, s), 7.99 – 8.14 (3H, m), 11.63 (1H, s). ^{13}C NMR (100MHz, DMSO): *δ* 26.60; 34.72; 43.03; 52.04; 106.77; 112.59; 115.59; 119.71; 120.46; 122.17; 124.71; 125.33; 134.70; 135.96; 137.47; 143.91. HRMS: *m/z* (EI+), calculated for: $C_{20}H_{21}N_5$ 332.1831 $[M]^+$, found: 332.1868 $[M]^+$. Melting temp. range: 152 – 155 °C.

- *5-(1H-indol-3-yl)-1-(piperidin-4-ylmethyl)-1H-benzo[d][1,2,3]triazole (***34***)*

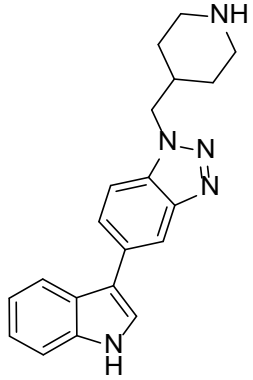

tert-butyl 3-(1-((1-(tert-butoxycarbonyl)piperidin-4-yl)methyl)-1H-benzo[d][1,2,3]triazol-5-yl)-1H-indole-1-carboxylate was obtained after coupling with **34d**. Purified by flash chromatography (Cyclohexane/EtOAc 1:0 ➔ 1:1).Quantitative yield. ^{1}H NMR (400MHz, $CDCl_3$): *δ* 1.36 – 1.27 (2H, m), 1.43 (9H, s), 1.67 (2H, s), 1.72 (9H, s), 2.34 – 2.20 (1H, m), 2.66 (2H, t, *J* = 12.3 Hz), 4.14 (2H, s), 4.55 (2H, d, *J* = 7.0 Hz), 7.34 (1H, t, *J* = 7.2 Hz), 7.42 (1H, t, *J* = 7.4 Hz), 7.73 – 7.62 (2H, m), 7.81 (2H, d, *J* = 7.4 Hz), 8.14 (1H, d, *J* = 8.5 Hz), 8.25 (1H, d, *J* = 7.8 Hz), 8.33 (1H, s).

tert-butyl 3-(1-((1-(tert-butoxycarbonyl)piperidin-4-yl)methyl)-1H-benzo[d][1,2,3]triazol-5-yl)-1H-indole-1-carboxylate was deprotected following procedure **C** to afford **34**. Purified by washing with diethylether. Yield: 76 %. ^{1}H NMR (400MHz, DMSO): *δ* 1.05 – 1.25 (2H, m), 1.43 (2H, d, J=11.15 Hz), 1.98 – 2.13 (1H, m), 2.38 (2H, t, J=11.55 Hz), 2.90 (2H, d, J=11.05 Hz), 4.60 (2H, d, J=6.48 Hz), 7.09 – 7.23 (2H, m), 7.49 (1H, d, J=7.68 Hz), 7.81 (1H, s), 7.88 – 8.01 (3H, q, J=7.16 Hz), 8.22 (1H, s), 11.51 (1H, s). ^{13}C NMR (100MHz, DMSO): *δ* 19.02; 26.60; 26.80; 34.71; 43.03; 52.04; 56.43; 56.52; 106.77; 112.55; 115.59; 119.72; 120.46; 122.18; 124.71; 125.33; 134.70; 135.96; 137.47; 143.91. HRMS: *m/z* (EI+), calculated for: $C_{20}H_{21}N_5$ 332.1831 $[M]^+$, found: 332.1868 $[M]^+$. Melting temp. range: 215 – 219 °C.

- *6-(1H-indol-3-yl)-1-(pyrrolidin-3-ylmethyl)-1H-benzo[d][1,2,3]triazole (***35***)*

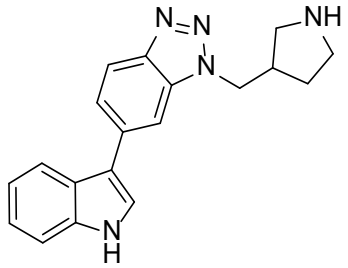

tert-butyl 3-(1-((1-(tert-butoxycarbonyl)pyrrolidin-3-yl)methyl)-1H-benzo[d][1,2,3]triazol-6-yl)-1H-indole-1-carboxylate was obtained after coupling with **35d**. Purified by flash chromatography (Cyclohexane/EtOAc 4:1 ➔ 1:2). Quantitative yield. ^{1}H NMR (400MHz, $CDCl_3$): δ 8.33 (1H, s), 8.25 (1H, d, *J* = 7.2 Hz), 7.82 (2H, dd, *J* = 20.2, 8.0 Hz), 7.60 (1H, d, *J* = 8.5 Hz), 7.37 (2H, dt, *J* = 30.0, 7.3 Hz), 4.68 (1H, s), 3.34 (7H, m), 1.71 (9H, s), 1.61 (2H, s), 1.46 (9H, s).

tert-butyl 3-(1-((1-(tert-butoxycarbonyl)pyrrolidin-3-yl)methyl)-1H-benzo[d][1,2,3]triazol-6-yl)-1H-indole-1-carboxylate was deprotected following procedure **C** to afford **35**. Purified by washing with diethylether. Yield: 85 %. ^{1}H NMR (400MHz, DMSO): δ 1.54 – 1.75 (1H, m), 1.85 – 2.04 (1H, m), 2.80 – 3.09 (3H, m), 3.17 (2H, s), 4.87 (2H, s), 7.18 (2H, t, J=8.29 Hz), 7.50 (2H, d, J=7.34 Hz), 7.79 (2H, d, J=8.36 Hz), 7.90 (1H, s), 8.00 – 8.12 (2H, m), 8.17 (1H, s), 11.65 (1H, s). ^{13}C NMR (100MHz, DMSO): δ 26.80; 28.63; 38.90; 45.00; 48.52; 49.49; 106.61; 112.58; 115.56; 119.74; 120.45; 122.16; 124.75; 125.30; 125.37; 134.48; 136.04; 137.47; 143.89. HRMS: *m/z* (EI+), calculated for : $C_{19}H_{19}N_5$ 318.1674 $[M]^+$, found: 318.1713 $[M]^+$. Melting temp. range: 72 – 82 °C.

- *5-(1H-indol-3-yl)-1-(pyrrolidin-3-ylmethyl)-1H-benzo[d][1,2,3]triazole (***36***)*

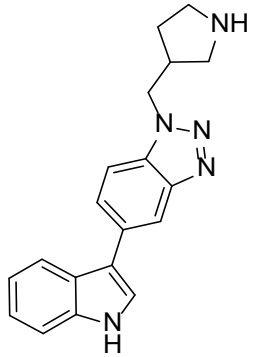

tert-butyl 3-(1-((1-(tert-butoxycarbonyl)pyrrolidin-3-yl)methyl)-1H-benzo[d][1,2,3]triazol-5-yl)-1H-indole-1-carboxylate was obtained after coupling

with **36d**. Purified by flash chromatography (Cyclohexane/EtOAc 1:0 ➔ 1:1). Yield: 80 %. ^{1}H NMR (400MHz, $CDCl_3$): δ 1.71 (9H, s), 2.91 – 3.05 (1H, m), 3.18 – 3.31 (1H, m), 3.31 – 3.45 (1H, m), 3.45 – 3.65 (2H, m), 4.64 – 4.72 (2H, m), 7.33 (1H, t, J=7.36 Hz), 7.41 (1H, t, J=7.55 Hz), 7.60 (1H, d, J=8.52 Hz), 7.77 – 7.82 (2H, m), 7.85 (1H, d, J=7.81 Hz), 8.22 – 8.29 (1H, m), 8.33 (1H, s).

tert-butyl 3-(1-((1-(tert-butoxycarbonyl)pyrrolidin-3-yl)methyl)-1H-benzo[d][1,2,3]triazol-5-yl)-1H-indole-1-carboxylate was deprotected following procedure **C** to afford **36**. Purified by washing with diethylether. Quantitative yield. ^{1}H NMR (400MHz, DMSO): δ 1.01 – 1.11 (1H, m), 2.79 – 2.88 (2H, m), 3.30 – 3.46 (multiplet under H_2O signal), 4.80 – 4.96 (2H, m), 7.11 – 7.25 (2H, m), 7.49 (1H, d, J=7.64 Hz), 7.75 (1H, d, J=8.46 Hz), 7.86 (1H, s), 7.99 – 8.07 (2H, m), 8.08 (1H, s), 11.53 (1H, s). ^{13}C NMR (100MHz, DMSO): δ 26.81; 45.44; 45.98; 54.63; 58.36; 65.39; 107.03; 112.57; 115.70; 119.57; 119.68; 120.37; 122.18; 124.50; 125.16; 125.37; 134.59; 135.52; 137.49; 143.98. HRMS: *m/z* (EI+), calculated for : $C_{19}H_{19}N_5$ 318.1674 $[M]^+$, found: 318.1711 $[M]^+$. Melting temp. range: 179 – 182 °C.

- *6-(1H-indol-3-yl)-1-(2-(piperazin-1-yl)ethyl)-1H-benzo[d][1,2,3]triazole (**37**)*

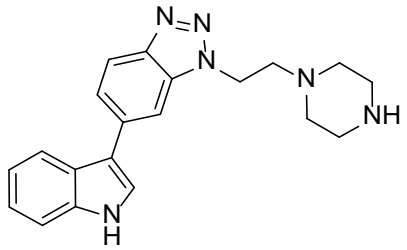

tert-butyl 3-(1-((1-(tert-butoxycarbonyl)piperidin-4-yl)methyl)-1H-benzo[d][1,2,3]triazol-6-yl)-1H-indole-1-carboxylate was obtained after coupling with **37d**. Purified by flash chromatography (Cyclohexane/EtOAc 1:1). Yield: 85 %. ^{1}H NMR (400MHz, DMSO): 2.35 – 2.44 (3H, m), 2.58 – 2.65 (3H, m), 2.83 (2H, t, J=6.21 Hz), 4.84 (2H, t, J=6.20 Hz), 7.14 (2H, t, J=7.08 Hz), 7.19 (2H, t, J=7.47 Hz), 7.49 (2H, d, J=7.93 Hz), 7.83 (2H, d, J=1.54 Hz), 7.89 – 7.98 (3H, m), 8.22 (2H, s), 11.50 (1H, s). ^{13}C NMR (100MHz, DMSO): δ 45.65; 46.01; 54.59; 58.23; 111.66; 112.52; 115.28; 115.66; 119.32; 120.26; 122.02; 124.49; 125.46; 127.73; 132.16; 132.41; 137.40; 146.56.

tert-butyl 3-(1-((1-(tert-butoxycarbonyl)piperidin-4-yl)methyl)-1H-benzo[d][1,2,3]triazol-6-yl)-1H-indole-1-carboxylate was deprotected using deprotection procedure **C** to afford **37**. Purified by washing with diethylether. Quantitative yield. ^{1}H NMR (400MHz, DMSO): δ 2.36 – 2.46 (4H, m), 2.56 – 2.64 (4H, m), 2.81 – 2.90 (2H, m), 4.85 – 4.93 (2H, m), 7.14 – 7.24 (2H, m), 7.50 (1H, d,

J=7.68 Hz), 7.77 (1H, d, J=8.56 Hz), 7.88 (1H, s), 8.01 – 8.08 (2H, m), 8.10 (1H, s), 11.55 (1H, s). ^{13}C NMR (100MHz, DMSO): *δ δ* 45.65; 46.01; 54.59; 58.23; 111.66; 112.52; 115.28; 115.66; 119.32; 120.26; 122.02; 124.49; 125.46; 127.73; 132.16; 132.41; 137.40; 146.56. HRMS: *m/z* (EI+), calculated for: $C_{20}H_{22}N_6$ 347.1939 $[M]^+$, found: 347.1978 $[M]^+$. Melting temp. range: 44 – 46 °C.

- *5-(1H-indol-3-yl)-1-(piperazin-4-yl)ethyl)-1H-benzo[d][1,2,3]triazole (***38***)*

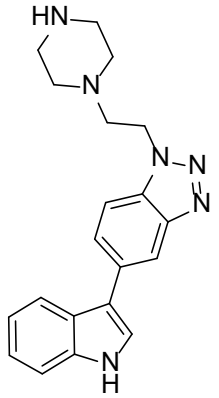

tert-butyl 3-(1-((4-(tert-butoxycarbonyl)piperazin-1-yl)methyl)-1H-benzo[d][1,2,3]triazol-5-yl)-1H-indole-1-carboxylate was obtained after coupling with **38d**. Purified by flash chromatography (Cyclohexane/EtOAc 1:1). Yield: 80 %. ^{1}H NMR (400MHz, $CDCl_3$): *δ* 2.43 – 2.55 (4H, m), 3.00 (1H, t, J=6.50 Hz), 3.35 – 3.44 (4H, m), 4.80 (2H, t, J=6.49 Hz), 7.33 (1H, t, J=7.49 Hz), 7.40 (1H, t, J=7.70 Hz), 7.64 (1H, d, J=8.55 Hz), 7.75 – 7.82 (2H, m), 7.85 (1H, d, J=7.79 Hz), 8.20 – 8.29 (1H, m), 8.31 (1H, s).

tert-butyl 3-(1-((4-(tert-butoxycarbonyl)piperazin-1-yl)methyl)-1H-benzo[d][1,2,3]triazol-5-yl)-1H-indole-1-carboxylate was deprotected using deprotection procedure **C** to afford **38**. Purified by washing with diethylether. Quantitative yield. ^{1}H NMR (400MHz, DMSO): *δ* 2.41 – 2.49 (3H, m), 2.61 – 2.67 (3H, m), 2.87 (2H, t, J=6.16 Hz), 4.89 (2H, t, J=6.17 Hz), 7.16 (1H, t, J=7.14 Hz), 7.21 (1H, t, J=7.45 Hz), 7.50 (1H, d, J=7.78 Hz), 7.77 (1H, d, J=8.68 Hz), 7.88 (1H, d, J=2.32 Hz), 8.01 – 8.07 (2H, m), 8.10 (1H, s). ^{13}C NMR (100MHz, DMSO): *δ* 31.01; 37.72; 46.04; 53.58; 111.47; 112.53; 115.34; 115.63; 119.30; 120.26; 122.01; 124.51; 125.45; 127.96; 132.30; 132.47; 137.39; 146.47. HRMS: *m/z* (EI+), calculated for: $C_{20}H_{22}N_6$ 347.1939 $[M]^+$, found: 347.1979 $[M]^+$. Melting temp. range: 177 – 185 °C.

6. Synthesis of 5-bromobenzochalcogendiazoles (48 – 51)

- *5-bromobenzo[c][1,2,5]thiadiazole (***48***).*

An RB flask was charged with thionyl chloride (3.5 mL, 48.4 mmol, 9 eq.) and 4-bromo-1,2-diaminobenzene (1 g, 5.3 mmol, 1 eq.) was added portion wise. After the addition, 0.16 mL of concentrated sulfuric acid (0.54 eq.). The resulting mixture was agitated under reflux for 1.5 hours. After cooling to room temperature, the mixture was poured on ice, extracted with dichloromethane. The OL was dried with $MgSO_4$ and concentrated in vacuo. Yield: 80 %. ^{1}H RMN (400MHz, DMSO): δ 7.85 (1H, dd, J=1.84, 9.25 Hz), 8.08 (1H, d, J=9.23 Hz), 8.47 (1H, d, J=1.31 Hz). ^{13}C RMN (100 MHz, DMSO): δ 123.04; 123.98; 124.53; 133.62; 153.37; 155.23.

- *6-bromo-[1,2,5]thiadiazolo[3,4-b]pyridine (**49**)*

The synthesis was performed according to a previously described procedure.[357] An RB flask was charged with 3 mL of toluene, dimethylformamide (50 μL) and 2,3-diamino-5-bromopyridine (0.5 g, 2.7 mmol) and heated to 70°C. Then, 1 mL of thionyl chloride were added and the final mixture was refluxed overnight at 90°C. After cooling down to room temperature, the precipitate was filtered and washed with H2O and ethanol to afford the desired compound. Yield: 77 %. ^{1}H RMN (400MHz, $CDCl_3$): δ 8.56 (1H, d, J=1.54 Hz), 9.09 (1H, s). ^{13}C RMN (100 MHz, $CDCl_3$): δ 121.25; 131.28; 147.96; 156.89; 160.01.

- *5-bromobenzo[c][1,2,5]selenadiazole (**50**)*

A solution of 4-bromo-1,2-diaminobenzene (1.2 g, 6.4 mmol, 1 eq.) in ethanol (9 mL) was heated to reflux temperature and selenium dioxide (0.8 g, 7 mmol, 1.1 eq.) was added. The addition of selenium dioxide resulted in an immediate precipitation of the desired product. After 10 minutes of reflux, the reaction mixture was cooled to 0°C and the precipitate was filtrated and washed with H_2O. Quantitative yield. ^{1}H RMN (400MHz, DMSO): δ 7.66 (1H, dd, J=1.74, 9.42 Hz), 7.81 (1H, d, J=9.40 Hz), 8.19 (1H, d, J=1.25 Hz). ^{13}C RMN (100 MHz, DMSO): δ 124.59; 124.64; 125.52; 132.83 (1C, s), 158.56 (1C, s), 160.21 (1C, s).

- *6-bromo-[1,2,5]selenadiazolo[3,4-b]pyridine (**51**)*

6-bromo-[1,2,5]selenadiazolo[3,4-b]pyridine was synthesised following a previously described procedure.[331] *In a mortar,* 2,3-diamino-5-bromopyridine was ground with selenium dioxide for 5 minutes. Then the reaction mixture was heated to 90°C and the crude residue was washed with H_2O. Quantitative yield. ^{1}H RMN (400MHz, DMSO): δ 8.72 (1H, d, J=2.24 Hz), 9.09 (1H, d, J=2.24 Hz). ^{13}C RMN (100 MHz, DMSO): δ 120.78; 133.10; 153.37; 157.20; 162.65.

7. Synthesis of compounds 45 – 47, 46*p* and 47*p*

- *Synthesis of 5-(1H-indol-3-yl)benzo[c][1,2,5]oxadiazole (**45**)*

The cross-coupled product was synthesised following the general coupling procedure using 5-bromo-2,1,3-benzoxadiazole (purchased from Fluorochem) and 1-(phenylsulfonyl)-3-(4,4,5,5-tetramethyl-1,3,2-dioxaborolan-2-yl)-1H-indole (**42**). Following the coupling, the resulting crude was filtrated through a silica pad and eluted with 1:4 mixture of ethyl acetate/cyclohexane. After concentration in vacuo, the residue containing the protected intermediate (*5-(1-(phenylsulfonyl)-1H-indol-3-yl)benzo[c][1,2,5]oxadiazole* ^{1}H RMN (400MHz, DMSO) : δ 7.40 (1H, t, J=7.30 Hz), 7.47 (1H, t, J=7.48 Hz), 7.62 (1H, t, J=7.20 Hz), 7.72 (1H, t, J=6.88 Hz), 7.93 (1H, d, J=9.20 Hz), 8.00 (1H, t, J=8.88 Hz), 7.90 – 8.09 (4H, m), 8.10 – 8.21 (3H, m), 8.44 (1H, s)). The protected intermediate underwent general SO_2Ph deprotection procedure **A** overnight to afford **45**. Yield over two steps: 80 %. ^{1}H RMN (400MHz, $CDCl_3$) : δ 7.28 – 7.31 (1H, m,), 7.32 – 7.35 (1H, m), 7.50 (1H, d, J=7.98 Hz), 7.59 (1H, d, J=2.67 Hz), 7.79 (1H, dd, J=1.37, 9.30 Hz), 7.87 (1H, dd, J=0.94, 9.30 Hz), 8.02 (1H, d, J=7.98 Hz), 8.06 (1H, t, J=0.99 Hz), 8.49 (1H, s). ^{13}C RMN (100 MHz, DMSO): δ 109.94; 111.90; 116.37; 116.42; 119.78; 121.44; 123.38; 123.84; 125.11; 133.68; 136.90; 138.55; 148.42; 150.05. HRMS: m/z (EI+), calculated for: $C_{14}H_9N_3O$ 236.0818 $[M+H]^+$, found: 236.0815 $[M+H]^+$.Melting range: 195.6 – 199.8 °C.

- *Synthesis of 5-(1H-indol-3-yl)benzo[c][1,2,5]thiadiazole (**46**)*

The cross-coupled product was synthesised following the general coupling procedure using 5-bromobenzo[*c*][1,2,5]thiadiazole (**48**) and tert-butyl 3-(4,4,5,5-tetramethyl-1,3,2-dioxaborolan-2-yl)-1H-indole-1-carboxylate (Fluorochem). Following the coupling, the resulting crude was filtrated through a silica pad and eluted with 1:3 mixture of ethyl acetate/cyclohexane. After concentration in vacuo, the residue underwent general Boc deprotection procedure **C** overnight to afford **46**. Yield over two steps: 76 %. ^{1}H RMN (400MHz, $CDCl_3$) : δ 7.28 (1H, t, J=7.41 Hz), 7.32 (1H, t, J=7.44 Hz), 7.49 (1H, d, J=7.98 Hz), 7.58 (1H, d, J=2.22 Hz), 7.97 (1H, dd, J=1.05, 9.03 Hz), 8.04 (1H, d, J=9.06 Hz), 8.07 (1H, d, J=7.86 Hz), 8.29 (1H, s), 8.43 (1H, s). ^{13}C RMN (100 MHz, $CDCl_3$): δ 111.71; 116.89; 117.08; 119.82; 121.08; 121.35; 123.05; 123.21; 125.40; 131.04; 136.88; 137.07; 153.78; 155.82. HRMS: m/z (EI+), calculated for: $C_{14}H_9N_3S$ 252.0590 $[M+H]^+$, found: 252.0580 $[M+H]^+$. Melting range: 183.1 – 183.6 °C.

- *Synthesis of 6-(1H-indol-3-yl)-[1,2,5]thiadiazolo[3,4-b]pyridine (**46*p*)*

The cross-coupled product was synthesised following the general coupling procedure using 6-bromo-[1,2,5]thiadiazolo[3,4-*b*]pyridine (**7**) and tert-butyl 3-(4,4,5,5-tetramethyl-1,3,2-dioxaborolan-2-yl)-1H-indole-1-carboxylate (Fluorochem). Following the coupling, the resulting crude was filtrated through a silica pad and eluted with 1:1 mixture of ethyl acetate/cyclohexane. After concentration in vacuo, the residue underwent general Boc deprotection procedure **C** overnight to afford **46*p***. Yield over two steps: 42 %. ^{1}H RMN (400MHz,

DMSO): δ 7.23 (1H, t, J=7.31 Hz), 7.27 (1H, t, J=7.36 Hz), 7.55 (1H, d, J=7.68 Hz), 8.11 (1H, d, J=7.62 Hz), 8.29 (1H, s), 8.66 (1H, s), 9.64 (1H, s), 11.86 (1H, s). ^{13}C RMN (100 MHz, DMSO): δ 111.48; 112.87; 119.81; 121.25; 121.62; 122.86; 125.21; 127.42; 133.19; 137.64; 148.58; 157.80; 159.94. HRMS: m/z (EI+), calculated for: $C_{13}H_9N_4S$ 253.0542 $[M+H]^+$, found: 253.0545 $[M+H]^+$. Melting range: 241.6 – 243.1 °C.

- *Synthesis of 5-(1H-indol-3-yl)benzo[c][1,2,5]selenadiazole (**47**)*

The cross-coupled product was synthesised following the general coupling procedure using 5-bromobenzo[*c*][1,2,5]selenadiazole (**50**) and 1-(phenylsulfonyl)-3-indolylboronic acid MIDA ester (**43**). Following the coupling, the resulting crude was filtrated through a silica pad and eluted with 1:1 mixture of ethyl acetate/cyclohexane. After concentration in vacuo, the residue was triturated in cyclohexane and the obtained precipitate was filtrated before undergoing general SO_2Ph deprotection procedure **A** for 1h to afford **3**. Yield over two steps: 79 %. ^{1}H RMN (400MHz, $CDCl_3$) : δ 7.27 – 7.35 (2H, m), 7.49 (1H, d, J=7.68 Hz), 7.60 (1H, d, J=2.44 Hz), 7.86 (1H, s), 8.09 (1H, d, J=7.64 Hz), 8.14 (1H, s), 8.47 (1H, s). ^{13}C RMN (100 MHz, DMSO): δ 111.73; 116.58; 118.35; 120.09; 121.14; 123.11; 123.19; 123.37; 125.36; 131.39; 136.95; 136.98; 159.74; 161.46. HRMS: m/z (EI+), calculated for: $C_{14}H_9N_3Se$ 300.0034 $[M+H]^+$, found: 300.0037 $[M+H]^+$. Melting range: 206.7 – 210.2

- *Synthesis of 6-(1H-indol-3-yl)-[1,2,5]selenadiazolo[3,4-b]pyridine (**47*****p*****)*

The cross-coupled product was synthesised following the general coupling procedure using 6-bromo-[1,2,5]selenadiazolo[3,4-*b*]pyridine (**51**) and 1-(phenylsulfonyl)-3-indolylboronic acid MIDA ester (**43**). Following the coupling, the resulting crude was filtrated through a silica pad and eluted with 1:1 mixture of ethyl acetate/cyclohexane. After concentration in vacuo, the residue was purified by flash chromatography (ethyl acetate/cyclohexane, 1:2 ➔ 1:0) to afford the protected intermediate *6-(1-(phenylsulfonyl)-1H-indol-3-yl)-[1,2,5]selenadiazolo[3,4-b]pyridine* ^{1}H RMN (400MHz, DMSO) : δ 7.39 – 7.54 (2H, m), 7.59 – 7.77 (3H, m), 8.07 (2H, dd, J=7.72, 15.89 Hz), 8.16 (2H, d, J=6.52 Hz), 8.59 (1H, s), 8.66 (1H, s), 9.54 (1H, s). The protected intermediate general SO_2Ph deprotection procedure **A** for 1h to afford **47*****p***. Yield over two steps: 34 %. ^{1}H RMN (400MHz, DMSO) : δ 7.23 (1H, t, J=6.96 Hz), 7.26 (1H, t, J=7.02 Hz), 7.54 (1H, d, J=7.98 Hz), 8.09 (1H, d, J=7.80 Hz), 8.30 (1H, s), 8.38 (1H, d, J=2.40 Hz), 9.58 (1H, d, J=2.40 Hz), 11.86 (1H, s). ^{13}C RMN (100 MHz, DMSO): δ 111.34; 112.88; 119.94; 121.22; 122.45; 122.86; 125.22; 127.42; 132.10; 137.69; 154.02; 158.59; 162.94. HRMS: m/z (EI+), calculated for: $C_{13}H_9N_4Se$ 300.9987 $[M+H]^+$, found: 300.9995 $[M+H]^+$ Melting range: 263.1 – 267.4 °C

8. Annex

Table S1. Inhibitory affinities (confidence intervals 95 % IC_{50}) of compounds against *h*TDO2 in the spectrophotometric assay and P815B cells

N_x	N°	Y	X	R_2	R_1	IC_{50}[a] *(μM)* Enz.	Cell
N_2	**7**				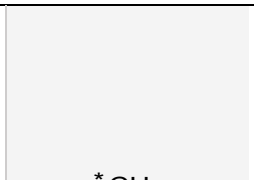	3.26 – 4.84	0.14 – 0.20
N_3	**8**					3.26 – 4.55	0.19 – 0.25
N_1	**9**					4.43 – 7.98	0.34 – 0.43
N_2	**10**			NH_2		2.21 – 5.57	0.35 – 0.51
N_3	**11**			NH_2		3.72 – 6.49	0.83– 1.16
N_1	**12**			NH_2		2.01 – 5.43	0.78 – 1.21
N_2	**13**		*N*			11.2 – 15.34	0.40 – 0.58
N_3	**14**		*N*			6.56 – 9.32	0.33 – 0.47
N_1	**15**		*N*			9.72 – 10.42	0.63 – 0.80
N_1	**16**			NO_2		0.69 – 1.93 *	2.44 – 4.25
N_3	**8a**	*F*				0.98 – 1.32	0.002 – 0.04
N_3	**17**				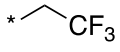	11.16 – 19.25	0.04 – 0.21
N_1	**18**					1.43 – 2.99	0.14 – 0.24
N_3	**19**				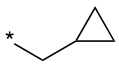	11.16 – 19.25	0.39 – 0.21
N_1	**20**					1.94 – 8.21	0.72 – 1.33
N_3	**21**				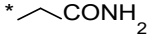	28.62 – 73.41	1.49 – 2.10
N_1	**22**					20.20 – 60.33	0.60 – 0.79
N_3	**23**				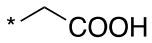	> 93.25	NI
N_1	**24**					58.34 – 127.20	NI
N_3	**25**				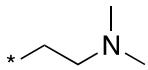	18.74 – 45.56	1.633 – 2.286
N_1	**26**					12.69 – 34.23	1.330 – 2.010
N_3	**27**				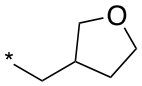	36.45 – 58.29	1.524 – 2.287
N_1	**28**					19.45 – 28.52	0.29 – 0.58
N_3	**29**				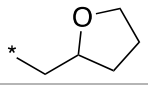	28.97 – 66.37	1.96 – 3.36
N_1	**30**					16.84 – 28.64	0.39 – 0.63
N_3	**31**					54.70 – 138.7	2.86 – 5.02

N_1	**32**		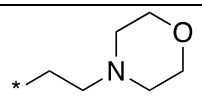	36.37 – 91.75	1.36 – 1.89
N_3	**33**		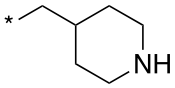	12.23 – 27.97	0.81 – 1.07
N_1	**34**			18.2 – 44.38	0.91 – 1.47
N_3	**35**		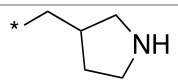	15.82 – 40.2	0.50 – 0.76
N_1	**36**			32.56 – 86.62	1.33 – 2.42
N_3	**37**		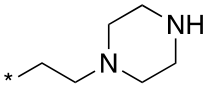	17.44 – 44.32	0.56 – 0.98
N_1	**38**			34.72 – 66.90	1.05 – 1.95
N_3	**37a**	*F*		2.38 – 8.46	0.18 – 0.29
N_3		**39**	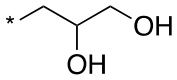	14.06 – 23.00	0.58 – 0.98
N_1		**40**		19.10 – 49.95	1.92 – 2.68

Figure S1. Epitope mapping of regioisomers 26, 27 (*a*) and 36, 37 (*b*).

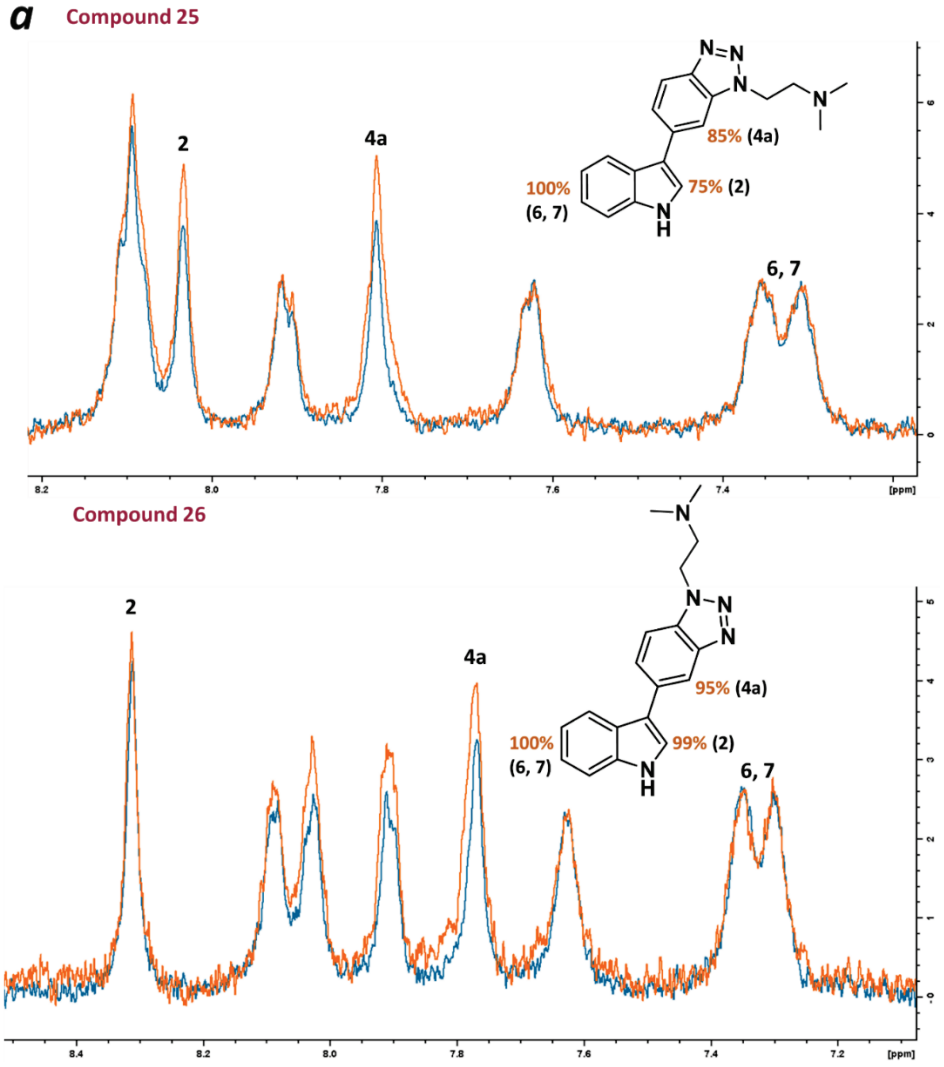

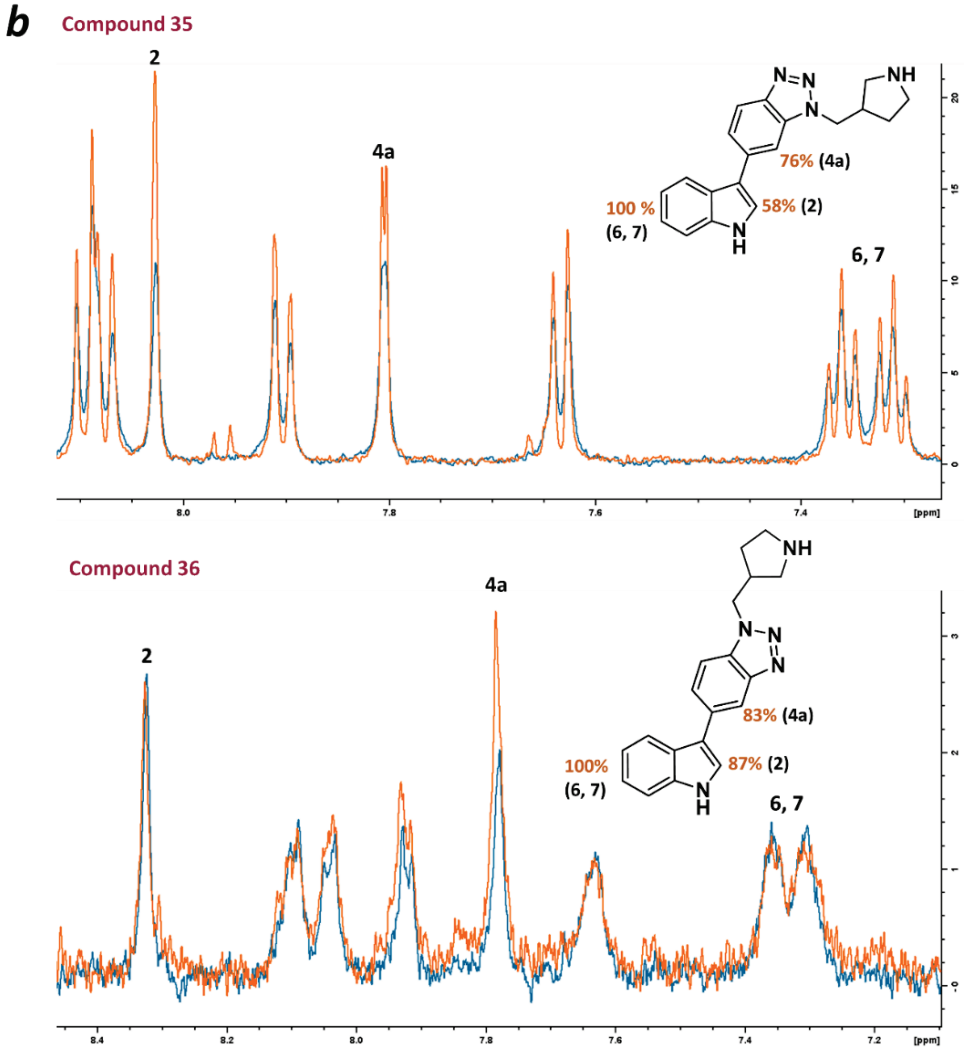
b
Compound 35
2
4a
6, 7
76% (4a)
58% (2)
100 %
(6, 7)
Compound 36
2
4a
6, 7
83% (4a)
87% (2)
100%
(6, 7)

Figure S2. Microsomal stability, half-life curves. (**a**) Recovery of the different studied compounds over time in the presence of microsomal extracts. (**b**) Closeup view on the 0 – 360 minutes portion of the curves. The plotted values are the result of two independent experiments. (**c**) Microsomal stability curves of benzochalcogendiazoles isosteres.

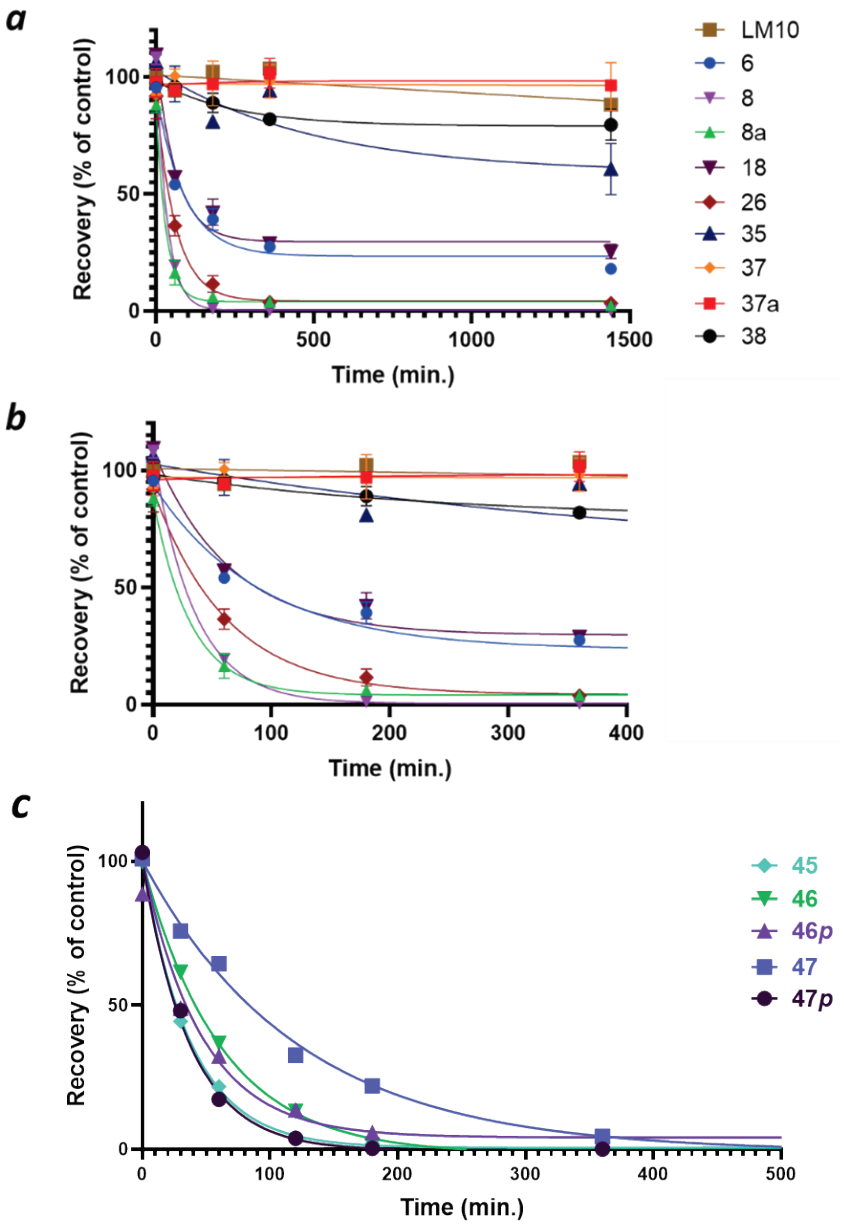

Figure S3. Log K_w traces for compounds 45 – 47, 46*p*, 47*p*.

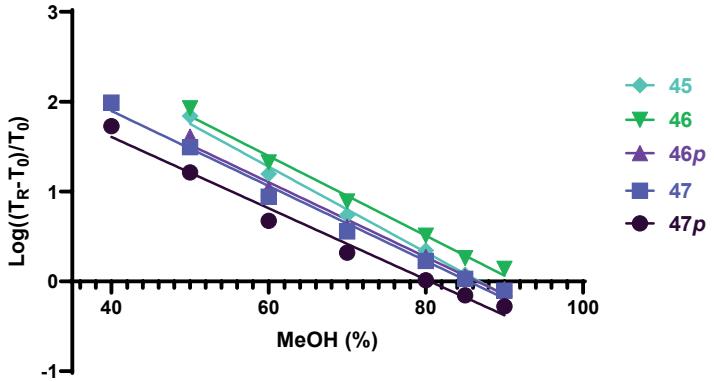

Figure S4. MTS-PMS survival curves following treatment with compounds 45 – 47, 46*p*, 47*p*.

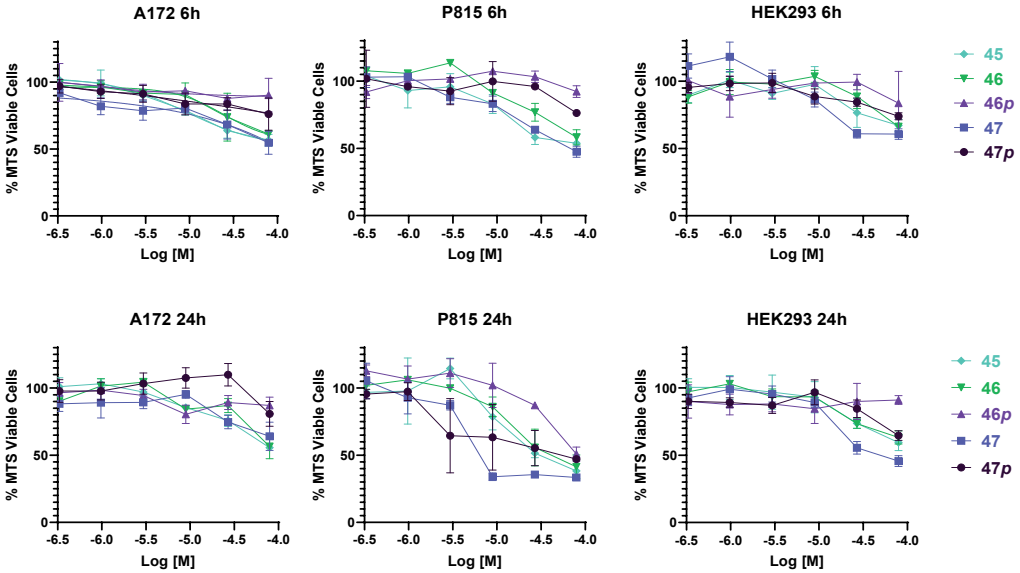

Figure S5. Annexin/PI analysis of the treatment of P815B cells with compound 47.

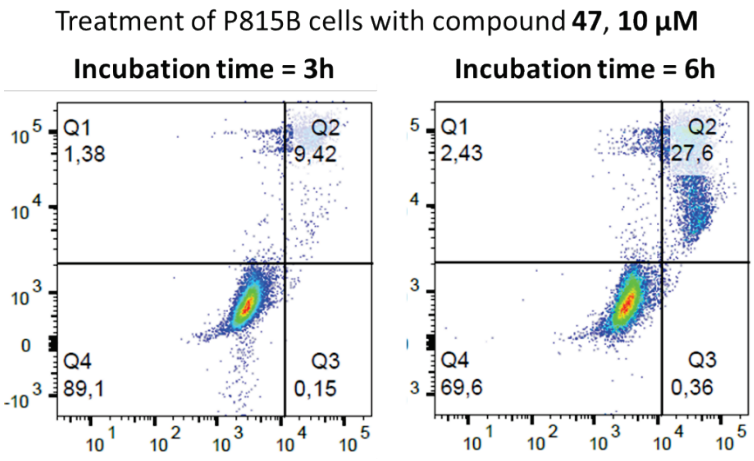

9. References

(1) Pardoll, D. M. The Blockade of Immune Checkpoints in Cancer Immunotherapy. *Nat. Rev. Cancer* **2012**, *12* (4), 252–264.

(2) Abbott, M.; Ustoyev, Y. Cancer and the Immune System: The History and Background of Immunotherapy. *Semin. Oncol. Nurs.* **2019**, *35* (5), 150923.

(3) Demaria, O.; Cornen, S.; Daëron, M.; Morel, Y.; Medzhitov, R.; Vivier, E. Harnessing Innate Immunity in Cancer Therapy. *Nature* **2019**, *574* (7776), 45–56.

(4) Feng, M.; Jiang, W.; Kim, B. Y. S.; Zhang, C. C.; Fu, Y. X.; Weissman, I. L. Phagocytosis Checkpoints as New Targets for Cancer Immunotherapy. *Nat. Rev. Cancer* **2019**, *19* (10), 568–586.

(5) Morvan, M. G.; Lanier, L. L. NK Cells and Cancer: You Can Teach Innate Cells New Tricks. *Nat. Rev. Cancer* **2016**, *16*, 7–19.

(6) Dranoff, G. Cytokines in Cancer Pathogenesis and Cancer Therapy. *Nat. Rev. Cancer* **2004**, *4* (1), 11–22.

(7) Bennett, S. R. M.; Carbone, F. R.; Karamalis, F.; Miller, J. F. A. P.; Heath, W. R. Induction of a CD8+ Cytotoxic T Lymphocyte Response by Cross-Priming Requires Cognate CD4+ T Cell Help. *J. Exp. Med.* **1997**, *186* (1), 65–70.

(8) Ahrends, T.; Spanjaard, A.; Pilzecker, B.; Bąbała, N.; Bovens, A.; Xiao, Y.; Jacobs, H.; Borst, J. CD4+ T Cell Help Confers a Cytotoxic T Cell Effector Program Including Coinhibitory Receptor Downregulation and Increased Tissue Invasiveness. *Immunity* **2017**, *47* (5), 848–861.e5.

(9) Takeuchi, A.; Saito, T. CD4 CTL, a Cytotoxic Subset of CD4+ T Cells, Their Differentiation and Function. *Front. Immunol.* **2017**, *8* (FEB), 194.

(10) Okeke, E. B.; Uzonna, J. E. The Pivotal Role of Regulatory T Cells in the Regulation of Innate Immune Cells. *Front. Immunol.* **2019**, *10* (APR), 680.

(11) Wang, H.; Franco, F.; Ho, P. C. Metabolic Regulation of Tregs in Cancer: Opportunities for Immunotherapy. *Trends Cancer.* **2017**, *3* (8), 583–592.

(12) Hald, S. M.; Bremnes, R. M.; Al-Shibli, K.; Al-Saad, S.; Andersen, S.; Stenvold, H.; Busund, L. T.; Donnem, T. CD4/CD8 Co-Expression Shows Independent Prognostic Impact in Resected Non-Small Cell Lung Cancer Patients Treated with Adjuvant Radiotherapy. *Lung Cancer* **2013**, *80* (2), 209–215.

(13) Sarvaria, A.; Madrigal, J. A.; Saudemont, A. B Cell Regulation in Cancer and Anti-Tumor Immunity. *Cell. Mol. Immunol.* **2017**, *14* (8), 662–674.

(14) Yuen, G. J.; Demissie, E.; Pillai, S. B Lymphocytes and Cancer: A Love–Hate Relationship. *Trends Cancer.* **2016**, *2* (12), 747–757.

(15) Gianchecchi, E.; Delfino, D. V.; Fierabracci, A. NK Cells in Autoimmune Diseases: Linking Innate and Adaptive Immune Responses. *Autoimmun. Rev.* **2018**, *17* (2), 142–154.

(16) Hanahan, D.; Weinberg, R. A. Hallmarks of Cancer: The next Generation. *Cell* **2011**, *144* (5), 646–674.

(17) Mueller, M. Inflammation and Angiogenesis: Innate Immune Cells as Modulators of Tumor Vascularization. *Tumor Angiogenes. Basic Mech. Cancer Ther.* **2008**, 351–362.

(18) Villalba, M.; Rathore, M. G.; Lopez-Royuela, N.; Krzywinska, E.; Garaude, J.; Allende-Vega, N. From Tumor Cell Metabolism to Tumor Immune Escape. *Int. J. Biochem. Cell Biol.* **2013**, *45* (1), 106–113.

(19) Cerezo, M.; Rocchi, S. Cancer Cell Metabolic Reprogramming: A Keystone for the Response to Immunotherapy. *Cell Death Dis.* **2020**, *11* (11), 1–10.

(20) Chen, J.; Cao, X.; Li, B.; Zhao, Z.; Chen, S.; Lai, S. W. T.; Muend, S. A.; Nossa, G. K.; Wang, L.; Guo, W.; Ye, J.; Lee, P. P.; Feng, M. Warburg Effect Is a Cancer Immune Evasion Mechanism Against Macrophage Immunosurveillance. *Front. Immunol.* **2021**, *11*, 3815.

(21) Bohn, T.; Rapp, S.; Luther, N.; Klein, M.; Bruehl, T. J.; Kojima, N.; Aranda Lopez, P.; Hahlbrock, J.; Muth, S.; Endo, S.; Pektor, S.; Brand, A.; Renner, K.; Popp, V.; Gerlach, K.; Vogel, D.; Lueckel, C.; Arnold-Schild, D.; Pouyssegur, J.; Kreutz, M.; Huber, M.; Koenig, J.; Weigmann, B.; Probst, H. C.; von Stebut, E.; Becker, C.; Schild, H.; Schmitt, E.; Bopp, T. Tumor Immunoevasion via Acidosis-Dependent Induction of Regulatory Tumor-Associated Macrophages. *Nat. Immunol.* **2018**, *19* (12), 1319–1329.

(22) Brand, A.; Singer, K.; Koehl, G. E.; Kolitzus, M.; Schoenhammer, G.; Thiel, A.; Matos, C.; Bruss, C.; Klobuch, S.; Peter, K.; Kastenberger, M.; Bogdan, C.; Schleicher, U.; Mackensen, A.; Ullrich, E.; Fichtner-Feigl, S.; Kesselring, R.; Mack, M.; Ritter, U.; Schmid, M.; Blank, C.; Dettmer, K.; Oefner, P. J.; Hoffmann, P.; Walenta, S.; Geissler, E. K.; Pouyssegur, J.; Villunger, A.; Steven, A.; Seliger, B.; Schreml, S.; Haferkamp, S.; Kohl, E.; Karrer, S.; Berneburg, M.; Herr, W.; Mueller-Klieser, W.; Renner, K.; Kreutz, M. LDHA-Associated Lactic Acid Production Blunts Tumor Immunosurveillance by T and NK Cells. *Cell Metab.* **2016**, *24* (5), 657–671.

(23) Colegio, O. R.; Chu, N. Q.; Szabo, A. L.; Chu, T.; Rhebergen, A. M.; Jairam, V.; Cyrus, N.; Brokowski, C. E.; Eisenbarth, S. C.; Phillips, G. M.; Cline, G. W.; Phillips, A. J.; Medzhitov, R. Functional Polarization of Tumour-Associated Macrophages by Tumour-Derived Lactic Acid. *Nature* **2014**, *513* (7519), 559–563.

(24) Sullivan, M. R.; Danai, L. V.; Lewis, C. A.; Chan, S. H.; Gui, D. Y.; Kunchok, T.; Dennstedt, E. A.; Heiden, M. G. V.; Muir, A. Quantification of Microenvironmental Metabolites in Murine Cancers Reveals Determinants of Tumor Nutrient Availability. *Elife* **2019**, *8*.

(25) Monteran, L.; Erez, N. The Dark Side of Fibroblasts: Cancer-Associated Fibroblasts as Mediators of Immunosuppression in the Tumor Microenvironment. *Front. Immunol.* **2019**, *10* (AUG), 1835.

(26) Sahai, E.; Astsaturov, I.; Cukierman, E.; DeNardo, D. G.; Egeblad, M.; Evans, R. M.; Fearon, D.; Greten, F. R.; Hingorani, S. R.; Hunter, T.; Hynes, R. O.; Jain, R. K.; Janowitz, T.; Jorgensen, C.; Kimmelman, A. C.; Kolonin, M. G.; Maki, R. G.; Powers, R. S.; Puré, E.; Ramirez, D. C.; Scherz-Shouval, R.; Sherman, M. H.; Stewart, S.; Tlsty, T. D.; Tuveson, D. A.; Watt, F. M.; Weaver, V.; Weeraratna, A. T.; Werb, Z. A Framework for Advancing Our Understanding of Cancer-Associated Fibroblasts. *Nature Reviews Cancer*. Nature Publishing Group January 24, 2020, pp 174–186.

(27) Takahashi, H.; Sakakura, K.; Kudo, T.; Toyoda, M.; Kaira, K.; Oyama, T.; Chikamatsu, K. Cancer-Associated Fibroblasts Promote an Immunosuppressive Microenvironment through the Induction and Accumulation of Protumoral Macrophages. *Oncotarget* **2017**, *8* (5), 8633–8647.

(28) Xiang, H.; Ramil, C. P.; Hai, J.; Zhang, C.; Wang, H.; Watkins, A. A.; Afshar, R.; Georgiev, P.; Sze, M. A.; Song, X. S.; Curran, P. J.; Cheng, M.; Miller, J. R.; Sun, D.; Loboda, A.; Jia, Y.; Moy, L. Y.; Chi, A.; Brandish, P. E. Cancer-Associated Fibroblasts Promote Immunosuppression by Inducing ROS-Generating Monocytic MDSCs in Lung Squamous Cell Carcinoma. *Cancer Immunol. Res.* **2020**, *8* (4), 436–450.

(29) Costa, A.; Kieffer, Y.; Scholer-Dahirel, A.; Pelon, F.; Bourachot, B.; Cardon, M.; Sirven, P.; Magagna, I.; Fuhrmann, L.; Bernard, C.; Bonneau, C.; Kondratova, M.; Kuperstein, I.; Zinovyev, A.; Givel, A. M.; Parrini, M. C.; Soumelis, V.; Vincent-Salomon, A.; Mechta-Grigoriou, F. Fibroblast Heterogeneity and Immunosuppressive Environment in Human Breast Cancer. *Cancer Cell* **2018**, *33* (3), 463–479.e10.

(30) Nishizuka, Y.; Sakakura, T. Thymus and Reproduction: Sex-Linked Dysgenesia of the Gonad after Neonatal Thymectomy in Mice. *Science (80-.).* **1969**, *166* (3906), 753–755.

(31) Chen, W. J.; Jin, W.; Hardegen, N.; Lei, K. J.; Li, L.; Marinos, N.; McGrady, G.; Wahl, S. M. Conversion of Peripheral CD4+CD25- Naive T Cells to CD4+CD25+ Regulatory T Cells by TGF-β Induction of Transcription Factor Foxp3. *J. Exp. Med.* **2003**, *198* (12), 1875–1886.

(32) Deng, G. Tumor-Infiltrating Regulatory T Cells: Origins and Features. *Am. J. Clin. Exp. Immunol.* **2018**, *7* (5), 81–87.

(33) Hori, S.; Nomura, T.; Sakaguchi, S. Control of Regulatory T Cell Development by the Transcription Factor Foxp3. *Science (80-.).* **2003**, *5609* (299), 1057–1061.

(34) Van Loosdregt, J.; Vercoulen, Y.; Guichelaar, T.; Gent, Y. Y. J.; Beekman, J. M.; Van Beekum, O.; Brenkman, A. B.; Hijnen, D. J.; Mutis, T.; Kalkhoven, E.; Prakken, B. J.; Coffer, P. J. Regulation of Treg Functionality by Acetylation-Mediated Foxp3 Protein Stabilization. *Blood* **2010**, *115* (5), 965–974.

(35) Martin, F.; Ladoire, S.; Mignot, G.; Apetoh, L.; Ghiringhelli, F. Human FOXP3 and Cancer. *Oncogene* **2010**, *29* (29), 4121–4129.

(36) Stockis, J.; Liénart, S.; Colau, D.; Collignon, A.; Nishimura, S. L.; Sheppard, D.; Coulie, P. G.; Lucas, S. Blocking Immunosuppression by Human Tregs in Vivo with Antibodies Targeting Integrin AVβ8. *Proc. Natl. Acad. Sci. U. S. A.* **2017**, *114* (47), E10161–E10168.

(37) Lu, L.; Barbi, J.; Pan, F. The Regulation of Immune Tolerance by FOXP3. *Nat. Rev. Immunol.* **2017**, *17*, 703–717.

(38) Ostrand-Rosenberg, S.; Sinha, P.; Beury, D. W.; Clements, V. K. Cross-Talk between Myeloid-Derived Suppressor Cells (MDSC), Macrophages, and Dendritic Cells Enhances Tumor-Induced Immune Suppression. *Semin. Cancer Biol.* **2012**, *22* (4), 275–281.

(39) Veglia, F.; Perego, M.; Gabrilovich, D. Myeloid-Derived Suppressor Cells Coming of Age. *Nat. Immunol.* **2018**, *19* (2), 108–119.

(40) Ugel, S.; De Sanctis, F.; Mandruzzato, S.; Bronte, V. Tumor-Induced Myeloid Deviation: When Myeloid-Derived Suppressor Cells Meet Tumor-Associated Macrophages. *J. Clin. Invest.* **2015**, *125* (9), 3365–3376.

(41) Jayasingam, S. D.; Citartan, M.; Thang, T. H.; Mat Zin, A. A.; Ang, K. C.; Ch'ng, E. S. Evaluating the Polarization of Tumor-Associated Macrophages Into M1 and M2 Phenotypes in Human Cancer Tissue: Technicalities and Challenges in Routine Clinical Practice. *Front. Oncol.* **2020**, *9*.

(42) Rivera, L. B.; Bergers, G. Myeloid Cell-Driven Angiogenesis and Immune Regulation in Tumors. *Trends Immunol.* **2015**, *36* (4), 240–249.

(43) de Haas, N.; de Koning, C.; Spilgies, L.; de Vries, I. J. M.; Hato, S. V. Improving Cancer Immunotherapy by Targeting the STATe of MDSCs. *Oncoimmunology* **2016**, *5* (7).

(44) Krneta, T.; Gillgrass, A.; Poznanski, S.; Chew, M.; Lee, A. J.; Kolb, M.; Ashkar, A. A. M2-Polarized and Tumor-Associated Macrophages Alter NK Cell Phenotype and Function in a Contact-Dependent Manner. *J. Leukoc. Biol.* **2017**, *101* (1), 285–295.

(45) Savage, N. D. L.; de Boer, T.; Walburg, K. V.; Joosten, S. A.; van Meijgaarden, K.; Geluk, A.; Ottenhoff, T. H. M. Human Anti-Inflammatory Macrophages Induce Foxp3 + GITR + CD25 + Regulatory T Cells, Which Suppress via Membrane-Bound TGFβ-1 . *J. Immunol.* **2008**, *181* (3), 2220–2226.

(46) Munn, D. H.; Sharma, M. D.; Baban, B.; Harding, H. P.; Zhang, Y.; Ron, D.; Mellor, A. L. GCN2 Kinase in T Cells Mediates Proliferative Arrest and Anergy Induction in Response to Indoleamine 2,3-Dioxygenase. *Immunity* **2005**, *22* (5), 633–642.

(47) Bronte, V.; Zanovello, P. Regulation of Immune Responses by L-Arginine Metabolism. *Nat. Rev. Immunol.* **2005**, *5* (8), 641–654.

(48) Corzo, C. A.; Cotter, M. J.; Cheng, P.; Cheng, F.; Kusmartsev, S.; Sotomayor, E.; Padhya, T.; McCaffrey, T. V.; McCaffrey, J. C.; Gabrilovich, D. I. Mechanism Regulating Reactive Oxygen Species in Tumor-Induced Myeloid-Derived Suppressor Cells. *J. Immunol.* **2009**, *182* (9), 5693–5701.

(49) Chen, X.; Song, M.; Zhang, B.; Zhang, Y. Reactive Oxygen Species Regulate T Cell Immune Response in the Tumor Microenvironment. *Oxid. Med. Cell. Longev.* **2016**, *2016*.

(50) Liu, Y.; Yu, Y.; Yang, S.; Zeng, B.; Zhang, Z.; Jiao, G.; Zhang, Y.; Cai, L.; Yang, R. Regulation of Arginase i Activity and Expression by Both PD-1 and CTLA-4 on the Myeloid-Derived Suppressor Cells. *Cancer Immunol. Immunother.* **2009**, *58* (5), 687–697.

(51) Davidov, V.; Jensen, G.; Mai, S.; Chen, S. H.; Pan, P. Y. Analyzing One Cell at a TIME: Analysis of Myeloid Cell Contributions in the Tumor Immune Microenvironment. *Front. Immunol.* **2020**, *11*, 1842.

(52) Goleva, E.; Lyubchenko, T.; Kraehenbuehl, L.; LaCouture, M. E.; Leung, D. Y. M.; Kern, J. A. Our Current Understanding of Checkpoint Inhibitor Therapy in Cancer Immunotherapy. *Ann. Allergy, Asthma Immunol.* **2021**.

(53) Schwartz, R. H. Costimulation of T Lymphocytes: The Role of CD28, CTLA-4, and B7/BB1 in Interleukin-2 Production and Immunotherapy. *Cell* **1992**, *71* (7), 1065–1068.

(54) Sinclair, N. R. S. C.; Anderson, C. C. Co-Stimulation and Co-Inhibition: Equal Partners in Regulation. *Scandinavian Journal of Immunology*. Blackwell Publishing Ltd June 3, 1996, pp 597–603.

(55) Ramsay, A. G. Immune Checkpoint Blockade Immunotherapy to Activate Anti-Tumour T-Cell Immunity. *Br. J. Haematol.* **2013**, *162* (3), 313–325.

(56) Acuto, O.; Michel, F. CD28-Mediated Co-Stimulation: A Quantitative Support for TCR Signalling. *Nat. Rev. Immunol.* **2003**, *3* (12), 939–951.

(57) Korman, A. J.; Peggs, K. S.; Allison, J. P. Checkpoint Blockade in Cancer Immunotherapy. *Adv. Immunol.* **2006**, *90*, 297–339.

(58) Buchbinder, E. I.; Desai, A. CTLA-4 and PD-1 Pathways Similarities, Differences, and Implications of Their Inhibition. *Am. J. Clin. Oncol. Cancer Clin. Trials* **2016**, *39* (1), 98–106.

(59) Seliger, B.; Marincola, F. M.; Ferrone, S.; Abken, H. The Complex Role of B7 Molecules in Tumor Immunology. *Trends Mol. Med.* **2008**, *14* (12), 550–559.

(60) Mueller, D. L.; Jenkins, M. K.; Schwartz, R. H. Clonal Expansion versus Functional Clonal Inactivation: A Costimulatory Signalling Pathway Determines the Outcome of T Cell Antigen Receptor Occupancy. *Annu. Rev. Immunol.* **1989**, *7*, 445–480.

(61) Fife, B. T.; Pauken, K. E.; Eagar, T. N.; Obu, T.; Wu, J.; Tang, Q.; Azuma, M.; Krummel, M. F.; Bluestone, J. A. Interactions between PD-1 and PD-L1 Promote Tolerance by Blocking the TCR-Induced Stop Signal. *Nat. Immunol.* **2009**, *10* (11), 1185–1192.

(62) Khattri, R.; Auger, J.; Griffin, M.; Sharpe, A.; Bluestone, J. Lymphoproliferative Disorder in CTLA-4 Knockout Mice Is Characterized by CD28-Regulated Activation of Th2 Responses. *J. Immunol.* **1999**, No. May 15;162(10), 5784–5791.

(63) Fife, B. T.; Bluestone, J. A. Control of Peripheral T-Cell Tolerance and Autoimmunity via the CTLA-4 and PD-1 Pathways. *Immunol. Rev.* **2008**, *224* (1), 166–182.

(64) Keir, M. E.; Butte, M. J.; Freeman, G. J.; Sharpe, A. H. PD-1 and Its Ligands in Tolerance and Immunity. *Annu. Rev. Immunol.* **2008**, *26*, 677–704.

(65) Ostrand-Rosenberg, S.; Horn, L. A.; Haile, S. T. The Programmed Death-1 Immune-Suppressive Pathway: Barrier to Antitumor Immunity. *J. Immunol.* **2014**, *193* (8), 3835–3841.

(66) Ishida, Y.; Agata, Y.; Shibahara, K.; Honjo, T. Induced Expression of PD-1, a Novel Member of the Immunoglobulin Gene Superfamily, upon Programmed Cell Death. *EMBO J.* **1992**, *11* (11), 3887–3895.

(67) Pfistershammer, K.; Klauser, C.; Pickl, W. F.; Stöckl, J.; Leitner, J.; Zlabinger, G.; Majdic, O.; Steinberger, P. No Evidence for Dualism in Function and Receptors: PD-L2/B7-DC Is an Inhibitory Regulator of Human T Cell Activation. *Eur. J. Immunol.* **2006**, *36* (5), 1104–1113.

(68) Wherry, E. J. T Cell Exhaustion. *Nat. Immunol.* **2011**, *12* (6), 492–499.

(69) Parry, R. V.; Chemnitz, J. M.; Frauwirth, K. A.; Lanfranco, A. R.; Braunstein, I.; Kobayashi, S. V.; Linsley, P. S.; Thompson, C. B.; Riley, J. L. CTLA-4 and PD-1 Receptors Inhibit T-Cell Activation by Distinct Mechanisms. *Mol. Cell. Biol.* **2005**, *25* (21), 9543–9553.

(70) Bennett, F.; Luxenberg, D.; Ling, V.; Wang, I.-M.; Marquette, K.; Lowe, D.; Khan, N.; Veldman, G.; Jacobs, K. A.; Valge-Archer, V. E.; Collins, M.; Carreno, B. M. Program Death-1 Engagement Upon TCR Activation Has Distinct Effects on Costimulation and Cytokine-Driven Proliferation: Attenuation of ICOS, IL-4, and IL-21, But Not CD28, IL-7, and IL-15 Responses. *J. Immunol.* **2003**, *170* (2), 711–718.

(71) Hulpke, S.; Tampé, R. The MHC I Loading Complex: A Multitasking Machinery in Adaptive Immunity. *Trends Biochem. Sci.* **2013**, *38* (8), 412–420.

(72) Paulson, K. G.; Tegeder, A.; Willmes, C.; Iyer, J. G.; Afanasiev, O. K.; Schrama, D.; Koba, S.; Thibodeau, R.; Nagase, K.; Simonson, W. T.; Seo, A.; Koelle, D. M.; Madeleine, M.; Bhatia, S.; Nakajima, H.; Sano, S.; Hardwick, J. S.; Disis, M. L.; Cleary, M. A.; Urgen, J.; Becker, C.; Nghiem, P. Downregulation of MHC-I Expression Is Prevalent but Reversible in Merkel Cell Carcinoma. *Cancer Immunol Res.* **2014**, No. Nov;2(11), 1071–1079.

(73) Bubeník, J. Tumour MHC Class I Downregulation and Immunotherapy (Review). *Oncol. Rep.* **2003**, *10* (6), 2005–2008.

(74) Cornel, A. M.; Mimpen, I. L.; Nierkens, S. MHC Class I Downregulation in Cancer: Underlying Mechanisms and Potential Targets for Cancer Immunotherapy. *Cancers (Basel).* **2020**, *12* (7), 1760.

(75) Garrido, F.; Cabrera, T.; Aptsiauri, N. “Hard” and “Soft” Lesions Underlying the HLA Class I Alterations in Cancer Cells: Implications for Immunotherapy. *Int. J. Cancer* **2010**, *127* (2), 249–256.

(76) Feenstra, M.; Veltkamp, M.; Van Kuik, J.; Wiertsema, S.; Slootweg, P.; Van den Tweel, J.; De Weger, R.; Tilanus, M. HLA Class 1 Expression and Chromosomal Deletions at 6p and 15q in Head and Neck Squamous Cell Carcinomas. *Tissue Antigens* **1999**, *54* (3), 235–245.

(77) Maleno, I.; Romero, J. M.; Cabrera, T.; Paco, L.; Aptsiauri, N.; Cozar, J. M.; Tallada, M.; López-Nevot, M. A.; Garrido, F. LOH at 6p21.3 Region and HLA Class Altered Phenotypes in Bladder Carcinomas. *Immunogenetics* **2006**, *58* (7), 503–510.

(78) Siddle, H. V.; Kreiss, A.; Tovar, C.; Yuen, C. K.; Cheng, Y.; Belov, K.; Swift, K.; Pearse, A. M.; Hamede, R.; Jones, M. E.; Skjødt, K.; Woods, G. M.; Kaufman, J. Reversible Epigenetic Down-Regulation of MHC Molecules by Devil Facial Tumour Disease Illustrates Immune Escape by a Contagious Cancer. *Proc. Natl. Acad. Sci. U. S. A.* **2013**, *110* (13), 5103–5108.

(79) Romero, J. M.; Jiménez, P.; Cabrera, T.; Cózar, J. M.; Pedrinaci, S.; Tallada, M.; Garrido, F.; Ruiz-Cabello, F. Coordinated Downregulation of the Antigen Presentation Machinery and HLA Class I/B2-Microglobulin Complex Is Responsible for HLA-ABC Loss in Bladder Cancer. *Int. J. Cancer* **2005**, *113* (4), 605–610.

(80) Rabinovich, G. A.; Gabrilovich, D.; Sotomayor, E. M. Immunosuppressive Strategies That Are Mediated by Tumor Cells. *Annu. Rev. Immunol.* **2007**, *25*, 267–296.

(81) Li, M. O.; Wan, Y. Y.; Sanjabi, S.; Robertson, A. K. L.; Flavell, R. A. Transforming Growth Factor-β Regulation of Immune Responses. *Annu. Rev. Immunol.* **2006**, *24*, 99–146.

(82) Liu, B.; Qu, L.; Yan, S. Cyclooxygenase-2 Promotes Tumor Growth and Suppresses Tumor Immunity. *Cancer Cell Int.* **2015**, *15* (1), 106.

(83) Murray, P. J. Amino Acid Auxotrophy as a System of Immunological Control Nodes. *Nat. Immunol. 2016 172* **2016**, *17* (2), 132–139.

(84) Coley, W. B. The Treatment of Inoperable Sarcoma by Bacterial Toxins (the Mixed Toxins of the Streptococcus Erysipelas and the Bacillus Prodigiosus). *Proc. R. Soc. Med.* **1910**, *3* (Surg_Sect), 1–48.

(85) Tsung, K.; Norton, J. A. Lessons from Coley's Toxin. *Surg. Oncol.* **2006**, *15* (1), 25–28.

(86) Morales, A.; Eidinger, D.; Bruce, A. W. Intracavitary Bacillus Calmette Guerin in the Treatment of Superficial Bladder Tumors. *J. Urol.* **1976**, *116* (2), 180–182.

(87) Herr, H. W.; Morales, A. History of Bacillus Calmette-Guerin and Bladder Cancer: An Immunotherapy Success Story. *J. Urol.* **2008**, *179* (1), 53–56.

(88) Kruger, S.; Ilmer, M.; Kobold, S.; Cadilha, B. L.; Endres, S.; Ormanns, S.; Schuebbe, G.; Renz, B. W.; D'Haese, J. G.; Schloesser, H.; Heinemann, V.; Subklewe, M.; Boeck, S.; Werner, J.; Von Bergwelt-Baildon, M. Advances in Cancer Immunotherapy 2019 - Latest Trends. *J. Exp. Clin. Cancer Res.* **2019**, *38* (1), 268.

(89) Hargadon, K. M.; Johnson, C. E.; Williams, C. J. Immune Checkpoint Blockade Therapy for Cancer: An Overview of FDA-Approved Immune Checkpoint Inhibitors. *International Immunopharmacology*. Elsevier September 1, 2018, pp 29–39.

(90) Robert, L.; Tsoi, J.; Wang, X.; Emerson, R.; Homet, B.; Chodon, T.; Mok, S.; Huang, R. R.; Cochran, A. J.; Comin-Anduix, B.; Koya, R. C.; Graeber, T. G.; Robins, H.; Ribas, A. CTLA4 Blockade Broadens the Peripheral T-Cell Receptor Repertoire. *Clin. Cancer Res.* **2014**, *20* (9), 2424–2432.

(91) Robert, C.; Schachter, J.; Long, G. V.; Arance, A.; Grob, J. J.; Mortier, L.; Daud, A.; Carlino, M. S.; McNeil, C.; Lotem, M.; Larkin, J.; Lorigan, P.; Neyns, B.; Blank, C. U.; Hamid, O.; Mateus, C.; Shapira-Frommer, R.; Kosh, M.; Zhou, H.; Ibrahim, N.; Ebbinghaus, S.; Ribas, A. Pembrolizumab versus Ipilimumab in Advanced Melanoma. *N. Engl. J. Med.* **2015**, *372* (26), 2521–2532.

(92) Weber, J. S.; D'Angelo, S. P.; Minor, D.; Hodi, F. S.; Gutzmer, R.; Neyns, B.; Hoeller, C.; Khushalani, N. I.; Miller, W. H.; Lao, C. D.; Linette, G. P.; Thomas, L.; Lorigan, P.; Grossmann, K. F.; Hassel, J. C.; Maio, M.; Sznol, M.; Ascierto, P. A.; Mohr, P.; Chmielowski, B.; Bryce, A.; Svane, I. M.; Grob, J. J.; Krackhardt, A. M.; Horak, C.; Lambert, A.; Yang, A. S.; Larkin, J. Nivolumab versus Chemotherapy in Patients with Advanced Melanoma Who Progressed after Anti-CTLA-4 Treatment (CheckMate 037): A Randomised, Controlled, Open-Label, Phase 3 Trial. *Lancet Oncol.* **2015**, *16* (4), 375–384.

(93) Weber, J.; Mandala, M.; Del Vecchio, M.; Gogas, H. J.; Arance, A. M.; Cowey, C. L.; Dalle, S.; Schenker, M.; Chiarion-Sileni, V.; Marquez-Rodas, I.; Grob, J.-J.; Butler, M. O.; Middleton, M. R.; Maio, M.; Atkinson, V.; Queirolo, P.; Gonzalez, R.; Kudchadkar, R. R.; Smylie, M.; Meyer, N.; Mortier, L.; Atkins, M. B.; Long, G. V.; Bhatia, S.; Lebbé, C.; Rutkowski, P.; Yokota, K.; Yamazaki, N.; Kim, T. M.; de Pril, V.; Sabater, J.; Qureshi, A.; Larkin, J.; Ascierto, P. A. Adjuvant Nivolumab versus Ipilimumab in Resected Stage III or IV Melanoma. *N. Engl. J. Med.* **2017**, *377* (19), 1824–1835.

(94) Vaddepally, R. K.; Kharel, P.; Pandey, R.; Garje, R.; Chandra, A. B. Review of Indications of FDA-Approved Immune Checkpoint Inhibitors per NCCN Guidelines with the Level of Evidence. *Cancers (Basel).* **2020**, *12* (3).

(95) Gaynor, N.; Crown, J.; Collins, D. M. Immune Checkpoint Inhibitors: Key Trials and an Emerging Role in Breast Cancer. *Semin. Cancer Biol.* **2020**.

(96) Liang, F.; Zhang, S.; Wang, Q.; Li, W. Clinical Benefit of Immune Checkpoint Inhibitors Approved by US Food and Drug Administration. *BMC Cancer* **2020**, *20* (1), 823.

(97) Hu, X.; Yu, H.; Zheng, Y.; Zhang, Q.; Lin, M.; Wang, J.; Qiu, Y. Immune Checkpoint Inhibitors and Survival Outcomes in Brain Metastasis: A Time Series-Based Meta-Analysis. *Front. Oncol.* **2020**, *10*.

(98) Yarchoan, M.; Hopkins, A.; Jaffee, E. M. Tumor Mutational Burden and Response Rate to PD-1 Inhibition. *N. Engl. J. Med.* **2017**, *377* (25), 2500–2501.

(99) Sharma, P.; Hu-Lieskovan, S.; Wargo, J. A.; Ribas, A. Primary, Adaptive, and Acquired Resistance to Cancer Immunotherapy. *Cell* **2017**, *168* (4), 707–723.

(100) Michot, J. M.; Bigenwald, C.; Champiat, S.; Collins, M.; Carbonnel, F.; Postel-Vinay, S.; Berdelou, A.; Varga, A.; Bahleda, R.; Hollebecque, A.; Massard, C.; Fuerea, A.; Ribrag, V.; Gazzah, A.; Armand, J. P.; Amellal, N.; Angevin, E.; Noel, N.; Boutros, C.; Mateus, C.; Robert, C.; Soria, J. C.; Marabelle, A.; Lambotte, O. Immune-Related Adverse Events with Immune Checkpoint Blockade: A Comprehensive Review. *Eur. J. Cancer* **2016**, *54*, 139–148.

(101) Postow, M. A.; Sidlow, R.; Hellmann, M. D. Immune-Related Adverse Events Associated with Immune Checkpoint Blockade. *N. Engl. J. Med.* **2018**, *378* (2), 158–168.

(102) Draghi, A.; Borch, T. H.; Radic, H. D.; Chamberlain, C. A.; Gokuldass, A.; Svane, I. M.; Donia, M. Differential Effects of Corticosteroids and Anti-TNF on Tumor-specific Immune Responses: Implications for the Management of IrAEs. *Int. J. Cancer* **2019**, *145* (5), 1408–1413.

(103) Oh, D. Y.; Cham, J.; Zhang, L.; Fong, G.; Kwek, S. S.; Klinger, M.; Faham, M.; Fong, L. Immune Toxicities Elicted by CTLA-4 Blockade in Cancer Patients Are Associated with Early Diversification of the T-Cell Repertoire. *Cancer Res.* **2017**, *77* (6), 1322–1330.

(104) Rodríguez Pérez; Campillo-Davo, D.; Van Tendeloo, V. F. I.; Benítez-Ribas, D. Cellular Immunotherapy: A Clinical State-of-the-Art of a New Paradigm for Cancer Treatment. *Clin. Transl. Oncol.* **2020**, *22* (11), 1923–1937.

(105) Rodríguez Pérez; Campillo-Davo, D.; Van Tendeloo, V. F. I.; Benítez-Ribas, D. Cellular Immunotherapy: A Clinical State-of-the-Art of a New Paradigm for Cancer Treatment. *Clin. Transl. Oncol.* **2020**, *22* (11), 1923–1937.

(106) Wang, K.; Wei, G.; Liu, D. CD19: A Biomarker for B Cell Development, Lymphoma Diagnosis and Therapy. *Exp. Hematol. Oncol.* **2012**, *1* (1), 36.

(107) Li, J.; Li, W.; Huang, K.; Zhang, Y.; Kupfer, G.; Zhao, Q. Chimeric Antigen Receptor T Cell (CAR-T) Immunotherapy for Solid Tumors: Lessons Learned and Strategies for Moving Forward. *J. Hematol. Oncol.* **2018**, *11* (1), 1–18.

(108) Shen, S. H.; Woroniecka, K.; Barbour, A. B.; Fecci, P. E.; Sanchez-Perez, L.; Sampson, J. H. CAR T Cells and Checkpoint Inhibition for the Treatment of Glioblastoma. *Expert Opin. Biol. Ther.* **2020**, *20* (6), 579–591.

(109) Fares, C. M.; Van Allen, E. M.; Drake, C. G.; Allison, J. P.; Hu-Lieskovan, S. Mechanisms of Resistance to Immune Checkpoint Blockade: Why Does Checkpoint Inhibitor Immunotherapy Not Work for All Patients? *Am. Soc. Clin. Oncol. Educ. Book* **2019**, No. 39, 147–164.

(110) Klemen, N. D.; Wang, M.; Feingold, P. L.; Cooper, K.; Pavri, S. N.; Han, D.; Detterbeck, F. C.; Boffa, D. J.; Khan, S. A.; Olino, K.; Clune, J.; Ariyan, S.; Salem, R. R.; Weiss, S. A.; Kluger, H. M.; Sznol, M.; Cha, C. Patterns of Failure after Immunotherapy with Checkpoint Inhibitors Predict Durable Progression-Free Survival after Local Therapy for Metastatic Melanoma. *Journal for Immunother. cancer* **2019**, *7* (1), 196.

(111) Kerr, W. G.; Chisholm, J. D. The Next Generation of Immunotherapy for Cancer: Small Molecules Could Make Big Waves. *J. Immunol.* **2019**, *202* (1), 11–19.

(112) van der Zanden, S. Y.; Luimstra, J. J.; Neefjes, J.; Borst, J.; Ovaa, H. Opportunities for Small Molecules in Cancer Immunotherapy. *Trends Immunol.* **2020**, *41* (6), 493–511.

(113) Cheng, B.; Yuan, W.-E.; Su, J.; Liu, Y.; Chen, J. Recent Advances in Small Molecule Based Cancer Immunotherapy. **2018**.

(114) Konieczny, M.; Musielak, B.; Kocik, J.; Skalniak, L.; Sala, D.; Czub, M.; Magiera-Mularz, K.; Rodriguez, I.; Myrcha, M.; Stec, M.; Siedlar, M.; Holak, T. A.; Plewka, J. Di-Bromo-Based Small-Molecule Inhibitors of the PD-1/PD-L1 Immune Checkpoint. *J. Med. Chem.* **2020**, *63* (19), 11271–11285.

(115) Magiera-Mularz, K.; Skalniak, L.; Zak, K. M.; Musielak, B.; Rudzinska-Szostak, E.; Berlicki, Ł.; Kocik, J.; Grudnik, P.; Sala, D.; Zarganes-Tzitzikas, T.; Shaabani, S.; Dömling, A.; Dubin, G.; Holak, T. A. Bioactive Macrocyclic Inhibitors of the PD-1/PD-L1 Immune Checkpoint. *Angew. Chemie Int. Ed.* **2017**, *56* (44), 13732–13735.

(116) Zhong, Y.; Li, X.; Yao, H.; Lin, K. The Characteristics of PD-L1 Inhibitors, from Peptides to Small Molecules. *Molecules* **2019**, *24* (10).

(117) Wu, Q.; Jiang, L.; Li, S. cheng; He, Q. jun; Yang, B.; Cao, J. Small Molecule Inhibitors Targeting the PD-1/PD-L1 Signaling Pathway. *Acta Pharmacol. Sin.* **2021**, *42* (1), 1–9.

(118) Powderly, J.; Patel, M. R.; Lee, J. J.; Brody, J.; Meric-Bernstam, F.; Hamilton, E.; Ponce Aix, S.; Garcia-Corbacho, J.; Bang, Y.-J.; Ahn, M.-J.; Rha, S. Y.; Kim, K.-P.; Gil Martin, M.; Wang, H.; Lazorchak, A.; Wyant, T.; Ma, A.; Agarwal, S.; Tuck, D.; Daud, A. CA-170, a First in Class Oral Small Molecule Dual Inhibitor of Immune Checkpoints PD-L1 and VISTA, Demonstrates Tumor Growth Inhibition in Pre-Clinical Models and Promotes T Cell Activation in Phase 1 Study. *Ann. Oncol.* **2017**, *28*, v405–v406.

(119) Javaid, N.; Choi, S. Toll-like Receptors from the Perspective of Cancer Treatment. *Cancers (Basel).* **2020**, *12* (2).

(120) Takeuchi, O.; Akira, S. Pattern Recognition Receptors and Inflammation. *Cell* **2010**, *140* (6), 805–820.

(121) Wang, Y.; Zhang, S.; Li, H.; Wang, H.; Zhang, T.; Hutchinson, M. R.; Yin, H.; Wang, X. Small-Molecule Modulators of Toll-like Receptors. *Acc. Chem. Res.* **2020**, *53* (5), 1046–1055.

(122) Urban-Wojciuk, Z.; Khan, M. M.; Oyler, B. L.; Fåhraeus, R.; Marek-Trzonkowska, N.; Nita-Lazar, A.; Hupp, T. R.; Goodlett, D. R. The Role of Tlrs in Anti-Cancer Immunity and Tumor Rejection. *Front. Immunol.* **2019**, *10* (OCT), 2388.

(123) Oldfield, V.; Keating, G. M.; Perry, C. M. Imiquimod: In Superficial Basal Cell Carcinoma. *Am. J. Clin. Dermatol.* **2005**, *6* (3), 195–200.

(124) Farrugia, M.; Baron, B. The Role of Toll-Like Receptors in Autoimmune Diseases through Failure of the Self-Recognition Mechanism. *Int. J. Inflam.* **2017**, *2017*.

(125) Nam Lee, S.; Mo Jin, S.; Sik Shin, H.; Taik Lim, Y. Chemical Strategies to Enhance the Therapeutic Efficacy of Toll-like Receptor Agonist Based Cancer Immunotherapy A Designer Scaffold with Immune Nanoconverters for Reverting Immunosuppression and Enhancing Immune Check. *Acc. Chem. Res* **2020**, *53*.

(126) Pradere, J. P.; Dapito, D. H.; Schwabe, R. F. The Yin and Yang of Toll-like Receptors in Cancer. *Oncogene* **2014**, *33* (27), 3485–3495.

(127) Shukla, N. M.; Malladi, S. S.; Mutz, C. A.; Balakrishna, R.; David, S. A. Structure-Activity Relationships in Human Toll-Like Receptor 7-Active Imidazoquinoline Analogues. *J. Med. Chem* **2010**, *53*, 4450–4465.

(128) Hopfner, K. P.; Hornung, V. Molecular Mechanisms and Cellular Functions of CGAS–STING Signalling. *Nat. Rev. Mol. Cell Biol.* **2020**, *21* (9), 501–521.

(129) Ishikawa, H.; Ma, Z.; Barber, G. N. STING Regulates Intracellular DNA-Mediated, Type i Interferon-Dependent Innate Immunity. *Nature* **2009**, *461* (7265), 788–792.

(130) Barber, G. N. STING: Infection, Inflammation and Cancer. *Nat. Rev. Immunol.* **2015**, *15* (12), 760–770.

(131) Ng, K. W.; Marshall, E. A.; Bell, J. C.; Lam, W. L. CGAS–STING and Cancer: Dichotomous Roles in Tumor Immunity and Development. *Trends Immunol.* **2018**, *39* (1), 44–54.

(132) Ahn, J.; Xia, T.; Konno, H.; Konno, K.; Ruiz, P.; Barber, G. N. Inflammation-Driven Carcinogenesis Is Mediated through STING. *Nat. Commun.* **2014**, *5*, 5166.

(133) Ishikawa, H.; Barber, G. N. STING Is an Endoplasmic Reticulum Adaptor That Facilitates Innate Immune Signalling. *Nature* **2008**, *455* (7213), 674–678.

(134) Meric-Bernstam, F.; Sandhu, S. K.; Hamid, O.; Spreafico, A.; Kasper, S.; Dummer, R.; Shimizu, T.; Steeghs, N.; Lewis, N.; Talluto, C. C.; Dolan, S.; Bean, A.; Brown, R.; Trujillo, D.; Nair, N.; Luke, J. J. Phase Ib Study of MIW815 (ADU-S100) in Combination with Spartalizumab (PDR001) in Patients (Pts) with Advanced/Metastatic Solid Tumors or Lymphomas. *https://doi.org/10.1200/JCO.2019.37.15_suppl.2507* **2019**, *37* (15_suppl), 2507–2507.

(135) Zandberg, D. P.; Ferris, R.; Laux, D.; Mehra, R.; Nabell, L.; Kaczmar, J.; Gibson, M. K.; Kim, Y. J.; Neupane, P.; Bauman, J.; Julian, R.; Adkins, D.; Cohen, E.; Burtness, B.; Bermingham, C.; Dupage, A.; Desbien, A.; Loi, A.; Nuyten, D. S. A.; Saba, N. F. 71P A Phase II Study of ADU-S100 in Combination with Pembrolizumab in Adult Patients with PD-L1+ Recurrent or Metastatic HNSCC: Preliminary Safety, Efficacy and PK/PD Results. *Ann. Oncol.* **2020**, *31*, S1446–S1447.

(136) Huang, K.-C.; Endo, A.; McGrath, S.; Chandra, D.; Wu, J.; Kim, D.-S.; Albu, D.; Ingersoll, C.; Tendyke, K.; Loiacono, K.; Noland, T.; Verbel, D.; Zhang, C.; Hao, M.-H.; Matijevic, M.; Dixit, V.; Hukkanen, R. R.; Hutz, J.; Wang, J.; Fang, F.; Bao, X.; Kolber-Simonds, D.; Akram, M.; Sarwar, N. Abstract 3269: Discovery and Characterization of E7766, a Novel Macrocycle-Bridged STING Agonist with Pan-Genotypic and Potent Antitumor Activity through Intravesical and Intratumoral Administration. *Cancer Res.* **2019**, *79* (13 Supplement), 3269–3269.

(137) Amouzegar, A.; Chelvanambi, M.; Filderman, J. N.; Storkus, W. J.; Luke, J. J. Sting Agonists as Cancer Therapeutics. *Cancers*. Multidisciplinary Digital Publishing Institute May 30, 2021, p 2695.

(138) DuBois, R. N.; Abramson, S. B.; Crofford, L.; Gupta, R. A.; Simon, L. S.; Putte, L. B. A.; Lipsky, P. E. Cyclooxygenase in Biology and Disease. *FASEB J.* **1998**, *12* (12), 1063–1073.

(139) Subbaramaiah, K.; Dannenberg, A. J. Cyclooxygenase 2: A Molecular Target for Cancer Prevention and Treatment. *Trends Pharmacol. Sci.* **2003**, *24* (2), 96–102.

(140) McCormack, P. L.; Lanas, A.; McKenna, F.; Patrignani, P.; Simon, L. S. Celecoxib: A Review of Its Use for Symptomatic Relief in the Treatment of Osteoarthritis, Rheumatoid Arthritis and Ankylosing Spondylitis. *Drugs* **2011**, *71* (18), 2457–2489.

(141) Lee, S. Y.; Choi, H. K.; Lee, K. J.; Jung, J. Y.; Hur, G. Y.; Jung, K. H.; Kim, J. H.; Shin, C.; Shim, J. J.; In, K. H.; Kang, K. H.; Yoo, S. H. The Immune Tolerance of Cancer Is Mediated by IDO That Is Inhibited by COX-2 Inhibitors through Regulatory T Cells. *J. Immunother.* **2009**, *32* (1), 22–28.

(142) Hennequart, M.; Pilotte, L.; Cane, S.; Hoffmann, D.; Stroobant, V.; De Plaen, E.; Van Den Eynde, B. J. Constitutive IDO1 Expression in Human Tumors Is Driven by Cyclooxygenase-2 and Mediates Intrinsic Immune Resistance. *Cancer Immunol. Res.* **2017**, *5* (8), 695–709.

(143) Rodriguez, P. C.; Ochoa, A. C.; Al-Khami, A. A. Arginine Metabolism in Myeloid Cells Shapes Innate and Adaptive Immunity. *Front. Immunol.* **2017**, *8* (FEB), 1.

(144) Leu, S.-Y.; Wang, S.-R. Clinical Significance of Arginase in Colorectal Cancer. *Cancer* **1992**, *70* (4), 733–736.

(145) Nussler, A. K.; Billiar, T. R. Inflammation, Immunoregulation, and Inducible Nitric Oxide Synthase. *J. Leukoc. Biol.* **1993**, *54* (2), 171–178.

(146) Zea, A. H.; Rodriguez, P. C.; Culotta, K. S.; Hernandez, C. P.; DeSalvo, J.; Ochoa, J. B.; Park, H. J.; Zabaleta, J.; Ochoa, A. C. L-Arginine Modulates CD3ζ Expression and T Cell Function in Activated Human T Lymphocytes. *Cell. Immunol.* **2004**, *232* (1–2), 21–31.

(147) Vanini, F.; Kashfi, K.; Nath, N. The Dual Role of INOS in Cancer. *Redox Biol.* **2015**, *6*, 334–343.

(148) Kashfi, K.; Vannini, F. Nitric Oxide and Cancer: To Inhibit or To Induce INOS: That Is the Question? *Ther. Appl. Nitric Oxide Cancer Inflamm. Disord.* **2019**, 93–111.

(149) Granados-Principal, S.; Liu, Y.; Guevara, M. L.; Blanco, E.; Choi, D. S.; Qian, W.; Patel, T.; Rodriguez, A. A.; Cusimano, J.; Weiss, H. L.; Zhao, H.; Landis, M. D.; Dave, B.; Gross, S. S.; Chang, J. C. Inhibition of INOS as a Novel Effective Targeted Therapy against Triple-Negative Breast Cancer. *Breast Cancer Res.* **2015**, *17* (1), 1–16.

(150) Sikora, A. G.; Gelbard, A.; Davies, M. A.; Sano, D.; Ekmekcioglu, S.; Kwon, J.; Hailemichael, Y.; Jayaraman, P.; Myers, J. N.; Grimm, E. A.; Overwijk, W. W. Targeted Inhibition of Inducible Nitric Oxide Synthase Inhibits Growth of Human Melanoma in Vivo and Synergizes with Chemotherapy. *Clin. Cancer Res.* **2010**, *16* (6), 1834–1844.

(151) Ivanenkov, Y. A.; Chufarova, N. V. Small-Molecule Arginase Inhibitors. *Pharmaceutical Patent Analyst*. Future Science Ltd London, UK December 20, 2014, pp 65–85.

(152) Borek, B.; Gajda, T.; Golebiowski, A.; Blaszczyk, R. Boronic Acid-Based Arginase Inhibitors in Cancer Immunotherapy. *Bioorganic Med. Chem.* **2020**, *28* (18), 115658.

(153) Baker, S. J.; Ding, C. Z.; Akama, T.; Zhang, Y. K.; Hernandez, V.; Xia, Y. Therapeutic Potential of Boron-Containing Compounds. *Future Medicinal Chemistry*. Future Med Chem October 2009, pp 1275–1288.

(154) Plescia, J.; Moitessier, N. Design and Discovery of Boronic Acid Drugs. *European Journal of Medicinal Chemistry*. Elsevier Masson June 1, 2020, p 112270.

(155) Naing, A.; Bauer, T.; Papadopoulos, K. P.; Rahma, O.; Tsai, F.; Garralda, E.; Naidoo, J.; Pai, S.; Gibson, M. K.; Rybkin, I.; Wang, D.; McDermott, D. F.; Fasolo, A.; de Miguel, M.; Shaheen, M.; Jenkins, Y.; Kallender, H.; Gogov, S.; Kuriakose, E.; Pishvaian, M. Phase I Study of the Arginase Inhibitor INCB001158 (1158) Alone and in Combination with Pembrolizumab (PEM) in Patients (Pts) with Advanced/Metastatic (Adv/Met) Solid Tumours. *Ann. Oncol.* **2019**, *30*, v160.

(156) Javle, M. M.; Bridgewater, J. A.; Gbolahan, O. B.; Jungels, C.; Cho, M. T.; Papadopoulos, K. P.; Thistlethwaite, F. C.; Canon, J.-L. R.; Cheng, L.; Ioannidis, S.; Gogov, S.; Naing, A. A Phase I/II Study of Safety and Efficacy of the Arginase Inhibitor INCB001158 plus Chemotherapy in Patients (Pts) with Advanced Biliary Tract Cancers. *J. Clin. Oncol.* **2021**, *39* (3_suppl), 311–311.

(157) Steggerda, S. M.; Bennett, M. K.; Chen, J.; Emberley, E.; Huang, T.; Janes, J. R.; Li, W.; MacKinnon, A. L.; Makkouk, A.; Marguier, G.; Murray, P. J.; Neou, S.; Pan, A.; Parlati, F.; Rodriguez, M. L. M.; Van de Velde, L. A.; Wang, T.; Works, M.; Zhang, J.; Zhang, W.; Gross, M. I. Inhibition of Arginase by CB-1158 Blocks Myeloid Cell-Mediated Immune Suppression in the Tumor Microenvironment. *Journal for Immunother. cancer* **2017**, *5* (1), 1–18.

(158) Tang, K.; Wu, Y. H.; Song, Y.; Yu, B. Indoleamine 2,3-Dioxygenase 1 (IDO1) Inhibitors in Clinical Trials for Cancer Immunotherapy. *Journal of Hematology and Oncology*. BioMed Central April 21, 2021, pp 1–21.

(159) Pardridge, W. M.; Fierer, G. Transport of Tryptophan into Brain from the Circulating, Albumin-Bound Pool in Rats and in Rabbits. *J. Neurochem.* **1990**, *54* (3), 971–976.

(160) Curzon, G.; Friedel, J.; Katamaneni, B. D.; Greenwood, M. H.; Lader, M. H. Unesterified Fatty Acids and the Binding of Tryptophan in Human Plasma. *Clin. Sci. Mol. Med.* **1974**, *47* (5), 415–424.

(161) Le Floc'h, N.; Otten, W.; Merlot, E. Tryptophan Metabolism, from Nutrition to Potential Therapeutic Applications. *Amino Acids* **2011**, *41* (5), 1195–1205.

(162) Pardridge, W. M. Tryptophan Transport through the Blood-Brain Barrier: In Vivo Measurement of Free and Albumin-Bound Amino Acid. *Life Sci.* **1979**, *25* (17), 1519–1528.

(163) Ruddick, J. P.; Evans, A. K.; Nutt, D. J.; Lightman, S. L.; Rook, G. A. W.; Lowry, C. A. Tryptophan Metabolism in the Central Nervous System: Medical Implications. *Expert Rev. Mol. Med.* **2006**, *8* (20), 1–27.

(164) Wolf, H.; Price, J. M.; Brown, R. R.; Madsen, P. O. Studies on Tryptophan Metabolism in Male Subjects Treated with Progestational Agents. *Scand. J. Clin. Lab. Invest.* **1970**, *25* (3), 237–249.

(165) Botting, N. P. Chemistry and Neurochemistry of the Kynurenine Pathway of Tryptophan Metabolism. *Chem. Soc. Rev.* **1995**, *24* (6), 401–412.

(166) Stefulj, J.; Hörtner, M.; Ghosh, M.; Schauenstein, K.; Rinner, I.; Wölfler, A.; Semmler, J.; Liebmann, P. M. Gene Expression of the Key Enzymes of Melatonin Synthesis in Extrapineal Tissues of the Rat. *J. Pineal Res.* **2001**, *30* (4), 243–247.

(167) Tan, P.; Bharath, A. Manipulation of Indoleamine 2,3 Dioxygenase; a Novel Therapeutic Target for Treatment of Diseases. *Expert Opin. Ther. Targets* **2009**, *13* (8), 987–1012.

(168) Fallarino, F.; Grohmann, U.; Vacca, C.; Bianchi, R.; Orabona, C.; Spreca, A.; Fioretti, M. C.; Puccetti, P. T Cell Apoptosis by Tryptophan Catabolism. *Cell Death Differ.* **2002**, *9* (10), 1069–1077.

(169) Grohmann, U.; Fallarino, F.; Puccetti, P. Tolerance, DCs and Tryptophan: Much Ado about IDO. *Trends Immunol.* **2003**, *24* (5), 242–248.

(170) Routy, J. P.; Routy, B.; Graziani, G. M.; Mehraj, V. The Kynurenine Pathway Is a Double-Edged Sword in Immune-Privileged Sites and in Cancer: Implications for Immunotherapy. *Int. J. Tryptophan Res.* **2016**, *9* (1), 67–77.

(171) Pilotte, L.; Larrieu, P.; Stroobant, V.; Colau, D.; Dolušić, E.; Frédérick, R.; De Plaen, E.; Uyttenhove, C.; Wouters, J.; Masereel, B.; Van Den Eynde, B. J. Reversal of Tumoral Immune Resistance by Inhibition of Tryptophan 2,3-Dioxygenase. *Proc. Natl. Acad. Sci. U. S. A.* **2012**, *109* (7), 2497–2502.

(172) Munn, D. H.; Shafizadeh, E.; Attwood, J. T.; Bondarev, I.; Pashine, A.; Mellor, A. L. Inhibition of T Cell Proliferation by Macrophage Tryptophan Catabolism. *J. Exp. Med.* **1999**, *189* (9), 1363–1372.

(173) Deval, C.; Chaveroux, C.; Maurin, A.-C.; Cherasse, Y.; Parry, L.; Carraro, V.; Milenkovic, D.; Ferrara, M.; Bruhat, A.; Jousse, C.; Fafournoux, P. Amino Acid Limitation Regulates the Expression of Genes Involved in Several Specific Biological Processes through GCN2-Dependent and GCN2-Independent Pathways. *FEBS J.* **2009**, *276* (3), 707–718.

(174) Sonner, J. K.; Deumelandt, K.; Ott, M.; Thomé, C. M.; Rauschenbach, K. J.; Schulz, S.; Munteanu, B.; Mohapatra, S.; Adam, I.; Hofer, A. C.; Feuerer, M.; Opitz, C. A.; Hopf, C.; Wick, W.; Platten, M. The Stress Kinase GCN2 Does Not Mediate Suppression of Antitumor T Cell Responses by Tryptophan Catabolism in Experimental Melanomas. *Oncoimmunology* **2016**, *5* (12), e1240858.

(175) Metz, R.; Rust, S.; DuHadaway, J. B.; Mautino, M. R.; Munn, D. H.; Vahanian, N. N.; Link, C. J.; Prendergast, G. C. IDO Inhibits a Tryptophan Sufficiency Signal That Stimulates MTOR: A Novel IDO Effector Pathway Targeted by D-1-Methyl-Tryptophan. *Oncoimmunology* **2012**, *1* (9), 1460–1468.

(176) Mautino, M. R.; Kumar, S.; Zhuang, H.; Waldo, J.; Jaipuri, F.; Potturi, H.; Brincks, E.; Adams, J.; Marcinowicz, A.; Allen, C. Van; Vahanian, N.; Link, C. J. Abstract 4076: A Novel Prodrug of Indoximod with Enhanced Pharmacokinetic Properties. *Exp. Mol. Ther.* **2017**, *77* (13 Supplement), 4076–4076.

(177) Fallarino, F.; Grohmann, U.; You, S.; McGrath, B. C.; Cavener, D. R.; Vacca, C.; Orabona, C.; Bianchi, R.; Belladonna, M. L.; Volpi, C.; Santamaria, P.; Fioretti, M. C.; Puccetti, P. The Combined Effects of Tryptophan Starvation and Tryptophan Catabolites Down-Regulate T Cell Receptor ζ-Chain and Induce a Regulatory Phenotype in Naive T Cells. *J. Immunol.* **2006**, *176* (11), 6752–6761.

(178) Mezrich, J. D.; Fechner, J. H.; Zhang, X.; Johnson, B. P.; William, J. Hydrocarbon Receptor Can Generate Regulatory T. *Receptor* **2011**, *185* (6), 3190–3198.

(179) Liu, Y.; Liang, X.; Dong, W.; Fang, Y.; Lv, J.; Zhang, T.; Fiskesund, R.; Xie, J.; Liu, J.; Yin, X.; Jin, X.; Chen, D.; Tang, K.; Ma, J.; Zhang, H.; Yu, J.; Yan, J.; Liang, H.; Mo, S.; Cheng, F.; Zhou, Y.; Zhang, H.; Wang, J.; Li, J.; Chen, Y.; Cui, B.; Hu, Z. W.; Cao, X.; Xiao-Feng Qin, F.; Huang, B. Tumor-Repopulating Cells Induce PD-1 Expression in CD8+ T Cells by Transferring Kynurenine and AhR Activation. *Cancer Cell* **2018**, *33* (3), 480–494.

(180) Campesato, L. F.; Budhu, S.; Tchaicha, J.; Weng, C. H.; Gigoux, M.; Cohen, I. J.; Redmond, D.; Mangarin, L.; Pourpe, S.; Liu, C.; Zappasodi, R.; Zamarin, D.; Cavanaugh, J.; Castro, A. C.; Manfredi, M. G.; McGovern, K.; Merghoub, T.; Wolchok, J. D. Blockade of the AHR Restricts a Treg-Macrophage Suppressive Axis Induced by L-Kynurenine. *Nat. Commun.* **2020**, *11* (1), 1–11.

(181) Mezrich, J. D.; Fechner, J. H.; Zhang, X.; Johnson, B. P.; Burlingham, W. J.; Bradfield, C. A. An Interaction between Kynurenine and the Aryl Hydrocarbon Receptor Can Generate Regulatory T Cells. *J. Immunol.* **2010**, *185* (6), 3190–3198.

(182) Heng, B.; Lim, C. K.; Lovejoy, D. B.; Bessede, A.; Gluch, L.; Guillemin, G. J. Understanding the Role of the Kynurenine Pathway in Human Breast Cancer Immunobiology. *Oncotarget* **2016**, *7* (6), 6506–6520.

(183) Wu, X.; Tian, J.; Wang, S. Insight into Non-Pathogenic Th17 Cells in Autoimmune Diseases. *Front. Immunol.* **2018**, *9* (MAY), 1112.

(184) Holmgaard, R. B.; Zamarin, D.; Li, Y.; Gasmi, B.; Munn, D. H.; Allison, J. P.; Merghoub, T.; Wolchok, J. D. Tumor-Expressed IDO Recruits and Activates MDSCs in a Treg-Dependent Manner. *Cell Rep.* **2015**, *13* (2), 412–424.

(185) Takenaka, M. C.; Gabriely, G.; Rothhammer, V.; Mascanfroni, I. D.; Wheeler, M. A.; Chao, C. C.; Gutiérrez-Vázquez, C.; Kenison, J.; Tjon, E. C.; Barroso, A.; Vandeventer, T.; de Lima, K. A.; Rothweiler, S.; Mayo, L.; Ghannam, S.; Zandee, S.; Healy, L.; Sherr, D.; Farez, M. F.; Pratt, A.; Antel, J.; Reardon, D. A.; Zhang, H.; Robson, S. C.; Getz, G.; Weiner, H. L.; Quintana, F. J. Control of Tumor-Associated Macrophages and T Cells in Glioblastoma via AHR and CD39. *Nat. Neurosci.* **2019**,

22 (5), 729–740.

(186) Sekkaï, D.; Guittet, O.; Lemaire, G.; Tenu, J. P.; Lepoivre, M. Inhibition of Nitric Oxide Synthase Expression and Activity in Macrophages by 3-Hydroxyanthranilic Acid, a Tryptophan Metabolite. *Arch. Biochem. Biophys.* **1997**, *340* (1), 117–123.

(187) Oh, G. S.; Pae, H. O.; Choi, B. M.; Chae, S. C.; Lee, H. S.; Ryu, D. G.; Chung, H. T. 3-Hydroxyanthranilic Acid, One of Metabolites of Tryptophan via Indoleamine 2,3-Dioxygenase Pathway, Suppresses Inducible Nitric Oxide Synthase Expression by Enhancing Heme Oxygenase-1 Expression. *Biochem. Biophys. Res. Commun.* **2004**, *320* (4), 1156–1162.

(188) Weber, W. P.; Feder-Mengus, C.; Chiarugi, A.; Rosenthal, R.; Reschner, A.; Schumacher, R.; Zajac, P.; Misteli, H.; Frey, D. M.; Oertli, D.; Heberer, M.; Spagnoli, G. C. Differential Effects of the Trytophan Metabolite 3-Hydroxyanthranilic Acid on the Proliferation of Human CD8 T Cells Induced by TCR Triggering or Homeostatic Cytokines. *Eur. J. Immunol.* **2006**, *36* (2), 296–304.

(189) Yan, Y.; Zhang, G.-X.; Gran, B.; Fallarino, F.; Yu, S.; Li, H.; Cullimore, M. L.; Rostami, A.; Xu, H. IDO Upregulates Regulatory T Cells via Tryptophan Catabolite and Suppresses Encephalitogenic T Cell Responses in Experimental Autoimmune Encephalomyelitis. *J. Immunol.* **2010**, *185* (10), 5953–5961.

(190) Krause, D.; Suh, H. S.; Tarassishin, L.; Cui, Q. L.; Durafourt, B. A.; Choi, N.; Bauman, A.; Cosenza-Nashat, M.; Antel, J. P.; Zhao, M. L.; Lee, S. C. The Tryptophan Metabolite 3-Hydroxyanthranilic Acid Plays Anti-Inflammatory and Neuroprotective Roles during Inflammation: Role of Hemeoxygenase-1. *Am. J. Pathol.* **2011**, *179* (3), 1360–1372.

(191) Muller, A. J.; Sharma, M. D.; Chandler, P. R.; DuHadaway, J. B.; Everhart, M. E.; Johnson, B. A.; Kahler, D. J.; Pihkala, J.; Soler, A. P.; Munn, D. H.; Prendergast, G. C.; Mellor, A. L. Chronic Inflammation That Facilitates Tumor Progression Creates Local Immune Suppression by Inducing Indoleamine 2,3 Dioxygenase. *Proc. Natl. Acad. Sci. U. S. A.* **2008**, *105* (44), 17073–17078.

(192) Prendergast, G. C.; Mondal, A.; Dey, S.; Laury-Kleintop, L. D.; Muller, A. J. Inflammatory Reprogramming with IDO1 Inhibitors: Turning Immunologically Unresponsive 'Cold' Tumors 'Hot.' *Trends Cancer.* **2018**, *4* (1), 38–58.

(193) Ogawa, T.; Matson, W. R.; Beal, M. F.; Myers, R. H.; Bird, E. D.; Milbury, P.; Saso, S. Kynurenine Pathway Abnormalities in Parkinson's Disease. *Neurology* **1992**, *42* (9), 1702–1706.

(194) Baran, H.; Jellinger, K.; Deecke, L. Kynurenine Metabolism in Alzheimer's Disease. *J. Neural Transm.* **1999**, *106* (2), 165–181.

(195) Myint, A.-M.; Schwarz, M. J.; Müller, N. The Role of the Kynurenine Metabolism in Major Depression. *J. Neural Transm.* **2012**, *119* (2), 245–251.

(196) Kegel, M. E.; Bhat, M.; Skogh, E.; Samuelsson, M.; Lundberg, K.; Dahl, M.-L.; Sellgren, C.; Schwieler, L.; Engberg, G.; Schuppe-Koistinen, I.; Erhardt, S. Imbalanced Kynurenine Pathway in Schizophrenia. *Int. J. Tryptophan Res.* **2014**, *7*, 15–22.

(197) Guillemin, G. J.; Brew, B. J. Implications of the Kynurenine Pathway and Quinolinic Acid in Alzheimer's Disease. *Redox Rep.* **2002**, *7* (4), 199–206.

(198) Schwarcz, R.; Bruno, J. P.; Muchowski, P. J.; Wu, H. Q. Kynurenines in the Mammalian Brain: When Physiology Meets Pathology. *Nat. Rev. Neurosci.* **2012**, *13* (7), 465–477.

(199) Guillemin, G. J. Quinolinic Acid, the Inescapable Neurotoxin. *FEBS J.* **2012**, *279* (8), 1356–1365.

(200) Phillips, R. S.; Iradukunda, E. C.; Hughes, T.; Phillip Bowen, J. Modulation of Enzyme Activity in the Kynurenine Pathway by Kynurenine Monooxygenase Inhibition. *Front. Mol. Biosci.* **2019**, *6* (FEB).

(201) Zwilling, D.; Huang, S. Y.; Sathyasaikumar, K. V.; Notarangelo, F. M.; Guidetti, P.; Wu, H. Q.; Lee, J.; Truong, J.; Andrews-Zwilling, Y.; Hsieh, E. W.; Louie, J. Y.; Wu, T.; Scearce-Levie, K.; Patrick, C.; Adame, A.; Giorgini, F.; Moussaoui, S.; Laue, G.; Rassoulpour, A.; Flik, G.; Huang, Y.; Muchowski, J. M.; Masliah, E.; Schwarcz, R.; Muchowski, P. J. Kynurenine 3-Monooxygenase Inhibition in Blood Ameliorates Neurodegeneration. *Cell* **2011**, *145* (6), 863–874.

(202) Smith, J. R.; Jamie, J. F.; Guillemin, G. J. Kynurenine-3-Monooxygenase: A Review of Structure, Mechanism, and Inhibitors. *Drug Discov. Today* **2016**, *21* (2), 315–324.

(203) Pham, K. N.; Lewis-Ballester, A.; Yeh, S. R. Conformational Plasticity in Human Heme-Based Dioxygenases. *J. Am. Chem. Soc.* **2021**, *143* (4), 1836–1845.

(204) Leeds, J. M.; Brown, P. J.; Mcgeehan, G. M.; Brown, F. K.; Wisemans, J. S. Isotope Effects and Alternative Substrate Reactivities for Tryptophan 2,3-Dioxygenase. *J. Biol. Chem.* **1993**, *268* (24), 17781–17786.

(205) Batabyal, D.; Yeh, S. R. Substrate-Protein Interaction in Human Tryptophan Dioxygenase: The Critical Role of H76. *J. Am. Chem. Soc.* **2009**, *131* (9), 3260–3270.

(206) Lewis-Ballester, A.; Batabyal, D.; Egawa, T.; Lu, C.; Lin, Y.; Marti, M. A.; Capece, L.; Estrin, D. A.; Yeh, S. R. Evidence for a Ferryl Intermediate in a Heme-Based Dioxygenase. *Proc. Natl. Acad. Sci. U. S. A.* **2009**, *106* (41), 17371–17376.

(207) Meng, B.; Wu, D.; Gu, J.; Ouyang, S.; Ding, W.; Liu, Z. J. Structural and Functional Analyses of Human Tryptophan 2,3-Dioxygenase. *Proteins.* **2014**, *82* (11), 3210–3216.

(208) Hayaishi, O. Properties and Function of Indoleamine 2,3-Dioxygenase. *J. Biochem.* **1976**, *79* (4), 13P–21P.

(209) Yamazaki, F.; Kuroiwa, T.; Takikawa, O.; Kido, R. Human Indolylamine 2,3-Dioxygenase. Its Tissue Distribution, and Characterization of the Placental Enzyme. *Biochem. J.* **1985**, *230* (3), 635–638.

(210) Terness, P.; Bauer, T. M.; Röse, L.; Dufter, C.; Watzlik, A.; Simon, H.; Opelz, G. Inhibition of Allogeneic T Cell Proliferation by Indoleamine 2,3-Dioxygenase-Expressing Dendritic Cells: Mediation of Suppression by Tryptophan Metabolites. *J. Exp. Med.* **2002**, *196* (4), 447–457.

(211) Taylor, M. W.; Feng, G. S. Relationship between Interferon-Gamma, Indoleamine 2,3-Dioxygenase, and Tryptophan Catabolism. *FASEB J.* **1991**, *5* (11), 2516–2522.

(212) Opitz, C. A.; Litzenburger, U. M.; Lutz, C.; Lanz, T. V.; Tritschler, I.; Köppel, A.; Tolosa, E.; Hoberg, M.; Anderl, J.; Aicher, W. K.; Weller, M.; Wick, W.; Platten, M. Toll-Like Receptor Engagement Enhances the Immunosuppressive Properties of Human Bone Marrow-Derived Mesenchymal Stem Cells by Inducing Indoleamine-2,3-Dioxygenase-1 via Interferon-β and Protein Kinase R. *Stem Cells* **2009**, *27* (4), 909–919.

(213) Lewis-Ballester, A.; Pham, K. N.; Batabyal, D.; Karkashon, S.; Bonanno, J. B.; Poulos, T. L.; Yeh, S. R. Structural Insights into Substrate and Inhibitor Binding Sites in Human Indoleamine 2,3-Dioxygenase. *Nat. Commun.* **2017**, *8* (1), 1–8.

(214) Munn, D. H.; Zhou, M.; Attwood, J. T.; Bondarev, I.; Conway, S. J.; Marshall, B.; Brown, C.; Mellor, A. L. Prevention of Allogeneic Fetal Rejection by Tryptophan Catabolism. *Science* **1998**, *281* (5380), 1191–1193.

(215) Moffett, J. R.; Namboodiri, M. A. Tryptophan and the Immune Response. *Immunol. Cell Biol.* **2003**, *81* (4), 247–265.

(216) Badawy, A. A.-B. Tryptophan Metabolism, Disposition and Utilization in Pregnancy. *Biosci. Rep.* **2015**, *35* (5).

(217) Badawy, A. A.-B.; Namboodiri, A. M. A.; Moffett, J. R. The End of the Road for the Tryptophan Depletion Concept in Pregnancy and Infection. *Clin. Sci. (Lond).* **2016**, *130* (15), 1327–1333.

(218) Uyttenhove, C.; Pilotte, L.; Théate, I.; Stroobant, V.; Colau, D.; Parmentier, N.; Boon, T.; Van den Eynde, B. J. Evidence for a Tumoral Immune Resistance Mechanism Based on Tryptophan Degradation by Indoleamine 2,3-Dioxygenase. *Nat. Med.* **2003**, *9* (10), 1269–1274.

(219) Yang Zhang; Seong A. Kang; Tathagata Mukherjee; Shridhar Bale; Brian R. Crane; Tadhg P. Begley, * and; Ealick*, S. E. Crystal Structure and Mechanism of Tryptophan 2,3-Dioxygenase, a Heme Enzyme Involved in Tryptophan Catabolism and in Quinolinate Biosynthesis. *Biochemistry* **2007**, *46* (1), 145–155.

(220) Lewis-Ballester, A.; Forouhar, F.; Kim, S. M.; Lew, S.; Wang, Y.; Karkashon, S.; Seetharaman, J.; Batabyal, D.; Chiang, B. Y.; Hussain, M.; Correia, M. A.; Yeh, S. R.; Tong, L. Molecular Basis for Catalysis and Substrate-Mediated Cellular Stabilization of Human Tryptophan 2,3-Dioxygenase. *Sci. Rep.* **2016**, *6* (35169).

(221) Miller, C. L.; Llenos, I. C.; Dulay, J. R.; Barillo, M. M.; Yolken, R. H.; Weis, S. Expression of the Kynurenine Pathway Enzyme Tryptophan 2,3-Dioxygenase Is Increased in the Frontal Cortex of Individuals with Schizophrenia. *Neurobiol. Dis.* **2004**, *15* (3), 618–629.

(222) Schramme, F.; Crosignani, S.; Frederix, K.; Hoffmann, D.; Pilotte, L.; Stroobant, V.; Preillon, J.; Driessens, G.; van den Eynde, B. J. Inhibition of Tryptophan-Dioxygenase Activity Increases the Antitumor Efficacy of Immune Checkpoint Inhibitors. *Cancer Immunol. Res.* **2020**, *8* (1), 32–45.

(223) Hoffmann, D.; Dvorakova, T.; Stroobant, V.; Bouzin, C.; Solvay, M.; Klaessens, S.; Letellier, M.; Baren, N. Van; Lelotte, J.; Marbaix, E. Tryptophan 2 , 3-Dioxygenase Expression Is Prominent in Human Hepatocarcinoma Cells , but Is Mostly Restricted to Pericytes in Other Human Tumors.

(224) Nakamura, T.; Niimi, S.; Nawa, K.; Noda, C.; Ichihara, A.; Takagi, Y.; Anai, M.; Sakaki, Y. Multihormonal Regulation of Transcription of the Tryptophan 2,3-Dioxygenase Gene in Primary Cultures of Adult Rat Hepatocytes with Special Reference to the Presence of a Transcriptional Protein Mediating the Action of Glucocorticoids. *J. Biol. Chem.* **1987**, *262* (2), 727–733.

(225) Badawy, A. A.-B. Kynurenine Pathway of Tryptophan Metabolism: Regulatory and Functional Aspects. *Int. J. Tryptophan Res.* **2017**, *10*, 1178646917691938.

(226) Holmgaard, R. B.; Zamarin, D.; Munn, D. H.; Wolchok, J. D.; Allison, J. P. Indoleamine 2,3-Dioxygenase Is a Critical Resistance Mechanism in Antitumor T Cell Immunotherapy Targeting CTLA-4. *J. Exp. Med.* **2013**, *210* (7), 1389–1402.

(227) Spranger, S.; Koblish, H. K.; Horton, B.; Scherle, P. A.; Newton, R.; Gajewski, T. F. Mechanism of Tumor Rejection with Doublets of CTLA-4, PD-1/PD-L1, or IDO Blockade Involves Restored IL-2 Production and Proliferation of CD8+ T Cells Directly within the Tumor Microenvironment. *Journal for Immunother. cancer* **2014**, *2* (1).

(228) Yue, E. W.; Douty, B.; Wayland, B.; Bower, M.; Liu, X.; Leffet, L.; Wang, Q.; Bowman, K. J.; Hansbury, M. J.; Liu, C.; Wei, M.; Li, Y.; Wynn, R.; Burn, T. C.; Koblish, H. K.; Fridman, J. S.; Metcalf, B.; Scherle, P. A.; Combs, A. P. Discovery of Potent Competitive Inhibitors of Indoleamine 2,3-Dioxygenase with in Vivo

Pharmacodynamic Activity and Efficacy in a Mouse Melanoma Model. *J. Med. Chem.* **2009**, *52* (23), 7364–7367.

(229) Yue, E. W.; Sparks, R.; Polam, P.; Modi, D.; Douty, B.; Wayland, B.; Glass, B.; Takvorian, A.; Glenn, J.; Zhu, W.; Bower, M.; Liu, X.; Leffet, L.; Wang, Q.; Bowman, K. J.; Hansbury, M. J.; Wei, M.; Li, Y.; Wynn, R.; Burn, T. C.; Koblish, H. K.; Fridman, J. S.; Emm, T.; Scherle, P. A.; Metcalf, B.; Combs, A. P. INCB24360 (Epacadostat), a Highly Potent and Selective Indoleamine-2,3-Dioxygenase 1 (IDO1) Inhibitor for Immuno-Oncology. *ACS Med. Chem. Lett.* **2017**, *8* (5), 486–491.

(230) Liu, X.; Shin, N.; Koblish, H. K.; Yang, G.; Wang, Q.; Wang, K.; Leffet, L.; Hansbury, M. J.; Thomas, B.; Rupar, M.; Waeltz, P.; Bowman, K. J.; Polam, P.; Sparks, R. B.; Yue, E. W.; Li, Y.; Wynn, R.; Fridman, J. S.; Burn, T. C.; Combs, A. P.; Newton, R. C.; Scherle, P. A. Selective Inhibition of IDO1 Effectively Regulates Mediators of Antitumor Immunity. *Blood* **2010**, *115* (17), 3520–3530.

(231) Gangadhar, T. C.; Hamid, O.; Smith, D. C.; Bauer, T. M.; Wasser, J. S.; Luke, J. J.; Balmanoukian, A. S.; Kaufman, D. R.; Zhao, Y.; Maleski, J.; Leopold, L.; Gajewski, T. F. Preliminary Results from a Phase I/II Study of Epacadostat (Incb024360) in Combination with Pembrolizumab in Patients with Selected Advanced Cancers. *Journal for Immunother. cancer* **2015**, *3* (2), 1–2.

(232) Wolchok, J. D.; Kluger, H.; Callahan, M. K.; Postow, M. A.; Rizvi, N. A.; Lesokhin, A. M.; Segal, N. H.; Ariyan, C. E.; Gordon, R.-A.; Reed, K.; Burke, M. M.; Caldwell, A.; Kronenberg, S. A.; Agunwamba, B. U.; Zhang, X.; Lowy, I.; Inzunza, H. D.; Feely, W.; Horak, C. E.; Hong, Q.; Korman, A. J.; Wigginton, J. M.; Gupta, A.; Sznol, M. Nivolumab plus Ipilimumab in Advanced Melanoma. *N. Engl. J. Med.* **2013**, *369* (2), 122–133.

(233) Nayak-Kapoor, A.; Hao, Z.; Sadek, R.; Dobbins, R.; Marshall, L.; Vahanian, N. N.; Jay Ramsey, W.; Kennedy, E.; Mautino, M. R.; Link, C. J.; Lin, R. S.; Royer-Joo, S.; Liang, X.; Salphati, L.; Morrissey, K. M.; Mahrus, S.; McCall, B.; Pirzkall, A.; Munn, D. H.; Janik, J. E.; Khleif, S. N. Phase Ia Study of the Indoleamine 2,3-Dioxygenase 1 (IDO1) Inhibitor Navoximod (GDC-0919) in Patients with Recurrent Advanced Solid Tumors. *Journal for Immunother. cancer* **2018**, *6* (1), 1–12.

(234) Jung, K. H.; LoRusso, P.; Burris, H.; Gordon, M.; Bang, Y. J.; Hellmann, M. D.; Cervantes, A.; Ochoa de Olza, M.; Marabelle, A.; Stephen Hodi, F.; Ahn, M. J.; Emens, L. A.; Barlesi, F.; Hamid, O.; Calvo, E.; McDermott, D.; Soliman, H.; Rhee, I.; Lin, R.; Pourmohamad, T.; Suchomel, J.; Tsuhako, A.; Morrissey, K.; Mahrus, S.; Morley, R.; Pirzkall, A.; Lindsey Davis, S. Phase I Study of the Indoleamine 2,3-Dioxygenase 1 (IDO1) Inhibitor Navoximod (GDC-0919) Administered with PD-L1 Inhibitor (Atezolizumab) in Advanced Solid Tumors. *Clin. Cancer Res.* **2019**, *25* (11), 3220–3228.

(235) Crosignani, S.; Bingham, P.; Bottemanne, P.; Cannelle, H.; Cauwenberghs, S.; Cordonnier, M.; Dalvie, D.; Deroose, F.; Feng, J. L.; Gomes, B.; Greasley, S.; Kaiser, S. E.; Kraus, M.; Négrerie, M.; Maegley, K.; Miller, N.; Murray, B. W.; Schneider, M.; Soloweij, J.; Stewart, A. E.; Tumang, J.; Torti, V. R.; Van Den Eynde, B.; Wythes, M. Discovery of a Novel and Selective Indoleamine 2,3-Dioxygenase (IDO-1) Inhibitor 3-(5-Fluoro-1H-Indol-3-Yl)Pyrrolidine-2,5-Dione (EOS200271/PF-06840003) and Its Characterization as a Potential Clinical Candidate. *J. Med. Chem.* **2017**, *60* (23), 9617–9629.

(236) Sono, M.; Cady, S. G. Enzyme Kinetic and Spectroscopic Studies of Inhibitor and Effector Interactions with Indoleamine 2,3-Dioxygenase. 1. Norharman and 4-Phenylimidazole Binding to the Enzyme as Inhibitors and Heme Ligands. *Biochemistry* **1989**, *28* (13), 5392–5399.

(237) Newton, R. C.; Scherle, P. A.; Bowman, K.; Liu, X.; Beatty, G. L.; O'Dwyer, P. J.; Gajewski, T.; Bowman, J.; Schaub, R.; Leopold, L. Pharmacodynamic Assessment of INCB024360, an Inhibitor of Indoleamine 2,3-Dioxygenase 1 (IDO1), in Advanced Cancer Patients. *J. Clin. Oncol.* **2012**, *30* (15_suppl), 2500–2500.

(238) Siu, L. L.; Gelmon, K.; Chu, Q.; Pachynski, R.; Alese, O.; Basciano, P.; Walker, J.; Mitra, P.; Zhu, L.; Phillips, P.; Hunt, J.; Desai, J. Abstract CT116: BMS-986205, an Optimized Indoleamine 2,3-Dioxygenase 1 (IDO1) Inhibitor, Is Well Tolerated with Potent Pharmacodynamic (PD) Activity, Alone and in Combination with Nivolumab (Nivo) in Advanced Cancers in a Phase 1/2a Trial. In *Cancer Research*; American Association for Cancer Research, 2017; Vol. 77, pp CT116-CT116.

(239) Mautino, M. R.; Jaipuri, F. A.; Waldo, J.; Kumar, S.; Adams, J.; Van Allen, C.; Marcinowicz-Flick, A.; Munn, D.; Vahanian, N.; Link, C. J. Abstract 491: NLG919, a Novel Indoleamine-2,3-Dioxygenase (IDO)-Pathway Inhibitor Drug Candidate for Cancer Therapy. *Immunology* **2013**, *73* (8 Supplement), 491–491.

(240) Mitchell, T. C.; Hamid, O.; Smith, D. C.; Bauer, T. M.; Wasser, J. S.; Olszanski, A. J.; Luke, J. J.; Balmanoukian, A. S.; Schmidt, E. V.; Zhao, Y.; Gong, X.; Maleski, J.; Leopold, L.; Gajewski, T. F. Epacadostat plus Pembrolizumab in Patients with Advanced Solid Tumors: Phase I Results from a Multicenter, Open-Label Phase I/II Trial (ECHO-202/KEYNOTE-037). *J. Clin. Oncol.* **2018**, *36* (32), 3223–3230.

(241) Long, G. V.; Dummer, R.; Hamid, O.; Gajewski, T. F.; Caglevic, C.; Dalle, S.; Arance, A.; Carlino, M. S.; Grob, J. J.; Kim, T. M.; Demidov, L.; Robert, C.; Larkin, J.; Anderson, J. R.; Maleski, J.; Jones, M.; Diede, S. J.; Mitchell, T. C. Epacadostat plus Pembrolizumab versus Placebo plus Pembrolizumab in Patients with Unresectable or Metastatic Melanoma (ECHO-301/KEYNOTE-252): A Phase 3, Randomised, Double-Blind Study. *Lancet Oncol.* **2019**, *20* (8), 1083–1097.

(242) Muller, A. J.; Manfredi, M. G.; Zakharia, Y.; Prendergast, G. C. Inhibiting IDO Pathways to Treat Cancer: Lessons from the ECHO-301 Trial and Beyond. *Semin. Immunopathol.* **2019**, *41* (1), 41–48.

(243) Van Den Eynde, B. J.; Van Baren, N.; Baurain, J. F. Is There a Clinical Future for IDO1 Inhibitors after the Failure of Epacadostat in Melanoma? *Annu. Rev. Cancer Biol.* **2020**, *4*, 241–256.

(244) Blair, A. B.; Kleponis, J.; Thomas, D. L.; Muth, S. T.; Murphy, A. G.; Kim, V.; Zheng, L. IDO1 Inhibition Potentiates Vaccine-Induced Immunity against Pancreatic Adenocarcinoma. *J. Clin. Invest.* **2019**, *129* (4), 1742–1755.

(245) Balog, A.; Lin, T.; Maley, D.; Gullo-Brown, J.; Kandoussi, E. H.; Zeng, J.; Hunt, J. T. Preclinical Characterization of Linrodostat Mesylate, a Novel, Potent, and Selective Oral Indoleamine 2,3-Dioxygenase 1 Inhibitor. *Mol. Cancer Ther.* **2021**, *20* (3), 467–476.

(246) Phan, T.; Nguyen, V. H.; D'Alincourt, M. S.; Manuel, E. R.; Kaltcheva, T.; Tsai, W.; Blazar, B. R.; Diamond, D. J.; Melstrom, L. G. Salmonella-Mediated Therapy Targeting Indoleamine 2, 3-Dioxygenase 1 (IDO) Activates Innate Immunity and Mitigates Colorectal Cancer Growth. *Cancer Gene Ther.* **2020**, *27* (3–4), 235–245.

(247) Kim, C.; Kim, J. H.; Kim, J. S.; Chon, H. J.; Kim, J.-H. A Novel Dual Inhibitor of IDO and TDO, CMG017, Potently Suppresses the Kynurenine Pathway and Overcomes Resistance to Immune Checkpoint Inhibitors. *J. Clin. Oncol.* **2019**, *37* (15_suppl), e14228–e14228.

(248) Hu, M.; Zhou, W.; Wang, Y.; Yao, D.; Ye, T.; Yao, Y.; Chen, B.; Liu, G.; Yang, X.; Wang, W.; Xie, Y. Discovery of the First Potent Proteolysis Targeting Chimera (PROTAC) Degrader of Indoleamine 2,3-Dioxygenase 1. *Acta Pharm. Sin. B* **2020**, *10* (10), 1943–1953.

(249) Röhrig, U. F.; Reynaud, A.; Majjigapu, S. R.; Vogel, P.; Pojer, F.; Zoete, V. Inhibition Mechanisms of Indoleamine 2,3-Dioxygenase 1 (IDO1). *J. Med. Chem.* **2019**, *62* (19), 8784–8795.

(250) Röhrig, U. F.; Majjigapu, S. R.; Reynaud, A.; Pojer, F.; Dilek, N.; Reichenbach, P.; Ascencao, K.; Irving, M.; Coukos, G.; Vogel, P.; Michielin, O.; Zoete, V. Azole-Based Indoleamine 2,3-Dioxygenase 1 (IDO1) Inhibitors. *J. Med. Chem.* **2021**, *64* (4), 2205–2227.

(251) Salter, M.; Hazelwood, R.; Pogson, C. I.; Iyer, R.; Madge, D. J. The Effects of a Novel and Selective Inhibitor of Tryptophan 2,3-Dioxygenase on Tryptophan and Serotonin Metabolism in the Rat. *Biochem. Pharmacol.* **1995**, *49* (10), 1435–1442.

(252) Opitz, C. A.; Litzenburger, U. M.; Sahm, F.; Ott, M.; Tritschler, I.; Trump, S.; Schumacher, T.; Jestaedt, L.; Schrenk, D.; Weller, M.; Jugold, M.; Guillemin, G. J.; Miller, C. L.; Lutz, C.; Radlwimmer, B.; Lehmann, I.; von Deimling, A.; Wick, W.; Platten, M. An Endogenous Tumour-Promoting Ligand of the Human Aryl Hydrocarbon Receptor. *Nature* **2011**, *478* (7368), 197–203.

(253) Dolusic, E.; Larrieu, P.; Moineaux, L.; Stroobant, V.; Pilotte, L.; Colau, D.; Pochet, L.; Eynde, V. Den; Masereel, B.; Wouters, J.; Frédérick, R. 3- (2- (Pyridyl) Ethenyl) Indoles as Potential Anticancer Immunomodulators. *J. Med. Chem.* **2011**, *54*, 5320–5334.

(254) Breda, C.; Sathyasaikumar, K. V.; Idrissi, S. S.; Notarangelo, F. M.; Estranero, J. G.; Moore, G. G. L.; Green, E. W.; Kyriacou, C. P.; Schwarcz, R.; Giorgini, F. Tryptophan-2,3-Dioxygenase (TDO) Inhibition Ameliorates Neurodegeneration by Modulation of Kynurenine Pathway Metabolites. *Proc. Natl. Acad. Sci. U. S. A.* **2016**, *113* (19), 5435–5440.

(255) Dolušić, E.; Frédérick, R. Indoleamine 2,3-Dioxygenase Inhibitors: A Patent Review (2008-2012). *Expert Opinion on Therapeutic Patents*. Informa Healthcare October 1, 2013, pp 1367–1381.

(256) Cheong, J. E.; Ekkati, A.; Sun, L. A Patent Review of IDO1 Inhibitors for Cancer. *Expert Opin. Ther. Pat.* **2018**, *28* (4), 317–330.

(257) Feng, X.; Liao, D.; Liu, D.; Ping, A.; Li, Z.; Bian, J. Development of Indoleamine 2,3-Dioxygenase 1 Inhibitors for Cancer Therapy and Beyond: A Recent Perspective. *J. Med. Chem.* **2020**, *63* (24), 15115–15139.

(258) Takikawa, O.; Kuroiwa, T.; Yamazaki, F.; Kido, R. Mechanism of Interferon-Gamma Action. Characterization of Indoleamine 2,3-Dioxygenase in Cultured Human Cells Induced by Interferon-Gamma and Evaluation of the Enzyme-Mediated Tryptophan Degradation in Its Anticellular Activity. *J. Biol. Chem.* **1988**, *263* (4), 2041–2048.

(259) Röhrig, U. F.; Majjigapu, S. R.; Vogel, P.; Zoete, V.; Michielin, O. Challenges in the Discovery of Indoleamine 2,3-Dioxygenase 1 (IDO1) Inhibitors. *J. Med. Chem.* **2015**, *58* (24), 9421–9437.

(260) Alegre, E.; López, A. S.; González, A. Tryptophan Metabolites Interfere with the Ehrlich Reaction Used for the Measurement of Kynurenine. *Anal. Biochem.* **2005**, *339* (1), 188–189.

(261) Kumar, S.; Jaller, D.; Patel, B.; LaLonde, J. M.; DuHadaway, J. B.; Malachowski, W. P.; Prendergast, G. C.; Muller, A. J. Structure Based Development of Phenylimidazole-Derived Inhibitors of Indoleamine 2,3-Dioxygenase. *J. Med. Chem.* **2008**, *51* (16), 4968–4977.

(262) IOmet Pharma Ltd. Pharmaceutical Compound. WO2016026772 (2016).

(263) Pei, Z.; Mendonca, R.; Gazzard, L.; Pastor, R.; Goon, L.; Gustafson, A.; Vanderporten, E.; Hatzivassiliou, G.; Dement, K.; Cass, R.; Yuen, P. W.; Zhang, Y.; Wu, G.; Lin, X.; Liu, Y.; Sellers, B. D. Aminoisoxazoles as Potent Inhibitors of Tryptophan 2,3-Dioxygenase 2 (TDO2). *ACS Med. Chem. Lett.* **2018**, *9* (5), 417–421.

(264) Newlink Genetics Corp. Fused Imidazole Derivatives Useful as IDO Inhibitors. WO2012142237 (2012), October 18, 2012.

(265) Newlink Genetics Corp. Tricyclic Compounds as Inhibitors of Immunosuppression Mediated by Tryptophan Metabolization. WO2014159248 (2014).

(266) Hangzhou Innogate Pharma Co Ltd. Heterocycles Useful as IDO and TDO Inhibitors. WO2016165613 (2016).

(267) RedX Pharma Plc. 4H-Imidazo[1,5-a]Indole Derivatives and Their Use as Indoleamine 2,3-Dioxygenase (IDO) and/or Tryptophan 2,3-Dioxygenase (TDO2) Modulators. WO2016051181 (2016).

(268) RedX Pharma Plc. 6,7-Heterocyclic Fused 5H-Pyrrolo[1,2-c]Imidazole Derivatives and Their Use as Indoleamine 2,3-Dioxygenase (IDO) and/or Tryptophan 2,3-Dioxygenase (TDO2) Modulators. WO2016059412 (2016).

(269) Genentech Inc. TDO2 Inhibitors. WO2017107979 (2017).

(270) Shanghai De Novo Pharmatech Co Ltd. Fused-Ring Compounds, Pharmaceutical Composition and Uses Thereof. WO2016131381 (2016).

(271) Shanghai Institute of Organic Chemistry. Indoleamine-2,3-Dioxygenase Inhibitor and Preparation Method Thereof. WO2018082567 (2018).

(272) SciFluor Life Sciences Inc. Fused Imidazole Derivatives as IDO/TDO Inhibitors. US20170121325 (2017).

(273) Emcure. Heterocyclic Compounds Useful as IDO and/or TDO Modulators. WO2017149469 (2017).

(274) Parr, B. T.; Pastor, R.; Sellers, B. D.; Pei, Z.; Jaipuri, F. A.; Castanedo, G. M.; Gazzard, L.; Kumar, S.; Li, X.; Liu, W.; Mendonca, R.; Pavana, R. K.; Potturi, H.; Shao, C.; Velvadapu, V.; Waldo, J. P.; Wu, G.; Yuen, P. W.; Zhang, Z.; Zhang, Y.; Harris, S. F.; Oh, A. J.; Dipasquale, A.; Dement, K.; La, H.; Goon, L.; Gustafson, A.; Vanderporten, E. C.; Mautino, M. R.; Liu, Y. Implementation of the CYP Index for the Design of Selective Tryptophan-2,3-Dioxygenase Inhibitors. *ACS Med. Chem. Lett.* **2020**, *11* (4), 541–549.

(275) Curadev Pharma. Inhibitors of the Kynurenine Pathway. WO2014186035 (2014).

(276) ITEOS Therapeutics. 4-(Indol-3-Yl)-Pyrazole Derivatives, Pharmaceutical Compositions and Methods for Use. WO2015067782 (2015).

(277) ITEOS Therapeutics. Novel 3-(Indol-3-Yl)-Pyridine Derivatives, Pharmaceutical Compositions and Methods for Use. US2015225367 (2015).

(278) ITEOS Therapeutics. Novel 3-Indol Substituted Derivatives, Pharmaceutical Compositions and Methods for Use. WO2015140717 (2015).

(279) ITEOS Therapeutics. Novel 3-Indol Substituted Derivatives, Pharmaceutical Compositions and Methods for Use. US2018222862 (2018).

(280) Netherlands Translational Research Center. Inhibitors of Tryptophan 2,3-Dioxygenase. WO2018011227 (2018).

(281) IOmet Pharma Ltd. Pharmaceutical Compound. WO2015082499 (2015).

(282) IOmet Pharma Ltd. Indole Derivatives for Use in Medicine. WO2015150097 (2015).

(283) IOmet Pharma Ltd. Inhibitors of Tryptophan 2,3-Dioxygenase or Indoleamine 2,3-Dioxygenase WO2016071283. (2016).

(284) BeiGene Ltd. Novel 5 or 8-Substituted Imidazo[1, 5-a] Pyridines as Indoleamine and/or Tryptophan 2,3-Dioxygenase Inhibitors. US20180072716 (2018).

(285) Auckland Uniservices Ltd. Inhibitors of Tryptophan Dioxygenases (IDO1 and TDO) and Their Use in Therapy. WO2016024233 (2016).

(286) Auckland Uniservices Ltd. Inhibitors of Tryptophan Dioxygenases (IDO1 and TDO) and Their Use in Therapy. WO2017034420 (2017).

(287) Yang, S.; Li, X.; Hu, F.; Li, Y.; Yang, Y.; Yan, J.; Kuang, C.; Yang, Q. Discovery of Tryptanthrin Derivatives as Potent Inhibitors of Indoleamine 2,3-Dioxygenase with Therapeutic Activity in Lewis Lung Cancer (LLC) Tumor-Bearing Mice. *J. Med. Chem.* **2013**, *56* (21), 8321–8331.

(288) Zhang, S.; Qi, F.; Fang, X.; Yang, D.; Hu, H.; Huang, Q.; Kuang, C.; Yang, Q. Tryptophan 2,3-Dioxygenase Inhibitory Activities of Tryptanthrin Derivatives. *Eur. J. Med. Chem.* **2018**, *160*, 133–145.

(289) Yang, D.; Zhang, S.; Fang, X.; Guo, L.; Hu, N.; Guo, Z.; Li, X.; Yang, S.; He, J. C.; Kuang, C.; Yang, Q. N-Benzyl/Aryl Substituted Tryptanthrin as Dual Inhibitors of Indoleamine 2,3-Dioxygenase and Tryptophan 2,3-Dioxygenase. *J. Med. Chem.* **2019**, *62* (20), 9161–9174.

(290) Li, Y.; Zhang, S.; Wang, R.; Cui, M.; Liu, W.; Yang, Q.; Kuang, C. Synthesis of Novel Tryptanthrin Derivatives as Dual Inhibitors of Indoleamine 2,3-Dioxygenase 1 and Tryptophan 2,3-Dioxygenase. *Bioorganic Med. Chem. Lett.* **2020**, *30* (11).

(291) Li, Y.; Zhang, S.; Wang, R.; Cui, M.; Liu, W.; Yang, Q.; Kuang, C. Synthesis of Novel Tryptanthrin Derivatives as Dual Inhibitors of Indoleamine 2,3-Dioxygenase 1 and Tryptophan 2,3-Dioxygenase. *Bioorganic Med. Chem. Lett.* **2020**, *30* (11), 127159.

(292) Dolušić, E.; Larrieu, P.; Moineaux, L.; Stroobant, V.; Pilotte, L.; Colau, D.; Pochet, L.; Van Den Eynde, B.; Masereel, B.; Wouters, J.; Frédérick, R. Tryptophan 2,3-Dioxygenase (TDO) Inhibitors. 3-(2-(Pyridyl)Ethenyl)Indoles as Potential Anticancer Immunomodulators. *J. Med. Chem.* **2011**, *54* (15), 5320–5334.

(293) Wen, J.; Lord, H.; Knutson, N.; Wikström, M. Nano Differential Scanning Fluorimetry for Comparability Studies of Therapeutic Proteins. *Anal. Biochem.* **2020**, *593*, 113581.

(294) Takikawa, O.; Kuroiwa, T.; Yamazaki, F.; Kido, R. Mechanism of Interferon-γ Action. Characterization of Indoleamine 2,3-Dioxygenase in Cultured Human Cells Induced by Interferon -γ and Evaluation of the Enzyme-Mediated Tryptophan Degradation in Its Anticellular Activity. *J. Biol. Chem.* **1988**, *263* (4), 2041–2048.

(295) Kozlova, A.; Frédérick, R. Current State on Tryptophan 2,3-Dioxygenase Inhibitors: A Patent Review. *Expert Opin. Ther. Pat.* **2019**, *29* (1), 11–23.

(296) Schultes, S.; De Graaf, C.; Haaksma, E. E. J.; De Esch, I. J. P.; Leurs, R.; Krämer, O. Ligand Efficiency as a Guide in Fragment Hit Selection and Optimization. *Drug Discov. Today Technol.* **2010**, *7* (3), 157–162.

(297) Hopkins, A. L.; Keserü, G. M.; Leeson, P. D.; Rees, D. C.; Reynolds, C. H. The Role of Ligand Efficiency Metrics in Drug Discovery. *Nat. Rev. Drug Discov.* **2014**, *13* (2), 105–121.

(298) Johnson, T. W.; Gallego, R. A.; Edwards, M. P. Lipophilic Efficiency as an Important Metric in Drug Design. *J. Med. Chem.* **2018**, *61* (15), 6401–6420.

(299) Mayer, M.; Meyer, B. Group Epitope Mapping by Saturation Transfer Difference NMR to Identify Segments of a Ligand in Direct Contact with a Protein Receptor. *J. Am. Chem. Soc.* **2001**, *123* (25), 6108–6117.

(300) Avonto, C.; Taglialatela-Scafati, O.; Pollastro, F.; Minassi, A.; Di-Marzo, V.; De-Petrocellis, L.; Appendino, G. An NMR Spectroscopic Method to Identify and Classify Thiol-Trapping Agents: Revival of Michael Acceptors for Drug Discovery? *Angew. Chemie - Int. Ed.* **2011**, *50* (2), 467–471.

(301) Al-Rifai, N.; Rücker, H.; Amslinger, S. Opening or Closing the Lock? When Reactivity Is the Key to Biological Activity. *Chem. Eur. J.* **2013**, *19* (45), 15384–15395.

(302) Jackson, P. A.; Widen, J. C.; Harki, D. A.; Brummond, K. M. Covalent Modifiers: A Chemical Perspective on the Reactivity of α,β-Unsaturated Carbonyls with Thiols via Hetero-Michael Addition Reactions. *J. Med. Chem.* **2017**, *60* (3), 839–885.

(303) Knapp, D. M.; Gillis, E. P.; Burke, M. D. A General Solution for Unstable Boronic Acids: Slow-Release Cross-Coupling from Air-Stable MIDA Boronates. *J. Am. Chem. Soc.* **2009**, *131* (20), 6961–6963.

(304) Röhrig, U. F.; Majjigapu, S. R.; Vogel, P.; Zoete, V.; Michielin, O. Challenges in the Discovery of Indoleamine 2,3-Dioxygenase 1 (IDO1) Inhibitors. *J. Med. Chem.* **2015**, *58* (24), 9421–9437.

(305) Brown, N. Bioisosteres in Medicinal Chemistry. *Bioisosteres Med. Chem.* **2012**, *54*,

1–237.

(306) May, S. W. Selenium-Based Drug Design. *Top. Med. Chem.* **2016**, *17*, 87–118.

(307) Wessjohann, L. A.; Schneider, A.; Abbas, M.; Brandt, W. Selenium in Chemistry and Biochemistry in Comparison to Sulfur. *Biol. Chem.* **2007**, *388* (10), 997–1006.

(308) Moroder, L. Isosteric Replacement of Sulfur with Other Chalcogens in Peptides and Proteins. *J. Pept. Sci.* **2005**, *11* (4), 187–214.

(309) Mishra, K. K.; Singh, S. K.; Ghosh, P.; Ghosh, D.; Das, A. The Nature of Selenium Hydrogen Bonding: Gas Phase Spectroscopy and Quantum Chemistry Calculations. *Phys. Chem. Chem. Phys.* **2017**, *19* (35), 24179–24187.

(310) Howard, D. L.; Kjaergaard, H. G. Hydrogen Bonding to Divalent Sulfur. *Phys. Chem. Chem. Phys.* **2008**, *10* (28), 4113–4118.

(311) Jacob, C.; Giles, G. I.; Giles, N. M.; Sies, H. Sulfur and Selenium: The Role of Oxidation State in Protein Structure and Function. *Angew. Chemie Int. Ed.* **2003**, *42* (39), 4742–4758.

(312) Slater, J. C. Atomic Radii in Crystals. *J. Chem. Phys.* **1964**, *41* (10), 3199–3204.

(313) Brown, K.; Arthur, J. Selenium, Selenoproteins and Human Health: A Review. *Public Health Nutr.* **2001**, *4* (2b), 593–599.

(314) Holben, D. H.; Smith, A. M. The Diverse Role of Selenium within Selenoproteins: A Review. *J. Am. Diet. Assoc.* **1999**, *99* (7), 836–843.

(315) Bellinger, F. P.; Raman, A. V.; Reeves, M. A.; Berry, M. J. Regulation and Function of Selenoproteins in Human Disease. *Biochem. J.* **2009**, *422* (1), 11–22.

(316) May, S. W. Selenium-Based Pharmacological Agents: An Update. *Expert Opin. Investig. Drugs* **2002**, *11* (9), 1261–1269.

(317) Klein, E. A.; Thompson, I. M.; Tangen, C. M.; Crowley, J. J.; Lucia, S.; Goodman, P. J.; Minasian, L. M.; Ford, L. G.; Parnes, H. L.; Gaziano, J. M.; Karp, D. D.; Lieber, M. M.; Walther, P. J.; Klotz, L.; Parsons, J. K.; Chin, J. L.; Darke, A. K.; Lippman, S. M.; Goodman, G. E.; Meyskens, F. L.; Baker, L. H. Vitamin E and the Risk of Prostate Cancer: The Selenium and Vitamin E Cancer Prevention Trial (SELECT). *JAMA - J. Am. Med. Assoc.* **2011**, *306* (14), 1549–1556.

(318) Ali, W.; Benedetti, R.; Handzlik, J.; Zwergel, C.; Battistelli, C. The Innovative Potential of Selenium-Containing Agents for Fighting Cancer and Viral Infections. *Drug Discovery Today*. Elsevier Current Trends January 1, 2021, pp 256–263.

(319) Müller, A.; Cadenas, E.; Graf, P.; Sies, H. A Novel Biologically Active Seleno-Organic Compound-1. Glutathione Peroxidase-like Activity in Vitro and Antioxidant Capacity of PZ 51 (Ebselen). *Biochem. Pharmacol.* **1984**, *33* (20), 3235–3239.

(320) Singh, N.; Halliday, A. C.; Thomas, J. M.; Kuznetsova, O.; Baldwin, R.; Woon, E. C. Y.; Aley, P. K.; Antoniadou, I.; Sharp, T.; Vasudevan, S. R.; Churchill, G. C. A Safe Lithium Mimetic for Bipolar Disorder. *Nat. Commun.* **2013**, *4* (1), 1–7.

(321) Masaki, C.; Sharpley, A. L.; Cooper, C. M.; Godlewska, B. R.; Singh, N.; Vasudevan, S. R.; Harmer, C. J.; Churchill, G. C.; Sharp, T.; Rogers, R. D.; Cowen, P. J. Effects of the Potential Lithium-Mimetic, Ebselen, on Impulsivity and Emotional Processing. *Psychopharmacology (Berl).* **2016**, *233* (14), 2655–2661.

(322) Parnham, M. J.; Sies, H. The Early Research and Development of Ebselen. *Biochem. Pharmacol.* **2013**, *86* (9), 1248–1253.

(323) Menéndez, C. A.; Byléhn, F.; Perez-Lemus, G. R.; Alvarado, W.; De Pablo, J. J. Molecular Characterization of Ebselen Binding Activity to SARS-CoV-2 Main Protease. *Sci. Adv* **2020**, *6*, 345–356.

(324) Jin, Z.; Du, X.; Xu, Y.; Deng, Y.; Liu, M.; Zhao, Y.; Zhang, B.; Li, X.; Zhang, L.; Peng, C.; Duan, Y.; Yu, J.; Wang, L.; Yang, K.; Liu, F.; Jiang, R.; Yang, X.; You, T.; Liu, X.; Yang, X.; Bai, F.; Liu, H.; Liu, X.; Guddat, L. W.; Xu, W.; Xiao, G.; Qin, C.; Shi, Z.; Jiang, H.; Rao, Z.; Yang, H. Structure of Mpro from SARS-CoV-2 and Discovery of Its Inhibitors. *Nature* **2020**, *582* (7811), 289–293.

(325) Wang, L.; Yang, Z.; Fu, J.; Yin, H.; Xiong, K.; Tan, Q.; Jin, H.; Li, J.; Wang, T.; Tang, W.; Yin, J.; Cai, G.; Liu, M.; Kehr, S.; Becker, K.; Zeng, H. Ethaselen: A Potent Mammalian Thioredoxin Reductase 1 Inhibitor and Novel Organoselenium Anticancer Agent. *Free Radic. Biol. Med.* **2012**, *52* (5), 898–908.

(326) Wiles, J. A.; Phadke, A. S.; Bradbury, B. J.; Pucci, M. J.; Thanassi, J. A.; Deshpande, M. Selenophene-Containing Inhibitors of Type IIA Bacterial Topoisomerases. *J. Med. Chem.* **2011**, *54* (9), 3418–3425.

(327) Ghiazza, A. C.; Billard, T.; Dickson, C.; Tlili, A.; Gampe, C. Chalcogen OCF3-Isosteres Modulate Drug Properties without Introducing Inherent Liabilities. *ChemMedChem* **2019**, *14* (17), 1586–1589.

(328) Plano, D.; Karelia, D. N.; Pandey, M. K.; Spallholz, J. E.; Amin, S.; Sharma, A. K. Design, Synthesis, and Biological Evaluation of Novel Selenium (Se-NSAID) Molecules as Anticancer Agents. *J. Med. Chem.* **2016**, *59* (5), 1946–1959.

(329) Zhao, L.; Zhao, G.; Xue, Q. Tizanidine (Hydrochloride) Inhibits A549 Lung Cancer Cell Proliferation and Motility through Regulating Nischarin. *Onco. Targets. Ther.* **2020**, *13*, 291–298.

(330) Xing, X. W.; Sun, Y. F.; Zhao, J.; Pan, Z. X.; Jiang, W. X. Tizanidine Hydrochloride Exhibits a Cytotoxic Effect on Osteosarcoma Cells through the PI3K/AKT Signaling Pathway. *J. Int. Med. Res.* **2019**, *47* (8), 3792–3802.

(331) Plano, D.; Moreno, E.; Font, M.; Encío, I.; Palop, J. A.; Sanmartín, C. Synthesis and in Vitro Anticancer Activities of Some Selenadiazole Derivatives. *Arch. Pharm. (Weinheim).* **2010**, *343* (11–12), 680–691.

(332) Ruberte, A. C.; Plano, D.; Encío, I.; Aydillo, C.; Sharma, A. K.; Sanmartín, C. Novel Selenadiazole Derivatives as Selective Antitumor and Radical Scavenging Agents. *Eur. J. Med. Chem.* **2018**.

(333) Kozlova, A.; Thabault, L.; Liberelle, M.; Klaessens, S.; Prévost, J. R. C.; Mathieu, C.; Pilotte, L.; Stroobant, V.; Van den Eynde, B.; Frédérick, R. Rational Design of Original Fused-Cycle Selective Inhibitors of Tryptophan 2,3-Dioxygenase. *J. Med. Chem.* **2021**, DOI: 10.1021/acs.jmedchem.1c00323.

(334) Thakur, A.; Zhang, K.; Louie, J. Suzuki-Miyaura Coupling of Heteroaryl Boronic Acids and Vinyl Chlorides. *Chem. Commun.* **2012**, *48* (2), 203–205.

(335) Terentis, A. C.; Freewan, M.; Sempértegui Plaza, T. S.; Raftery, M. J.; Stocker, R.; Thomas, S. R. The Selenazal Drug Ebselen Potently Inhibits Indoleamine 2,3-Dioxygenase by Targeting Enzyme Cysteine Residues. *Biochemistry* **2010**, *49* (3), 591–600.

(336) ACD/Percepta, 14.1.0 (Build 2921), Advanced Chemistry Development, Inc., Toronto, On, Canada, Www.Acdlabs.Com, 2021.

(337) Swain, M. Chemicalize.Org. *J. Chem. Inf. Model.* **2012**, *52* (2), 613–615.

(338) Tombline, G.; Donnelly, D. J.; Holt, J. J.; You, Y.; Ye, M.; Gannon, M. K.; Nygren, C. L.; Detty, M. R. Stimulation of P-Glycoprotein ATPase by Analogues of Tetramethylrosamine: Coupling of Drug Binding at the "R" Site to the ATP Hydrolysis Transition State. *Biochemistry* **2006**, *45* (26), 8034–8047.

(339) Tsopelas, F.; Tsantili-Kakoulidou, A.; Ochsenkühn-Petropoulou, M. Investigation of the Chromatographic Behaviour of Some Selenium Species-Comparison with Their Octanol-Water Partitioning. *Talanta* **2007**, *73* (1), 127–133.

(340) Ayouni, L.; Cazorla, G.; Chaillou, D.; Herbreteau, B.; Rudaz, S.; Lantéri, P.; Carrupt, P. A. Fast Determination of Lipophilicity by HPLC. *Chromatographia* **2005**, *62* (5–6), 251–255.

(341) Elmansi, H.; Nasr, J. J.; Rageh, A. H.; El-Awady, M. I.; Hassan, G. S.; Abdel-Aziz, H. A.; Belal, F. Assessment of Lipophilicity of Newly Synthesized Celecoxib Analogues Using Reversed-Phase HPLC. *BMC Chem.* **2019**, *13* (1), 84.

(342) Curiel, T. J.; Coukos, G.; Zou, L.; Alvarez, X.; Cheng, P.; Mottram, P.; Evdemon-Hogan, M.; Conejo-Garcia, J. R.; Zhang, L.; Burow, M.; Zhu, Y.; Wei, S.; Kryczek, I.; Daniel, B.; Gordon, A.; Myers, L.; Lackner, A.; Disis, M. L.; Knutson, K. L.; Chen, L.; Zou, W. Specific Recruitment of Regulatory T Cells in Ovarian Carcinoma Fosters Immune Privilege and Predicts Reduced Survival. *Nat. Med.* **2004**, *10* (9), 942–949.

(343) Musiol, R. An Overview of Quinoline as a Privileged Scaffold in Cancer Drug Discovery. *Expert Opin. Drug Discov.* **2017**, *12* (6), 583–597.

(344) Mao, Y.; Soni, K.; Sangani, C.; Yao, Y. An Overview of Privileged Scaffold: Quinolines and Isoquinolines in Medicinal Chemistry as Anticancer Agents. *Curr. Top. Med. Chem.* **2020**, *20* (28), 2599–2633.

(345) Barreiro, E. J. Chapter 1: Privileged Scaffolds in Medicinal Chemistry: An Introduction. In *RSC Drug Discovery Series*; Royal Society of Chemistry, 2016; Vol. 2016–Janua, pp 1–15.

(346) Polanski, J.; Kurczyk, A.; Bak, A.; Musiol, R. Privileged Structures - Dream or Reality: Preferential Organization of Azanaphthalene Scaffold. *Curr. Med. Chem.* **2012**, *19* (13), 1921–1945.

(347) Sun, X.; Rao, Y. PROTACs as Potential Therapeutic Agents for Cancer Drug Resistance. *Biochemistry* **2019**, *59* (3), 240–249.

(348) Wang, K.; Zhou, H. Proteolysis Targeting Chimera (PROTAC) for Epidermal Growth Factor Receptor Enhances Anti-Tumor Immunity in Non-Small Cell Lung Cancer. *Drug Dev. Res.* **2021**, *82* (3), 422–429.

(349) Smith, B. E.; Wang, S. L.; Jaime-Figueroa, S.; Harbin, A.; Wang, J.; Hamman, B. D.; Crews, C. M. Differential PROTAC Substrate Specificity Dictated by Orientation of Recruited E3 Ligase. *Nat. Commun.* **2019**, *10* (1), 1–13.

(350) Toure, M.; Crews, C. M. Small-Molecule PROTACS: New Approaches to Protein Degradation. *Angew. Chemie - Int. Ed.* **2016**, *55* (6), 1966–1973.

(351) Burslem, G. M.; Crews, C. M. Proteolysis-Targeting Chimeras as Therapeutics and Tools for Biological Discovery. *Cell* **2020**, *181* (1), 102–114.

(352) Petrylak, D. P.; Gao, X.; Vogelzang, N. J.; Garfield, M. H.; Taylor, I.; Dougan Moore, M.; Peck, R. A.; Burris, H. A. First-in-Human Phase I Study of ARV-110, an Androgen Receptor (AR) PROTAC Degrader in Patients (Pts) with Metastatic Castrate-Resistant Prostate Cancer (MCRPC) Following Enzalutamide (ENZ) and/or Abiraterone (ABI). *J. Clin. Oncol.* **2020**, *38* (15_suppl), 3500–3500.

(353) Jerabek-Willemsen, M.; André, T.; Wanner, R.; Roth, H. M.; Duhr, S.; Baaske, P.; Breitsprecher, D. MicroScale Thermophoresis: Interaction Analysis and Beyond. *J. Mol. Struct.* **2014**, *1077*, 101–113.

(354) Greco, F. A.; Coletti, A.; Custodi, C.; Dolciami, D.; Di Michele, A.; Carotti, A.; Marinozzi, M.; Schlinck, N.; Macchiarulo, A. Binding Properties of Different Categories of IDO1 Inhibitors: A Microscale Thermophoresis Study. *Future Med. Chem.* **2017**, *9* (12), 1327–1338.

(355) Trott, O.; Olson, A. J. AutoDock Vina: Improving the Speed and Accuracy of Docking with a New Scoring Function, Efficient Optimization, and Multithreading. *J. Comput. Chem.* **2009**, *31* (2), 455–461.

(356) Carta, A.; Piras, S.; Boatto, G.; Paglietti, G. 1H,6H-Triazolo[4,5-e]Benzotriazole-3-Oxides and 5,5'-(Z)-Diazene-1,2-Diylbis(2-Methyl-2H-1,2,3-Benzotriazole) Derived from Chloronitrobenzotriazoles and Hydrazine. *Heterocycles* **2005**, *65* (10), 2471–2481.

(357) Schiemann, K.; Stieber, F.; Esdar, C. Azaheterocyclic Compounds. WO/2014/086453, 2014.